General Disclaimer

One or more of the Following Statements may affect this Document

- This document has been reproduced from the best copy furnished by the organizational source. It is being released in the interest of making available as much information as possible.

- This document may contain data, which exceeds the sheet parameters. It was furnished in this condition by the organizational source and is the best copy available.

- This document may contain tone-on-tone or color graphs, charts and/or pictures, which have been reproduced in black and white.

- This document is paginated as submitted by the original source.

- Portions of this document are not fully legible due to the historical nature of some of the material. However, it is the best reproduction available from the original submission.

Produced by the NASA Center for Aerospace Information (CASI)

(NASA-CR-168031) DILUTION JET MIXING PROGRAM, PHASE 1 (Garrett Turbine Engine Co.) 236 p HC A11/MF A01 CSCL 20D

N83-15590

Unclas
G3/34 02429

NASA CR-168031
GARRETT 21-4302

DILUTION JET MIXING PROGRAM
PHASE I REPORT

by

R. SRINIVASAN
A. BERENFELD
H.C. MONGIA

JAN 1983
RECEIVED
NASA STI FACILITY
ACCESS DEPT.

Garrett Turbine Engine Company
A Division of the Garrett Corporation

November 1982

Prepared for

National Aeronautics and Space Administration
NASA-Lewis Research Center

Contract NAS3-22110

ORIGINAL PAGE IS
OF POOR QUALITY

1. Report No. CR-168031	2. Government Accession No.	3. Recipient's Catalog No.
4. Title and Subtitle Dilution Jet Mixing Phase I Program		5. Report Date November 1982 6. Performing Organization Code
7. Author(s) R. Srinivasan A. Berenfeld H.C. Mongia		8. Performing Organization Report No. Garrett 21-4302 10. Work Unit No.
9. Performing Organization Name and Address Garrett Turbine Engine Co. A Division of the Garrett Corporation Phoenix, Arizona 85010		11. Contract or Grant No. NAS3-22110 13. Type of Report and Period Covered PHASE I COMPLETION
12. Sponsoring Agency Name and Address National Aeronautics and Space Administration Washington, D.C. 20546		14. Sponsoring Agency Code

15. Supplementary Notes

Project Manager: Dr. J.D. Holdeman
NASA-Lewis Research Center
Cleveland, Ohio

16. Abstract

The main objective of the NASA Dilution Jet Mixing Phase I Program was to quantify by means of parametric tests the effect of the following on the mixing of a row of jets with a confined cross-flow.

- Jet to mainstream density ratio
- Flow area convergence as encountered in transition sections.
- Non-uniform mainstream profile upstream of dilution orifices.

The general conclusions derived from Phase I work are:

- Jet spreading rate in transverse direction is increased with increasing J, H/D and with decreasing S/D.
- The density ratio has only a second order effect on the jet mixing characteristics for a constant momentum ratio.
- The temperature distributions in the jet mixing region are strongly influenced by the undisturbed mainstream profile. Therefore, a superposition of the mainstream profile on the correlations for isothermal mainstream conditions yields good agreement with data.
- Flow area convergence enhances mixing in radial and transverse directions. An asymmetric convergent duct with flat wall injection has the same jet mixing characteristics as a symmetric convergent duct. An asymmetric convergent duct with slant wall injection has a faster jet spreading rate in the transverse direction.

17. Key Words (Suggested by Author(s)) DILUTION-ZONE JET-MIXING COMBUSTION	18. Distribution Statement

19. Security Classif. (of this report) Unclassified	20. Security Classif. (of this page) Unclassified	21. No. of Pages	22. Price*

* For sale by the National Technical Information Service, Springfield, Virginia 22161

NASA-C-168 (Rev. 10-75)

TABLE OF CONTENTS

		Page
1.0	SUMMARY	1
2.0	INTRODUCTION AND OBJECTIVES	2
3.0	TEST RIG AND FACILITY DESCRIPTIONS	6
	3.1 Test Rig	6
	3.1.1 Profile Generator	7
	3.1.2 Test Sections	7
	3.1.3 Dilution Orifice Plate Geometry	10
	3.2 Test Facilities	10
4.0	DATA ACQUISITION AND REDUCTION	12
	4.1 Data Acquisition	12
	4.2 Data Reduction	13
5.0	EXPERIMENTAL DATA	18
	5.1 Series 1 Tests	18
	5.1.1 Conclusions for Series 1 Tests	26
	5.2 Series 2 Tests	27
	5.2.1 Conclusions for Series 2 Tests	32
	5.3 Series 3 Tests	33
	5.3.1 Symmetric Convergence Test Sections	33
	5.3.2 Asymmetric Convergence Test Sections	39
	5.3.3 Conclusions for Series 3 Tests	44
	5.4 Series 4 Tests	45
	5.4.1 Conclusions for Series 4 Tests	47
6.0	JET MIXING CORRELATIONS DEVELOPMENT	49
	6.1 NASA/Aerojet Correlations	50
7.0	CONCLUSIONS AND RECOMMENDATIONS	57
	APPENDIXES	
	A Symbols	148
	B References	149
DISTRIBUTION LIST		150

PRECEDING PAGE BLANK NOT FILMED

LIST OF ILLUSTRATIONS

Figure	Title	Page
1	Multiple Jet Study Coordinate System and Important Nomenclature	60
2	Jet Mixing Rig Schematic	61
3	Partially Assembled Dilution Jet Mixing Test Rig	62
4	Profile Generator	63
5	Jet Mixing Test Sections	64
6	Test Section Wall Statics and Thermocouples	65
7	Dilution Orifice Plate Configurations	66
8	Total Pressure, Thermocouple, and Static Pressure Rake	67
9	X-Y-Z Actuator with the Rake Mounted	68
10	Jet Mixing Rig as Viewed from Rig Discharge End	69
11	Typical Comparison Between Data from NASA/Aerojet and Present Investigation	70
12	Measured Theta Distributions for Test No. 1 with T_m = Constant, J = 5.74, S/D = 2, and H_o/D = 4.	71
13	Predicted Theta Distributions for Test No. 1 with T_m = Constant, J = 5.74, S/D = 2, and H_o/D = 4.	72
14	Measured Theta Distributions for Test No. 2 with T_m = Constant, J= 21.59, S/D = 2, and H_o/D = 4.	73
15	Predicted Theta Distributions for Test No. 2 with T_m = Constant, J = 21.59, S/D = 2, and H_o/D = 4.	74
16	Measured Theta Distributions for Test No. 3 with T_m = Constant, J = 6.14, S/D = 4, and H_o/D = 4.	75

LIST OF ILLUSTRATIONS (CONTD)

Figure	Title	Page
17	Predicted Theta Distributions for Test No. 3 with T_m = Constant, J= 6.14, S/D = 4, and H_o/D = 4.	76
18	Measured Theta Distributions for Test No. 4 with T_m = Constant, J = 26.7, S/D = 4, and H_o/D = 4.	77
19	Predicted Theta Distributions for Test No. 4 with T_m = Constant, J = 26.7, S/D = 4, and H_o/D = 4.	78
20	Measured Theta Distributions for Test No. 5 with T_m = Constant, J = 25.32, S/D = 2, and H_o/D = 8.	79
21	Predicted Theta Distributions for Test No. 5 with T_m = Constant, J = 25.32, S/D = 2, and H_o/D = 8.	80
22	Measured Theta Distributions for Test No. 6 with T_m = Constant, J = 107.8, S/D = 2, H_o/D = 8.	81
23	Predicted Theta Distributions for Test No. 6 with T_m = Constant, J = 107.8, S/D = 2, and H_o/D = 8.	82
24	Measured Theta Distributions for Test No. 7 with T_m = Constant, J = 26.3, S/D = 4, and H_o/D = 8.	83
25	Predicted Theta Distributions for Test No. 7 with T_m = Constant, J = 26.3, S/D = 4, and H_o/D = 8.	84
26	Measured Theta Distributions for Test No. 8 with T_m = Constant, J = 109.0, S/D = 4, and H_o/D = 8.	85
27	Predicted Theta Distributions for Test No. 8 with T_m = Constant, J = 109.0, S/D = 4, and H_o/D = 8.	86
28	Measured Theta Distributions for Test No. 9 with Hot Jets, J = 31.0, S/D = 2, and H_o/D = 4.	87

LIST OF ILLUSTRATIONS (CONTD)

Figure	Title	Page
29	Predicted Theta Distributions for Test No. 9 with Hot Jets, J = 31.0, S/D = 2, and H_o/D = 4.	88
30	Measured Theta Distributions for Test No. 10 with Hot Jets, J = 30.64, S/D = 4, and H_o/D = 4.	89
31	Predicted Theta Distributions for Test No. 10 with Hot Jets, J = 30.64, S/D = 4, and H_o/D = 4.	90
32	Measured Theta Distributions for Test No. 11 with Hot Jets, J = 30.19, S/D = 2, and H_o/D = 8.	91
33	Predicted Theta Distributions for Test No. 11 with Hot Jets, J = 30.19, S/D = 2, and H_o/D = 8.	92
34	Measured Theta Distributions for Test No. 12 with Hot Jets, J = 30.53, S/D = 4, and H_o/D = 8.	93
35	Predicted Theta Distributions for Test No. 12 with Hot Jets, J = 30.53, S/D = 4, and H_o/D = 8.	94
36	Profiled Mainstream Theta Distributions used in Series 2 Tests.	95
37	Measured Theta Distributions for Test No. 13 with Top Cold Profile, J = 22.63, S/D = 2, and H_o/D = 4.	96
38	Predicted Theta Distributions for Test No. 13 with Top Cold Profile, J = 22.63, S/D = 2, and H_o/D = 4	97
39	Measured Theta Distributions for Test No. 14 with Top Cold Profile, J = 7.5, S/D = 4, and H_o/D = 4.	98
40	Predicted Theta Distributions for Test No. 14 with Top Cold Profile, J = 7.5, S/D = 4, and H_o/D = 4.	99

LIST OF ILLUSTRATIONS (CONTD)

Figure	Title	Page
41	Measured Theta Distributions for Test No. 15 with Top Cold Profile, J = 109.9, S/D = 2, and H_o/D = 8.	100
42	Predicted Theta Distributions for Test No. 15 with Top Cold Profile, J = 109.9, S/D = 2, and H_o/D = 8.	101
43	Measured Theta Distributions for Test No. 16 with Top Cold Profile, J = 22.55, S/D = 4, and H_o/D = 8.	102
44	Predicted Theta Distributions for Test No. 16 with Top Cold Profile, J = 22.55, S/D = 4, and H_o/D = 8.	103
45	Measured Theta Distributions for Test No. 17 with Top Hot Profile, J = 22.14, S/D = 2, and H_o/D = 8.	104
46	Predicted Theta Distributions for Test No. 17 with Top Hot Profile, J = 22.14, S/D = 2, and H_o/D = 8.	105
47	Measured Theta Distributions for Test No. 18 with Top Hot Profile, J = 27.69, S/D = 4, and H_o/D = 8.	106
48	Predicted Theta Distributions for Test No. 18 with Top Hot Profile, J = 27.69, S/D = 4, and H_o/D = 8.	107
49	Measured Theta Distributions for Test No. 19 with Test Section II, J = 27.09, S/D = 4, and H_o/D = 8.	108
50	Predicted Theta Distributions for Test No. 19 with Test Section II, J = 27.09, S/D = 4, and H_o/D = 8.	109
51	Measured Theta Distributions for Test No. 20 with Test Section II, J = 102.5, S/D = 4, and H_o/D = 8.	110
52	Predicted Theta Distributions for Test No. 20 with Test Section II, J = 102.5, S/D = 4, and H_o/D = 8.	111

LIST OF ILLUSTRATIONS (CONTD)

Figure	Title	Page
53	Measured Theta Distributions for Test No. 21 with Test Section II, J = 6.76, S/D = 2, and H_o/D = 4.	112
54	Predicted Theta Distributions for Test No. 21 with Test Section II, J = 6.76, S/D = 2, and H_o/D = 4.	113
55	Measured Theta Distributions for Test No. 22 with Test Section II, J = 26.07, S/D = 2, and H_o/D = 4.	114
56	Predicted Theta Distributions for Test No. 22 with Test Section II, J = 26.07, S/D = 2, and H_o/D = 4.	115
57	Measured Theta Distributions for Test No. 23 with Test Section IV, J = 21.07, S/D = 4, and H_o/D = 8.	116
58	Predicted Theta Distributions for Test No. 23 with Test Section IV, J = 21.07, S/D = 4, and H_o/D = 8.	117
59	Measured Theta Distributions for Test No. 24 with Test Section IV, J = 85.84, S/D = 4, and H_o/D = 8.	118
60	Predicted Theta Distributions for Test No. 24 with Test Section IV, J = 85.84, S/D = 4, and H_o/D = 8.	119
61	Measured Theta Distributions for Test No. 25 with Test Section IV, J = 6.73, S/D = 4, and H_o/D = 8	120
62	Predicted Theta Distributions for Test No. 25 with Test Section IV, J = 6.73, S/D = 4, and H_o/D = 8.	121
63	Measured Theta Distributions for Test No. 26 with Test Section IV, J = 26.73, S/D = 2, and H_o/D = 4.	122
64	Predicted Theta Distributions for Test No. 26 with Test Section IV, J = 26.73, S/D = 2, and H_o/D = 4.	123

LIST OF ILLUSTRATIONS (CONTD)

Figure	Title	Page
65	Measured Theta Distributions for Test No. 27 with Test Section V, J = 27.13, S/D = 4, and H_o/D = 8.	124
66	Predicted Theta Distributions for Test No. 27 with Test Section V, J = 27.13, S/D = 4, and H_o/D = 8.	125
67	Measured Theta Distributions for Test No. 28 with Test Section V, J = 106.7, S/D = 4, and H_o/D = 8.	126
68	Predicted Theta Distributions for Test No. 28 with Test Section V, J = 106.7, S/D = 4, and H_o/D = 8.	127
69	Measured Theta Distributions for Test No. 29 with Test Section V, J = 7.07, S/D = 2, and H_o/D = 8.	128
70	Predicted Theta Distributions for Test No. 29 with Test Section V, J = 7.07, S/D = 2, and H_o/D = 8.	129
71	Measured Theta Distributions for Test No. 30 with Test Section V, J = 27.31, S/D = 2, and H_o/D = 4.	130
72	Predicted Theta Distributions for Test No. 30 with Test Section V, J = 27.31, S/D = 2, and H_o/D = 4.	131
73	Measured Theta Distributions for Test No. 31 with Test Section VI, J = 26.59, S/D = 4, and H_o/D = 8.	132
74	Predicted Theta Distributions for Test No. 31 with Test Section VI, J = 26.59, S/D = 4, and H_o/D = 8.	133
75	Measured Theta Distributions for Test No. 32 with Test Section VI, J = 107.8, S/D = 4, and H_o/D = 8.	134
76	Predicted Theta Distributions for Test No. 32 with Test Section VI, J = 107.8, S/D = 4, and H_o/D = 8.	135

LIST OF ILLUSTRATIONS (CONTD)

Figure	Title	Page
77	Measured Theta Distributions for Test No. 33 with Test Section VI, J = 7.05, S/D = 2, and H_o/D = 4.	136
78	Predicted Theta Distributions for Test No. 34 with Test Section VI, J = 7.05, S/D = 2, and H_o/D = 4.	137
79	Measured Theta Distributions for Test No. 34 with Test Section VI, J = 26.4, S/D = 2, and H_o/D = 4.	138
80	Predicted Theta Distributions for Test No. 34 with Test Section VI, J = 26.4, S/D = 2, and H_o/D = 4.	139
81	Measured Theta Distributions for Test No. 35 with Top Cold Profile, Test Section V, J = 26.82, S/D = 4, and H_o/D = 8.	140
82	Predicted Theta Distributions for Test No. 35 with Top Cold Profile, Test Section V, J = 26.82, S/D = 4, and H_o/D = 8.	141
83	Measured Theta Distributions for Test No. 36 with Top Cold Profile, Test Section V, J = 109.8, S/D = 4, and H_o/D = 8.	142
84	Predicted Theta Distributions for Test No. 36 with Top Cold Profile, Test Section V, J = 109.8, S/D = 4, and H_o/D = 8.	143
85	Measured Theta Distributions for Test No. 37 with Top Hot Profile, Test Section V, J = 8.51, S/D = 4, and H_o/D = 8.	144
86	Predicted Theta Distributions for Test No. 37 with Top Hot Profile, Test Section V, J = 8.51, S/D = 4, and H_o/D = 8.	145
87	Measured Theta Distributions for Test No. 38 with Top Hot Profile, Test Section V, J = 30.24, S/D = 4, and H_o/D = 8.	146
88	Predicted Theta Distributions for Test No. 38 with Top Hot Profile, Test Section V, J = 30.24, S/D = 4, and H_o/D = 8.	147

LIST OF TABLES

Table	Title	Page
I	Definition of Test Sections	8
II	Description of Dilution Orifice Plates	10
III	Series 1 Test Configurations and Flow Conditions	18
IV	Series 2 Test Configurations and Flow Conditions	28
V	Series 3 Test Configurations and Flow Conditions	34
VI	Series 4 Test Configurations and Flow Conditions	45

1.0 SUMMARY

The main objective of the NASA Dilution Jet Mixing Phase I Program was to quantify by means of parametric tests the effect of the following on the mixing of a row of jets with a confined cross-flow.

- Jet to mainstream density ratio
- Flow area convergence as encountered in transition sections
- Non-uniform mainstream profile upstream of dilution orifices.

The general conclusions derived from Phase I work are:

- Jet spreading rate in transverse direction is increased with increasing J, H/D and with decreasing S/D.
- The density ratio has only a second order effect on the jet mixing characteristics for a constant momentum ratio.
- The temperature distributions in the jet mixing region are strongly influenced by the undisturbed mainstream profile. Therefore, a superposition of the mainstream profile on the correlations for isothermal mainstream conditions yields good agreement with data.
- Flow area convergence enhances mixing in radial and transverse directions. An asymmetric convergent duct with flat wall injection has the same jet mixing characteristics as a symmetric convergent duct. An asymmetric convergent duct with slant wall injection has a faster jet spreading rate in the transverse direction.

2.0 INTRODUCTION AND OBJECTIVES

Advanced aircraft propulsion gas turbine engines for civil and military applications must provide increased power density usually expressed in terms of thrust or horsepower per unit airflow. Higher cycle pressure ratio and turbine inlet temperature (TIT) offer the greatest potential for increasing engine performance and reducing engine weight and size. However, because of the higher average TIT, the gas temperature distribution must be closely tailored for acceptable radial temperature profile and minimal peak gas temperature.

The combustor discharge temperature quality is influenced by nearly all aspects of the combustor design and in particular by the dilution zone. Due to increasing burner inlet air temperature and fuel/air ratio, an increasingly higher fraction of the combustor through-flow air is needed for combustion and cooling with correspondingly reduced airflow available for dilution purposes.

An improved understanding of dilution jet mixing processes will result in effective utilization of the available dilution air. The present program has been undertaken to acquire a data base of dilution jet mixing characteristics to develop empirical jet mixing correlations and validate combustor analytical design models.

The penetration and mixing of air jets directed into a cross-stream have been investigated by many researchers. Jet trajectory and mixing models have been developed both empirically and analytically. In the majority of the studies, the models are not directly applicable to flows in gas turbine combustion systems due to either an inappropriate range of flow conditions or unrealistic test geometries. In almost all cases, correlations have been derived using single jets discharging into a uniform cross-flow in relatively large ducts. In gas turbine combustion systems, a

number of dilution orifices in single or multiple rows normally inject the cooler air into relatively small annular ducts with non-uniform flow fields, resulting in jet interaction with adjacent jets and the liner walls. The availability of experimental data to extend current jet mixing models to account for these factors is limited, which results in only qualitative application of the models by combustion engineers in actual design practice.

The work reported in References 1 through 4 for multiple-jet injection into a confined cross-stream provided the basis for the program reported here. The nominal cross-flow test conditions in those studies were: U_m = 15 m/sec; T_∞ = 600°K with uniform temperature and velocity profiles. Dilution jet velocities (V_j) varied over the range of 25 m/sec to 85 m/sec with jets at an ambient temperature T_j = 300°K. The test conditions were established based primarily on jet to mainstream momentum ratio ($J = \rho_j V_j^2/\rho_m U_m^2$) variation from 6 to 60, with density-ratio (ρ_j/ρ_m) variation from 1.5 to 2.5.

Jet mixing correlations were developed (References 2 and 4) in terms of the momentum ratio and the following geometric variables:

o	$2 \leq S/D \leq 6$	D =	Dilution orifice diameter
o	$4 \leq H_o/D \leq 16$	H_o =	Channel height at injection plane
o	$0.25 \leq X/H_o \leq 2$	X =	Axial flow direction
o	$0 \leq Z/S \leq 0.5$	Z =	Lateral flow direction
		S =	Orifice spacing along the transverse direction

The main objective of the NASA Dilution Jet Mixing Phase I Program was to quantify the effect of the following factors on jet penetration and mixing:

- J, H_c/D, S/D, ρ_j/ρ_∞
- Non-uniform cross-stream temperature and velocity main profiles upstream of dilution orifices
- Cold versus hot jet injection
- Cross-stream flow area convergence (accelerating cross-stream) as encountered in practical dilution-zone geometries.

The experimental effort was divided into four series of tests:

Series 1 test objectives were to evaluate current data in relation to previous data and correlations at comparable conditions for jet mixing in a uniform cross-stream and to compare mixing characteristics of a cold jet injected into a hot stream versus a hot jet injected into a cold stream.

The effects of mainstream velocity and temperature profiles on jet mixing processes were investigated in Series 2 test. Two types of cross-stream temperature profiles were studied. A profile generator was used to inject a cooler stream near the jet injector wall with an increasing temperature profile away from the injection wall. A decreasing radial temperature profile was used in the second set of investigations.

Dilution zone geometric details, including flow area convergence rate and shape (symmetric or asymmetric convergence),

affect jet penetration and downstream radial profiles. The effect of mainstream acceleration on jet mixing behavior was studied in Series 3 tests. Both symmetric and asymmetric converging test sections were used in this test series.

Practical dilution zone designs include both flow convergence and profiled cross-stream. A limited study was done in Series 4 tests on quantifying the effect of flow convergence as well as cross-stream profile on jet spreading.

In addition to the four test series described above, limited model validation and correlation were done based upon the extension of the correlations developed by Holdeman and Walker (Reference 2).

3.0 TEST RIG AND FACILITY DESCRIPTIONS

3.1 Test Rig

A schematic layout of the jet mixing test rig is presented in Figure 2 and a partially assembled rig in Figure 3. The mainstream airflow is ducted from the test cell main air supply through a 15.24-cm internal diameter pipe. A transition section connects the inlet pipe to a rectangular cross section of constant width (30.48 cm) and adjustable height.

A perforated plate with 25 holes of 1.43-cm diameter provides a relatively uniform airstream upstream of the profile generator plenum. The profile generator duct incorporates an adjustable bottom wall to match the test section inlet height, which can vary from 10.16 cm to 15.24 cm.

A separate air supply enables the profile generator to provide the desired radial profile of temperature and velocity upstream of the jet-injection plane.

A third air supply allows the dilution injection orifices to vary jet velocity and density. A number of interchangeable dilution orifice plates and test section geometries were used to study confined jet mixing with the mainstream. To minimize the rig heat losses, the rig walls were insulated with a 2.54-cm thick layer of Kaolite insulation.

In addition to a traversing $P_t/P_s/T$ rake, as shown in Figure 2, the rig instrumentation includes a number of wall static pressure taps and flow thermocouples.

A brief description of the profile generator, test sections, and dilution orifice plates is provided in the following paragraphs.

3.1.1 Profile Generator

A profile generator (Figure 4) provides a desired radial profile in the mainstream. This is achieved by varying independently the flow conditions of the approaching mainstream and the flow injected from the profile generator. As shown in Figure 2, a separate air supply is used to vary the temperature and velocity of the air supplied to the profile generator slot, which is 2.54-cm high and 29.2-cm wide. The slot is fed uniformly through an inclined perforated plate having 50 orifices of 1.47-cm diameter; these orifices can be seen in Figure 4. The supply-air duct dumps the air into a rectangular plenum (or settling chamber) of 30.48 x 16.75 x 12.7-cm dimensions.

Three wall static pressure taps and one thermocouple were used to control the plenum air pressure and temperature levels, which, along with the main supply flow condition, control the mainstream radial profile.

3.1.2 Test Sections

In the present study, jet mixing was characterized for four different test sections, as pictured in Figure 5; their important dimensional parameters are summarized in Table I. Both constant-height and variable-height test sections were investigated.

Test Section I has a constant channel height (H_o = 10.16 cm) and slightly more than $2H_o$ length to allow radial profile measurements at X/H_o = 0.5, 0.75, 1.5, and 2.0.

TABLE I. DEFINITION OF TEST SECTIONS

ORIGINAL PAGE IS
OF POOR QUALITY

Test Section Number	Description	Test Section Height (cm)		Jet Injection Angle α (Degrees)	Test Section Convergence Rate $-\frac{dh}{dx}$
		Injection Plane	Exit Plane		
I	Constant Height	10.16	10.16	90.0	0
II	Symmetric Convergence	10.16	5.08	97.1	0.25
III	Symmetric Convergence	10.16	7.62	97.1	0.25
IV	Symmetric Convergence	10.16	5.08	104.0	0.50
V	Asymmetric Flat-Wall Injection	10.16	5.08	90.0	0.50
VI	Asymmetric Inclined-Wall Injection	10.16	5.08	116.6	0.50

The same piece of hardware was used for Test Sections II and III, which are symmetrically converging with a wall inclination angle equal to 7.1 degrees. Consequently, the jet injection angle is 97.1 degrees. The test section flow area convergence rate (defined as -dh/dx) is 0.25. Test Section II exit-plane height is 5.08 cm at $X = 2\ H_o$, and the corresponding injection to exit plane area ratio is 2.0. Test Section III is assumed to be 10.16-cm long with attendant exit-plane height of 7.62 cm and area ratio equal to 1.33.

ORIGINAL PAGE IS
OF POOR QUALITY

Test Section IV is symmetrically converging with a convergence rate of 0.5; the corresponding inclination angle is 14.0 degrees for both top and bottom walls. Therefore, the jet injection angle is 104 degrees. The test section injection to exit plane area ratio is 2.0.

Test Sections V and VI are asymmetric with a convergence rate equal to that of Test Section IV. The bottom wall of Test Section V is horizontal and the top wall inclination is 26.6 degrees with an attendant jet injection angle of 116.6 degrees. By turning Test Section V, the top wall becomes flat (horizontal) and the jet injection angle becomes 90 degrees.

It should be noted that all test sections have a 10.16-cm channel height at the injection plane. Consequently, the inlet channel heights of the test sections range between 10.16 and 15.24 cm. To match the test section height, the profile generator section height was adjusted by means of a moveable wall.

To insure well-controlled boundary layer profile at the injection plane, a boundary-layer trip (0.41-cm high and 0.33-cm wide) was welded to all four walls of the test sections. The trip is located 15.24 cm upstream of the jet injection plane.

A number of static pressure taps are installed on all four walls of the test sections. As delineated in Figure 6 for Test Section I, a total of 32 wall statics are used to measure static pressure distribution. Four thermocouples (two thermocouples extending from the top wall and two through the bottom wall) are used for monitoring the mainstream gas temperature levels. These thermocouples are immersed 1.27 and 3.81 cm from the bottom and top walls, respectively.

ORIGINAL PAGE IS
OF POOR QUALITY

3.1.3 Dilution Orifice Plate Geometry

Four circular orifice configurations, illustrated in Figure 7, were used on the present investigation. These plates are designated by 3-set numerals indicating aspect ratio, S/D, and H_o/D. The aspect ratio is unity for the circular orifices. Two orifice spacings (S/D = 2 and 4) were investigated. Similarly, two orifice sizes (D = 1.27 and 2.54 cm) were employed, producing H_o/D = 8 and 4, where H_o (test section height at the injection plane) is equal to 10.16 cm. Table II gives important dimensions of the four dilution orifice plates used in the present study.

TABLE II. DESCRIPTION OF DILUTION ORIFICE PLATES

Designation	Orifice Diameter, D (cm)	Number of Orifices	S/D	H_o/D	S/H_o
01/02/04	2.54	6	2	4	0.50
01/04/04	2.54	3	4	4	1.00
01/02/08	1.27	12	2	8	0.25
01/04/08	1.27	6	4	8	0.50

3.2 Test Facilities

The test rig was installed in the combustion test cell, C-100. Three air supplies were used for setting up the required flow conditions for the mainstream, profile generator, and dilution jets. Nonvitiated air from the laboratory compressors and heaters was used throughout the present investigation.

The mainstream air temperature can be regulated from ambient to 725°K. A special preheater is used for obtaining air temperatures above 750°K. For the majority of the test cases the mainstream nominal temperature and flow rate were 644°K and 0.25 kg/sec, respectively. For the test cases involving hot jet injection the mainstream nominal temperature and flow rate were 310°K and 0.56 kg/sec, respectively. The mainstream temperature was measured by thermocouples located at the test section entrance. A standard ASME orifice section installed in a 15-cm inside diameter pipe was used for measuring the mainstream airflow rate.

A second, separately controlled air supply was used for the profile generator, which can be installed in either the top or bottom walls of the test rig. The mainstream profile was adjusted by varying the pressure drop across the profile generator and the attendant airflow rate. The airflow rate was measured by an ASME orifice in a 7.62-cm inside diameter pipe.

A third air supply was used for controlling the dilution jet flow conditions, including jet velocity and temperature. For a majority of test cases, the dilution jet air was at ambient temperature and therefore no external heater was required. For hot jet injection, an external heater supplied a nominal dilution air temperature of 450°K. The dilution airflow rate was measured by an orifice section in accordance with standard ASME airflow measurement procedures.

4.0 DATA ACQUISITION AND REDUCTION

4.1 Data Acquisition

The dilution jet mixing characteristics were determined by measuring temperature and pressure distribution within the test section at different axial stations. A traversing probe, shown in Figure 8, was used for this purpose.

The probe consists of a 20-element thermocouple rake surrounded by 20 total-pressure sensors on one side and 20 static-pressure rakes on the other side. The nominal transverse spacing between the thermocouple rake and the total pressure rake is 5.08 mm; similarly, the spacing between the thermocouple and the static pressure elements is 5.08 mm.

The center-to-center height of the probe is 9.35 cm. The first element is therefore located 4.05 mm from the top wall of the constant-height test section, i.e., 0.16 D for a 2.54-cm dilution jet diameter. All the elements are equally spaced in the vertical direction, providing a nominal spacing of 4.92 mm.

The total-pressure sensor elements are made of Inconel tubes with an outside diameter of 0.16 cm and a wall thickness of 0.023 cm. The internal conical design of the tube at the inlet provides a ±15 degree flow insensitivity angle. The static pressure tubes, similar to the total pressure sensors, are dead-ended with four bleeding holes of 0.03-cm diameter 90 degrees apart and 0.7 cm from the tip. The total temperature sensors are type K thermocouple wires with insulated junctions encased in 0.10-cm inside diameter tubes, supported by 0.21 cm inside diameter enveloping tubes. The insulated junction tubes exposed to the air stream are 0.76-cm long. All the sensing elements have a straight length of 1.52 cm or more before the first bend to the probe core

where all tubes are inserted in a rectangular probe shield, 4.32 cm x 0.67 cm.

The probe is mounted on a traversing system (Figure 9) that allows travel in three directions. This system allows 30.48 cm traverse in the X-direction (mainstream flow direction) and 22.86 cm in the radial (Y) and lateral (Z) directions with an accuracy of ±0.015 percent. The flow field mapping in the Z direction is done over a distance equal to the hole spacing (S) for any given orifice plate. The measurements in the Z direction were made at the planes identified by Z/S = 0, 0.1, 0.2, 0.3, 0.4, 0.5, 0.6, 0.7, 0.8, 0.9, and 1.0, where Z/S = 0 denotes center of the orifice. The measurements in the X-direction were made at the planes X/H_o = 0.5, 0.75, 1.0, 1.5, and 2.0. The probe was traversed over a matrix of 11 x 5 survey locations.

The temperature and pressure values from the test rig instrumentation were recorded on magnetic tapes through a central computerized data acquisition system. An on-line data display system provided real-time information on selected raw data for monitoring the flow conditions. The raw data from the magnetic tape were later used for detail data reduction, analysis, and correlation.

4.2 Data Reduction

The rectangular grid network at which the measurements were made can be described with the aid of Figures 1 and 10. The X-axis is the axis along the length of the duct in the direction of the bulk flow. The X=0 station is located at the jet injection plane. The Y-axis (radial direction) is the direction along the jet injection direction. The Y=0 plane is located at the jet orifice exit plane. The Z-axis is in the cross-stream direction. The Z=0 plane is the vertical X, Y plane at a jet centerline. The

streamwise (X) and radial (Y) distances are nondimensionalized by H_o, the channel height at the jet injection plane. The lateral distance, Z, is nondimensionalized by S, the dilution orifice spacing.

The measured gas temperature distributions are presented in a nondimensionalized form as:

$$\theta(X, Y, Z) = \frac{T_m - T(X, Y, Z)}{T_m - T_j}$$

where,

T_m or TMAIN = Mainstream stagnation temperature

T_j or TJET = Jet stagnation temperature

T(X, Y, Z) = Stagnation temperature at the point (X, Y, Z) in the flow field.

θ is a measure of the temperature change due to the jet at any point (X, Y, Z) compared to the maximum possible temperature change. θ can vary from 0.0 to 1.0. $\theta = 0.0$ when the local temperature equals the mainstream temperature and $\theta = 1.0$ when the local temperature equals the jet temperature. When the jet and the mainstream are perfectly mixed, the local temperature reaches ideal equilibrium temperature, T_{EB}, given by

$$T_{EB} = \left(\frac{\dot{m}_\infty T_\infty + \dot{m}_j T_j}{\dot{m}_\infty + \dot{m}_j}\right)$$

The ideal equilibrium theta (θ_{EB} or THEB) is defined as

$$\theta_{EB} = \frac{T_m - T_{EB}}{T_m - T_j}$$

This parameter, θ_{EB}, provides a measure of the quality of the jet mixing. The arithmetic average temperature (T_{av}) at any X plane and the corresponding θ_{av} $\left(= \frac{T_m - T_{av}}{T_m - T_j}\right)$ are also presented with the reduced data to provide the information on the average value of the temperature field at that plane.

The measured θ values are presented in three-dimensional (isometric) plots at each X-station. The measured θ values are also presented in the form of isopleths for each X-station for the purpose of detailed comparison with correlations. These plots are presented over a 2S span in the Z direction by assuming symmetry of the θ distribution with respect to the midplane between two orifices. This assumption was invoked only for the purpose of improving the clarity of visual presentation of the temperature distribution. The accuracy of this assumption depends upon the uniformity of flow distribution across the jet orifices. Preliminary tests were performed to ensure that the jet mass flow was uniformly distributed over the entire orifice plate configuration. The isometric plots provide a convenient means of presenting the jet trajectory and mixing. Furthermore, a comparison of the data and correlations is presented in a two-dimensional (2-D) plot of θ versus Y/H_o along the jet centerplane at each of the X/H_o stations.

The pressure recordings from the probe rake were used to compute the velocity $\left(V(X,Y,Z)\right)$ at the point (X,Y,Z). An interpolation scheme was used to compute the total pressure (P_t) and static pressure (P_s) values at the point where probe thermocouples are located. From these total and static pressures, a nondimensionalized velocity, $V(X,Y,Z)/V_j$, was computed. V(X,Y,Z) is obtained from

$$V(X,Y,Z) = [2\left(P_t\ (X,Y,Z) - P_s\ (X,Y,Z)\right)/\rho(X,Y,Z)]^{1/2}$$

The jet velocity, V_j, is calculated from

ORIGINAL PAGE IS OF POOR QUALITY

$$V_j = 4\ \dot{m}_j\ /\ \left(\rho_j\ N\pi D^2\ C_D\right)$$

where D is the orifice diameter, N is the number of orifices, ρ_j is the jet density (P_j/RT_j), and C_D is the orifice discharge coefficient.

The orifice discharge coefficients were determined by measuring the pressure drop across the orifice plate (without crossflow) for a range of mass flow rates. The discharge coefficient, C_D, was obtained from the relation

$$\frac{\Delta P}{P} = 1.99\left[\frac{\dot{w}_c}{AC_D}\right]^2$$

where, $\dot{w}_c$ is the corrected flow rate in lbm/sec and A is the geometric area of the orifices in square inches.

$$\text{Note: } \dot{w}_c = \dot{w}_a\ \frac{\sqrt{\beta}}{\delta},\quad \beta = \frac{T(^\circ R)}{517},\ \text{and}\quad \delta = \frac{P(psi)}{14.696}$$

The velocity vector in the vicinity of the jet injection plane is predominantly in the radial direction. In such regions, the velocity values obtained from the rake probe are not expected to be accurate. For the sake of brevity, the measured velocity distributions are not presented in this report. However, tables of nondimensional velocity distribution, $V(X,Y,Z)/V_j$, will be provided for each test case in the Comprehensive Data Report (CDR) on this program.

An important parameter relevant to the jet description is the jet momentum ratio, J, defined as

$$J = \rho_j V_j^2 / (\rho_m V_m^2)$$

where

ρ_j = Jet density

ρ_m = Mainstream density = $P_m/(RT_m)$

V_j or VJET = Jet velocity at the orifice Vena Contracta

V_m or VMAIN = Mainstream Velocity = $\dot{m}_m/(P_m A_m)$

Other flow parameters of interest are:

Blowing rate, M or BLORAT = $\rho_j V_j / \rho_m V_m$

Temperature ratio, TRATIO = T_j/T_m

Density ratio, DENRATIO = ρ_j/ρ_m

Velocity ratio = V_j/V_m

The geometric parameters of importance associated with the orifice configuration are: S/D_j and H_o/D_j, where D_j is the effective jet diameter defined by

$$D_j = D\sqrt{C_D}$$

The quantities defined in this section define the geometric and flow conditions of each test and are reported along with the reduced data.

ORIGINAL PAGE IS
OF POOR QUALITY

5.0 EXPERIMENTAL DATA

5.1 Series 1 Tests

The purpose of this series was to investigate penetration, radial, and lateral mixing characteristics of cold and hot dilution jets with an isothermal, confined cross-flow in a constant channel height of 10.16 cm. The main objectives of this series were the following:

- o Comparison with the NASA/Aerojet data
- o Relative mixing characteristics of cold versus hot jet injection.

A total of 12 data sets were taken with the orifice geometrical description and nominal flow conditions listed in Table III. Tests 1 through 8 were repeats of the cases selected from the Aerojet study to demonstrate reproducibility of the jet mixing data from two different rigs. Typical comparison of data from Aerojet and the present investigation is presented in Figure 11 for the jet centerline plane at three axial stations

TABLE III. SERIES 1 TEST CONFIGURATIONS AND FLOW CONDITIONS

Test No.	Orifice Dia (D) (cm)	S/D	H_o/D	Mainstream Velocity VMAIN (m/sec)	Mainstream Temp. TMAIN (o_K)	Jet Velocity VJET (m/sec)	Jet Temp. TJET (o_K)	Momentum Ratio J	Density Ratio DENRATIO	Equilibrium Temp THEB	Region of Axial Direction (X/H_o)	Measurements in Transverse Direction Z/S
1	2.54	2.0	4.0	15.8	650	26.0	308	5.7	2.11	0.176	0.5 - 2.0	0.0 to 1.0
2	2.54	2.0	4.0	16.3	651	52.0	308	21.6	2.13	0.270	0.5 - 2.0	0.0 to 1.0
3	2.54	4.0	4.0	15.2	649	25.9	307	6.1	2.12	0.107	0.5 - 2.0	-0.5 to +0.5
4	2.54	4.0	4.0	14.9	651	52.2	304	26.7	2.17	0.191	0.5 - 2.0	-0.5 to +0.5
5	1.27	2.0	8.0	15.0	649	51.9	308	25.3	2.13	0.169	0.5 - 2.0	0.0 to 1.0
6	1.27	2.0	8.0	15.1	650	103.6	299	107.8	2.29	0.302	0.5 - 2.0	0.0 to 1.0
7	1.27	4.0	8.0	15.2	651	52.8	302	26.3	2.19	0.105	0.5 - 2.0	-0.5 to +0.5
8	1.27	4.0	8.0	15.1	649	104.1	299	109.0	2.30	0.181	0.5 - 2.0	-0.5 to +0.5
9	2.54	2.0	4.0	15.4	306	109.4	511	31.0	0.62	0.183	0.5 - 2.0	0.0 to 1.0
10	2.54	4.0	4.0	15.2	293	103.3	408	30.6	0.66	0.102	0.5 - 2.0	-0.5 to +0.5
11	1.27	2.0	8.0	15.2	290	102.2	445	30.2	0.67	0.102	0.5 - 2.0	-0.5 to +0.5
12	1.27	4.0	8.0	15.3	293	97.6	457	30.5	0.65	0.062	0.5 - 2.0	0.0 to 1.0

(X/H_o = 0.5, 1.0, and 2.0) for two values of jet momentum ratios (J = 6.1 and 26.7) with S/D = 4 and H_o/D = 4. The comparison, as shown for Tests 3 and 4, of data from two different rigs is quite good. Also shown in Figure 11 is the predicted radial profiles, using the NASA/Aerojet correlations.

The measured distribution of the nondimensionalized temperature, θ, for a momentum ratio (J) of 5.74 and uniform mainstream temperature, using the orifice plate 01/02/04 (S/D = 2, H_o/D = 4) is presented in Figure 12. The top part of this figure shows the isometric plot of the θ profiles at five axial planes of X/H_o = 0.5, 0.75, 1.0, 1.5, and 2.0. The geometrical and flow parameters of interest are provided at the top of this figure. The bottom part of the figure shows the measured θ contours for the corresponding axial planes. The contour values were selected to cover the range of θ values observed in the test. One of the contour values selected is also the value equal to θ_{EB}, which is 0.1759 in this case. The locations of jet centerline and jet direction are indicated by the arrows at the top of each contour plot and in the isometric plots.

The mixing performance for any given configuration can be estimated from the deviation of θ distribution about θ_{EB}. A small deviation from θ_{EB} characterizes nearly complete mixing of the jet and the mainstream. The θ_{EB} value for Test 1 is 0.1759, which corresponds to Contour 3. θ_{EB} contours are deformed by the penetration of the jets. This deformation is gradually smoothed out farther downstream. The location of the jet centerline can be identified from the location of the largest contour value. For Test 1, at X/H = 0.5, the jet centerline is inside Contour 9, which is at Y/H = 0.34.

The spreading of the jets in the transverse direction can be determined from the smoothness of the contour shapes. For this test, the presence of the individual jets can be seen at X/H = 0.5

and the jets quickly merge beyond X/H = 0.75. The locations of the theta contour in the radial direction are not significantly different as X/H_o increases beyond 1.0. From the θ profiles at X/H_o = 2.0 it can be seen that approximately the top half of the test section has an air temperature less than the equilibrium temperature, T_{EB}, whereas the bottom half has hotter gases. This indicates the jets have not penetrated the test section to the bottom wall.

The predicted theta distributions for Test 1 (J = 5.74, S/D = 2, H_o/D = 4) are presented in Figure 13. The predictions are obtained using NASA/Aerojet correlations. The top part of this figure shows the predicted theta contours while the bottom part provides a comparison between measured and predicted radial profiles of theta along the jet centerplane. Details of the NASA/Aerojet correlations are presented in Paragraph 6.1.

Although the predicted radial profiles are in good agreement with the measured theta profiles, significant differences in the theta contours can be observed. The predicted theta distributions for this test case underestimate the transverse spreading of the jets.

The measured theta distributions for Test 2 (J = 21.59, S/D = 2, H_o/D = 4) with uniform mainstream temperature (T_m) are presented in Figure 14. In this case, θ_{EB} is equal to 0.2705. The measurements show that for J = 21.59, the jet centerline at X/H_o = 0.5 is located at about Y/H = 0.6 compared to 0.34 for J = 5.7 (Figure 12). At X/H_o = 0.5, the two jets can be separately identified and they merge gradually as X/H_o increases. The variation in the radial penetration of the jets with increasing downstream distance is insignificant. As in Test 1, there is a top-cold and bottom-hot profile distribution.

The predicted theta distributions for Test 2 are portrayed in Figure 15. The agreement between the correlations and the data is good up to $X/H_o = 1.0$. Beyond this station, some differences in the profiles are seen.

The measured data for Test 3, with uniform T_m, J = 6.14, S/D = 4 and $H_o/D = 4$, are presented in Figure 16. In this test case, the jets are located farther apart than the first two tests and $\theta_{EB} = 0.1074$. For a constant value of J, H_o/D, the effect of S/D on the jet mixing characteristics can be inferred by comparing Figures 12 and 16. For S/D = 4, the data clearly shows the presence of two separate jets at all the axial stations. If the half-width values (from the contours) are used, it can be seen that the jets begin to merge only at $X/H_o = 2.0$, whereas Figure 12 shows that the merging is essentially complete at $X/H_o = 1.0$. Spreading of the contours in the radial direction is significantly higher in Test 3 than in Tests 1 and 2. This demonstrates that an increase in S/D results in improving the radial mixing and decreasing the lateral spreading rate.

The predicted theta values for Test 3 are portrayed in Figure 17. The NASA/Aerojet correlations slightly underpredict the jet penetration and overpredict the θ_{max} for this configuration.

The measured results for Test 4 with uniform T_m, J = 26.7, S/D = 4, and $H_o/D = 4$ are provided in Figure 18. For this test condition with $\theta_{EB} = 0.1915$, data reveals the jets are impinging on the opposing test section wall. The mixing in both the radial and transverse directions is substantially enhanced farther downstream as compared to Test 2 with S/D = 2 (Figure 14).

An optimum dilution orifice spacing is quite important to achieving the desired radial profiles. The profiles from Test 2

(Figure 14) and Test 4 (Figure 18) clearly illustrate this importance. The amount of dilution air in Test 2 is approximately twice that of Test 4. At the same values of orifice diameter and J, Test 2 provided a hub-peak (hot near the bottom wall) profile, whereas in Test 4 a tip-peak profile was achieved.

The predicted results for Test 4 are presented in Figure 19. Initially the correlations underpredict jet penetration, but farther down, jet impingement is predicted to occur between 1.0 and 1.5 H_o. The predicted radial profiles are in good agreement with the data at X/H = 2.0.

In the next four tests, the effects of H_o/D parameters on the mixing characteristics were studied. In these tests, the jet orifice diameter was reduced to 1.27 cm and the channel height was unchanged. The resultant value of H_o/D was 8.

The measured theta distributions for Test 5 with uniform T_m, J = 25.32, S/D = 2, and H_o/D = 8 are presented in Figure 20. This orifice plate (01/02/08) is characterized by 12 closely spaced, small holes (D = 1.27 cm) and a large duct height to diameter ratio. For this plate at a momentum ratio of 25.32, the data shows the jets have spread quickly in the transverse direction and no individual jet shapes can be identified even at X = 0.75 H_o. The gradual radial spreading of the contours demonstrates the slow radial jet spreading rate.

The predicted results for Test 5 are included in Figure 21. The predicted profiles are in good agreement with the data. The theta contour lines in both predicted and measured data are essentially horizontal, indicating the completeness of the mixing in the transverse direction. The predicted radial profiles are in very good agreement with the data in the entire mixing region of interest.

The data for Test 6 with uniform T_m, J = 107.8, S/D = 2, and H_o/D = 8 are depicted in Figure 22. As observed in the results for Test 5, the jet spreading in the transverse direction is nearly complete, even at X/H_o = 0.5 compared to 0.75 in the previous test with J = 25. The data shows that even for the high momentum ratio of 107.8, the jets do not impinge on the opposing wall. This results in bottom-hot profiles at all axial planes.

The predicted results for Test 6 are presented in Figure 23. The predicted profiles are in good agreement with the data up to X/H = 1.0. Beyond this station, the predictions show different trends compared to the data.

The measured data for Test 7 with uniform T_m, J = 26.3, S/D = 4, and H_o/D = 8 are portrayed in Figure 24. In this test, an orifice plate with six holes of 1.27-cm diameter was used. For this test condition, the data shows that at X/H = 0.5, the two jets are separately identifiable. The two jets spread in the transverse direction gradually as X/H_o increases. The gradual spreading of the contours in the radial direction with increasing X/H_o describes the radial mixing characteristics. The mixing characteristics for this orifice plate (01/04/08) are similar to that of orifice plate 01/02/04 (compare Figures 14 and 24) at the same momentum ratio, J.

The predicted results for Test 7 are presented in Figure 25. The predicted profiles are in good agreement with the data. With increasing hole spacing(S), the jet penetration is increased, as was shown previously for the 2.54-cm orifice diameter.

Figure 26 portrays the measured data for Test 8 with uniform T_m, J = 109.0, S/D = 4, and H_o/D = 8. For this momentum ratio, the data reveals that the jets impinge on the opposite wall at X/H_o = 0.5. The contour plots show significantly enhanced radial and transverse directions at stations farther downstream. It may be

recalled that for a comparable J value no impingement was observed with orifice plate 01/02/08, again indicating an increase in penetration with increasing S/D. The predicted results for Test 8 are presented in Figure 27. The predictions underestimate the jet penetration at X/H_o = 0.5 and 0.75. Jet impingement is predicted at X/H_o = 1.0, while the data shows jet impingement at X/H_o = 0.5. A similar trend was also observed for orifice plate 01/04/04.

The next four tests demonstrate the effect of density ratio. In these tests, a cold mainstream and hot jets were used. Tests were conducted with all four orifice plates and uniform mainstream temperature distribution.

Figure 28 portrays the measured data for Test 9 with heated jets at J = 31.0, S/D = 2, and H_o/D = 4. Comparison of these data with the results for cold jets at a comparable momentum ratio, J, and the same S/D and H_o/D (Figure 14) reveals very similar θ distributions.

The predicted results for Test 9 are presented in Figure 29. It is emphasized that the NASA/Aerojet correlations do not explicitly include the effects of density ratio since it was considered to be of second order in magnitude. However, the density ratio is taken into account in determining the nondimensional equilibrium temperature, θ_{EB}, which is used for predicting the theta distribution. Comparison between Figures 29 and 15 shows very nearly the same type of profiles. These comparisons reveal the effect of density ratio on the jet mixing characteristics is relatively weak.

Test 10 was performed with heated jets at J = 30.64, using orifice plate 01/04/04 (S/D = 4, H_o/D = 4). The measured theta distributions for Test 10 are depicted in Figure 30. For this case, jet impingement is observed at X/H_o = 1.0. At X/H_o = 0.5 and 0.75, the jets are separate. Beyond the point of impingement, an

enhanced mixing in radial as well as transverse direction is evident.

The predicted results for Test 10 are provided in Figure 31. The predicted profiles are in good agreement with the data. Comparison of this figure with Figure 19 shows that for a comparable momentum ratio, jet impingement on the opposite wall is observed with cold jets even at $X/H_o = 0.5$. However, the θ profiles for hot and cold jet cases are very similar.

Figure 32 shows the data for Test 11 with hot jets, J = 30.19, S/D = 2, and $H_o/D = 8$. The jet spreading in transverse direction is faster compared to that in the radial direction.

The predicted results for Test 11 are presented in Figure 33. The predicted θ profiles are in good agreement with the data although the predicted θ values are slightly higher than the measured values. Notwithstanding this difference, which is of second-order magnitude, the correlations show the same nature of jet mixing characteristics as the data. The data for this case are very similar to the characteristics for cold jet injection (Figure 20).

The measured theta distributions for Test 12 with heated jets, J = 30.53, S/D = 4, and $H_o/D = 8$ are presented in Figure 34. The data shows the presence of two individual jets at $X/H_o = 0.5$. The two jets mix well with each other rapidly, and at $X/H_o = 1.5$, the mixing is nearly complete, as indicated by nearly horizontal contour lines. The radial jet spreading rate is slower compared to that in the transverse direction.

The predicted results for Test 12 are presented in Figure 35. The predicted profiles have the same shape as the data, and the predicted θ values are slightly higher than the measured values. The θ distributions for heated jets are quite similar to that for

cold jets, indicating a weak influence of density ratio on jet mixing characteristics.

The first 12 tests presented thus far cover the Series 1 tests. In analyzing these tests, the parameter, orifice spacing (S) to duct height (H) ratio, S/H, was considered only implicitly. For the orifice plate 01/02/08, S/H = 0.25, while S/H = 0.5 for orifice plates 01/02/04 and 01/04/08 and S/H = 1.0 for orifice plate 01/04/04. From the results presented in this paragraph (5.1), it is seen that the transverse or lateral mixing is enhanced as S/H decreases. Furthermore, the jet penetration is increased with increasing value of S/H. As reported in Reference 2, the coupling of J and S/H parameters is thus an important criterion for describing the jet penetration and mixing characteristics.

5.1.1 Conclusions for Series 1 Tests

The Series 1 tests were conducted with constant duct height and uniform cross-flow temperature distribution. Four different orifice plate geometries were used to study the jet mixing characteristics. From these test data, the following conclusions are made:

- A good agreement between the present data and previous data and correlations (References 1 through 4) has been obtained.

- The jet penetration distance (Y_c/H_o) increases with increasing momentum ratio (J) and orifice diameter (D).

- For a given duct height to diameter ratio (H_o/D), the lateral mixing, that is, the jet spreading rate in the transverse direction, is enhanced with increasing

momentum ratio, J, and decreasing spacing to diameter ratio, S/D.

- For a given S/D, the lateral mixing is increased with increasing J and H_o/D.

- The radial mixing, that is, the jet spreading rate in the vertical direction, is enhanced with increased jet penetration. This is highlighted in the case of jet impingement on the opposite wall.

- The penetration of a hot jet in a cold cross-flow is very similar to that of a cold jet in a hot cross-flow at constant J. Although the hot jet penetration is slightly smaller (less than 5 percent) than the cold jet penetration at $X/H_o = 0.5$, the differences are minimal farther downstream. The density ratio effects are, at best, of second-order magnitude and can be neglected for a first-order approximation, provided the momentum ratio values, J, are the same.

- The NASA/Aerojet correlations are accurate to first order and provide a useful tool for predicting the jet thermal centerline trajectory and temperature profiles. The temperature profiles are well described by the correlations except very close to the jet injection plane, especially when jet impingement occurs.

5.2 Series 2 Tests

The objective of this series of tests was to investigate the interaction of the jets with a non-uniform cross-flow temperature distribution in a constant area duct. A non-uniform mainstream temperature profile is generated by using the profile generator as

ORIGINAL PAGE IS
OF POOR QUALITY

described in Section 3.0. Six tests were conducted in Series 2 with orifice geometries and nominal flow conditions as listed in Table IV.

TABLE IV. SERIES 2 TEST CONFIGURATIONS AND FLOW CONDITIONS

Test No.	Orifice Dia (D) (cm)	S/D	H_o/D	Mainstream Velocity VMAIN (m/sec)	Mainstream Temp. TMAIN (o_K)	Jet Velocity VJET (m/sec)	Jet Temp. TJET (o_K)	Momentum Ratio J	Density Ratio DENRATIO	Equilibrium Temp THEB	Region of Axial Direction (X/H_o)	Measurements in Transverse Direction Z/S
13	2.54	2.0	4.0	16.9	524	59.7	394	22.6	1.81	0.312	0.5 - 2.0	0.0 to 1.0
14	2.54	4.0	4.0	15.4	672	28.4	305	7.5	2.21	0.114	0.5 - 2.0	-0.5 to +0.5
15	1.27	2.0	8.0	15.5	616	109.3	297	109.9	2.07	0.303	0.5 - 2.0	-0.5 to +0.5
16	1.27	4.0	8.0	18.1	567	63.0	311	22.6	1.86	0.100	0.5 - 2.0	0.0 to 1.0
17	2.54	2.0	4.0	16.5	538	57.9	303	22.1	1.80	0.305	0.5 - 2.0	0.0 to 1.0
18	1.27	4.0	8.0	18.2	545	72.2	317	27.7	1.76	0.107	0.5 - 2.0	-0.5 to +0.5

Tests 13 through 16 were conducted with the mainstream temperature profile cold near the jet exit plane (top) and hot at the bottom of the duct. These test conditions are referred to as "top cold".

Tests 17 and 18 were conducted with an inverted temperature profile: hot at the top and cold at the bottom. These two test conditions are identified as "top hot".

The temperature profiles used for these six tests are depicted in Figure 36, in a nondimensionalized form, θ_p:

$$\theta_p(y) = \frac{T_{max} - T_p(y)}{T_{max} - T_j}$$

where

T_{max} = Maximum value of the profiled mainstream stagnation temperature

T_p (y) = Local value of the mainstream stagnation temperature upstream of the jet injection plane.

T_j = Jet stagnation temperature.

The nondimensionalized temperature variable, θ, represents the ratio of the actual temperature change due to the dilution jets to the maximum possible temperature change for any given flow condition. Consequently, the value of θ will always be between 0 and 1. For Series 2 tests, the maximum possible temperature change is $(T_{max} - T_j)$. Thus, the definition of θ is modified for the tests with profiled mainstream as

$$\theta = \frac{(T_{max} - T)}{(T_{max} - T_j)}$$

where T is the local temperature in the mixing region. To be consistent with this definition of theta, the NASA/Aerojet correlations were also modified. Details of the modifications are included in Paragraph 6.1.

The measured theta distributions for Test 13 with top cold profile, J = 22.63, ℓ/D = 2, and H_o/D = 4 are presented in Figure 37. An extent of the radial and lateral jet spreading rates can be obtained from the distortion and spreading of the contours.

For Test 13, at X/H_o = 0.5, two distinct jets can be associated with the dip in the contours around the jet injection locations. However, at X/H_o = 1.0 and farther downstream, the contour lines tend towards a horizontal line, indicating a tendency towards complete lateral mixing. It is also interesting to note that once the contour lines become nearly horizontal, the spreading in the radial direction is enhanced.

Figure 38 portrays the predicted theta distributions for Test 13. The predicted results were obtained by superposing the mainstream theta profile, $\theta_p(Y)$, on the NASA/Aerojet correlations

for uniform mainstream temperature. Detailed descriptions of these correlations are provided in Paragraph 6.1. The predicted theta profiles are not in good agreement with the data, although they show the same qualitative profiles. This suggests that the superposition method is perhaps valid if a suitable scaling parameter is employed for the profiled mainstream theta, $\theta_p(Y)$.

The measured theta distributions for Test 14 with top cold profile, J = 7.5, S/D = 4, and H/D = 4 are presented in Figure 39. In these figures, the modulation of the θ contours around the location of the jets is evident. Comparison of these figures with those in Figure 37 shows a substantial reduction in both lateral and radial mixing. This is largely due to the lower J value and a higher S/H_o ratio.

The predicted theta distributions for Test 14 are presented in Figure 40. The predicted profiles seem to overestimate the lateral mixing, while the jet centerplane radial profiles are in qualitative agreement with the measured profiles. It is also interesting to note that the major part of the differences between the data and correlations is in the region where the profiled mainstream temperature is cold (near the top for this test case).

The data for Test 15 are depicted in Figure 41. This test was conducted with top cold profile, J = 109.9, S/D = 2, and H_o/D = 8. The θ contours are nearly flat, even at X/H_o = 0.5, indicating a high lateral mixing. The gradual movement of the contour locations toward the top wall provides an idea of the relatively slow jet spreading rate in the radial direction. The dominance of the mainstream profile is clearly seen in the isometric plots.

The predicted results for Test 15 are portrayed in Figure 42. The predicted contours are horizontal lines, indicating the high lateral mixing rate. The radial profiles between the data and correlations are again in qualitative agreement.

Figure 43 depicts the measured theta distributions for Test 16, with top cold profile, J = 22.55, S/D = 4, and H_o/D = 8. At X/H_o = 0.5, the θ contours are modulated by the jet and these distortions are gradually smoothed out farther downstream. The spread of the contours in the radial direction is gradual, indicating a slow radial mixing rate.

The predicted results for Test 16 are presented in Figure 44. The radial profiles are in good agreement near the bottom and in qualitative agreement near the top. This trend was also noted in Tests 13 through 15.

The next two tests were conducted with an inverted mainstream temperature profile, namely, hot at the top and cold at the bottom. Figure 45 portrays the measured results for Test 17 with top hot mainstream temperature profile, J = 22.14, S/D = 2, and H_o/D = 4. The isometric plots show the dominance of the profiled mainstream. At X/H_o = 0.5, the distortion of the θ contours around the jet injection indicates the extent of jet penetration. These distortions are smoothed out at X/H_o = 1.5. The radial mixing characteristics are seen from the relatively rapid changes in the contour locations in the radial direction.

Figure 46 portrays the predicted theta distributions for Test 17. The predicted profiles are in good agreement with the data, especially at X/H_o = 0.5. It is also interesting to note that the differences in the profiles between data and correlations are more pronounced in the colder part of the duct (near the bottom in this test case).

The measured theta distributions for Test 18 with top hot mainstream temperature profile, J = 27.69, S/D = 4, and H_o/D = 8 are presented in Figure 47. As observed in the previous test case,

the lateral mixing appears to be rapid. The dominance of the profiled mainstream on the theta distribution throughout the mixing region is seen clearly in the isometric plots.

Figure 48 presents the predicted theta distributions for Test 18. The predicted profiles are in good agreement with the measurements, especially at stations closer to the jet injection plane (X/H_o = 0.5 - 1.0).

5.2.1 Conclusions for Series 2 Tests

Series 2 tests consisted of six tests with constant height duct and profiled mainstream temperature distribution. The mainstream temperature profiles employed included both top cold and top hot profiles. Four orifice plate configurations were used to study the jet mixing characteristics. The following conclusions are made from these tests:

- A new definition for nondimensional temperature, θ, is needed for analyzing the jet mixing characteristics.

- The jet spreading characteristics with profiled mainstream are very similar to those with uniform mainstream temperature profile.

- The radial temperature profiles in the mixing region are strongly influenced by the mainstream profiles upstream of the jet injection plane.

- The superposition procedure used for modifying the NASA/Aerojet correlations is reasonably good. This is seen from the good qualitative agreement between the data and correlations. Some of the differences in the

agreements may be due to the distortion of the mainstream temperature profile downstream of the jet injection plane. These differences between correlations and data can be reduced by using an appropriate scaling parameter on the superposition scheme employed.

5.3 Series 3 Tests

The objective of the Series 3 tests was to investigate the penetration and mixing characteristics of cold dilution jets injected into an isothermal cross-flow in a converging duct. These tests can be divided into two segments based upon the geometry of the convergent ducts:

- Symmetric convergence (Test Sections II and IV)
- Asymmetric convergence (Test Sections V and VI)

For each of the test sections, two orifice plates (01/02/04 and 01/04/08) were used, and two momentum ratios were selected for each orifice plate. A total of 16 tests were performed in Series 3 with orifice geometrical description and nominal flow conditions as listed in Table V. Tests 19 through 26 were conducted with symmetrical convergence, and Tests 27 through 34 were conducted with an asymmetrically convergent test section. All the convergent test sections used in these tests (shown in Figure 5) have the same area ratio, $A_o/A_{min} = 2$, where A_o is the duct area at the jet injection plane and A_{min} is the minimum area of the duct. The results for symmetric convergence are presented in Paragraph 5.3.1 and for asymmetric convergence in Paragraph 5.3.2.

5.3.1 Symmetric Convergence Test Sections

The two symmetric convergence test sections used in these tests were Test Sections II and IV. (See Figure 5.) Uniform

ORIGINAL PAGE IS
OF POOR QUALITY

TABLE V. SERIES 3 TEST CONFIGURATIONS AND FLOW CONDITIONS

Test No.	Orifice Dia (D) (cm)	S/D	H_o/D	Mainstream Velocity VMAIN (m/sec)	Mainstream Temp. TMAIN (o_K)	Jet Velocity VJET (m/sec)	Jet Temp. TJET (o_K)	Momentum Ratio J	Density Ratio DENRATIO	Equilibrium Temp THEB	Region of Axial Direction (X/H_o)	Measurements in Transverse Direction Z/S
19	1.27	4.0	8.0	15.9	656	5[illegible].1	330	27.1	2.02	0.106	0.25 to 2.0	0.0 to 1.0
20	1.27	4.0	8.0	15.5	645	106.4	314	102.5	2.19	0.188	0.25 to 2.0	0.0 to 1.0
21	2.54	2.0	4.0	15.8	654	28.1	308	6.7	2.13	0.197	0.50 to 2.0	0.0 to 1.0
22	2.54	2.0	4.0	15.8	654	54.5	304	26.1	2.18	0.307	0.50 to 2.0	0.0 to 1.0
23	1.27	4.0	8.0	17.0	646	[illegible]	312	21.1	2.10	0.097	0.25 to 1.0	-0.5 to +0.5
24	1.27	4.0	8.0	16.9	643	105.1	311	85.8	2.07	0.178	0.25 to 1.0	-0.5 to +0.5
25	2.54	2.0	4.0	15.1	[illegible]	27.7	322	6.7	2.00	0.183	0.50 to 1.0	0.0 to 1.0
26	1.27	4.0	8.0	14.9	641	55.1	330	26.7	1.96	0.299	0.50 to 1.0	0.0 to 1.0
27	1.27	4.0	8.0	16.1	646	58.[illegible]	320	27.2	2.05	0.107	0.25 to 1.0	0.0 to 1.0
28	1.27	4.0	8.0	16.0	645	112.[illegible]	319	106.7	2.02	0.189	0.25 to 1.0	0.0 to 1.0
29	2.54	2.0	4.0	15.7	645	29.1	314	7.1	2.06	0.198	0.50 to 1.0	-0.5 to +0.5
30	2.54	2.0	4.0	15.6	646	56.4	314	27.3	2.09	0.315	0.50 to 1.0	-0.5 to +0.5
31	1.27	4.0	8.0	16.4	649	58.6	320	26.6	2.07	0.107	0.25 to 1.0	-0.5 to +0.5
32	1.27	4.0	8.0	16.5	[illegible]	116.0	321	107.8	2.18	0.189	0.25 to 1.0	-0.5 to +0.5
33	1.27	2.0	4.0	16.3	[illegible]	29.5	301	7.1	2.17	0.197	0.50 to 1.0	-0.5 to +0.5
34	2.54	2.0	4.0	16.2	651	55.9	297	26.4	2.23	0.314	0.50 to 1.0	-0.5 to +0.5

mainstream temperature and velocity profiles were generated at the jet injection plane. All these test sections have a duct height (H_o) of 10.16 cm at the jet injection plane.

Test Section II is a symmetrically convergent duct with channel height reduction from 10.16 cm (4 in.) to 5.08 cm (2 in.) over a length of 20.32 cm (8 in.). Test Section IV has a channel height reduction from 10.16 cm (4 in.) to 5.08 cm (2 in.) over a length of 10.16 cm (4 in.).

Since the Series 3 tests were performed with uniform mainstream temperature profiles, the definition of theta needed for analyzing these data is identical to those used in Series 1, namely,

$$\theta = \frac{T_m - T}{T_m - T_j}$$

where

T_m = Mainstream stagnation temperature
T = Local stagnation temperature
T_j = Jet stagnation temperature

The measured theta distributions for Test 19 with Test Section II, J = 27.09, S/D = 4, and H_o/D = 8 are portrayed in Figure 49. For Test Section II, the jet injection angle is 97.1 degrees and measurements were made at four axial planes. For orifice plate 01/04/08, the measurements were taken at X/H_o = 0.25, 0.5, 1.0, and 2.0. Figure 49 shows the presence of two distinct jets at X/H_o = 0.25 and 0.5. At X/H_o = 1.0, the two jets begin to diffuse with each other and at X/H_o = 2, the contour lines are almost horizontal, indicating nearly complete mixing in the lateral direction.

Comparison of Figures 49 and 24 reveals the effect of convergence on the jet mixing characteristics. These two figures correspond to the same orifice configuration at a comparable momentum ratio. For both cases, the jet centerline is located at about 50 percent of local channel height at X/H_o = 0.5 and 1.0. The jet spreading rate in the radial direction is significantly faster in the convergent duct than in the constant area duct. The jet spreading rates in the transverse direction for the two cases are nearly the same.

The predicted theta distributions for Test 19 were obtained by modifying the NASA/Aerojet correlations for a convergent duct. In a convergent duct, the local mainstream velocity, $V_m(X)$, increases with X according to the relation

$$\frac{V_m(X)}{V_o} = \frac{A_o}{A(X)}$$

where A_o is the duct cross-sectional area at the jet injection plane, A(X) is the local duct cross-sectional area, and V_o is the mainstream velocity at the jet injection plane. For low Mach numbers, the density variation with X can be neglected. Thus, the equivalent momentum ratio at any axial station can be expressed as:

$$J_{eq} = \frac{\rho_j V_j^2}{\rho_m V_m^2(X)} = \frac{\rho_j V_j^2}{\rho_m V_o^2} \frac{V_o^2}{V_m^2(X)}$$

Thus,

$$J_{eq} = J_o \left(\frac{A(X)}{A_o}\right)^2$$

where J_o is the momentum ratio at the jet injection plane. Predictions for convergent ducts were obtained by using the equivalent momentum ratio, J_{eq}, in the NASA/Aerojet correlations. These results are presented in Figure 50 for Test 19. The predicted radial theta profiles are in very good agreement with the data at X/H_o = 0.25 and 0.5. The agreement between data and correlations is qualitatively good at X/H_o = 1.0 and X/H_o = 2.0. The accelerating flow in the convergent duct enhances mixing in radial and transverse directions. Although the correlations correctly predict the jet penetrations, the enhanced mixing due to convergence is not properly taken into account.

Figure 51 illustrates the measured theta distributions for Test 20 with Test Section II, J = 102.5, S/D = 4, and H_o/D = 8. For this condition, the jets impinge on the opposite wall even at X/H_o = 0.25, followed by a rapid mixing in the transverse direction. The theta distributions for this case are similar in characteristics to those with constant area duct. (See Figure 26.)

The predicted results for Test 20 are presented in Figure 52. The predicted profiles are in very good agreement with the data at

X/H_o = 1.0 and 2.0. In regions closer to the jet injection plane, the jet penetration is underpredicted. It is recalled that even in Series 1 test cases, the NASA/Aerojet correlations underpredicted the jet penetrations for high momentum ratios.

The measured theta distributions for Test 21 are shown in Figure 53. Test 21 was performed with Test Section II, J = 6.7, S/D = 2, and H_o/D = 4. For this orifice plate, measurements were taken at X/H_o = 0.5, 0.75, 1.0, and 2.0. At the momentum ratio of 6.76, the jets penetrate to about Y/H = 0.4 at X/H_o = 0.5 and gradually diffuse in radial and transverse directions. The radial mixing rates in this case are slightly faster than that with uniform duct height at the same momentum ratio. (See Figure 12.)

The predicted results for Test 21 are presented in Figure 54. The predicted theta profiles are in good agreement with the data at X/H_o = 0.5. Beyond this station, the predicted theta values are slightly larger, but the shapes of the θ profiles are correctly predicted.

The measured theta distributions for Test 22 with Test Section II, J = 26.07, S/D = 2, and H_o/D = 4 are illustrated in Figure 55. For this momentum ratio, the jet penetration is about 60 percent of the local duct height at X/H_o = 0.5, the jets gradually diffuse deeper, and at X/H_o = 2.0, the jet centerline is located near Y/H = 1.0.

The predicted theta values for Test 22 are portrayed in Figure 56. The predicted radial profiles are in good agreement with the data, especially in regions close to the jet injection plane. The predicted theta values are slightly higher than the measured values although the profile shapes are correctly predicted.

The next four test cases correspond to the measurements taken with Test Section IV. The measured theta distribution with Test

Section IV, J = 21.07, S/D = 4, and H_o/D = 8 are presented in Figure 57. At X = 0.25, two separate jets are observed which rapidly diffuse in the lateral direction. For Test Section IV, the jets are injected at an angle of 104 degrees. The upstream component of the jet momentum tends to enhance the mixing in both radial and transverse directions.

Comparison of Figures 57 and 49 shows the effects of different convergence rates. For Test Section IV, at X/H_o = 1, the area ratio, A_o/A, is 2.0. For Test Section II, at X/H_o = 1, the area ratio, A_o/A, is 1.33. With increasing convergence rate (area ratio), jet penetration is also increased. Furthermore, the lateral jet spreading rate is increased with increasing area ratio.

The predicted results for Test 23 are presented in Figure 58. The predicted distributions are at best in qualitative agreement with the data. The correlations underpredict the jet penetration. Some of these differences are due tc the effects of jet injection angle, which are neglected in the correlations. Furthermore, the predicted theta values are slightly higher than the measured values.

The measured theta distributions for Test 24 with Test Section IV, J = 85.84, S/D = 4, and H_o/D = 8 are presented in Figure 59. For this momentum ratio, the jets impinge on the opposite wall, followed by an enhanced lateral mixing. Figure 60 illustrates the predicted theta profiles for Test 24. The predicted profiles are in poor agreement with the data. The correlations underpredict the jet penetration.

The measured theta values for Test 25 with Test Section IV, J = 6.73, S/D = 2, and H_o/D = 4 are shown in Figure 61. For the low momentum ratio of 6.73, the jets penetrate up to about 40 percent of the local channel height. The mixing in the transverse direction

is very slow, as evidenced by the contour shapes. The predicted results for Test 25 are portrayed in Figure 62. For this case, the correlations overpredict the penetration and the predicted theta values are significantly higher than the measured values.

Comparison of Figures 61 and 53 shows that the mixing characteristics for Test Section IV are very similar to that of Test Section II.

The data for Test 26 with Test Section IV, J = 26.73, S/D = 2, and H_o/D = 4 are illustrated in Figure 63. In this case, the jets penetrate up to about 65 percent of the channel height at X/H_o = 0.5 and gradually reach the bottom wall at X/H_o = 1.0. The individual jet contours are clearly seen until the jet centerline reaches the opposing wall. The predicted results for Test 26 are presented in Figure 64. The predicted profiles are in good qualitative agreement with the data. The predicted theta values are higher in magnitude compared to the measured theta values. The jet mixing characteristics for this case are very similar to those with Test Section II. (See Figure 55.)

5.3.2 Asymmetric Convergence Test Sections

The following eight tests (Tests 27 through 34) were performed with asymmetric Test Sections V and VI. Test Section V is a duct with rectangular cross-section with a flat wall on one side and a slant wall on the opposite side, such that the channel height reduces from 10.16 cm (4 in.) to 5.08 cm (2 in.) over a length of 10.16 cm (4 in.). The jets are injected from the flat wall (jet injection angle is 90 degrees).

Test Section VI has the same geometry as Test Section V, but the jets are injected from the slant wall. The geometry of the test sections is illustrated in Figure 5.

The tests with asymmetric converging ducts were performed with orifice plates 01/02/04 and 01/04/08, with two momentum ratios for each orifice plate as listed in Table V. Measurements were made at X/H_o = 0.25, 0.5, and 1.0 with orifice plate 01/04/08 and at X/H_o = 0.5, 0.75, and 1.0 with orifice plate 01/02/04.

The measured theta distributions with Test Section V, J = 27.18, S/D = 4, and H_o/D = 8 are portrayed in Figure 65. At X/H_o = 0.25, the jet centerline penetration is at about Y/H = 0.5 and the jet gradually penetrates farther with increasing X/H_o, but does not reach the opposite wall.

Figures 57 and 65 provide a comparison between the jet mixing characteristics for symmetric convergence and asymmetric convergence with flat wall injection. These two figures show nearly the same theta distribution at all X/H_o locations. This suggests that the jet mixing characteristics for flat wall injection are almost identical to that in a symmetrically convergent duct at the same orifice and flow conditions.

The predicted results for Test 27 are presented in Figure 66. The predicted profiles are in very good agreement with the data except at X/H_o = 1.0. The theta values predicted are slightly higher than the measured values at most of the axial stations.

The measured theta values for Test 28 with Test Section V, J = 106.7, S/D = 4, and H_o/D = 8 are presented in Figure 67. For this momentum ratio, the jets impinge on the opposite wall at X/H_o = 0.25. The jets mix rapidly in both radial and transverse directions. The jets merge with each other at X/H_o = 0.5. The predicted results for Test 28 are shown in Figure 68. The predicted theta radial profiles are in good agreement with the data.

In this test case, measurements were made only up to Y/H = 0.75 at X/H_o = 0.25. However, the contour plots for these cases were obtained by using extrapolated values beyond that region. The extrapolated values were obtained by using a cubic spline

curve fit. This was done only for the purpose of clarity in presenting the data.

Comparison of Figures 67 and 59 shows that the asymmetric convergence with flat wall injection has the same theta distribution as the symmetric convergence with the same area reduction.

The test results for Test 29 with Test Section V, J = 7.07, S/D = 2, and H_o/D = 4 are illustrated in Figure 69. At this low momentum ratio, the jets remain separate as far downstream as X/H_o = 1.0. The radial and lateral mixing rates are quite slow as evidenced by the shape and size of the contours. The predicted results for Test 29 are presented in Figure 70. The predicted radial profiles are in qualitative agreement with the data, and the predicted theta values are significantly higher than the measured values. This trend has been observed for most of the Series 3 tests. Furthermore, the predicted jet penetrations are slightly deeper than that seen from the test data for this case. The theta distributions for this test case are very similar to those with symmetric convergence. (See Figures 61 and 69.)

The measured theta values for Test 30 with Test Section V, J = 27.31, S/D = 2, and H_o/D = 4 are presented in Figure 71. At X/H_o = 0.5, the jets penetrate up to about 65 percent of local channel height and they gradually reach the opposite (slant) wall at X/H_o = 1. The jet spreading rate in the radial direction appears to be faster than that in the transverse direction. The predicted theta distributions for Test 30 are portrayed in Figure 72. For this test condition, the predicted and the measured radial profiles are in good agreement at X/H_o = 0.5 and are in only qualitative agreement farther downstream. As observed in the other test cases in Series 3, the predicted theta values are slightly higher than the measured values. Figures 71 and 72 show distributions very similar to those in Figures 63 and 64. This re-emphasizes the similarity in the jet mixing characteristics of Test Sections IV and V.

The following four test cases were taken with Test Section VI, where the dilution jets were injected from the slant test section wall. The jet injection angle for these cases is 106.6 degrees. The jets are injected in the upstream direction, and are expected to alter the mixing characteristics compared to the 90-degree injection case associated with Test Section V. Comparison of the data for these two test sections provides information about the mixing characteristics at two different injection angles with asymmetric convergence.

The measured theta distributions for Test 31 with Test Section VI, J = 26.59, S/D = 4, and H_o/D = 8 are given in Figure 73. At X/H_o = 0.25, the jet penetration is at about 60 percent of local duct height and the penetration gradually increases farther downstream. The lateral mixing is significantly higher for this test section compared to that with Test Section V. (See Figure 65.) This is primarily due to the upstream injection.

The predicted theta distributions for Test 31 are portrayed in Figure 74. The correlations underpredict the jet penetration and overestimate the theta values compared to the measurements. The correlations do not properly account for the effects of the jet injection angle, which is primarily responsible for the poor agreement with the data.

Comparison of Figures 74 and 66 reveals that the correlations predict the profiles more accurately for flat wall injection than for slant side injection. Furthermore, it is seen that the jet penetration with slant side injection is deeper than that with flat wall injection.

The measured data for Test 32 with Test Section VI, J = 107.8, S/D = 4, and H_o/D = 8 are illustrated in Figure 75. For this momentum ratio, the jets impinge on the opposite (flat) wall. A comparison of Figure 75 with Figure 67 for flat wall injection

at a comparable momentum ratio shows that with the slant wall injection, the jet spreading rate in the transverse direction is significantly faster, while the radial jet spreading rates are nearly the same. The predicted results for Test 32 are illustrated in Figure 76. The correlations underpredict the penetration at X/H_o = 0.25 and 0.5, and the agreement between data and correlations is poor. At X/H_o = 1.0, the agreement between the two centerplane profiles is very good.

Figure 77 illustrates the data for Test 33, with Test Section VI, J = 7.05, S/D = 2, and H_o/D = 4. The jets penetrate to about 40 percent of the duct height at X/H_o = 0.5 and the jet centerline and gradually return to the injection wall. Comparison of this figure with Figure 69 shows that for slant wall injection at J = 7.05, the lateral jet spreading rate is slightly faster than that for flat wall injection. The radial jet spreading rates are not significantly different between these two cases. The predicted results for Test 33 are portrayed in Figure 78. The predicted jet penetrations are slightly deeper than the measured ones and the predicted theta values are higher than the measured values. The correlations are, however, in good qualitative agreement with the data.

The data for Test 34, with Test Section VI, J = 26.4, S/D = 2, and H_o/D = 4 are illustrated in Figure 79. At X/H_o = 0.5, the jets penetrate up to about 70 percent of the local duct height and reach the opposite (flat) wall at X/H_o = 0.75. Comparing this test case with Test 30 (Figure 71) shows that the lateral mixing is enhanced with slant wall injection. The mixing in the radial direction is accelerated after the jet centerline reaches the opposite wall. The predicted theta values for Test 34 are portrayed in Figure 80. The correlations slightly underpredict the jet penetration and overpredict the theta values. The higher theta values are a result of underestimating the mixing rate in the correlations.

5.3.3 Conclusions for Series 3 Tests

Interactions between a row of jets with cross-flow in a convergent duct were studied. Two geometric orifice configurations and two flow conditions for each convergent duct were considered. Symmetric and asymmetric convergent test sections with uniform mainstream temperature and velocity profiles were used in Series 3 tests. The following conclusions are drawn from these tests:

- Mixing is generally enhanced by flow area convergence. The jet spreading in radial and transverse directions occurs within a shorter distance from the jet injection plane than in the case with a constant area duct.

- The jet penetration is slightly reduced in symmetric convergence Test Section II compared to those in a constant cross-sectional area duct. For Test Section IV, the jets are injected upstream at a higher angle toward a region of higher cross-sectional area, where the mainstream velocities are lower. Regions of lower mainstream velocities can be associated with a higher apparent jet momentum ratio and hence the jet penetration in those regions is deeper.

- For asymmetric Test Section V with flat wall injection, the jet mixing characteristics are the same as those of the symmetric convergent Test Section IV.

- In the asymmetric Test Section VI with slant wall injection (jet injection angle of 116.6 degrees), the mixing in the transverse direction is significantly enhanced while the radial mixing is very similar to that with flat wall injection.

ORIGINAL PAGE IS
OF POOR QUALITY

- The modified NASA/Aerojet correlations with equivalent momentum ratio (J_{eq}) yield qualitatively good comparison with the data. However, the predicted theta values are higher than the measured values. The differences between the two results are larger with increasing jet injection angle. Further refinements in the correlations are needed to improve the agreement between data and correlations.

5.4 Series 4 Tests

The objective of these tests was to study the combined effects of flow area convergence and profiled mainstream temperature. These tests were taken with Test Section V (flat wall injection) and with orifice plate 01/04/08. Both top cold and top hot profiles were employed with two momentum ratios for each profile. The test configuration and flow conditions employed in this series are listed in Table VI. Measurements were taken at two axial stations, X/H_o = 0.25 and 1.0.

TABLE VI. SERIES 4 TEST CONFIGURATIONS AND FLOW CONDITIONS

Test No.	Orifice Dia (D) (cm)	S/D	H_o/D	Mainstream Velocity VMAIN (m/sec)	Mainstream Temp. TMAIN (^oK)	Jet Velocity VJET (m/sec)	Jet Temp. TJET (^oK)	Momentum Ratio J	Density Ratio DENRATIO	Equilibrium Temp TWEE	Region of Axial Direction (X/H_o)	Measurements In Transverse Direction Z/S
35	1.27	4.0	8.0	16.7	561	70.9	308	26.8	1.86	0.100	0.25 to 1.0	0.0 to 1.0
36	1.27	4.0	8.0	18.8	568	139.1	305	109.8	2.01	0.177	0.25 to 1.0	0.0 to 1.0
37	1.27	4.0	8.0	16.0	417	40.7	319	8.5	1.32	0.064	0.25 to 1.0	0.0 to 1.0
38	1.27	4.0	8.0	16.0	416	75.4	315	30.2	1.36	0.107	0.25 to 1.0	0.0 to 1.0

As stated in Paragraph 5.2 for the Series 2 tests, the definition of theta used to analyze these data is

$$\theta = \frac{T_{max} - T}{T_{max} - T_j}$$

where:

T_{max} = Maximum temperature of the profiled mainstream.

T = Local stagnation temperature in the mixing region.

T_j = Jet stagnation temperature.

The measured theta distributions for Test 35 with top cold profile, J = 26.82, S/D = 4, and H_o/D = 8 are depicted in Figure 81. The jet penetration in this case is about 40 percent of the channel height at X/H_o = 0.25. The jets retain their individual shapes at both X/H_o = 0.25 and 1.0. The mainstream temperature (top cold) profile seems to inhibit the lateral and radial mixing. This is evident by comparing Figure 81 with the data for uniform mainstream profile (Figure 65). The predicted theta values for Test 35 are portrayed in Figure 82. The predictions are obtained by superposing the mainstream theta profile [$\theta_p(y)$] on the NASA/Aerojet correlations with equivalent momentum ratio, J_{eq}, in a manner similar to the one described in Paragraph 5.2. The predicted radial profiles along the jet centerplanes are in qualitative agreement with the data at X/H_o = 0.25 and in poor agreement with the data at X/H_o = 1.0.

The data for Test 36 with top cold profile, J = 109.8, S/D = 4, and H_o/D = 8 are illustrated in Figure 83. At X/H_o = 0.25, the jet centerlines are located at about 60 percent of local channel height. The mixing in the transverse direction is much slower than in the corresponding test case with uniform mainstream temperature profile (Figure 67). The predicted theta distributions for Test 36 are presented in Figure 84. The comparison of predicted and measured radial profiles is poor.

The measured theta distributions with Test Section V, top hot mainstream temperature profile, J = 8.51, S/D = 4, and H_o/D = 8

are depicted in Figure 85. At $X/H_o = 0.25$, the jets retain their individual shapes and mix rapidly in the transverse direction. This characteristic is contrary to the trend observed with the top cold mainstream profile. The predicted theta values for Test 37 are portrayed in Figure 86. At $X/H_o = 0.25$, the agreement between data and correlations is good. At $X/H_o = 1$, the agreement is poor.

The measured theta values for Test 38 with top hot profile, $J = 30.24$, $S/D = 4$, and $H_o/D = 8$ are presented in Figure 87. At $X/H_o = 0.25$, the jets penetrate to about 50 percent of the channel height and gradually penetrate to the opposite wall at $X/H_o = 1.0$. The shape and location of the contours indicate enhanced mixing in both radial and transverse directions in comparison with those with top cold profiles (Figure 81). The predicted theta distributions for Test 38 are presented in Figure 88. The correlations and data are in good agreement at $X/H_o = 0.25$, while the agreement is poor at $X/H_o = 1.0$.

5.4.1 Conclusions for Series 4 Tests

Confined jet mixing characteristics were studied with flow area convergence and profiled mainstream temperature. Four tests were performed with orifice plate 01/04/08, including top cold and top hot mainstream temperature profiles.

The following conclusions are drawn from the data:

- Mixing of the jets in radial and transverse directions is inhibited with top cold mainstream temperature profile and is not significantly affected with top hot profile when compared to tests with isothermal mainstream conditions.

- The mainstream temperature profile has a dominant influence on the temperature distribution throughout the mixing region.

- The superposition scheme used in the correlations is inadequate for predicting the temperature distribution with flow area convergence and profiled mainstream.

6.0 JET MIXING CORRELATIONS DEVELOPMENT

A number of empirical and semiempirical methods have been developed by various researchers for predicting jet interaction with a cross-flow. These models were mostly concerned with jet blockage, entrainment, and mixing in the wake region (References 5, 6, and 7). Empirical models have been proposed for jet trajectory, jet spread, and mixing rate. The main differences between the various models were in the postulated mechanisms for jet entrainment and trajectory.

Most of the popular approximate predictive techniques (References 8 through 12) employ integral methods with simplifying assumptions introduced for mathematical simplicity.

One of the unknowns in integral mixing field prediction methods is usually the shape of the jet cross section. The complex jet cross-section geometries are often approximated by rectangles, circles, or ellipses for satisfying the conservation of mass, momentum, and energy. The second unknown is a velocity profile parameter, which is usually modeled by an appropriate similarity assumption. These models are invalid for curved jets.

The jet deflection is treated in two ways: The first approach treats the jet as a solid body and uses discharge coefficients for the cylinders or ellipses, together with a pressure differential across the jet in the mainstream direction to compute the jet deflection. The second approach deals with mass and momentum entrained from the mainstream into the jet through empirical models and this approach is generally considered to be more accurate. The correlations used in this study are the NASA/Aerojet correlations, which are described in the following paragraph.

6.1 NASA/Aerojet Correlations

ORIGINAL PAGE IS
OF POOR QUALITY

The correlations developed by Holdeman and Walker (Reference 2) are based upon experimental data involving a row of jets injected into a confined cross-flow. The jet centerline trajectory is given as:

Correlations for Predicting the Centerplane Temperature Profiles

Thermal Trajectory (Centerline):

$$\frac{Y_{c,o}}{D_j} = 0.539\ J^{0.25} \left(\frac{S}{D_j}\right)^{0.14} \left(\frac{H}{D_j}\right)^{0.38} \left(\frac{X}{D_j}\right)^{0.17} e^{-b} \qquad (5.1)$$

where

$$b = \left[0.091 \left(\frac{X}{H}\right)^2 \left(\frac{H}{S} - \frac{\sqrt{J}}{3.5}\right)\right]$$

The results for temperature field are presented in nondimensional form by using

$$\theta = (T_m - T) \ / \ (T_m - T_j)$$

where T_m is the undisturbed mainstream stagnation temperature, T is the local stagnation temperature in the mixing region, and T_j is the stagnation temperature of the jet. The variable θ represents the ratio of actual temperature change to the maximum possible temperature change due to the dilution jets. The centerline temperature is correlated by the following expression:

Centerline Temperature Difference Ratio:

$$\theta_{c,o} = \theta_{EB} + (1-\theta_{EB}) \left[1.452\ J^{-0.35} / \left(\frac{X}{D_j}\right)\right]^f \qquad (5.2)$$

ORIGINAL PAGE IS
OF POOR QUALITY

where

$$f = 1.15 \sqrt{\frac{S}{H} \Big/ \left(1 + \frac{S}{H}\right)}$$

and

$$\theta_{EB} = \frac{\dot{m}_m T_m + \dot{m}_j T_j}{(\dot{m}_m + \dot{m}_j)}$$

The temperature difference ratio, θ, at any point in the flow field is determined from:

$$\theta = \theta^{\pm}_{min} + (\theta_c - \theta^{\pm}_{min}) \exp \left[\left(-\ln 2\right) \left(\frac{Y - Y_c}{W^{\pm}_{1/2}}\right)^2\right] \tag{5.3}$$

where $\theta^{\pm}_{min}$ and $W^{\pm}_{1/2}$ are defined as follows:

Minimum Centerplane Temperature Difference Ratios:

$$\frac{\theta^{+}_{min,o}}{\theta_{c,o}} = 1 - e^{-c^+} \tag{5.4}$$

where

$$c^+ = 0.038\ J^{1.62} \left(\frac{S}{D_j}\right)^{1.5} \left(\frac{H}{D_j}\right)^{-3.67} \left(\frac{X}{D_j}\right)^{1.1}$$

$$\frac{\theta^{-}_{min,o}}{\theta_{c,o}} = 1 - e^{-c^-} \tag{5.5}$$

where

$$c^- = 1.57\ J^{-0.3} \left(\frac{S}{D_j}\right)^{-1.4} \left(\frac{X}{D_j}\right)^{0.9}$$

Centerplane Half-Widths:

$$\frac{W^{+}_{1/2,o}}{D_j} = 0.162\ J^{0.18} \left(\frac{S}{D_j}\right)^{-0.25} \left(\frac{H}{D_j}\right)^{0.5} \left(\frac{X}{D_j}\right)^{0.5} \tag{5.6}$$

ORIGINAL PAGE IS
OF POOR QUALITY

$$\frac{W^{-}_{1/2,o}}{D_j} = 0.20\ J^{0.15} \left(\frac{S}{D_j}\right)^{0.27} \left(\frac{H}{D_j}\right)^{0.5} \left(\frac{X}{D_j}\right)^{0.12} \tag{5.7}$$

The half-widths $W^{\pm}_{1/2}$ are the distance between the jet centerline and the location where $\theta = (\theta_c + \theta^{\pm}_{min})/2$.

Correlations for Predicting the Off-Centerplane Variation of the Temperature Profile Scaling Parameters

Off-Centerplane Penetration

$$\frac{Y_{c,Z}}{Y_{c,o}} = 1 - \left(\frac{Z}{S/2}\right)^2 e^{-g} \tag{5.8}$$

where

$$g = 0.227\ J^{0.67} \left(\frac{S}{D_j}\right)^{-1} \left(\frac{X}{D_j}\right)^{0.54}$$

Off-Centerplane Maximum Temperature Difference Ratio

$$\frac{\theta_{c,Z}}{\theta_{c,o}} = 1 - \left(\frac{Z}{S/2}\right)^2 e^{-d} \tag{5.9}$$

where

$$d = 0.452\ J^{0.53} \left(\frac{S}{D_j}\right)^{-1.53} \left(\frac{X}{D_j}\right)^{0.83}$$

Off-Centerplane Minimum Temperature Difference Ratios and Half-Widths

$$\frac{\theta^{\pm}_{min,Z}}{\theta_{c,Z}} = \frac{\theta^{\pm}_{min,o}}{\theta_{c,o}} \tag{5.10}$$

These correlations provide a useful and reasonably accurate prediction of the temperature profiles along the jet centerplanes. However, the predicted off centerplane temperature profiles are not very accurate and need refinement. Furthermore, the correlations are inaccurate for high momentum ratios when the jets penetrate to the opposite wall.

The NASA/Aerojet correlations described in this Paragraph (6.1) were derived for a uniform flow area and uniform mainstream conditions. When a non-uniform mainstream temperature profile exists, the NASA/Aerojet correlations for theta, θ_{NA}, can be assumed to represent the changes in the local mainstream temperature distribution by dilution jets. In other words,

$$\theta_{NA} = (T_m(y) - T) / (T_m(y) - T_j) \qquad (5.11)$$

Here, θ_{NA} represents the results from equation (5.3).

For flows with non-uniform profiled mainstream, the ratio of actual temperature change to the maximum possible temperature change due to the jets is obtained from the following definition of nondimensionalized temperature difference ratio:

$$\theta = (T_{max} - T) / (T_{max} - T_j) \qquad (5.12)$$

where:

T_{max} = Maximum stagnation temperature of the undisturbed mainstream profile

T = Local stagnation temperature

T_j = Jet stagnation temperature.

ORIGINAL PAGE IS
OF POOR QUALITY

Using equation (5.12), the profiled mainstream theta, θ_m (y), can be defined as

$$\theta_m(y) = [T_{max} - T_m(y)] \ / \ (T_{max} - T_j) \qquad (5.13)$$

From equations (5.11), (5.12), and (5.13) it is seen that

$$\theta = \theta_m(y) + [1 - \theta_m(y)] \quad \theta_{NA} \qquad (5.14)$$

Equation (5.14) is used to generate the predicted theta values for test cases in Series 2 and 4. It is important to note that the variation of the nondimensionalized temperature, θ, is conveniently scaled between 0.0 and 1.0. The nondimensional temperature distribution, θ_{NA}, is obtained from the NASA/Aerojet correlations (Equation 5.3).

For test cases with flow area convergence, the following modifications are used in obtaining predictions. For converging ducts at low Mach numbers, the average mainstream velocity increases by the relation

$$V_m(x) = V_o \left(\frac{A_o}{A(X)}\right) \qquad (5.15)$$

where:

$V_m(X)$ = Average mainstream velocity in the duct at any given axial Station X

V_o = Average mainstream velocity at the jet injection plane (X = 0)

A(X) = Cross-sectional area of the duct at the axial Station X

A_o = Cross-sectional area of the duct at the jet injection plane (X = 0)

ORIGINAL PAGE IS
OF POOR QUALITY

Thus, $$\rho_m(X)V_m^2(X) = \rho_o V_o^2 \left(\frac{A_o}{A(X)}\right)^2$$

Due to the acceleration induced by the flow area convergence, the equivalent jet-to-mainstream momentum ratio is given by

$$J_{eq} = \frac{\rho_j \; V_j^2}{\rho_m(X) \; V_m^2(X)} = \frac{\rho_j \; V_j^2}{\rho_o \; V_o^2} \left(\frac{A(X)}{A_o}\right)^2$$

Thus, $$J_{eq} = J_o \left(\frac{A(X)}{A_o}\right)^2 \qquad (5.16)$$

Where, J_o is the momentum ratio at the jet injection plane.

The correlations for convergent ducts are obtained by substituting the equivalent momentum ratio, J_{eq}, wherever J is used in the NASA/Aerojet correlations. This approach was found to yield improved results compared to the results obtained from the original NASA/Aerojet correlations. However, the correlations do not account for the effects of jet injection angle, which have been observed to have significant effect on the jet spreading rates. Further work on the correlations is required to properly account for these effects.

For test cases with flow area convergence and profiled mainstream, the correlations were obtained by combining the procedures described for convergent ducts and profiled mainstream. The predictions obtained from these correlations are inadequate for correctly describing the jet mixing characteristics in Series 4 tests. This is partly due to the fact that the distortion of the mainstream temperature profile (without the jets) by the flow area convergence is ignored in the correlations.

The NASA/Aerojet correlations, along with the modifications suggested in this section, provide an excellent analytical design tool for predicting the jet mixing characteristics in the dilution zone of a combustor. These correlations were formed to yield excellent qualitative agreement (and good quantitative agreement in some of the test cases) with the measurements made in this program. Additional work is needed to improve the predictions obtained from the correlations.

7.0 CONCLUSIONS AND RECOMMENDATIONS

The tests made in Phase I of the NASA Dilution Jet Mixing Program were directed toward better understanding of the mixing processes of a row of jets injected into a ducted cross-flow. The following conclusions are drawn from these tests:

- The jet penetration distance increases with increasing the momentum ratio, J, and jet orifice diameter, D.

- The jet spreading rate in the transverse direction increases with increasing the momentum ratio, J, and duct height to hole diameter ratio, H_o/D, and decreasing the hole spacing to diameter ratio, S/D.

- The jet spreading in the radial direction is enhanced with increased jet penetration.

- The jet-to-mainstream density ratio, ρ_j/ρ_m, has only a second-order effect on the mixing characteristics for a given momentum ratio.

- The temperature distribution in the jet mixing region is strongly influenced by the mainstream temperature profile. The jet spreading rates with profiled mainstream are similar to those with uniform mainstream. This suggests that a superposition principle could be applied to predict temperature profiles with profiled mainstream.

- Jet mixing is generally enhanced by flow area convergence. The jet penetration is increased with increasing upstream injection angle.

- The jet mixing characteristics with asymmetric convergence and flat wall injection are similar to those in a symmetric convergent test section of the same area ratio.

- The asymmetric test section with slant wall injection has a significantly faster jet spreading rate in the transverse direction.

- The radial and lateral jet spreading rates with "top cold" mainstream profile and flow area convergence are significantly slower compared to those with uniform mainstream profile and flow area convergence. The jet spreading rates are not appreciably altered with a "top hot" mainstream temperature profile.

- The NASA/Aerojet correlations adequately predict the theta profiles for constant area duct and uniform mainstream profile. For the case of constant area duct with profiled mainstream, the superposition of mainstream theta profiles on the correlations yield good qualitative results. An improved scaling parameter is needed to obtain a good quantitative agreement with data.

- The modified NASA/Aerojet correlations with equivalent momentum ratio, J_{eq}, provide improved predictions of nondimensionalized temperature profiles. However, this model does not properly account for the effects of jet injection angles.

- For situations involving flow area convergence and profiled mainstream, the superposition of mainstream temperature profile on the NASA/Aerojet correlations is

inadequate for predicting the temperature profiles in the mixing region. This is mainly due to the decay of the mainstream temperature profile due to flow area convergence. Further work on the correlations is needed to improve the predictions.

The correlations used in this program provide a very useful and simple analytical tool for designing the dilution zone of a combustor. However, additional work is needed to further refine the correlations for convergent ducts and non-uniform mainstream conditions.

ORIGINAL PAGE IS
OF POOR QUALITY

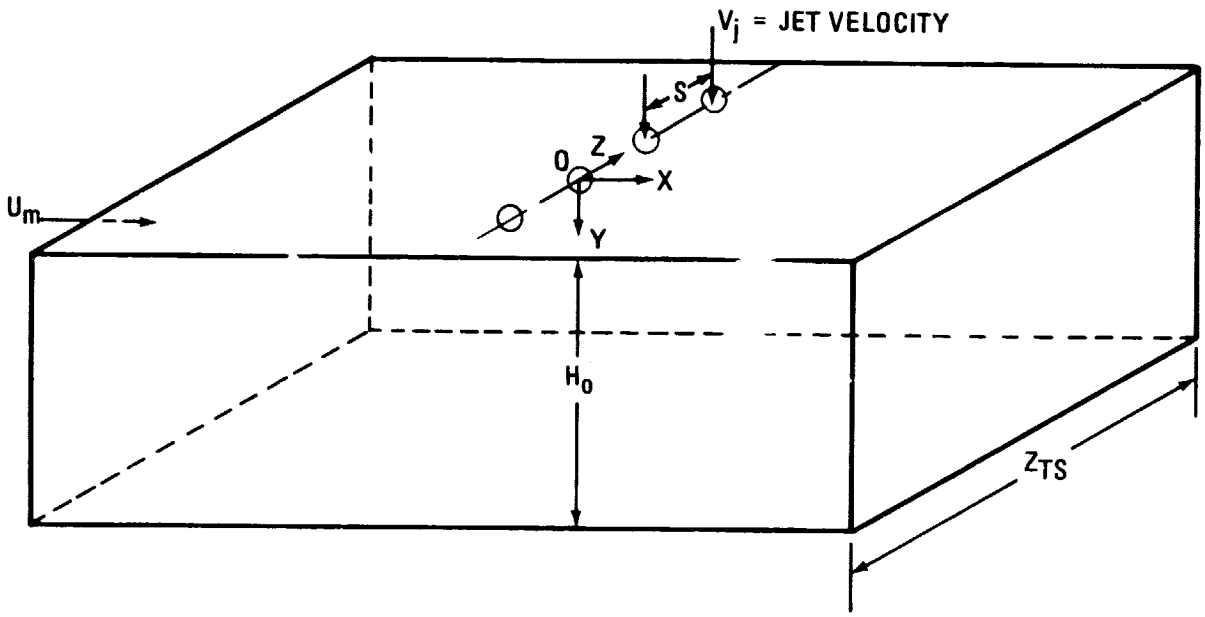

COORDINATE ORIGIN IS LOCATED AT CENTER OF ORIFICE

U_m, ρ_m, T_m	=	MAINSTREAM VELOCITY, DENSITY, AND TEMPERATURE
V_j, ρ_j, T_j	=	INITIAL JET VELOCITY, DENSITY, AND TEMPERATURE
H_0	=	TEST-SECTION HEIGHT AT INJECTION PLANE
H	=	TEST-SECTION HEIGHT AT ANY X-Y PLANE
S	=	ORIFICE SPACING ALONG Z (TRANSVERSE) DIRECTION
D	=	ORIFICE DIAMETER
D_j	=	$\sqrt{C_D}\, D$
Z_{TS}	=	TEST-SECTION TRANSVERSE DIMENSION = 305mm

Figure 1. Multiple Jet Study Coordinate System and Important Nomenclature.

ORIGINAL PAGE IS
OF POOR QUALITY

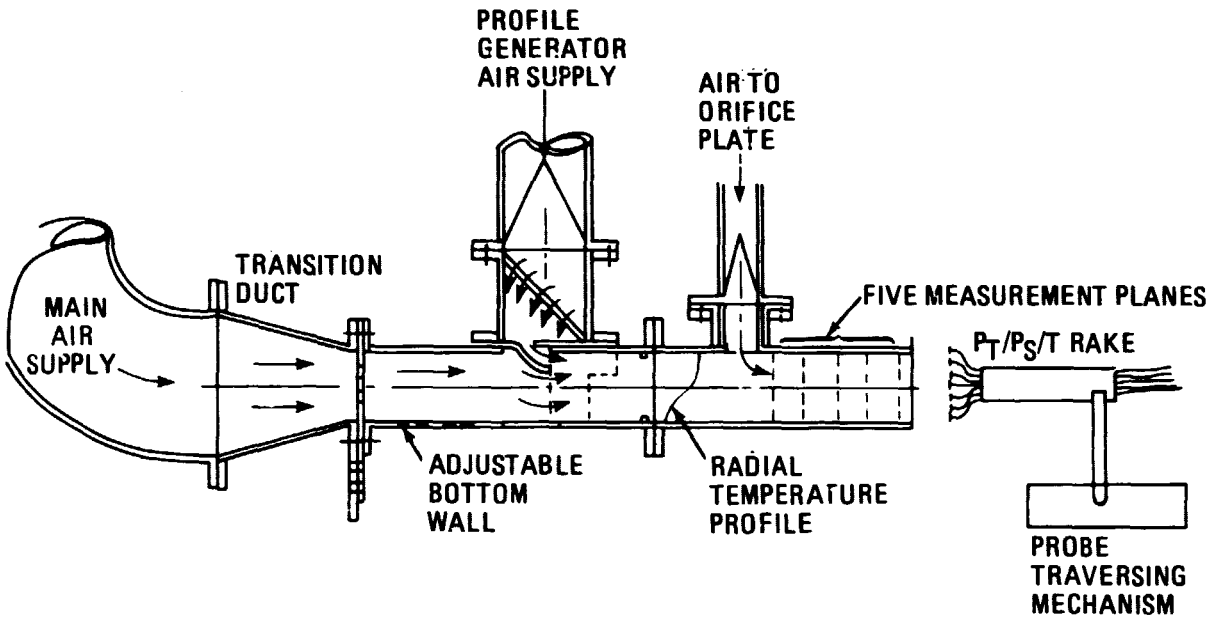

Figure 2. Jet Mixing Rig Schematic.

ORIGINAL PAGE
BLACK AND WHITE PHOTOGRAPH

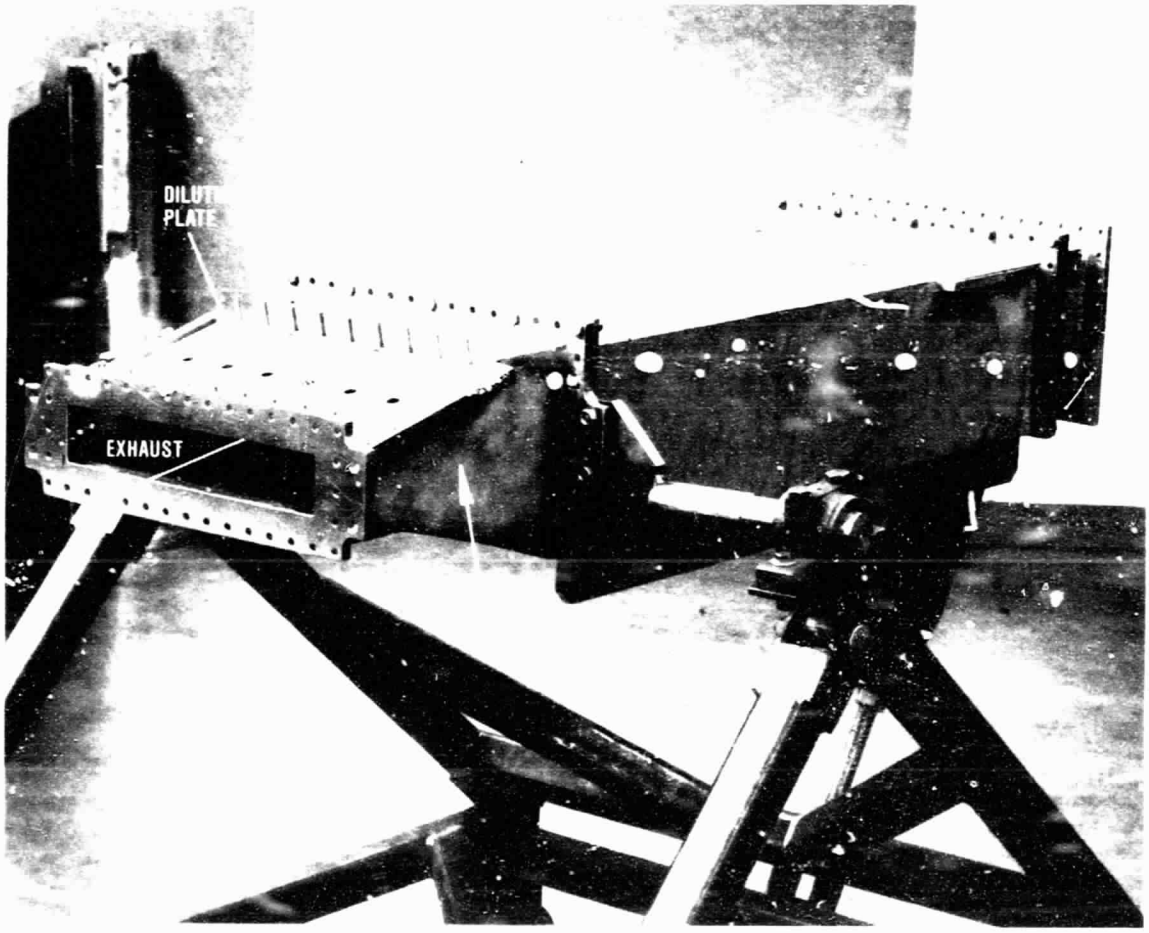

Figure 3. Partially Assembled Dilution Jet Mixing Test Rig.

ORIGINAL PAGE IS
BLACK AND WHITE PHOTOGRAPH

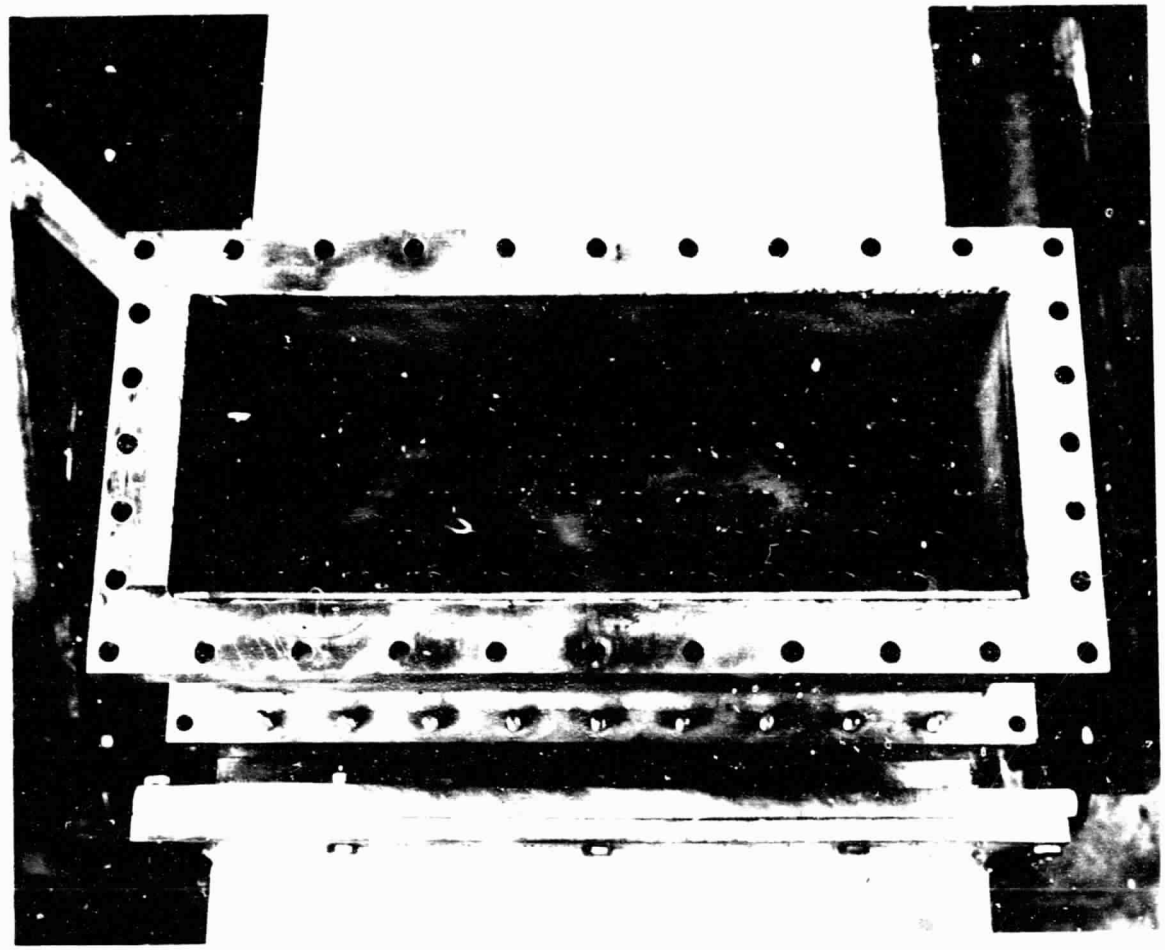

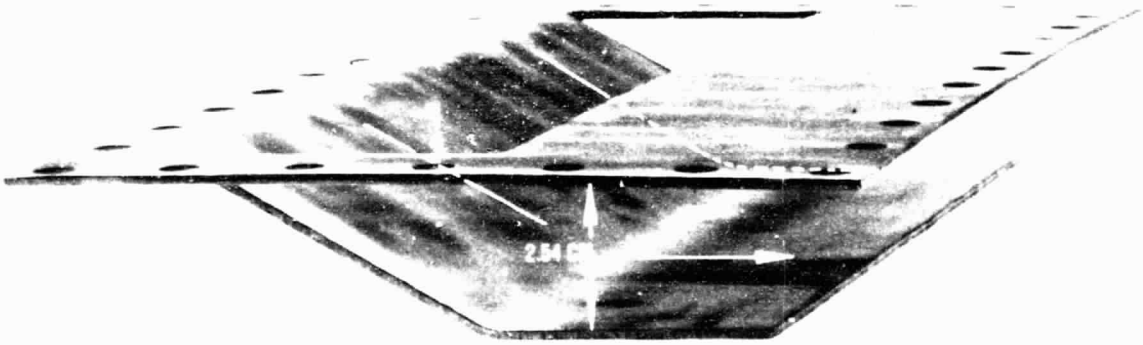

Figure 4. Profile Generator.

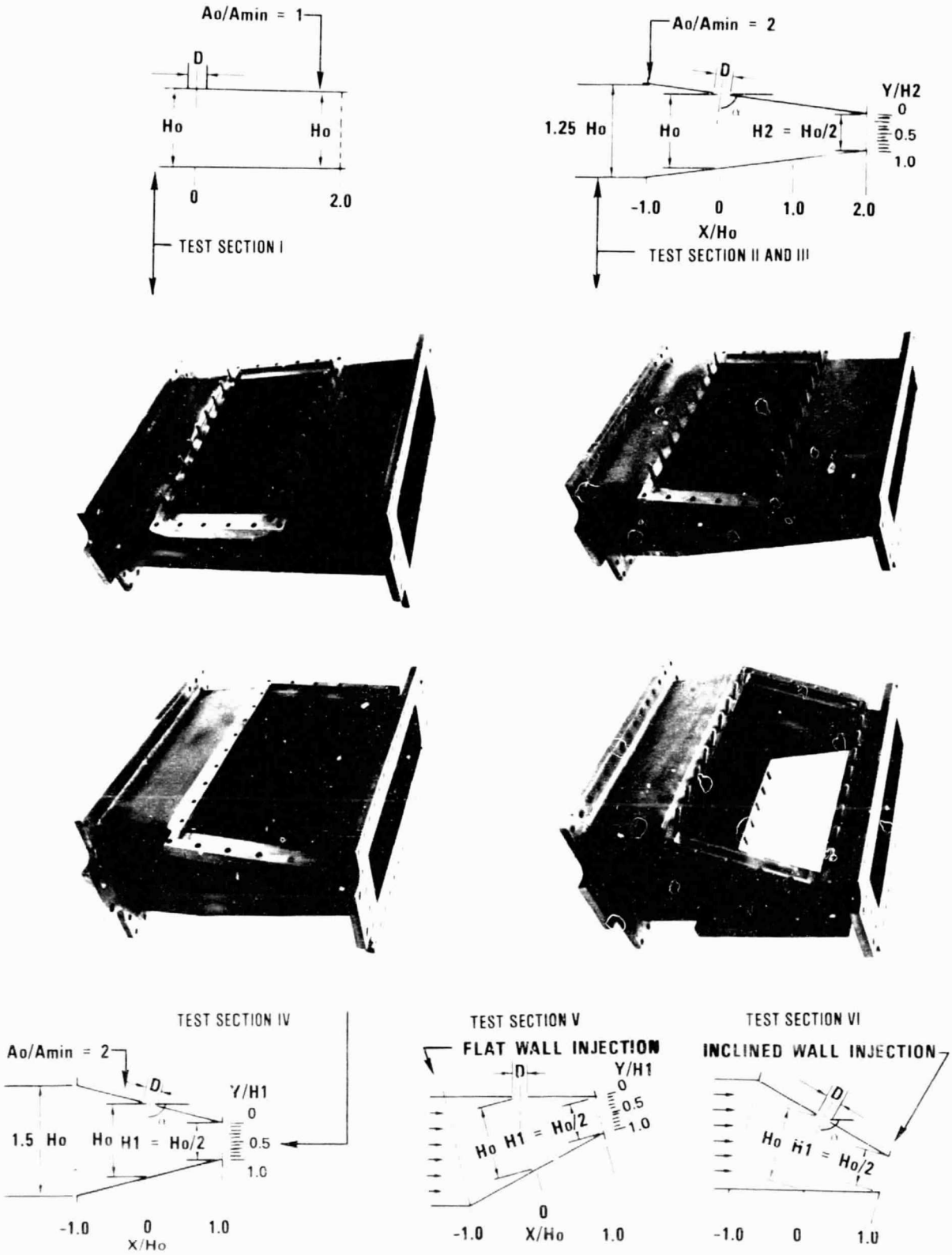

Figure 5. Jet Mixing Test Sections. H_o = 10.16 cm.

ORIGINAL PAGE
BLACK AND WHITE PHOTOGRAPH

ORIGINAL PAGE IS
OF POOR QUALITY

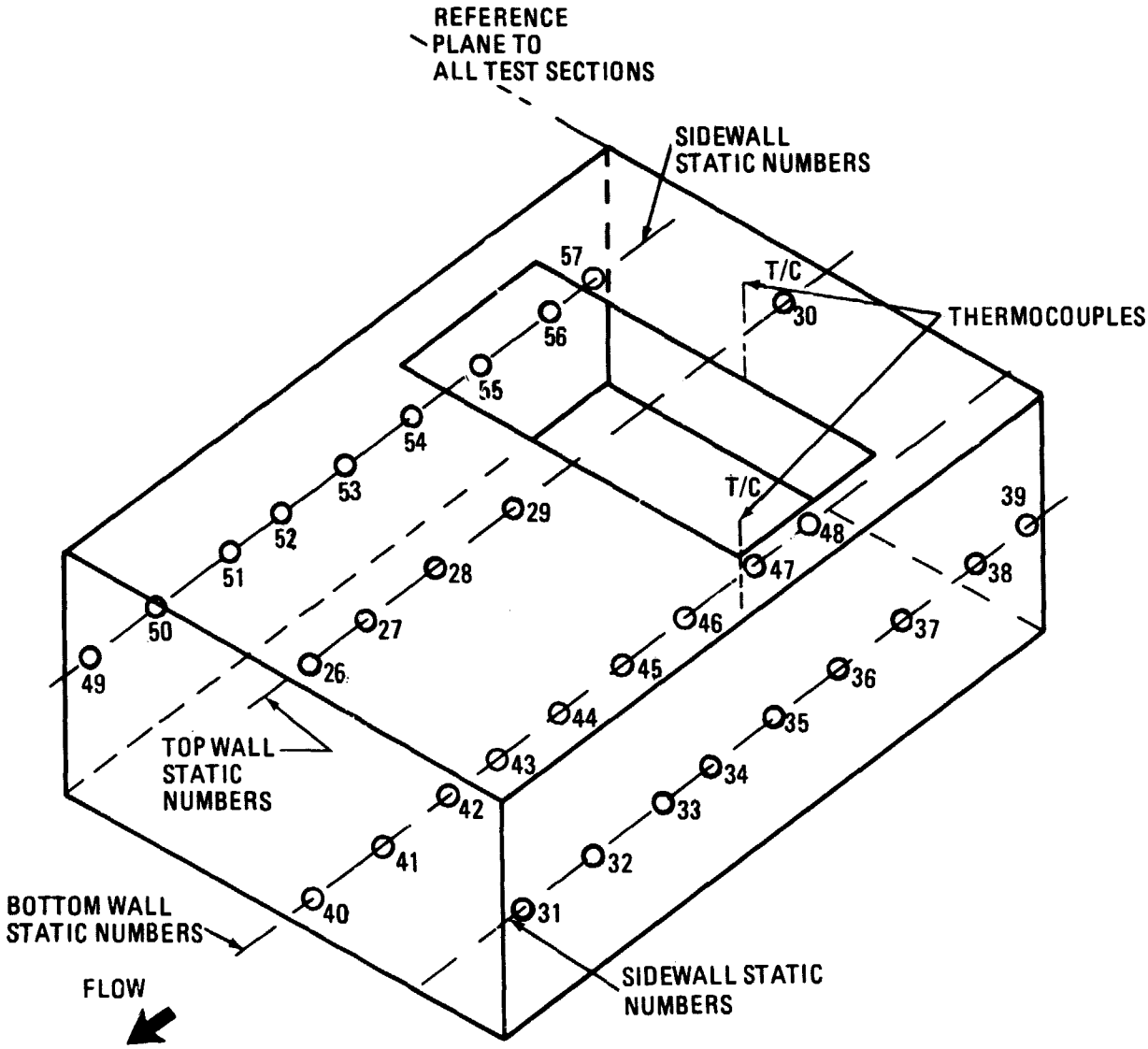

Figure 6. Test Section Wall Statics and Thermocouples.

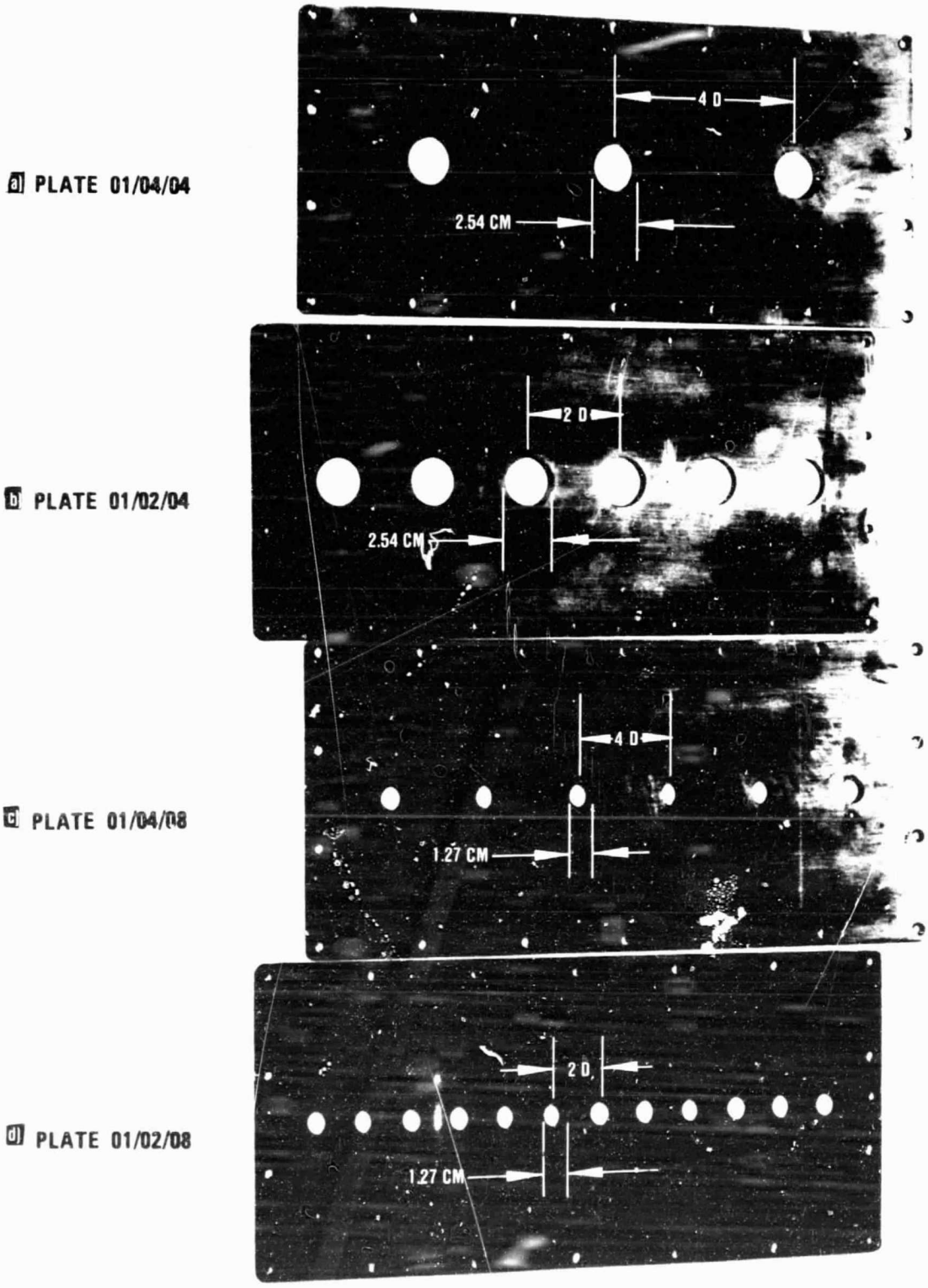

Figure 7. Dilution Orifice Plate Configurations.

ORIGINAL PAGE
BLACK AND WHITE PHOTOGRAPH

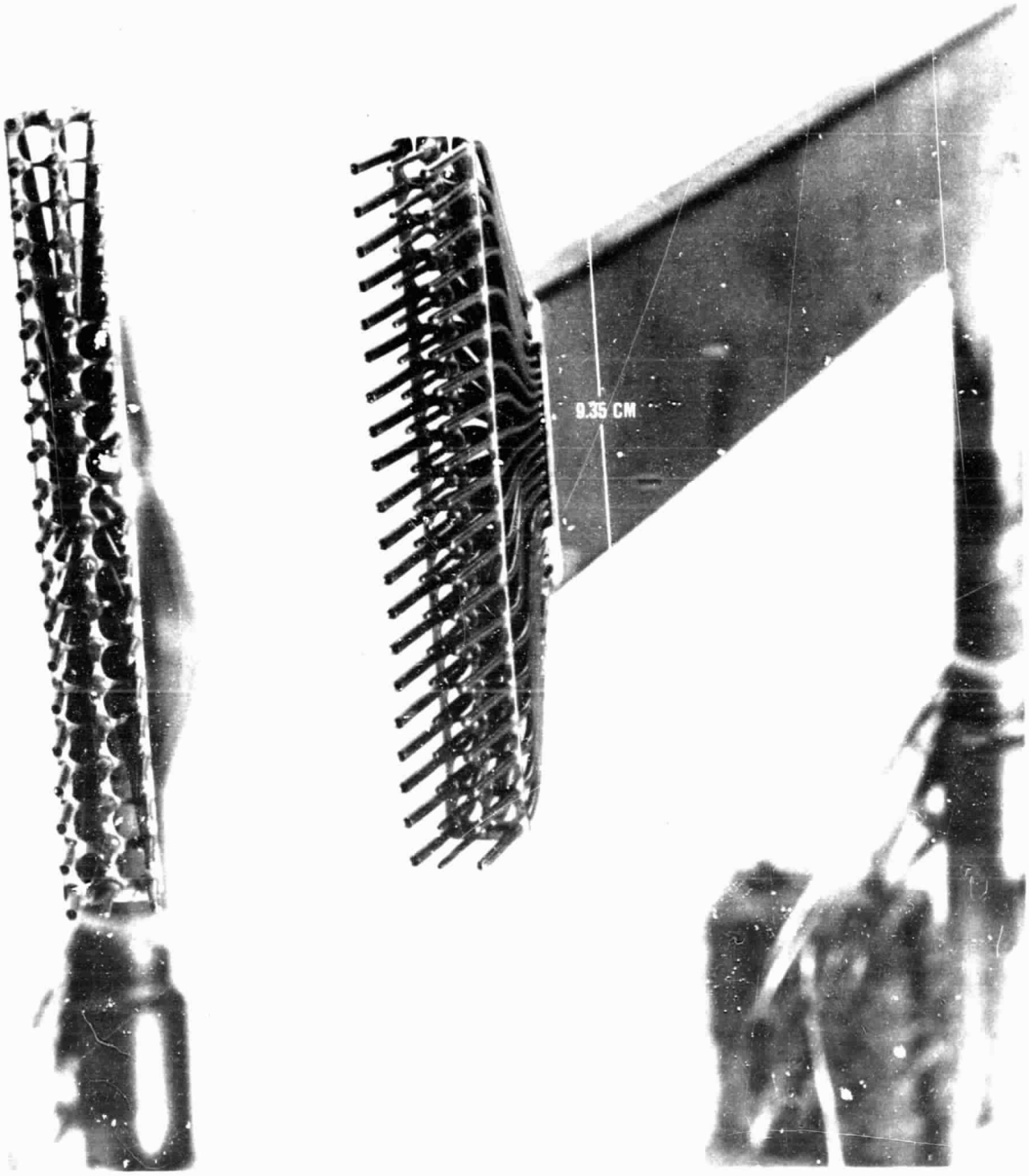

Figure 8. Total Pressure, Thermocouple, and Static Pressure Rake.

ORIGINAL PAGE
BLACK AND WHITE PHOTOGRAPH

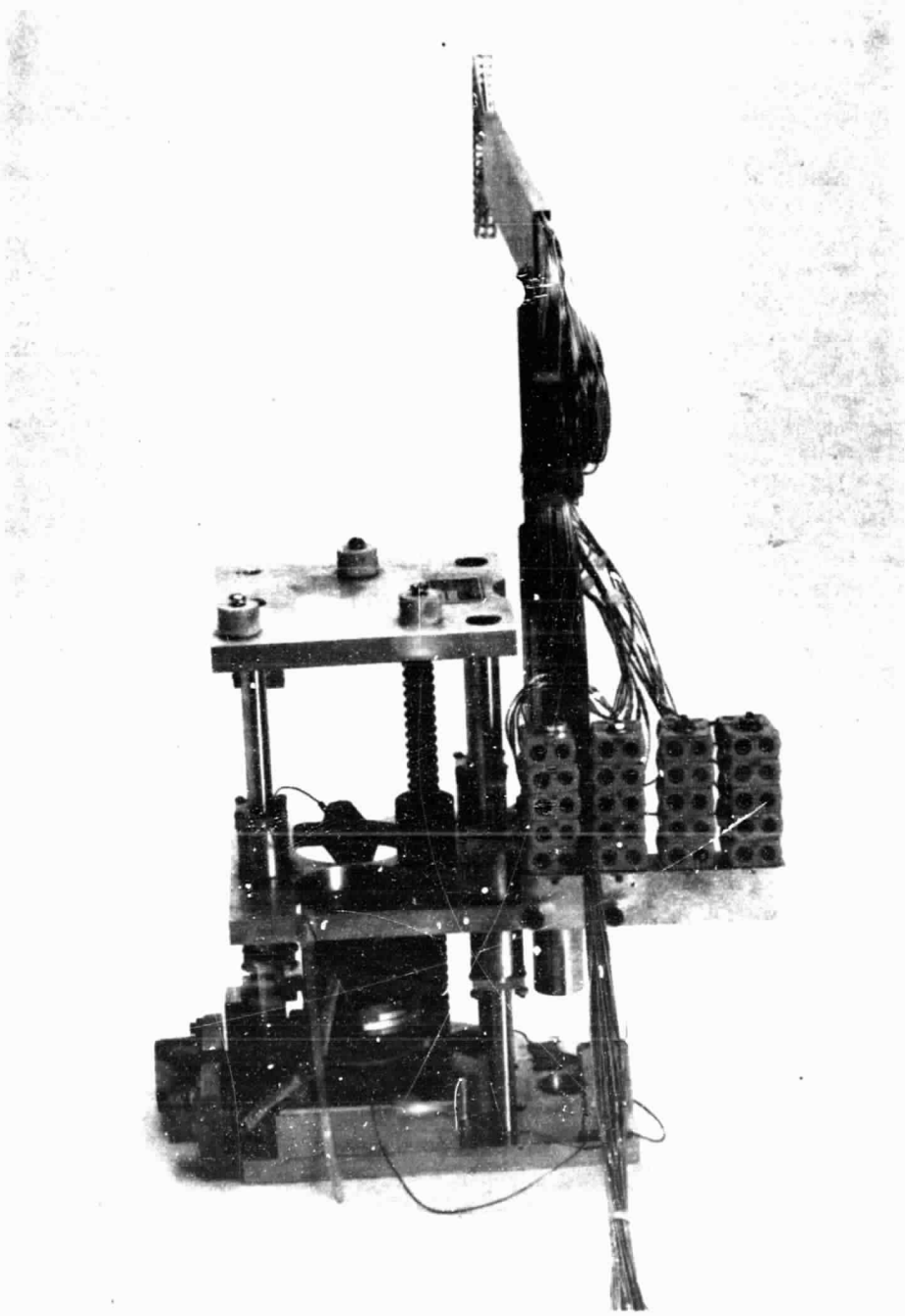

Figure 9. X-Y-Z Actuator with the Rake Mounted.

ORIGINAL PAGE
BLACK AND WHITE PHOTOGRAPH

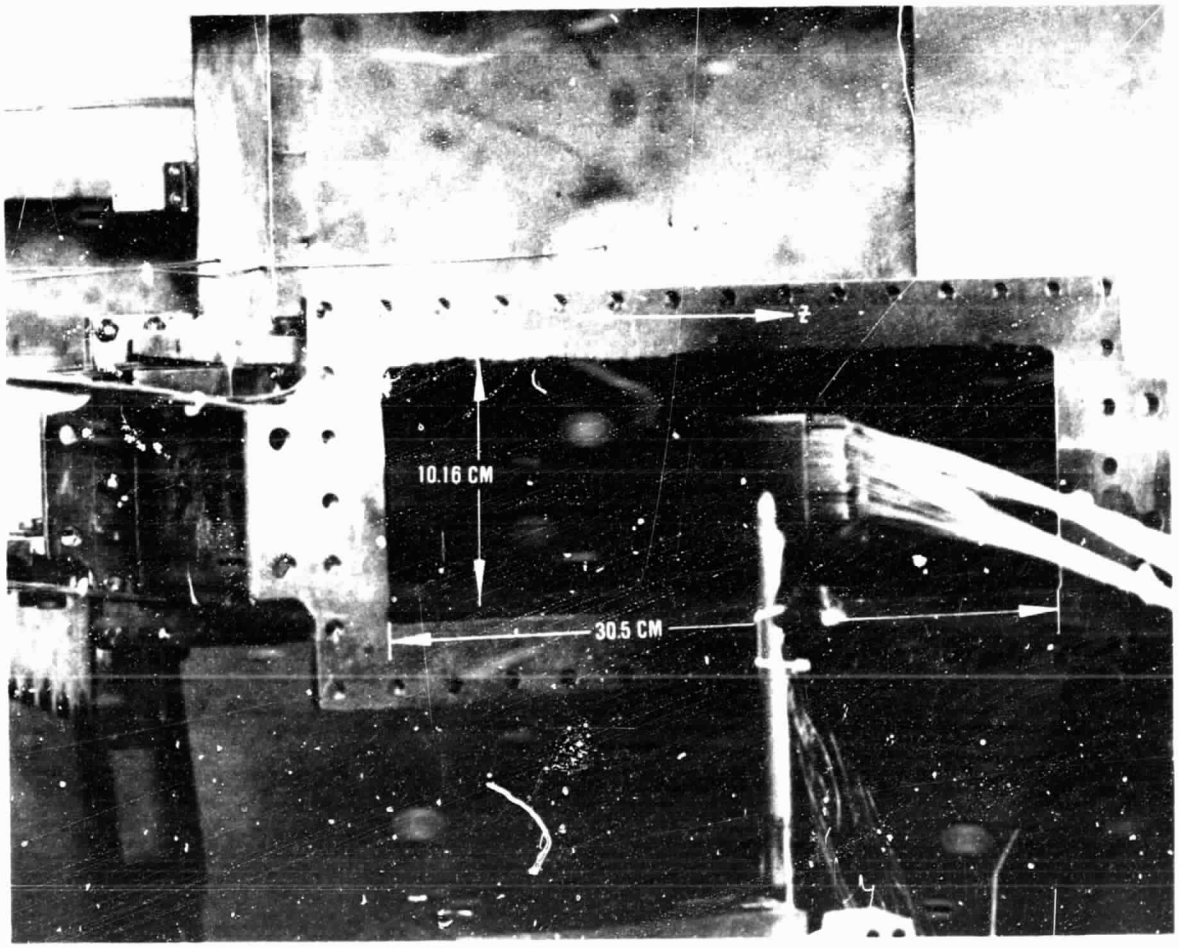

Figure 10. Jet Mixing Rig as Viewed from Rig Discharge End.

ORIGINAL PAGE
BLACK AND WHITE PHOTOGRAPH

ORIGINAL PAGE
COLOR PHOTOGRAPH

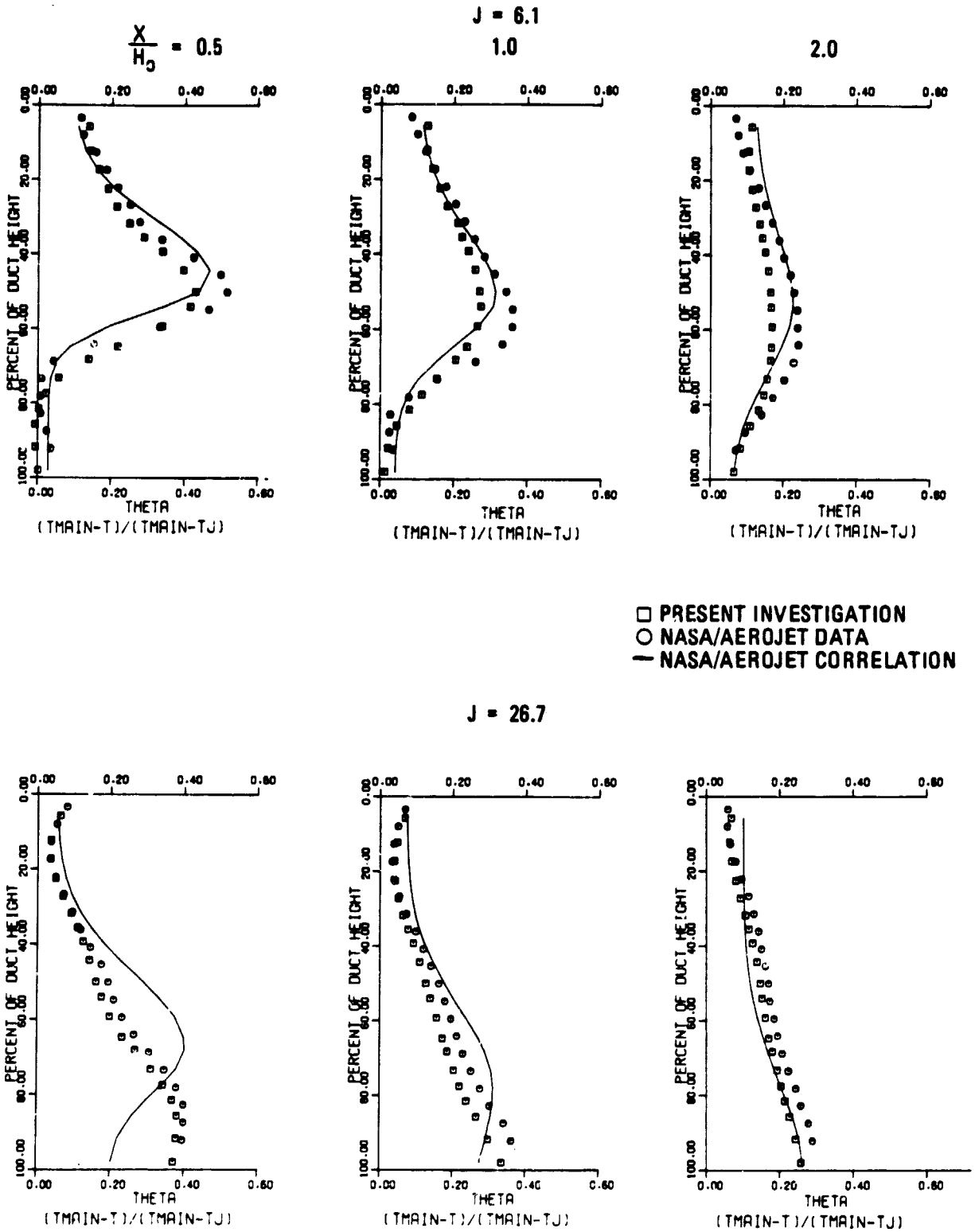

Figure 11. Typical Comparison Between Data From NASA/Aerojet and Present Investigation for S/D = 4 and H_o/D = 4.

S = 0.0508 METERS S/DJ = 2.443 HO/DJ = 4.687 VMAIN = 15.8 M/SEC VJET = 26.0 M/SEC TMAIN = 649.8 K

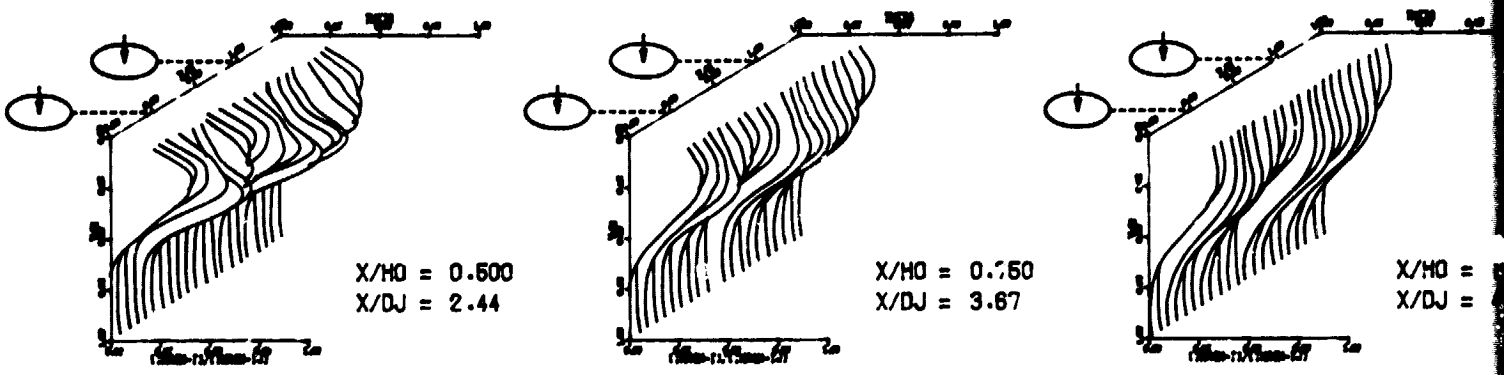

MEASURED THETA PROFILES FOR TEST NO. 1, TEST SECTION I, TMAIN=CONST.,

CONTOUR	1	2	3	4	5	6
VALUE	0.0500	0.1000	0.1759	0.2000	0.2500	0.3000

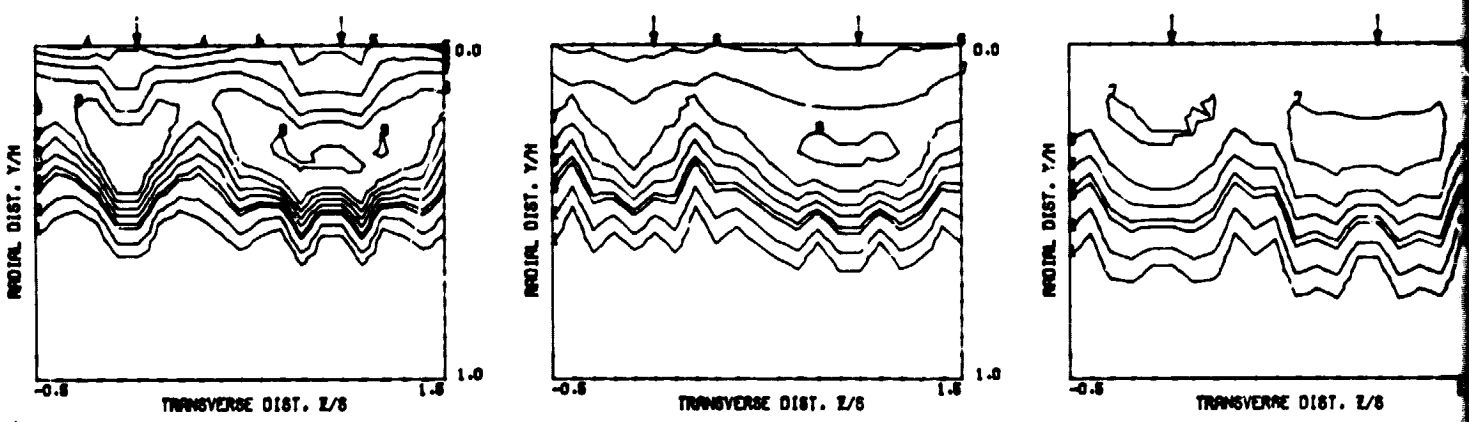

MEASURED THETA CONTOURS FOR TEST NO.1, TMAIN=CONST.

ORIGINAL PAGE IS OF POOR QUALITY

FOLDOUT FRAME

M/SEC TMAIN = 649.8 K TJET = 308.1 K THEB = 0.1759 BLORAT= 3.243 DENRATIO= 2.113 TRATIO=0.474

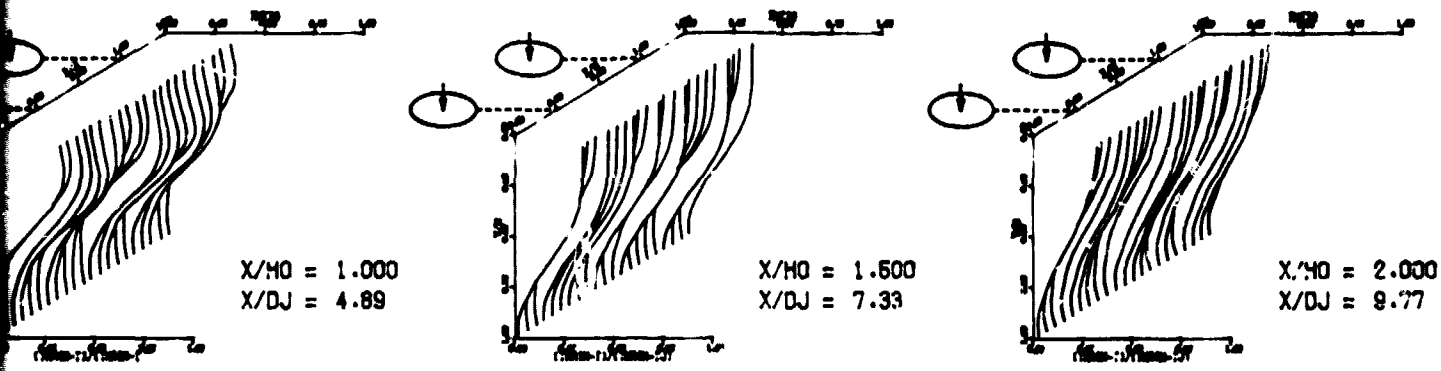

I. TMAIN=CONST. , J = 5.74 , S/D = 2.00 , H/D = 4.00

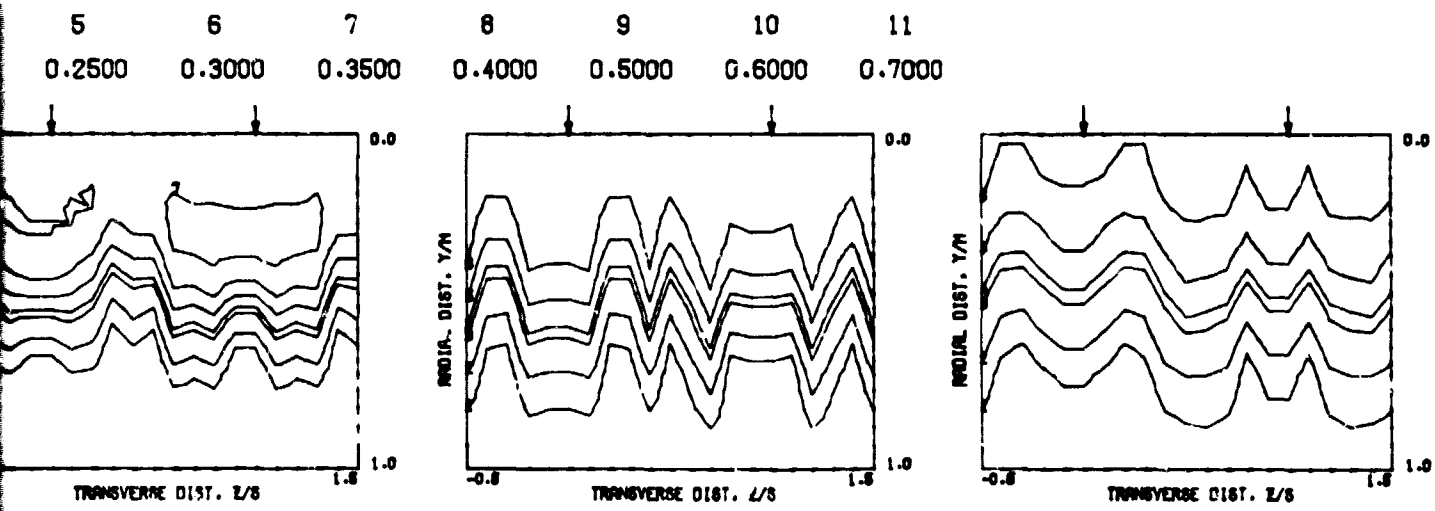

ST NO.1. TMAIN=CONST. J=5.74. S/D=2.0. H/D=4.0

Figure 12

ORIGINAL PAGE IS
OF POOR QUALITY

FOLDOUT FRAME

CONTOUR	1	2	3	4	5	6	7
VALUE	0.0500	0.1000	0.1759	0.2000	0.2500	0.3000	0.3500

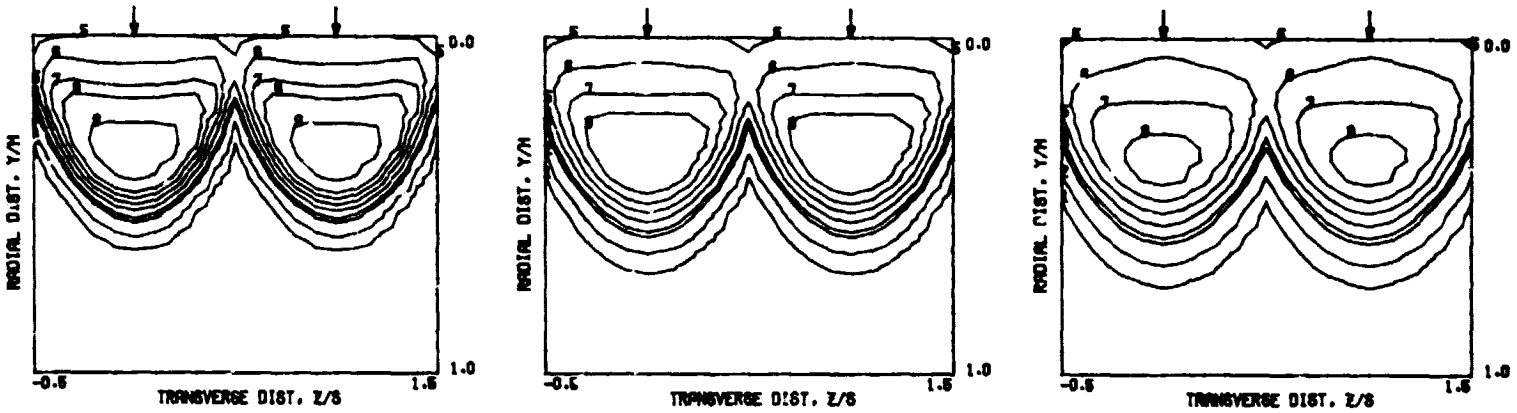

PREDICTED THETA CONTOURS FOR TEST NO. 1. TMAIN=CONST. J

S/DJ = 2.44 HO/DJ = 4.89 VRATIO = 1.65 TRATIO = 0.474 DENRATIO=2.113 TMAI

X/H = 0.50 X/DJ =2.44 X/H = 0.75 X/DJ =3.67 X/H = 1.00 X/DJ =4.89

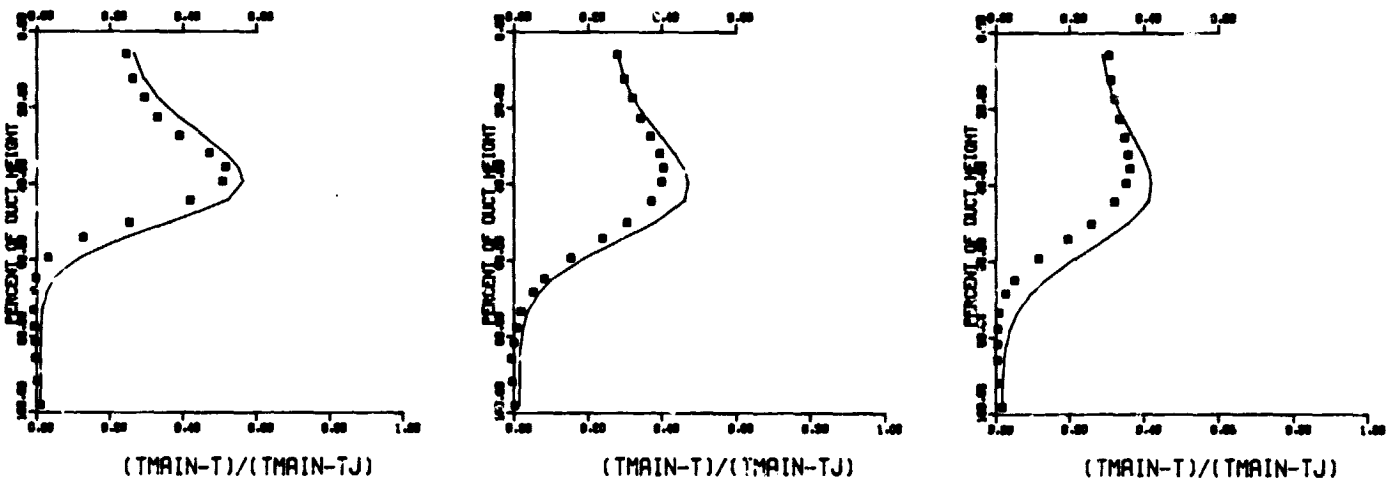

COMPARISON BETWEEN DATA AN CORRELATIONS FOR TEST NO. 1. TEST SECTION I. TMAI

FOLDOUT FRAME

ORIGINAL PAGE IS
OF POOR QUALITY

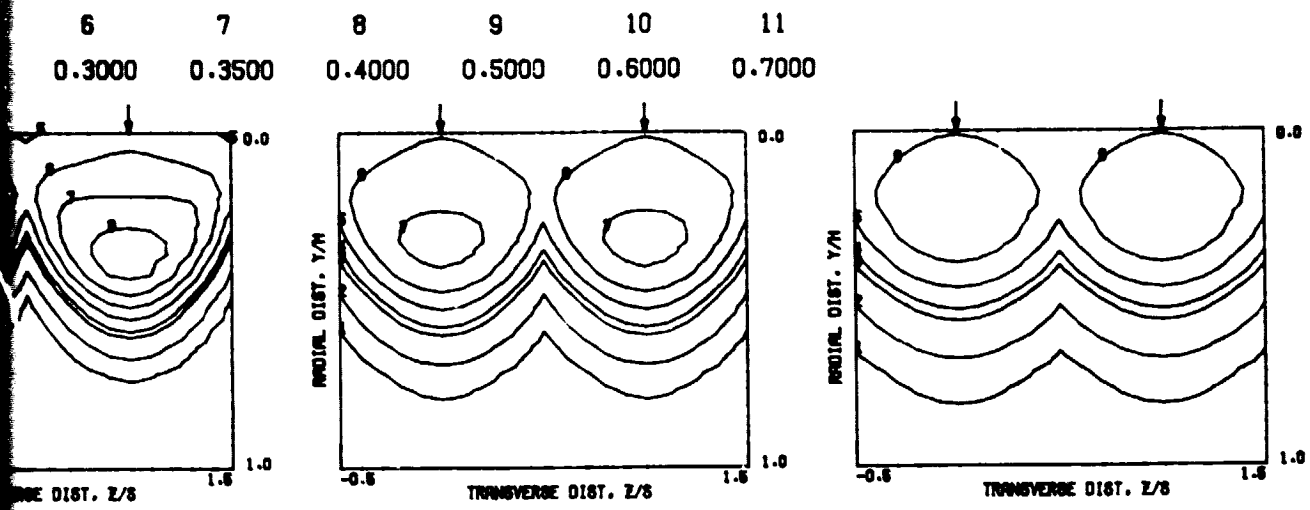

1. TMAIN=CONST. J=5.74. S/D=2.0 H/D=4.0

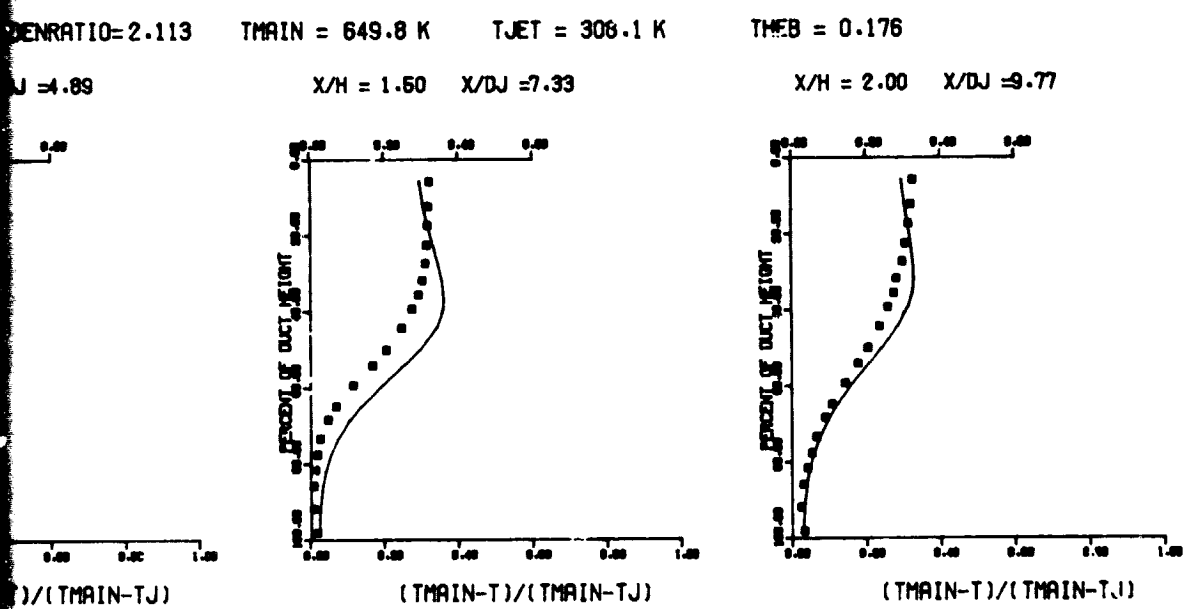

SECTION I. TMAIN = CONST. J = 5.74 , S/D =2.00 , H/D =4.00

Figure 13

2 FOLDOUT FRAME
ORIGINAL PAGE IS
OF POOR QUALITY

S = 0.0508 METERS S/DJ = 2.582 HO/DJ = 5.164 VMAIN = 16.3 M/SEC VJET = 52.0 M/SEC TMAIN = 651.2 K TJET

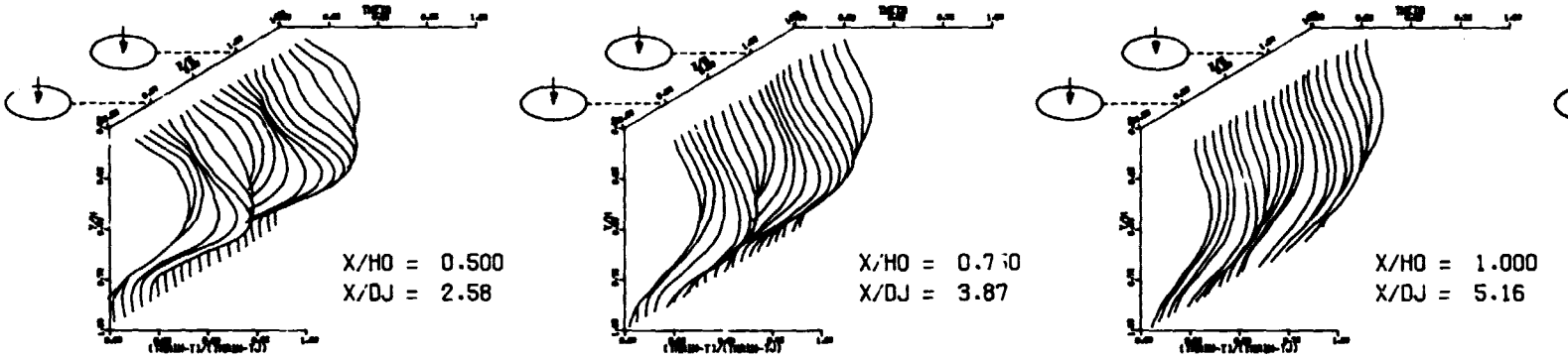

MEASURED THETA PROFILES FOR TEST NO. 2, TEST SECTION I, TMAIN=CONST. , J = 21

CONTOUR	1	2	3	4	5
VALUE	0.0600	0.1200	0.1800	0.2400	0.2705

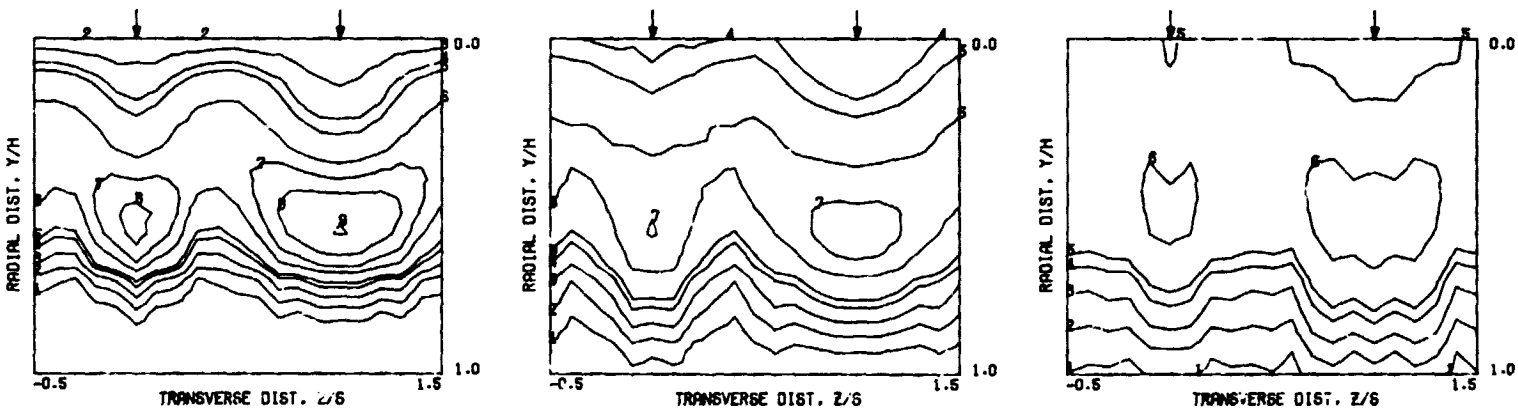

MEASURED THETA CONTOURS FOR TEST NO. 2, TMAIN=CONST, J=

ORIGINAL PAGE IS OF POOR QUALITY

FOLDOUT FRAME

M/SEC TMAIN = 651.2 K TJET = 308.0 K THEB = 0.2705 BLORAT= 6.281 DENRATIO= 2.132 TRATIO= 0.473

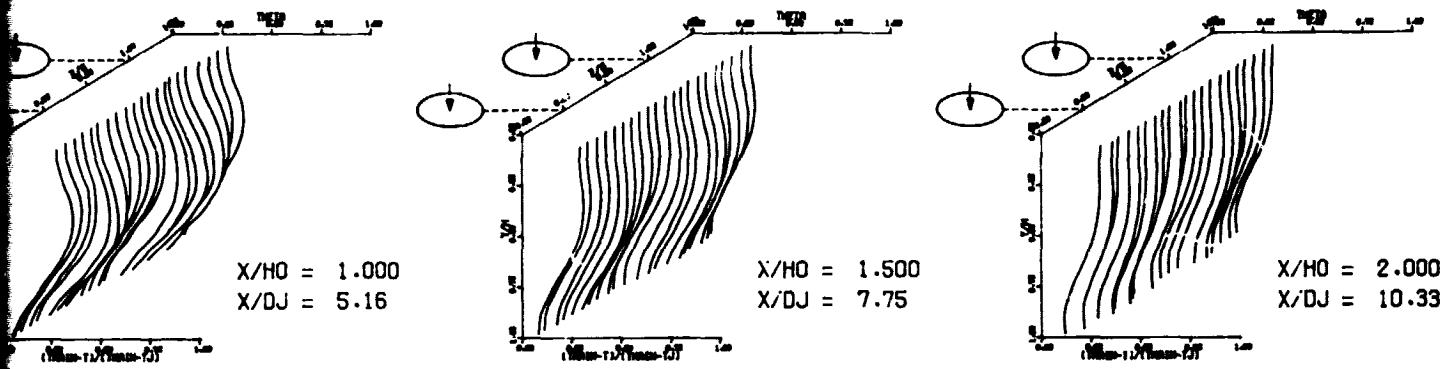

I, TMAIN=CONST. , J = 21.59 , S/D = 2.00 , H/D = 4.00

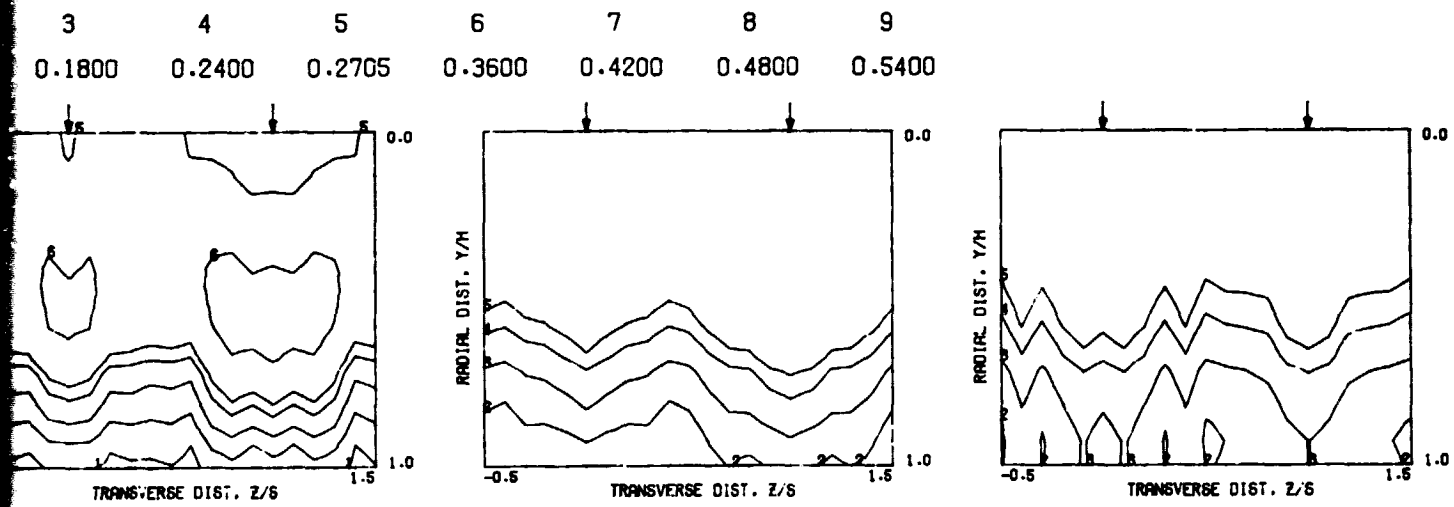

EST NO. 2, TMAIN=CONST, J=21.59, S/D=2.0, H/D=4.0

Figure 14

2 FOLDOUT FRAME

ORIGINAL PAGE IS
OF POOR QUALITY

CONTOUR	1	2	3	4	5	6
VALUE	0.0600	0.1200	0.1800	0.2400	0.2705	0.360

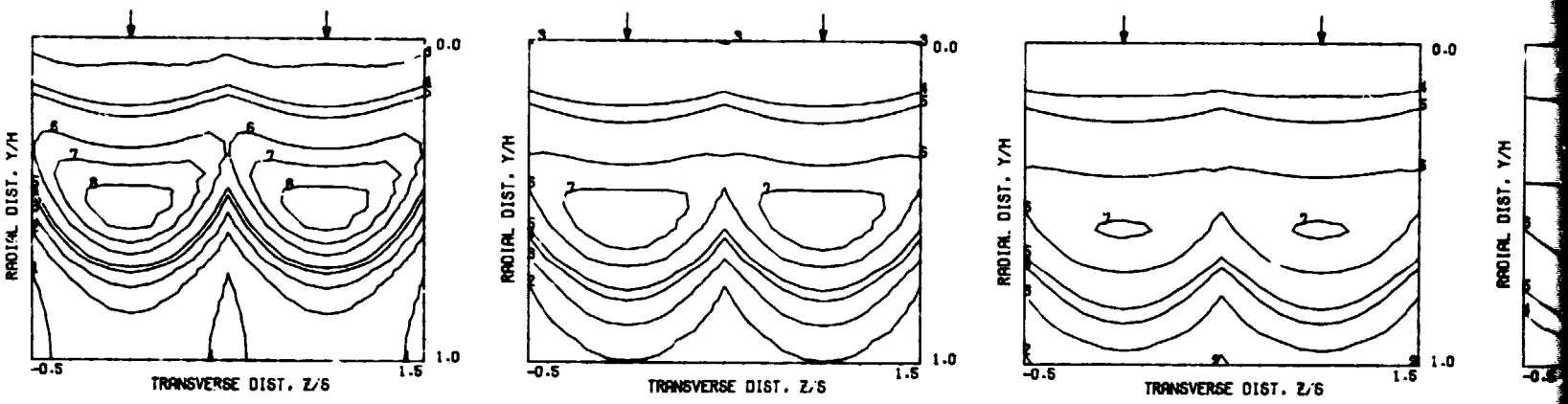

PREDICTED THETA CONTOURS FOR TEST NO.2, TMAIN=CONST. J=21.59

S/DJ = 2.58 HO/DJ = 5.16 VRATIO = 3.18 TRATIO = 0.473 DENRATIO=2.132 TMAIN = 651

X/H = 0.50 X/DJ =2.58 X/H = 0.75 X/DJ =3.87 X/H = 1.00 X/DJ =5.16 X/H =

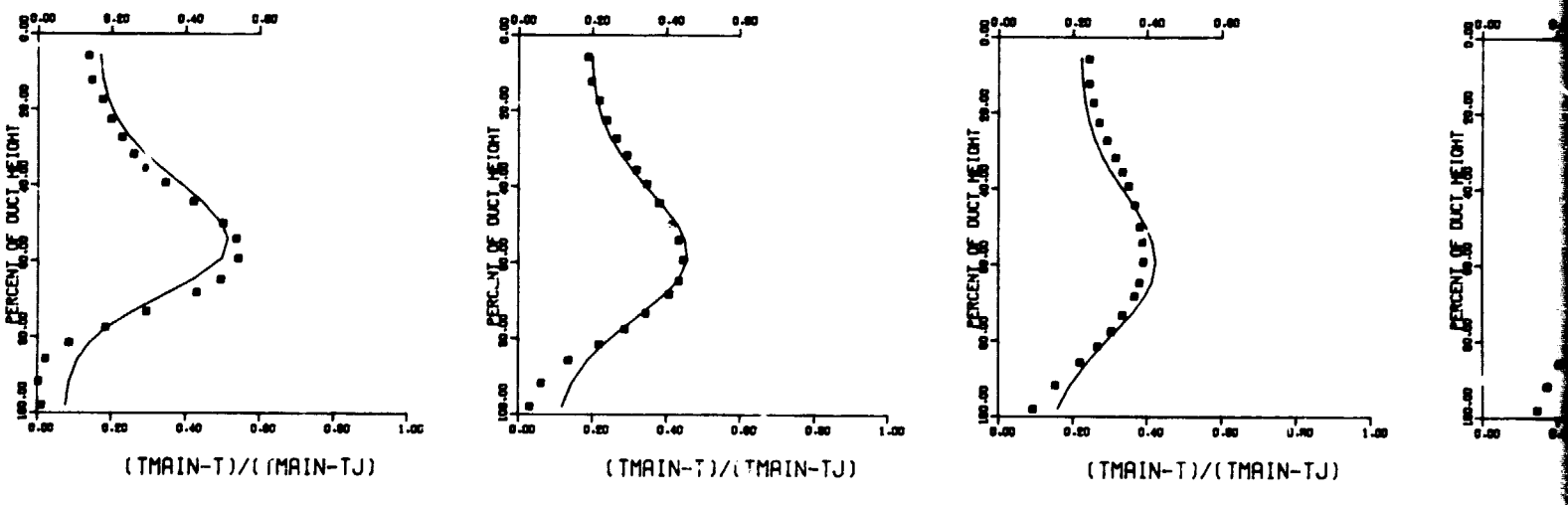

COMPARISON BETWEEN DATA AND CORRELATION. FOR TEST NO. 2, TEST SECTION I ,UNIFORM TMAI

FOLDOUT FRAME

ORIGINAL PAGE IS
OF POOR QUALITY

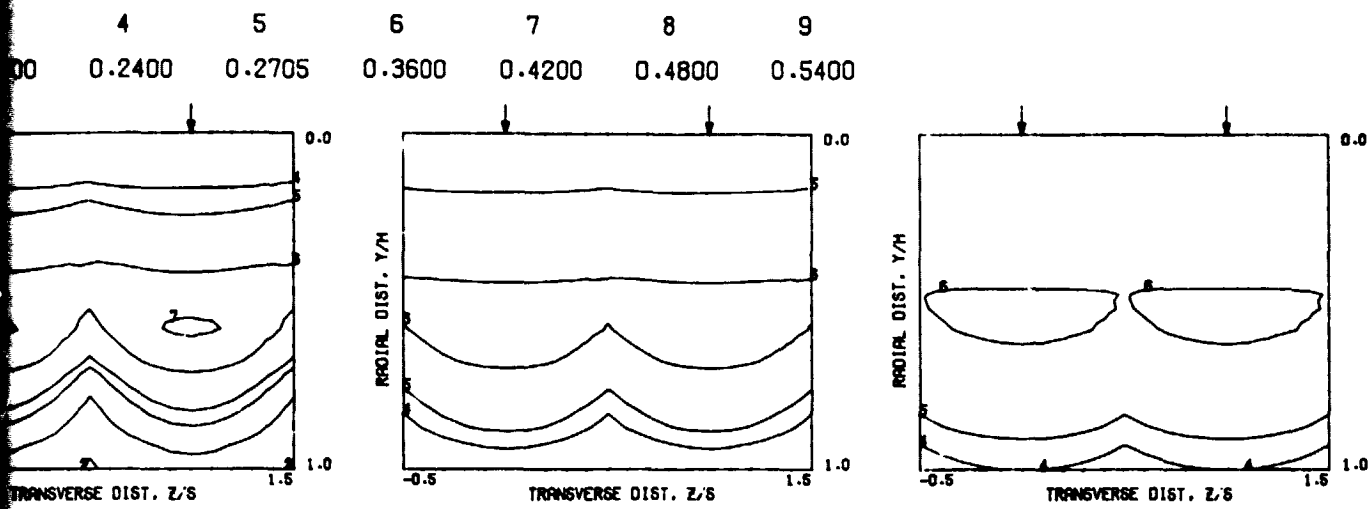

NO.2, TMAIN=CONST, J=21.59, S/D=2.0, H/D=4.0

DENRATIO=2.132 TMAIN = 651.2 K TJET = 308.0 K THEB = 0.271

X/DJ =5.16 X/H = 1.50 X/DJ =7.75 X/H = 2.00 X/DJ =10.33

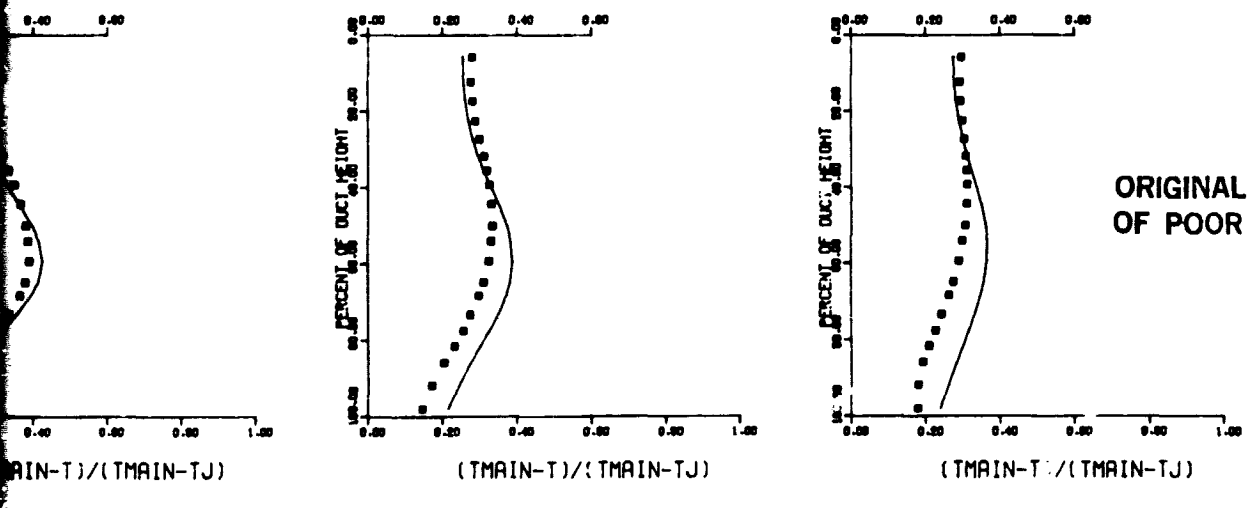

ORIGINAL PAGE IS
OF POOR QUALITY

EST SECTION I UNIFORM TMAIN, J = 21.59 , S/D =2.00 , H/D =4.00

Figure 15

FOLDOUT FRAME

S = 0.1016 METERS S/DJ = 4.682 HO/DJ = 4.682 VMAIN = 15.2 M/SEC VJET = 25.9 M/SEC TMAIN = 649.3 K TJ

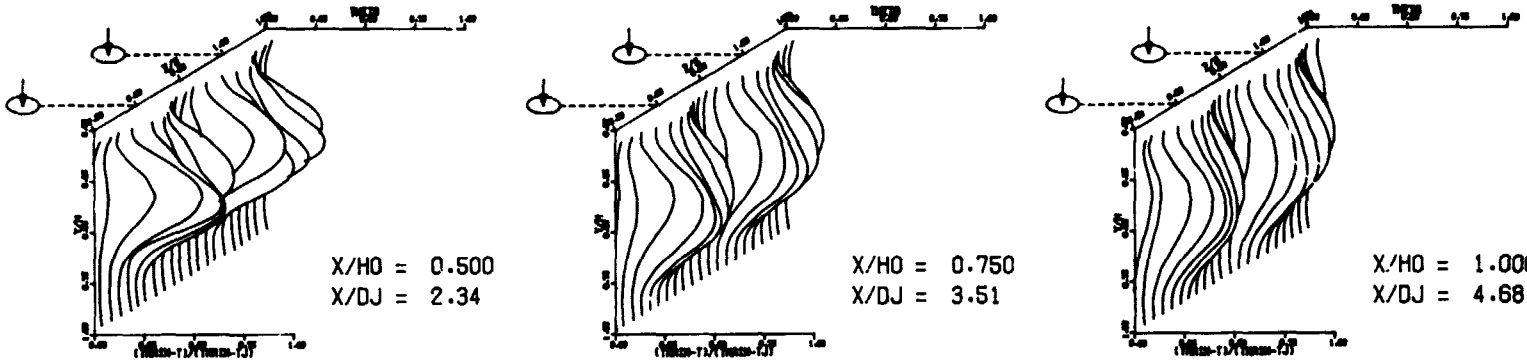

MEASURED THETA PROFILES FOR TEST NO. 3, TEST SECTION I, TMAIN=CONST. , J =

CONTOUR	1	2	3	4	5
VALUE	0.0250	0.0750	0.1074	0.1750	0.2250

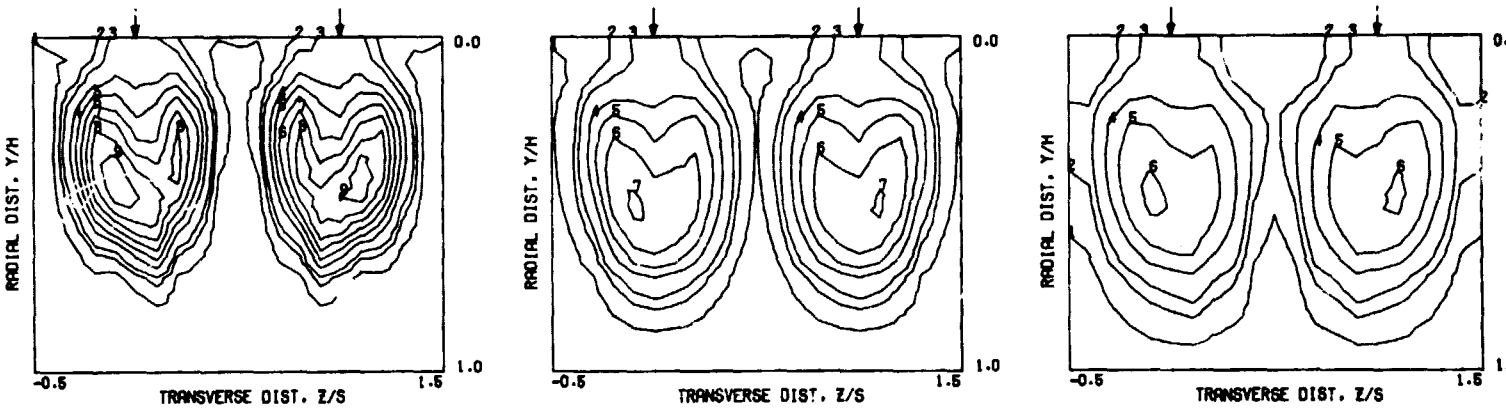

MEASURED THETA CONTOURS FOR TEST NO. 3, TMAIN=CONST. J

FOLDOUT FRAME

ORIGINAL PAGE IS
OF POOR QUALITY

M/SEC TMAIN = 649.3 K TJET = 306.9 K THEB = 0.1074 BLORAT= 3.356 DENRATIO= 2.122 TRATIO=0.473

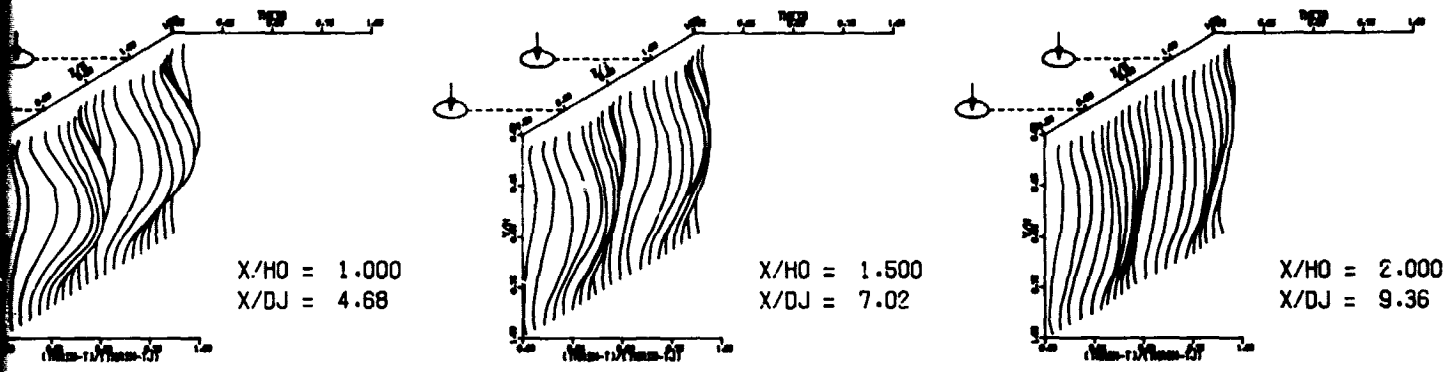

I, TMAIN=CONST. , J = 6.14 , S/D = 4.00 , H/D = 4.00

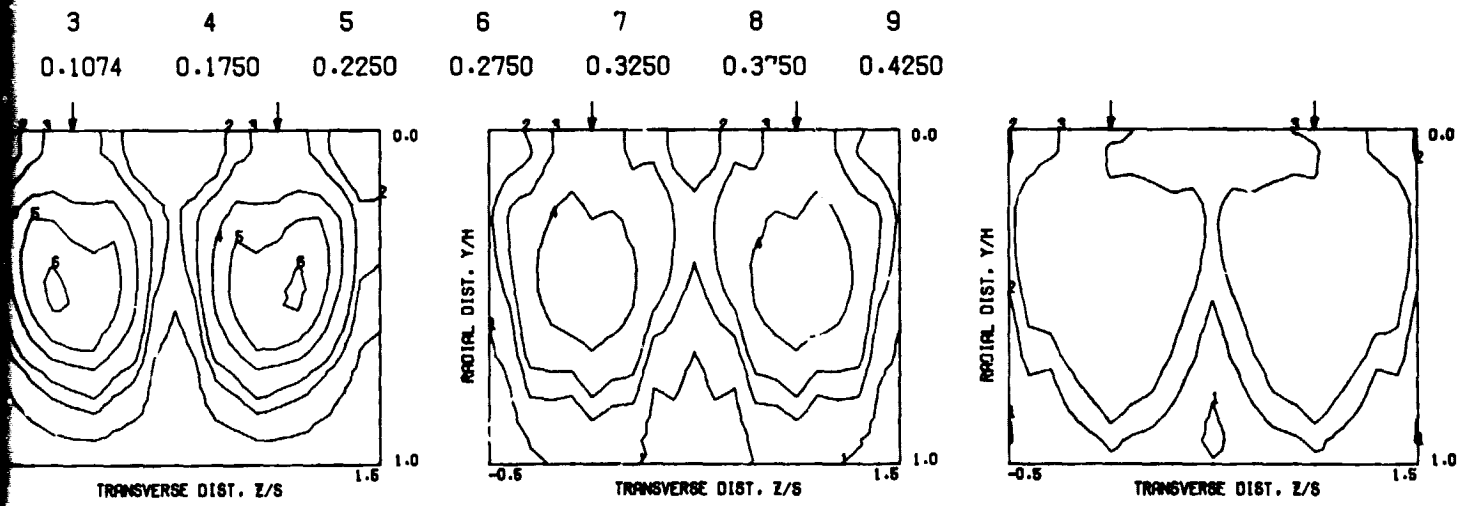

EST NO. 3, TMAIN=CONST, J=6.14, S/D=4.0, H/D=4.0

ORIGINAL PAGE IS
OF POOR QUALITY

Figure 16

FOLDOUT FRAME

CONTOUR	1	2	3	4	5
VALUE	0.0250	0.0750	0.1074	0.1750	0.2250

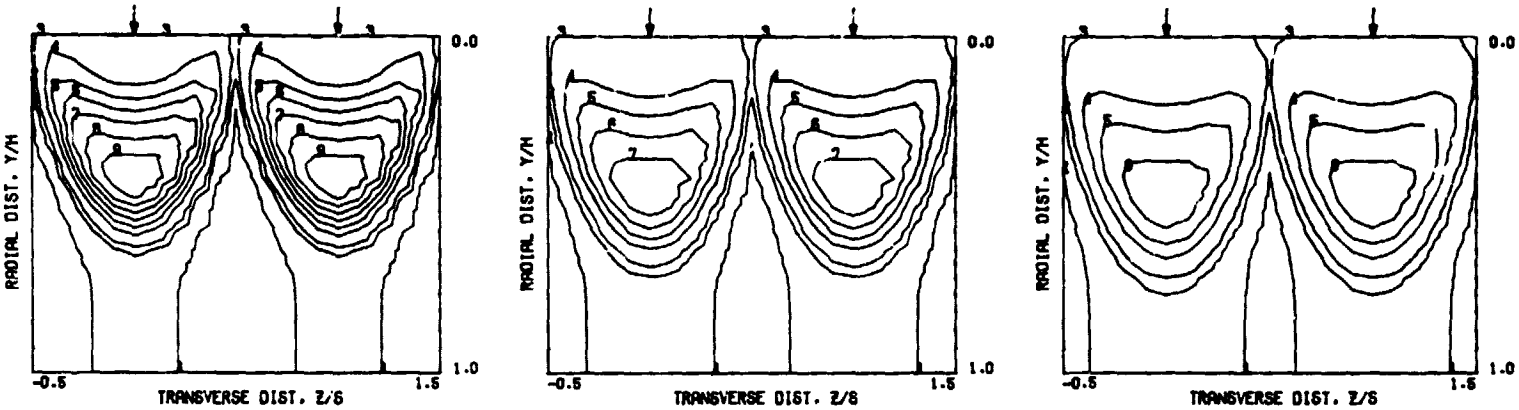

PREDICTED THETA CONTOURS FOR TEST NO.3. TMAIN=CONST. J=6.

ORIGINAL PAGE IS
OF POOR QUALITY

S/DJ = 4.68 HO/DJ = 4.68 VRATIO = 1.70 TRATIO = 0.473 DENRATIO=2.122 TMAIN

X/H = 0.50 X/DJ =2.34 X/H = 0.75 X/DJ =3.51 X/H = 1.00 X/DJ =4.68

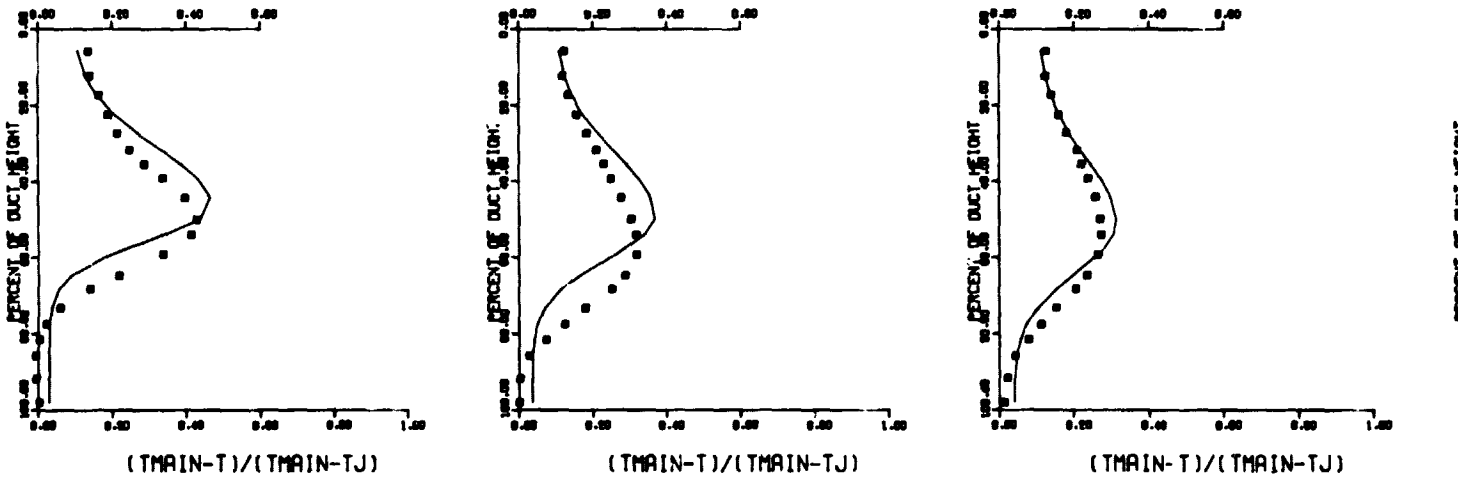

COMPARISON BETWEEN DATA AND CORRELATIONS FOR TEST NO. 3. TEST SECTION I .UNIFORI

FOLDOUT FRAME

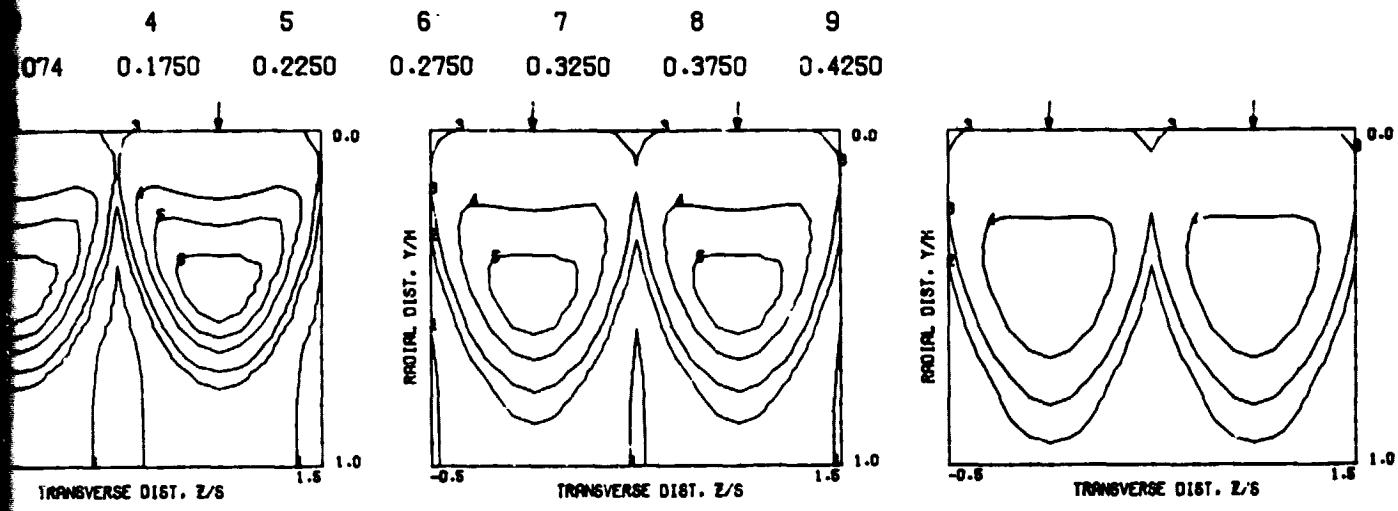

NO.3. TMAIN=CONST. J=6.14. S/D=4.0. H/D=4.0

ORIGINAL PAGE IS
OF POOR QUALITY

73 DENRATIO=2.122 TMAIN = 649.3 K TJET = 306.9 K THEB = 0.107

00 X/DJ =4.68 X/H = 1.50 X/DJ =7.02 X/H = 2.00 X/DJ =9.36

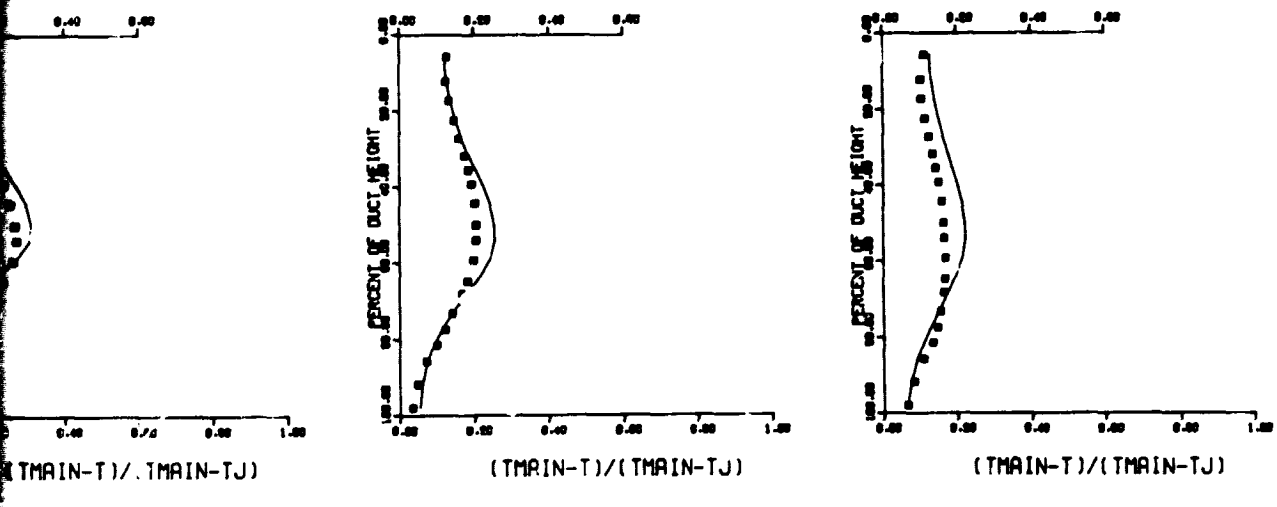

TEST SECTION I .UNIFORM TMAIN. J = 6.14 . S/D =4.00 . H/D =4.00

Figure 17

2 FOLDOUT FRAME

S = 0.1016 METERS S/DJ = 4.869 HO/DJ = 4.869 VMAIN = 14.9 M/SEC VJET = 52.2 M/SEC TMAIN = 651.

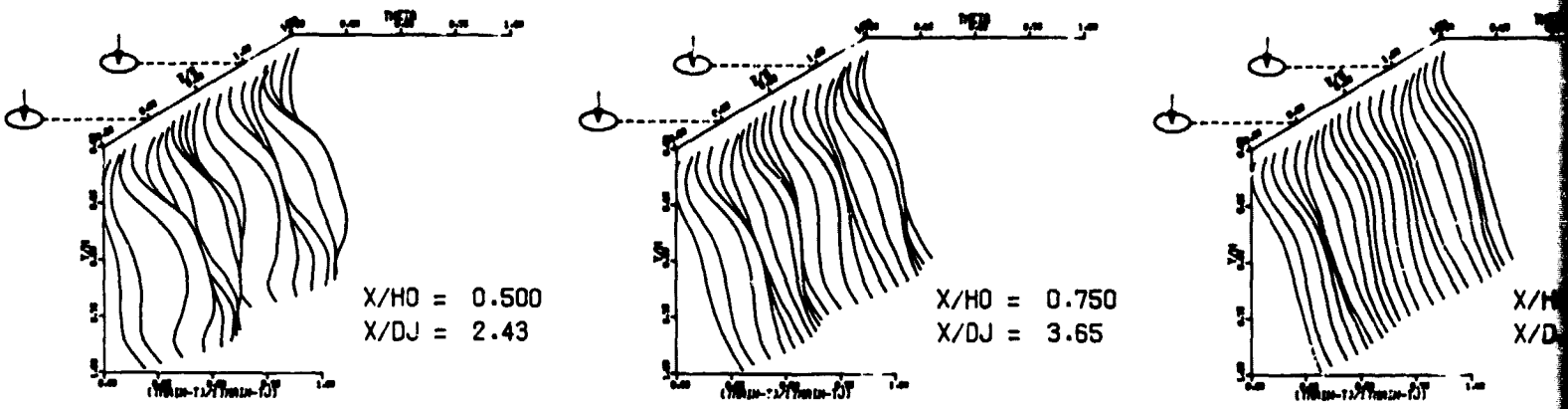

MEASURED THETA PROFILES FOR TEST NO. 4, TEST SECTION I, TMAIN=CONST.

CONTOUR	1	2	3	4
VALUE	0.0500	0.1000	0.1500	0.1915

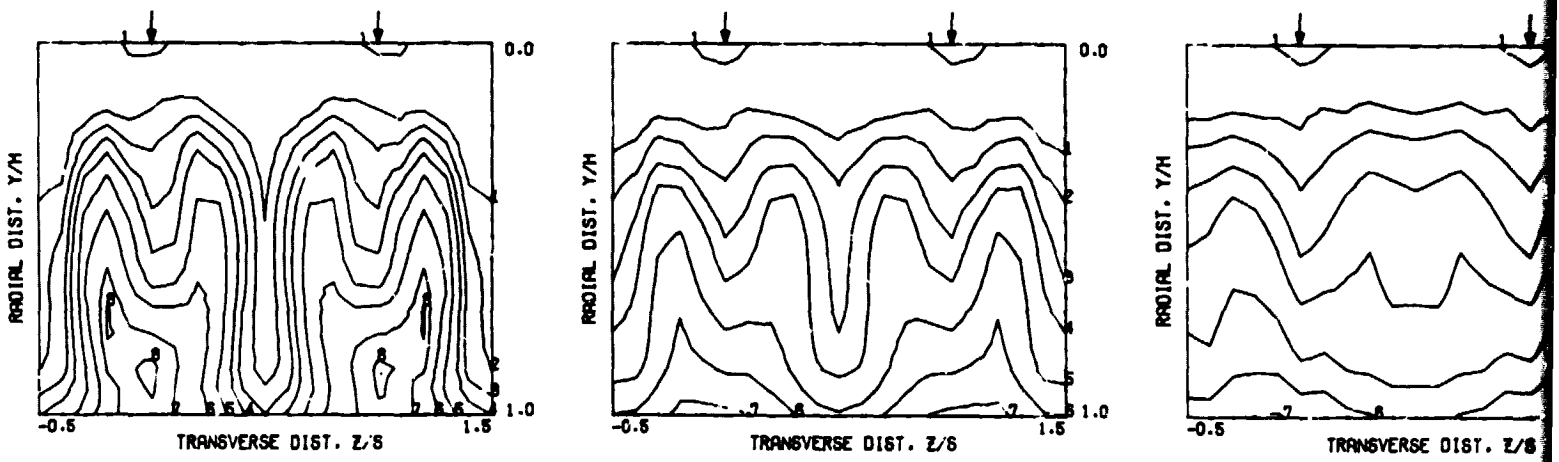

MEASURED THETA CONTOURS FOR TEST NO. 4, TMAIN=

FOLDOUT FRAME

ORIGINAL PAGE IS
OF POOR QUALITY

TMAIN = 651.2 K TJET = 304.0 K THEB = 0.1915 BLORAT= 7.148 DENRATIO= 2.174 TRATIO=0.467

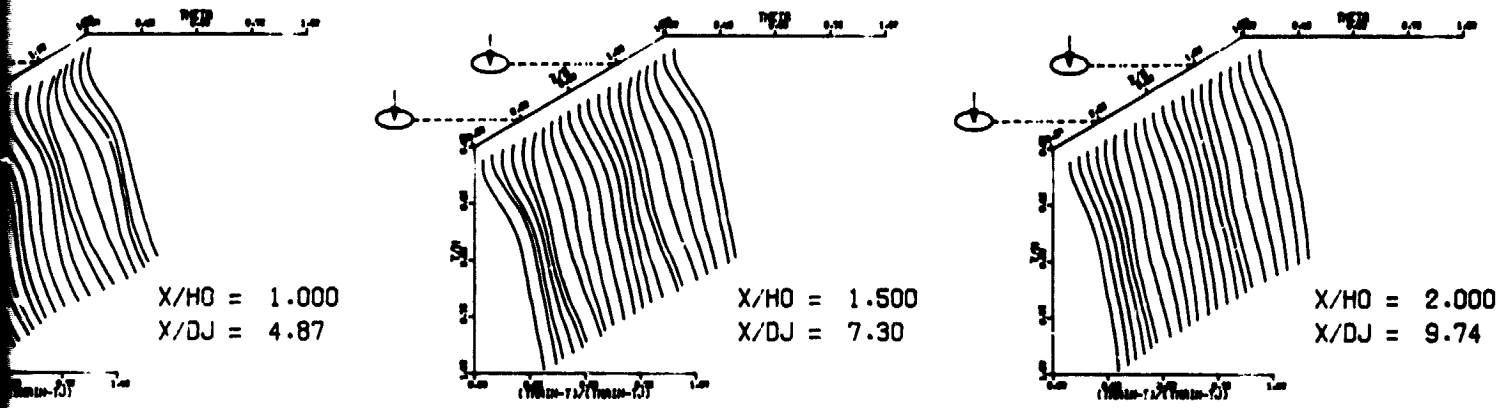

MAIN=CONST. , J = 26.68 , S/D = 4.00 , H/D = 4.00

4 5 6 7 8

0.1915 0.2500 0.3000 0.3500 0.3750

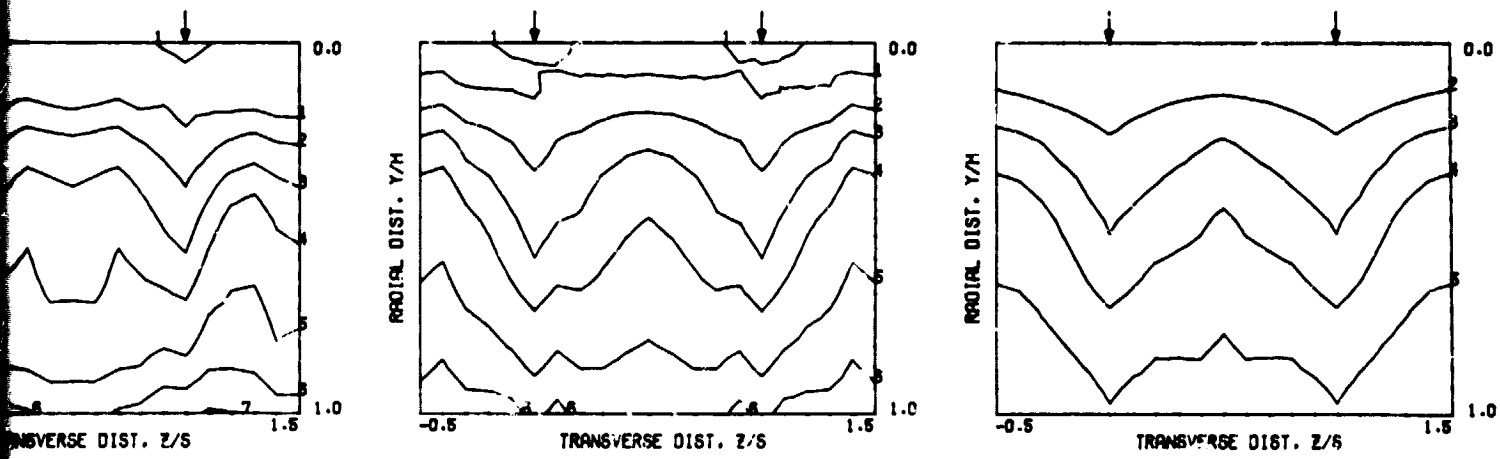

4. TMAIN=CONST. J=26.7. S/D=4.0. H/D=4.0

FOLDOUT FRAME

ORIGINAL PAGE IS
OF POOR QUALITY

Figure 18

CONTOUR	1	2	3	4	5
VALUE	0.0500	0.1000	0.1500	0.1915	0.2500

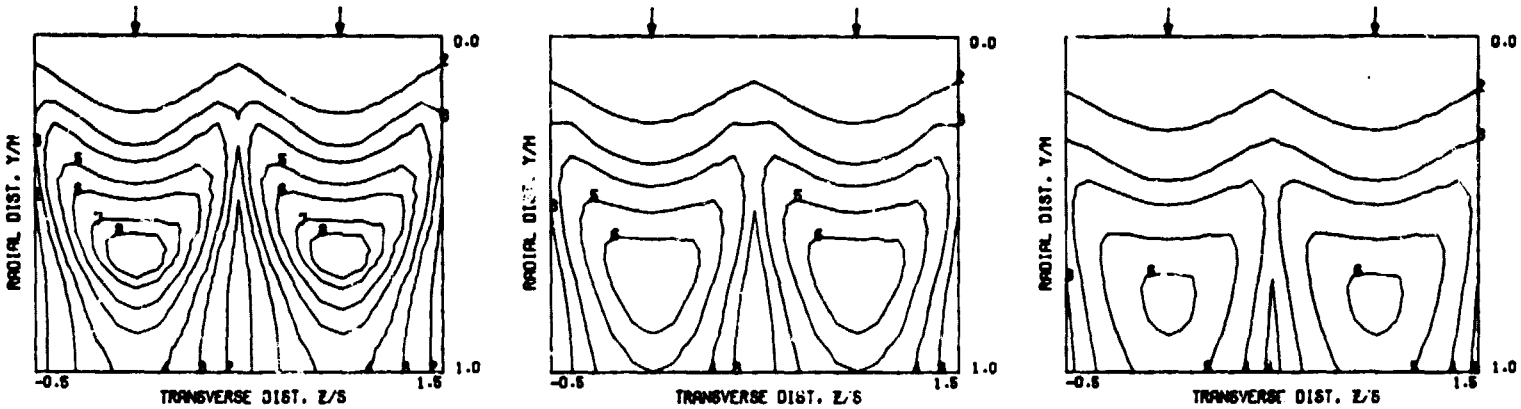

PREDICTED THETA CONTOURS FOR TEST NO.4. TMAIN=CONST. J=26

ORIGINAL PAGE IS
OF POOR QUALITY

S/DJ = 4.87 HO/DJ = 4.87 VRATIO = 3.50 TRATIO = 0.467 DENRATIO=2.174 TMAIN

X/H = 0.50 X/DJ = 2.43 X/H = 0.75 X/DJ =3.65 X/H = 1.00 X/DJ =4.87

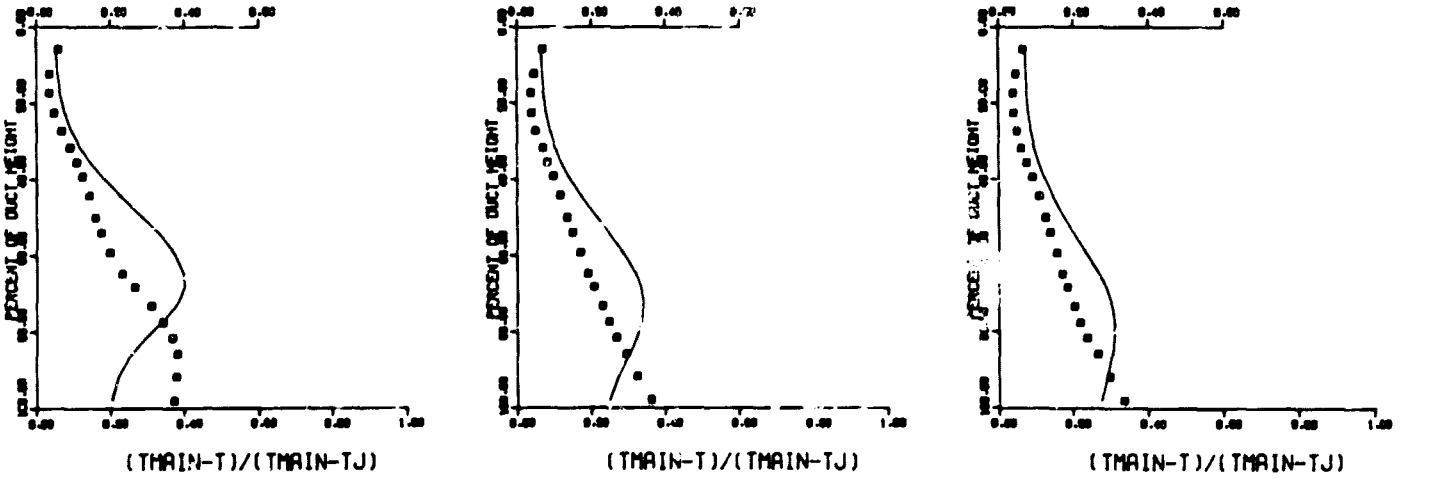

FOLDOUT FRAME

COMPARISON BETWEEN DATA AND CORRELATIONS FOR TEST NO. 4. TEST SECTION 1 .UNIFORM

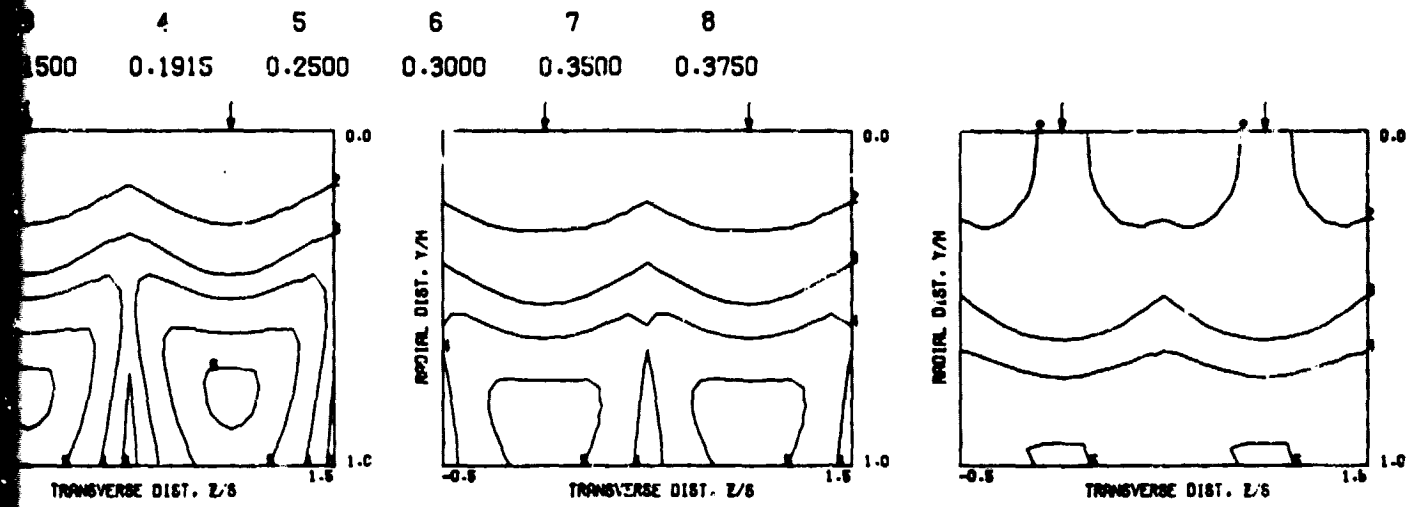

NO.4. TMAIN=CONST. J=26.7. S/D=4.0. H/D=4.0

ORIGINAL PAGE IS
OF POOR QUALITY

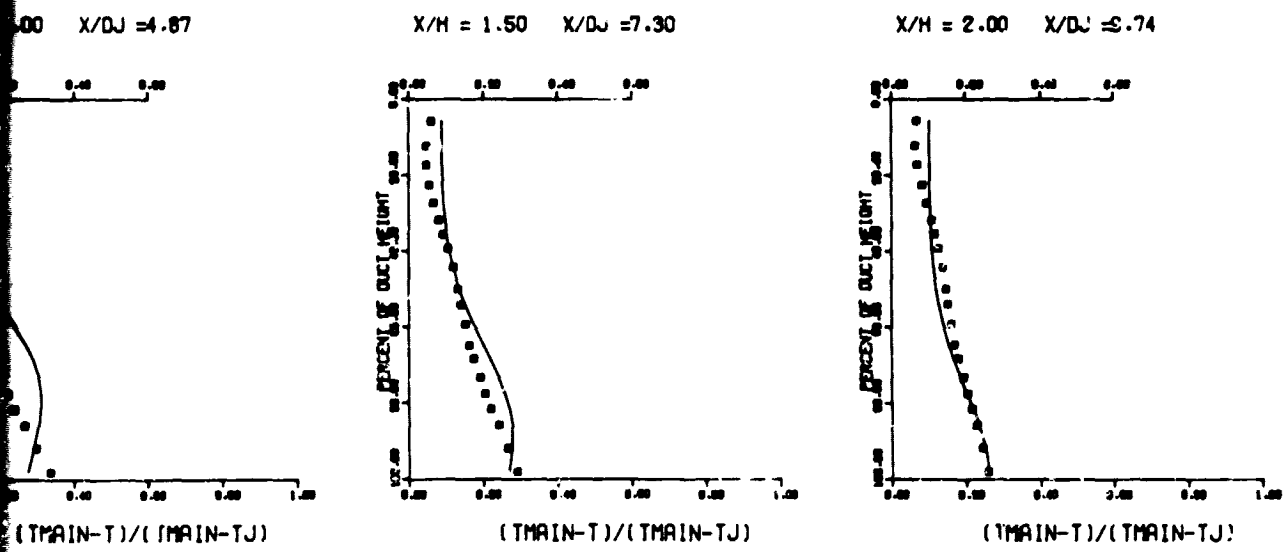

2 FOLDOUT FRAME

Figure 19

. TEST SECTION I .UNIFORM TMAIN. J = 26.68 . S/D =4.00 . H/D =4.00

S = 0.0254 METERS S/DJ = 2.582 HO/DJ = 10.328 VMAIN = 15.0 M/SEC VJET = 51.9 M/SEC TMAIN = 648.7 K

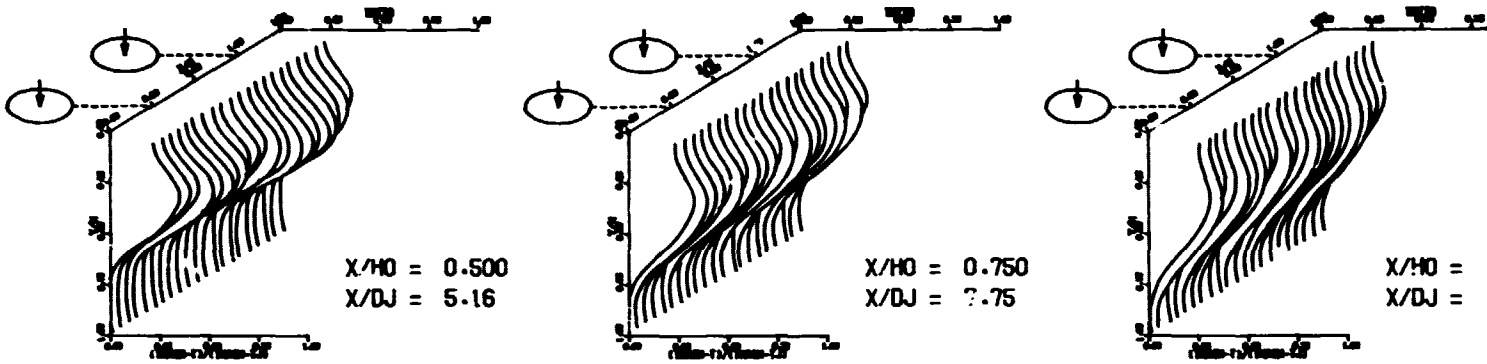

MEASURED THETA PROFILES FOR TEST NO. 5, TEST SECTION I, TMAIN=CONST. ,

CONTOUR	1	2	3	4	5
VALUE	0.0500	0.1000	0.1687	0.2000	0.2

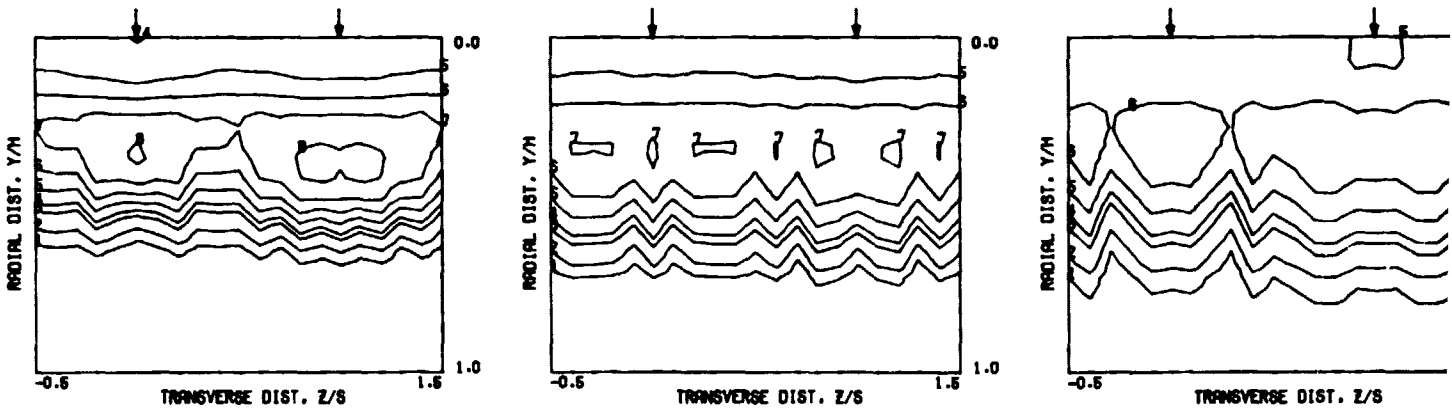

MEASURED THETA CONTOURS FOR TEST NO. 5, TMAIN=CONS

FOLDOUT FRAME

C-2

ORIGINAL PAGE IS
OF POOR QUALITY

EC TMAIN = 648.7 K TJET = 308.3 K THEB = 0.1687 BLORAT= 6.890 DENRATIO= 2.128 TRATIO=0.475

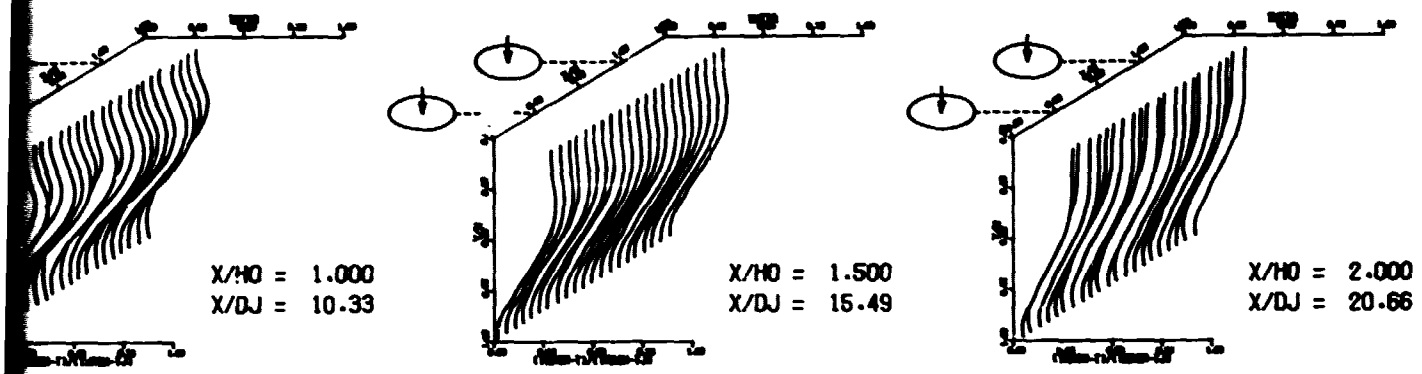

TMAIN=CONST. , J = 25.32 , S/D = 2.00 , H/D = 8.00

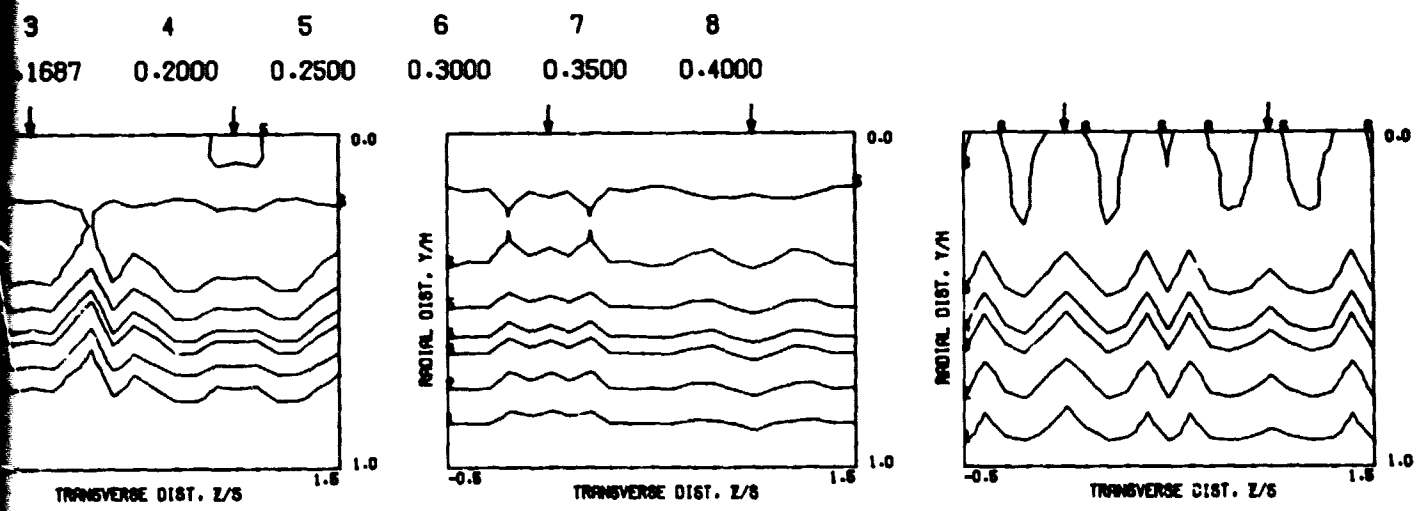

NO. 5. TMAIN=CONST. J=25.32. S/D=2.0. H/D=8.0

ORIGINAL PAGE IS
OF POOR QUALITY

Figure 20

2 FOLDOUT FRAME

CONTOUR	1	2	3	4	5
VALUE	0.0500	0.1000	0.1687	0.2000	0.2500

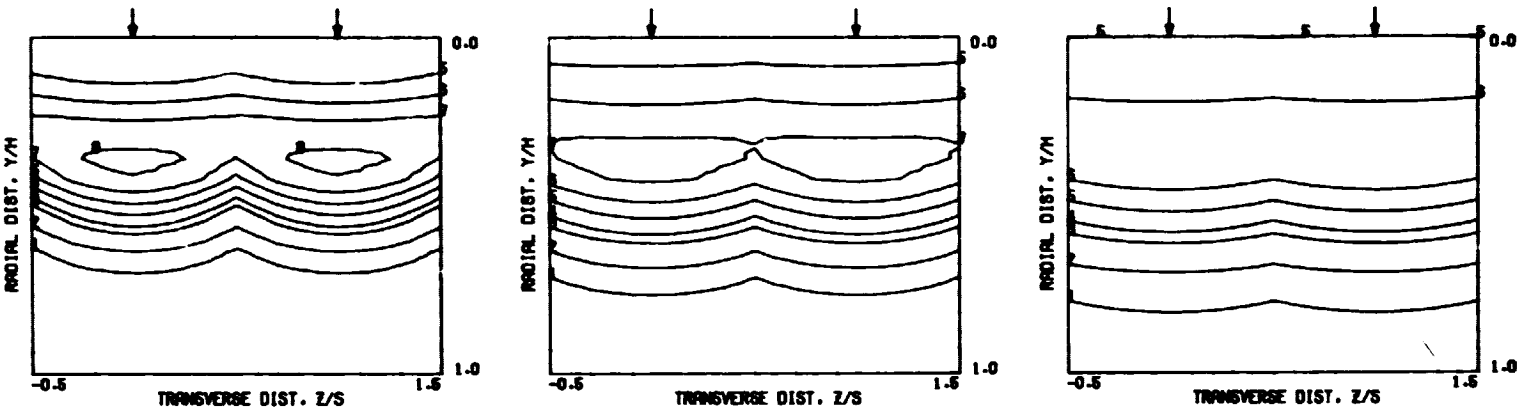

PREDICTED THETA CONTOURS FOR TEST NO.5. TMAIN=CONST. J=2

S/DJ = 2.58 HO/DJ = 10.33 VRATIO = 3.45 TRATIO = 0.475 DENRATIO=2.128 TMAIN

X/H = 0.50 X/DJ =5.16 X/H = 0.75 X/DJ =7.75 X/H = 1.00 X/DJ =10.33

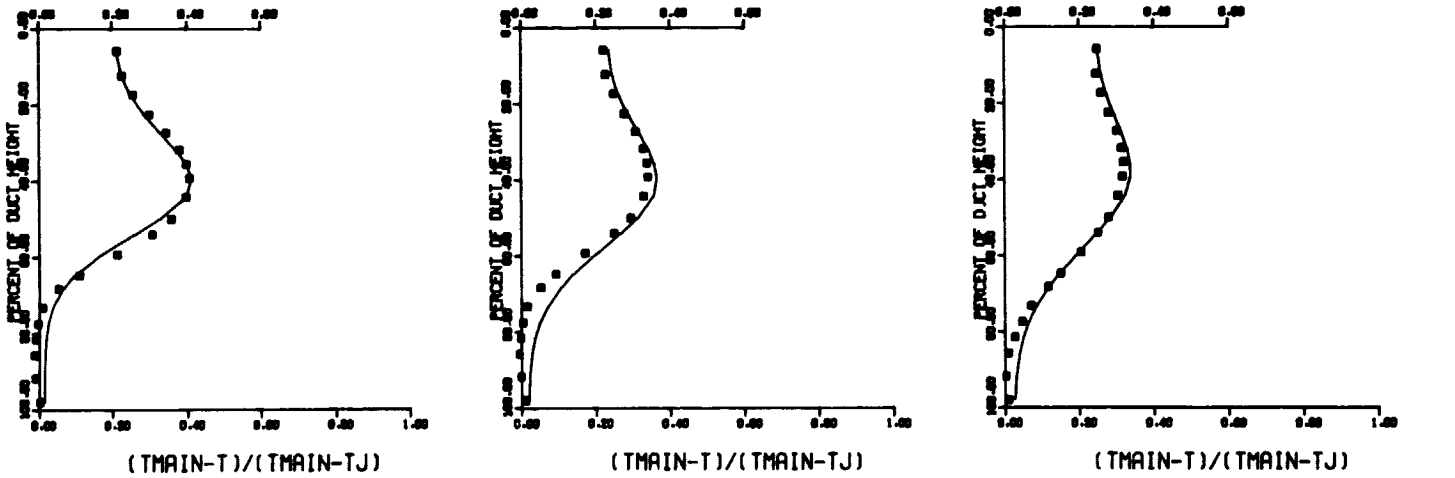

FOLDOUT FRAME

COMPARISON BETWEEN DATA AND CORRELATIONS FOR TEST NO. 5. TEST SECTION I ,UNIFORM

ORIGINAL PAGE IS
OF POOR QUALITY

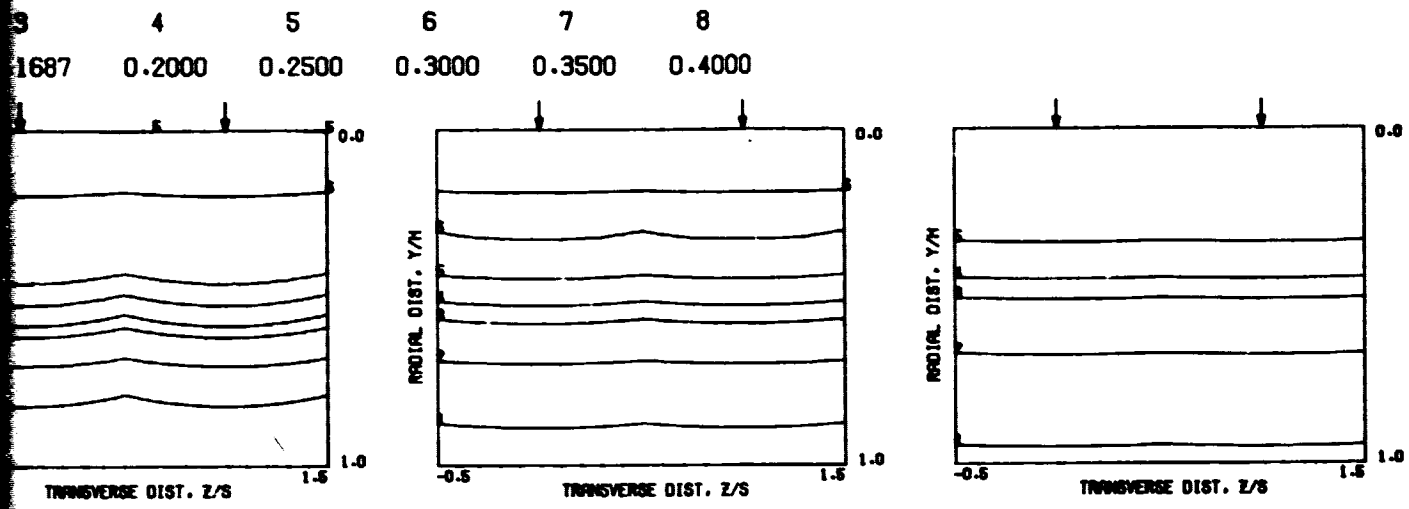

NO.5, TMAIN=CONST, J=25.3, S/D=2.0, H/D=8.0

75 DENRATIO=2.128 TMAIN = 648.7 K TJET = 308.3 K THEB = 0.169

00 X/DJ =10.33 X/H = 1.50 X/DJ =15.49 X/H = 2.00 X/DJ =20.66

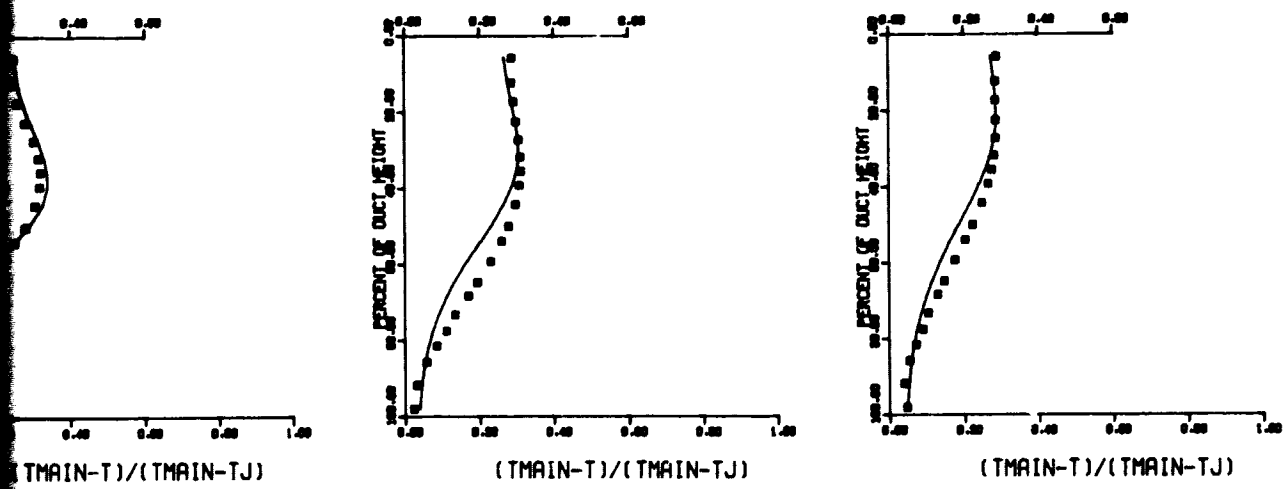

2 FOLDOUT FRAME

Figure 21

TEST SECTION I ,UNIFORM TMAIN, J = 25.32 , S/D =2.00 , H/D =8.00

ORIGINAL PAGE IS
OF POOR QUALITY

S = 0.0254 METERS S/DJ = 2.571 HO/DJ = 10.285 VMAIN = 15.1 M/SEC VJET = 103.6 M/SEC TMAIN = 649.7 K TJE

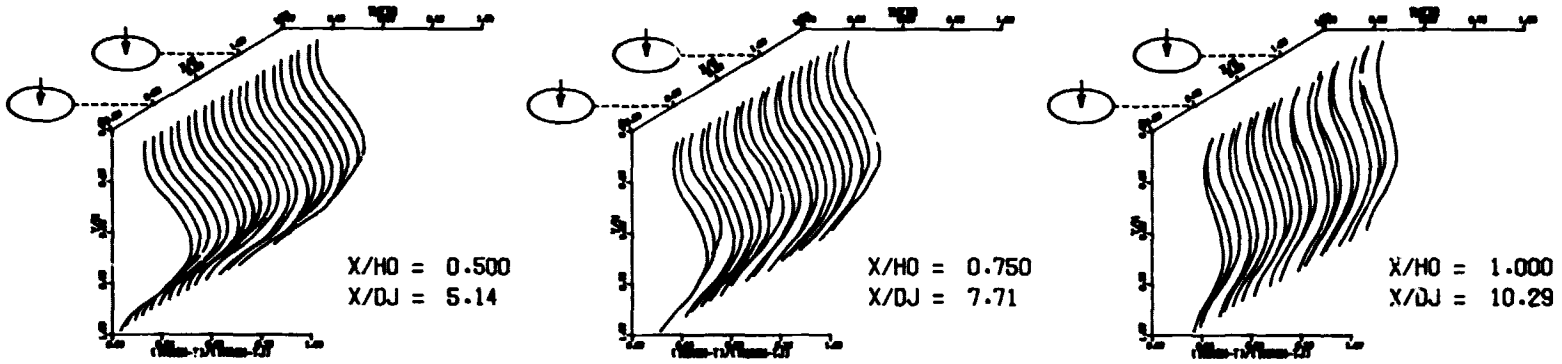

MEASURED THETA PROFILES FOR TEST NO. 6, TEST SECTION I, TMAIN=CONST. , J =

CONTOUR	1	2	3	4	5	6	7
VALUE	0.0500	0.1000	0.1500	0.2000	0.2500	0.3018	0.3500

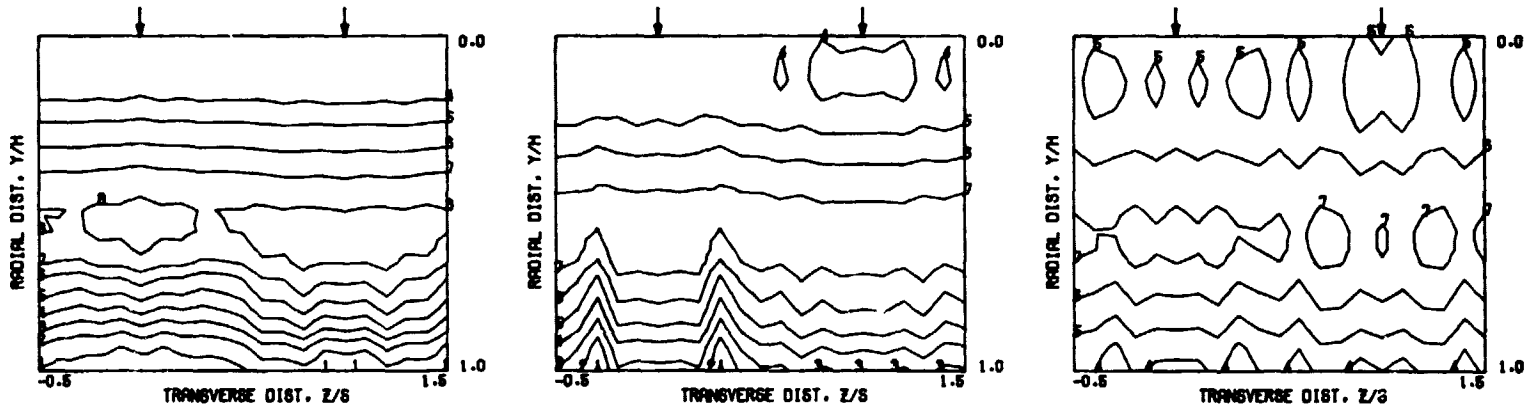

MEASURED THETA CONTOURS FOR TEST NO. 6, TMAIN=CONST, J

ORIGINAL PAGE IS
OF POOR QUALITY

FOLDOUT FRAME

/SEC TMAIN = 649.7 K TJET = 299.2 K THEB = 0.3018 BLORAT= 14.554 DENRATIO= 2.287 TRATIO= 0.460

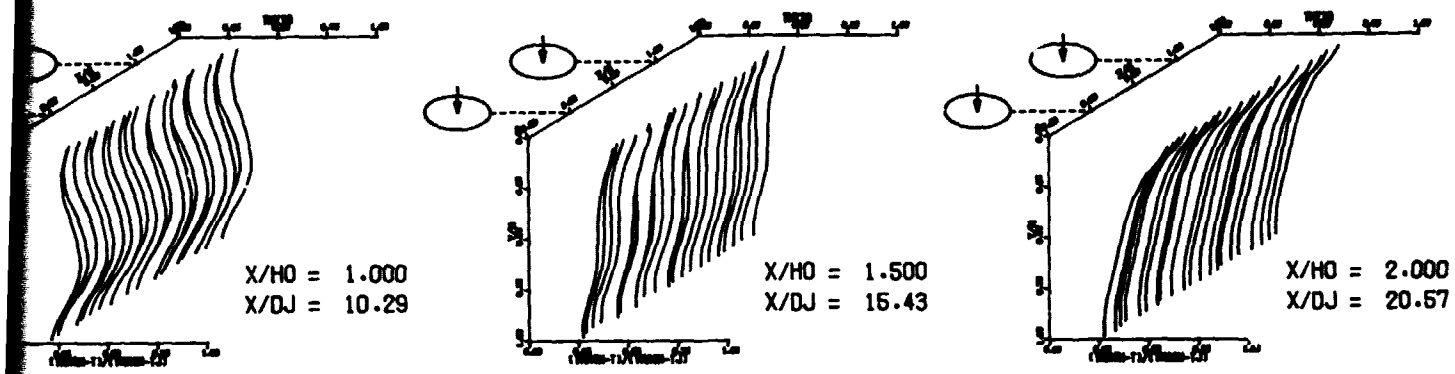

I, TMAIN=CONST. , J = 107.78 , S/D = 2.00 , H/D = 8.00

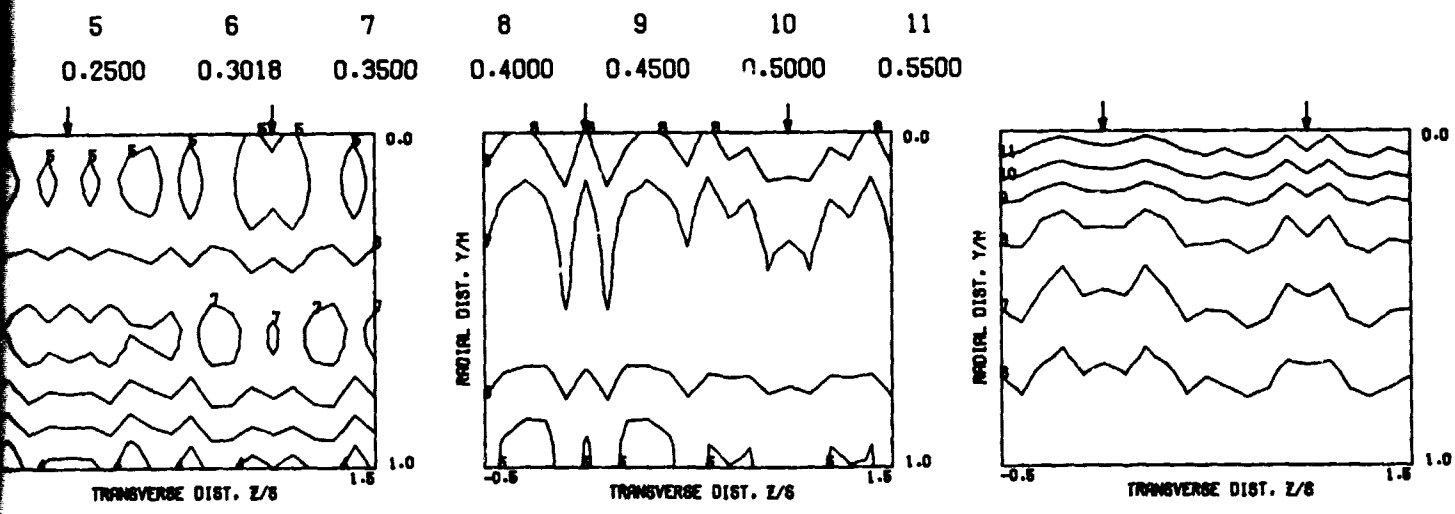

EST NO. 6, TMAIN=CONST, J=107.8, S/D=2.0, H/D=8.0

2 FOLDOUT FRAME

Figure 22

ORIGINAL PAGE IS OF POOR QUALITY

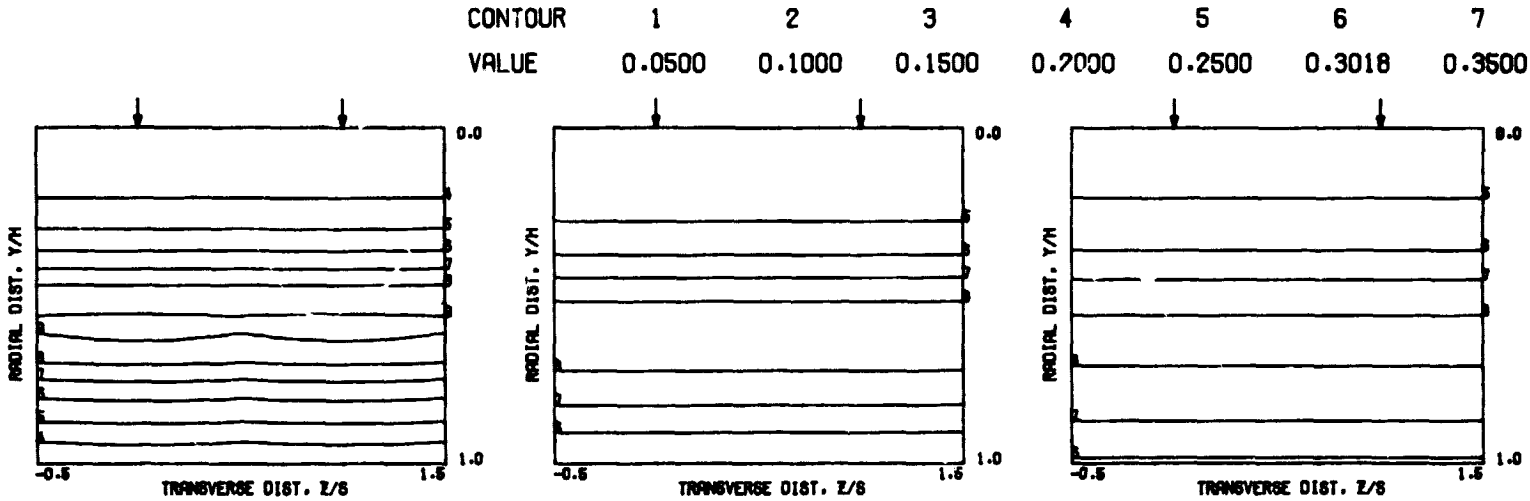

PREDICTED THETA CONTOURS FOR TEST NO.6, TMAIN=CONST, J=10

S/DJ = 2.57 HO/DJ = 10.29 VRATIO = 6.85 TRATIO = 0.460 DENRATIO=2.287 TMAIN

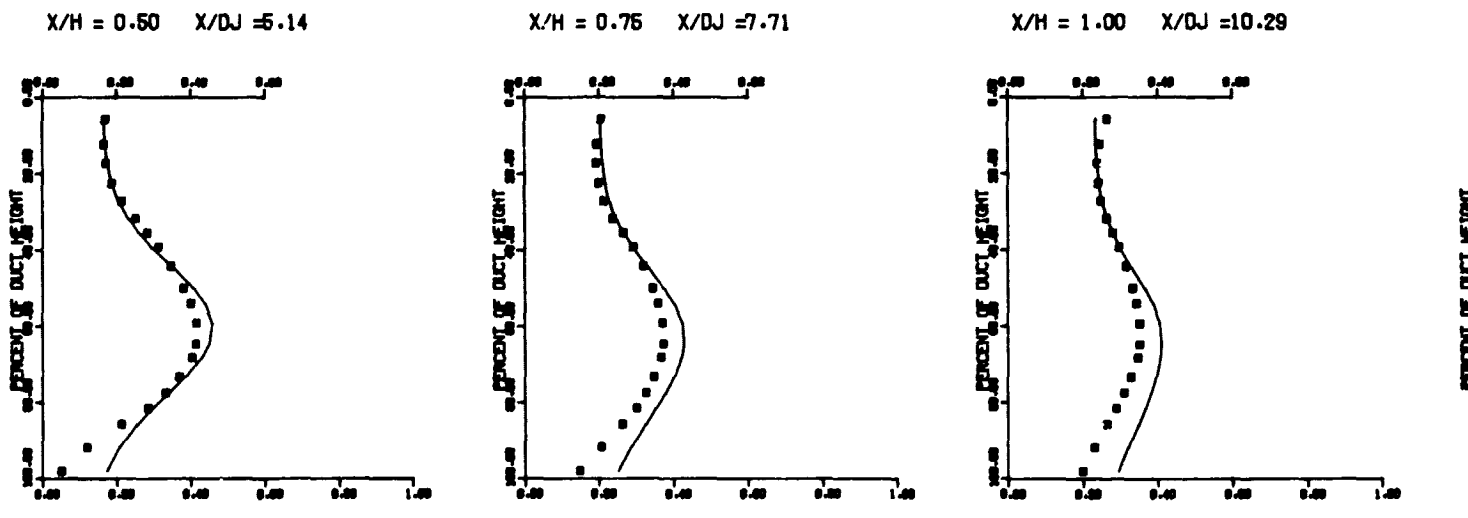

ORIGINAL PAGE IS
OF POOR QUALITY

COMPARISON BETWEEN DATA AND CORRELATIONS FOR TEST NO. 6, TEST SECTION I ,UNIFORM

FOLDOUT FRAME

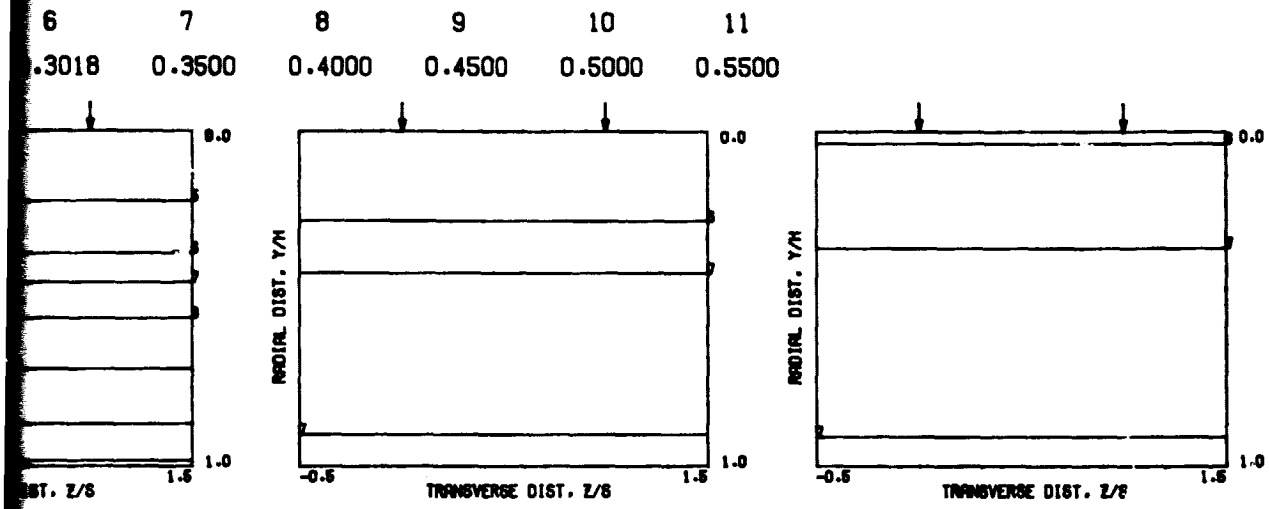

MAIN=CONST, J=107.8, S/D=2.0, H/D=8.0

ATIO=2.287 TMAIN = 649.7 K TJET = 299.2 K THEB = 0.302

.29 X/H = 1.50 X/DJ =15.43 X/H = 2.00 X/DJ =20.57

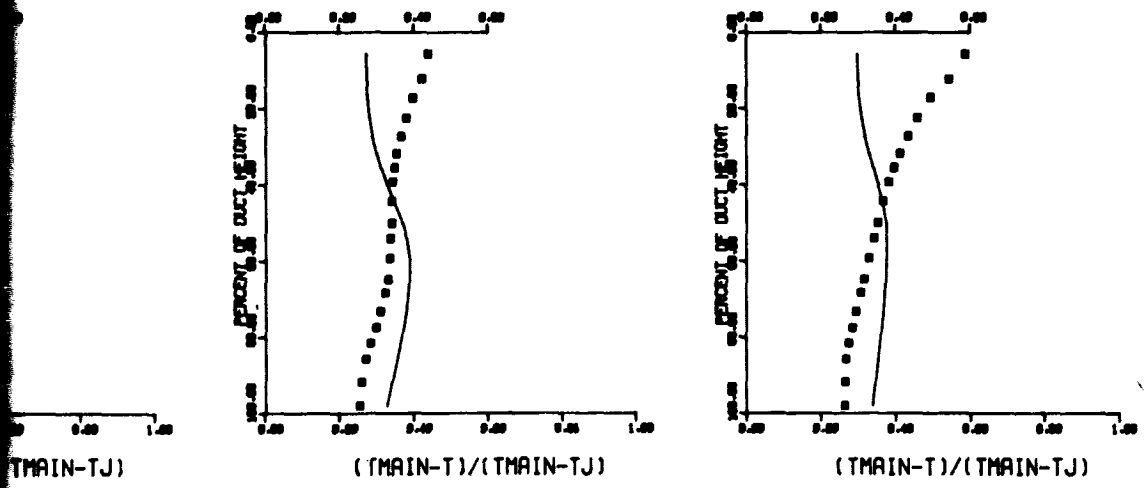

ORIGINAL PAGE IS
OF POOR QUALITY

CTION I ,UNIFORM TMAIN, J = 107.78 , S/D =2.00 , H/D =8.00

Figure 23

2 FOLDOUT FRAME

S = 0.0508 METERS S/DJ = 5.143 HO/DJ = 10.285 VMAIN = 15.2 M/SEC VJET = 52.8 M/SEC TMAIN = 651.4 K

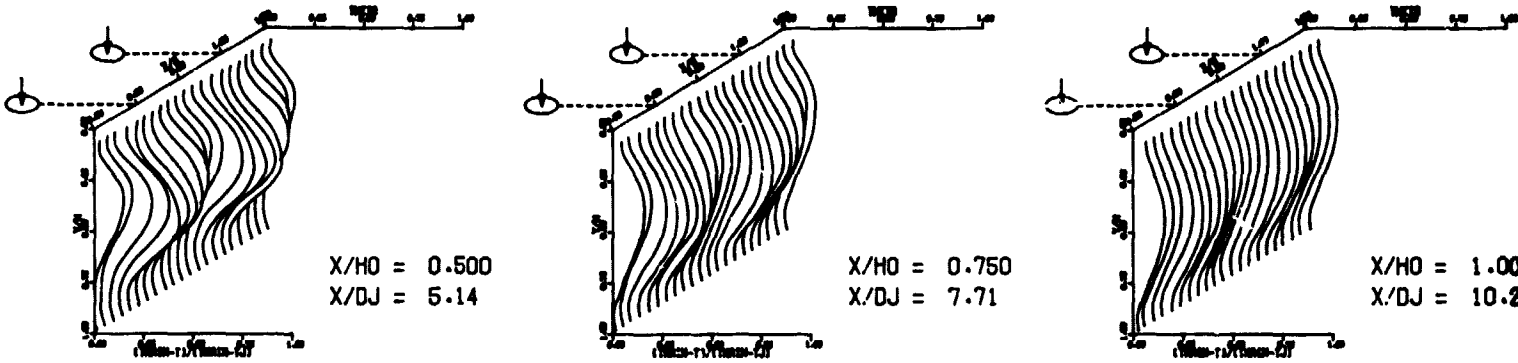

MEASURED THETA PROFILES FOR TEST NO. 7, TEST SECTION I, TMAIN=CONST. , J =

CONTOUR	1	2	3	4	5
VALUE	0.0500	0.0750	0.1048	0.1250	0.1500

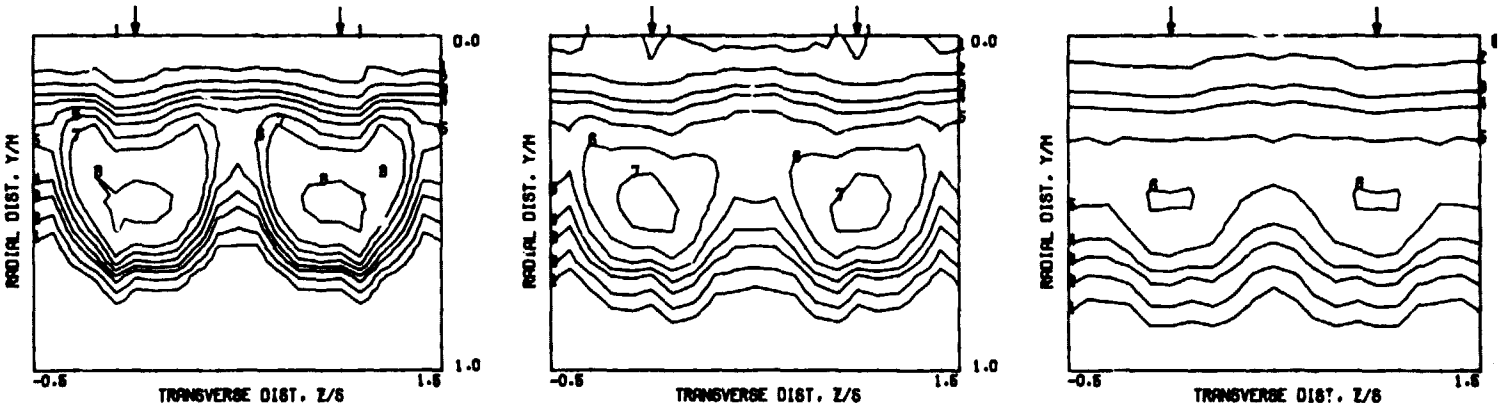

MEASURED THETA CONTOURS FOR TEST NO. 7, TMAIN=CONST.

FOLDOUT FRAME

ORIGINAL PAGE IS
OF POOR QUALITY

M/SEC TMAIN = 651.4 K TJET = 302.1 K THEB = 0.1048 BLORAT= 7.127 DENRATIO= 2.192 TRATIO= 0.464

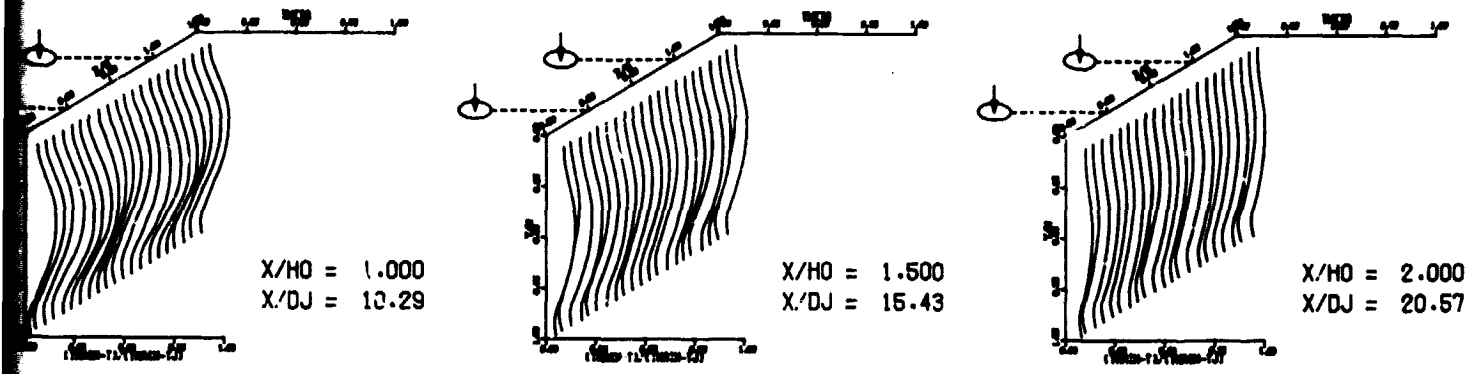

I, TMAIN=CONST. , J = 26.34 , S/D = 4.00 , H/D = 8.00

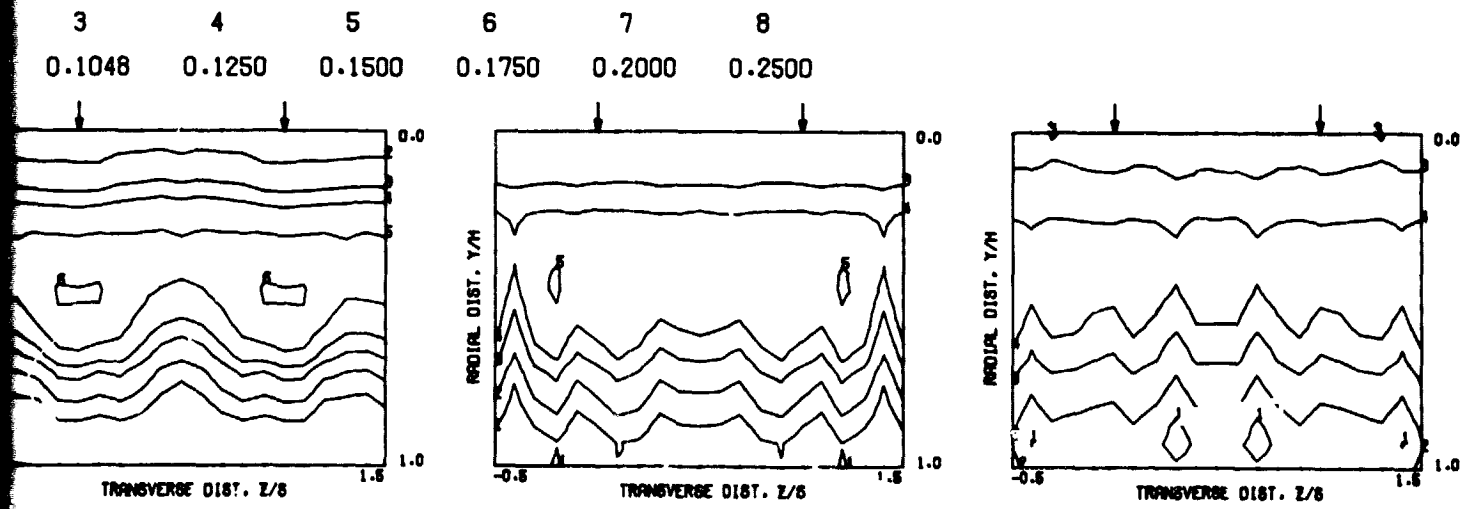

EST NO. 7, TMAIN=CONST, J=26.3, S/D=4.0, H/D=8.0

2 FOLDOUT FRAME

Figure 24

ORIGINAL PAGE IS
OF POOR QUALITY

CONTOUR	1	2	3	4	5
VALUE	0.0500	0.0750	0.1048	0.1250	0.150

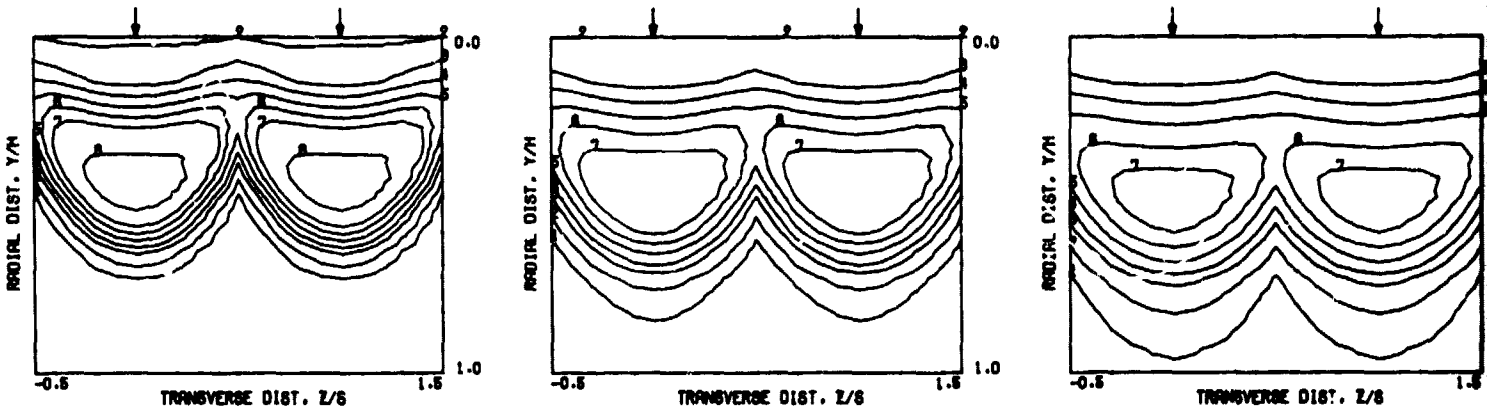

PREDICTED THETA CONTOURS FOR TEST NO.7. TMAIN=CONST.

S/DJ = 5.14 HO/DJ = 10.29 VRATIO = 3.47 TRATIO = 0.464 DENRATIO=2.192

X/H = 0.50 X/DJ =5.14 X/H = 0.75 X/DJ =7.71 X/H = 1.00 X/DJ =10.29

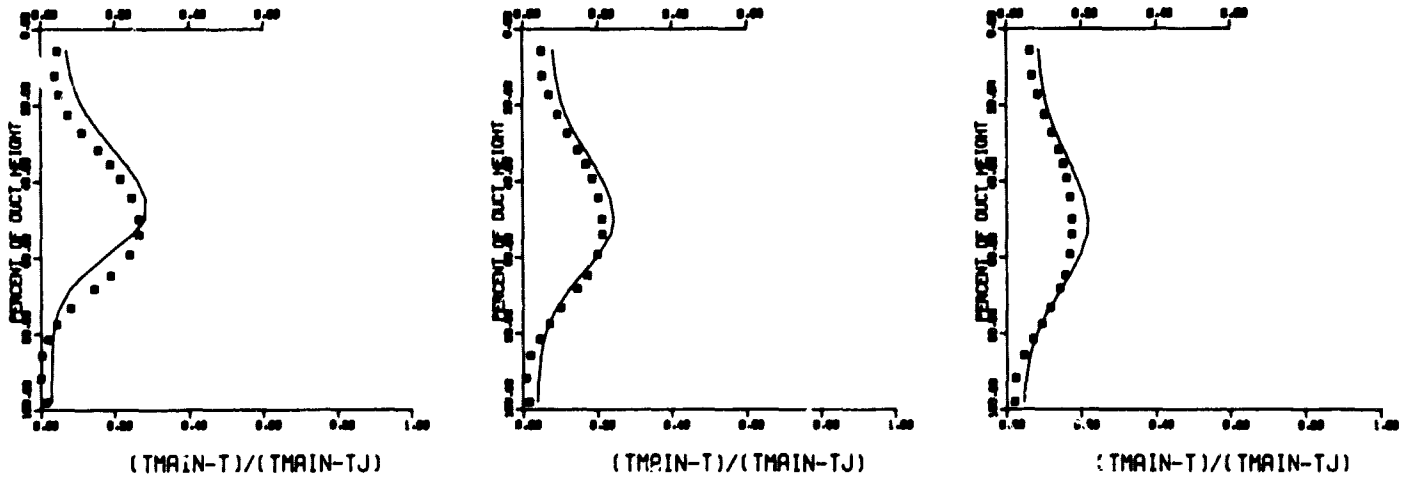

ORIGINAL PAGE IS
OF POOR QUALITY

COMPARISON BETWEEN DATA AND CORRELATIONS FOR TEST NO. 7. TEST SECTION I .UN

FOLDOUT FRAME

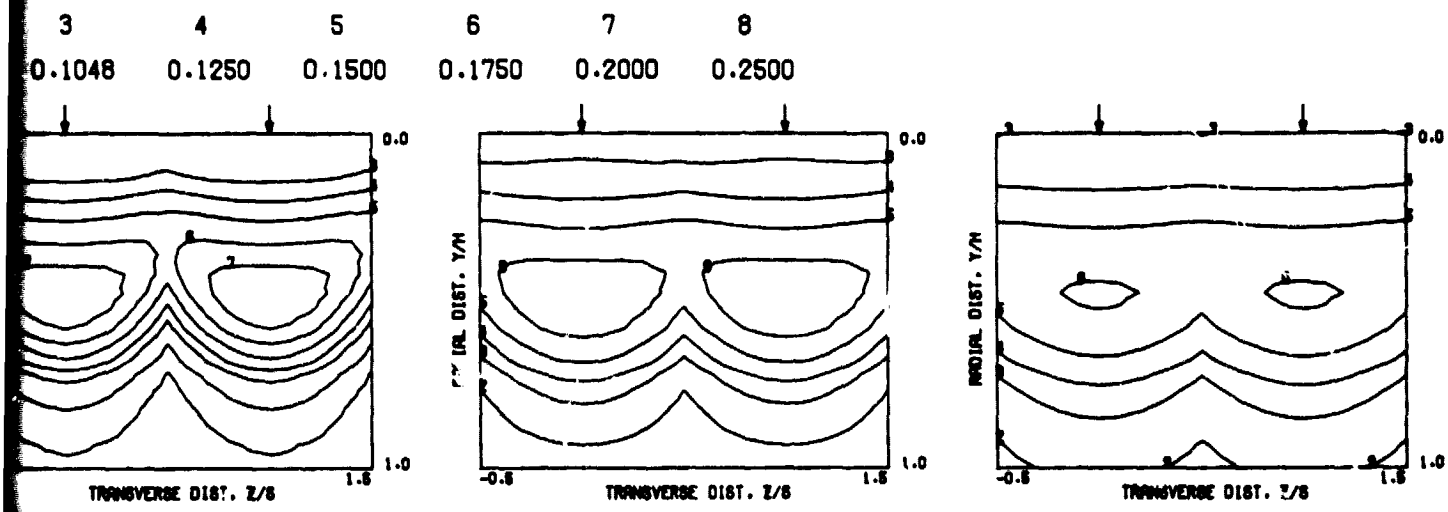

EST NO.7, TMAIN=CONST, J=26.34, S/D=4.0, H/D=8.0

0.464 DENRATIO=2.192 TMAIN = 651.4 K TJET = 302.1 K THEB = 0.105

= 1.00 X/DJ =10.29 X/H = 1.50 X/DJ =15.43 X/H = 2.00 X/DJ =20.57

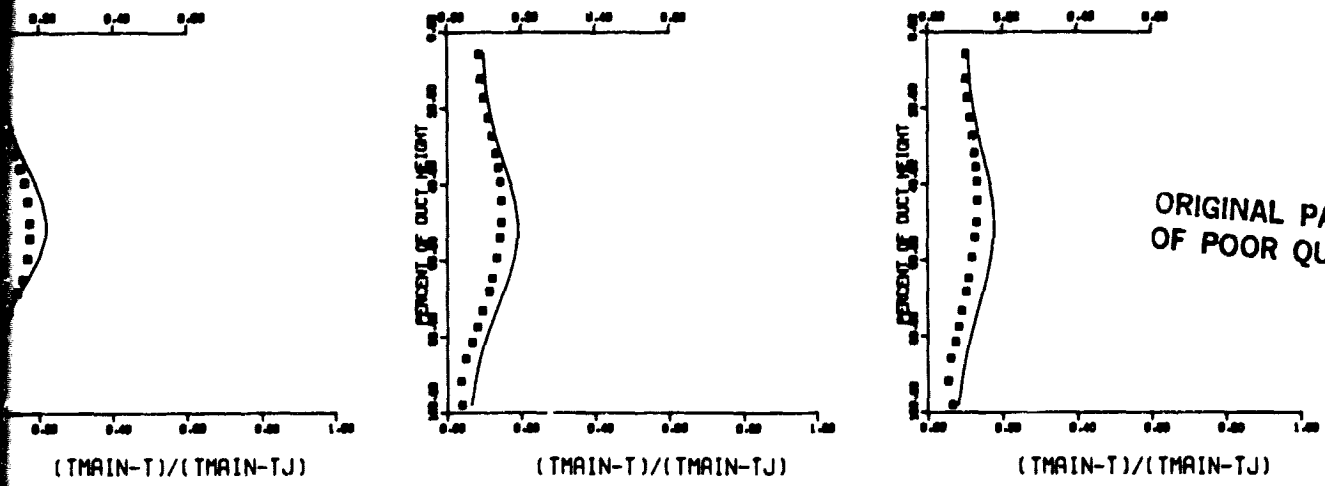

ORIGINAL PAGE IS
OF POOR QUALITY

7, TEST SECTION I ,UNIFORM TMAIN, J = 26.34 , S/D =4.00 , H/D =8.00

Figure 25

FOLDOUT FRAME

S = 0.0508 METERS S/DJ = 5.143 HO/DJ = 10.285 VMAIN = 15.1 M/SEC VJET = 104.1 M/SEC TMAIN = 649.2 K TJET

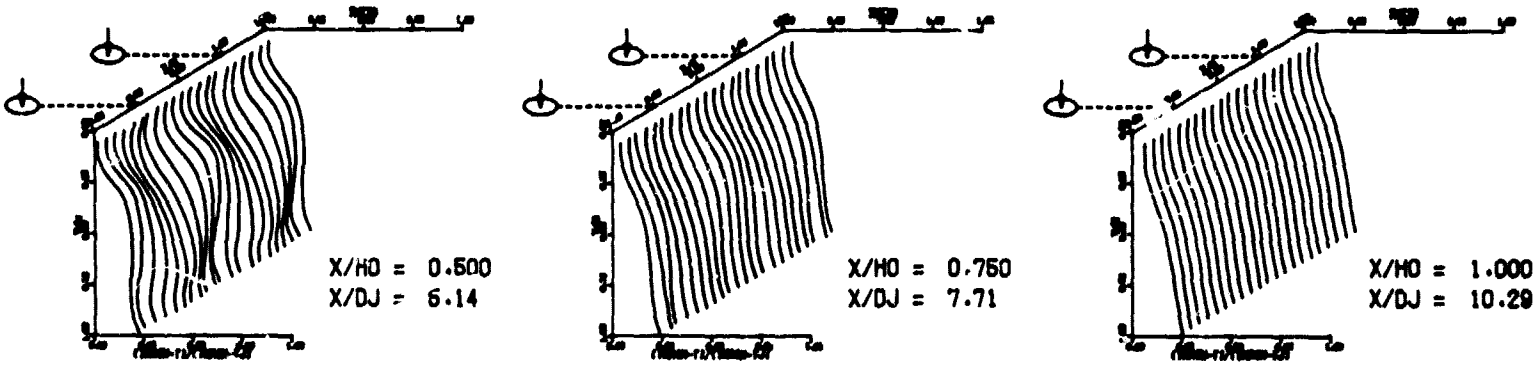

MEASURED THETA PROFILES FOR TEST NO. 8, TEST SECTION I, TMAIN=CONST. , J = 10

CONTOUR	1	2	3	4	5
VALUE	0.0500	0.0750	0.1000	0.1250	0.1809

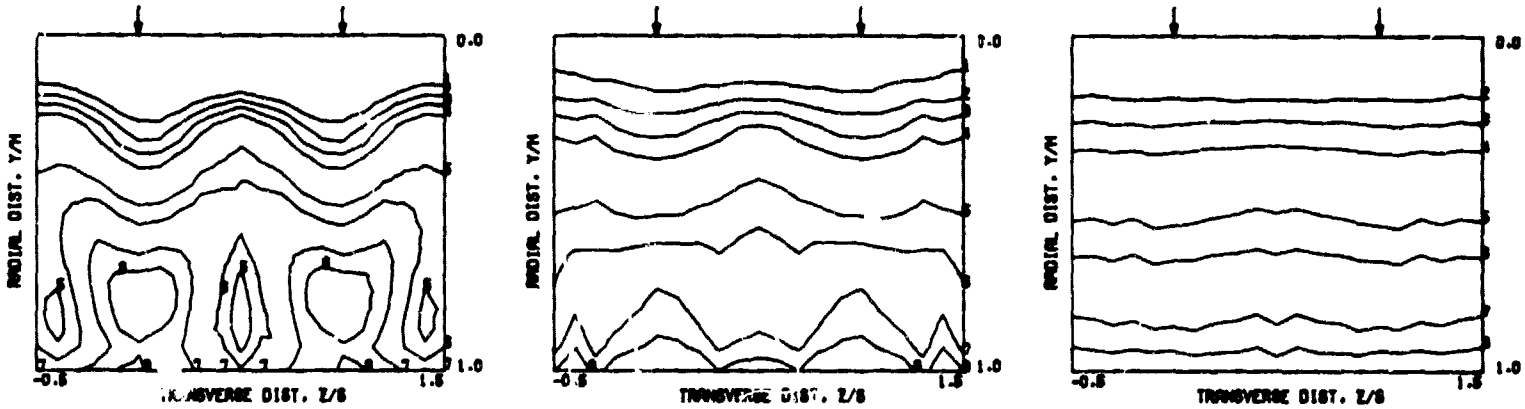

MEASURED THETA CONTOURS FOR TEST NO. 8, TMAIN=CONST, J=1

ORIGINAL PAGE IS
OF POOR QUALITY

FOLDOUT FRAME

.1 M/SEC TMAIN = 649.2 K TJET = 298.7 K THEB = 0.1808 BLORAT= 14.866 DENRATIO= 2.303 TRATIO= 0.460

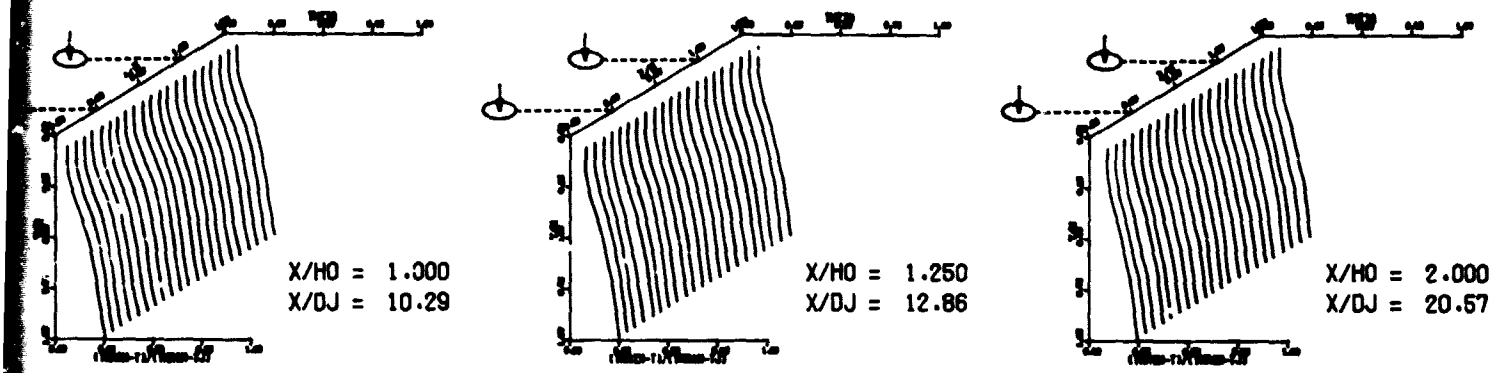

ON I, TMAIN=CONST. , J = 108.97 , S/D = 4.00 , H/D = 8.00

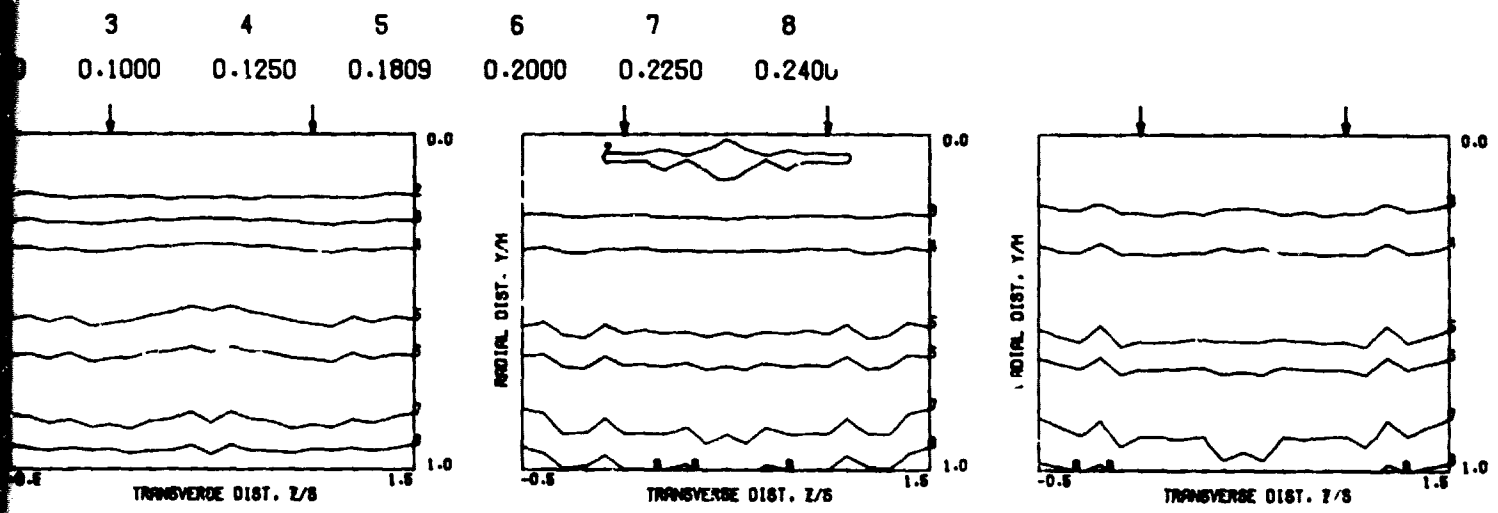

TEST NO. 8, TMAIN=CONST, J=109.0, S/D=4.0, H/D=8.0

FOLDOUT FRAME

Figure 26

ORIGINAL PAGE IS
OF POOR QUALITY

CONTOUR	1	2	3	4	5
VALUE	0.0500	0.0750	0.1000	0.1250	0..809

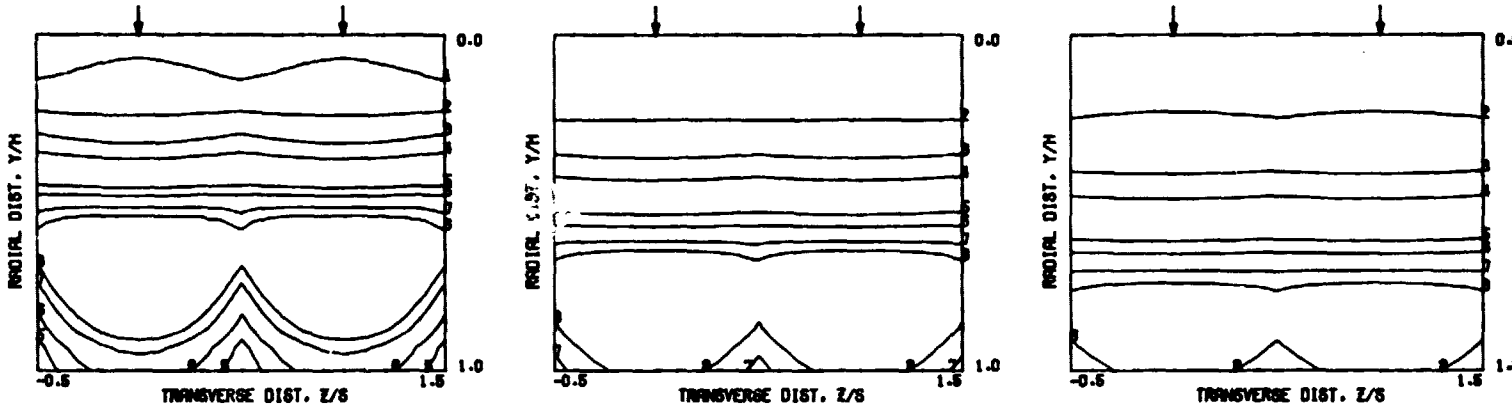

PREDICTED THETA CONTOURS FOR TEST NO.8. TMAIN=CONST. .

S/DJ = 5.14 HO/DJ = 10.29 VRATIO = 6.88 TRATIO = 0.460 DENRATIO=2.303 TM

X/H = 0.50 X/DJ =5.14 X/H = 0.75 X/DJ =7.71 X/H = 1.00 X/DJ =10.29

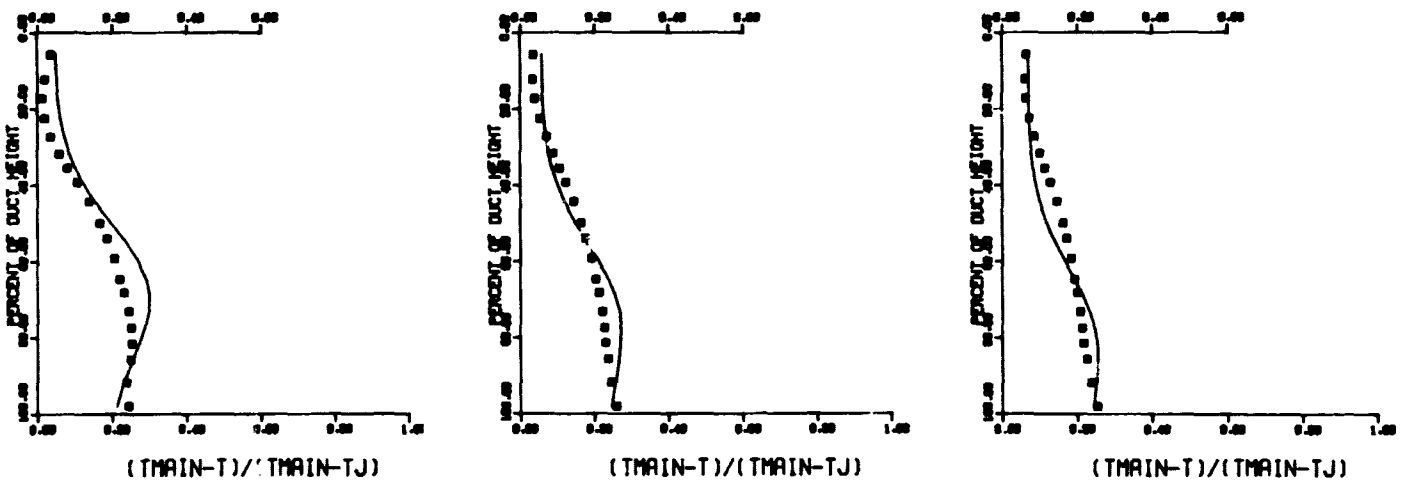

ORIGINAL PAGE IS OF POOR QUALITY

COMPARISON BETWEEN DATA AND CORRELATIONS FOR TEST NO. 8. TEST SECTION I .UNIF

FOLDOUT FRAME

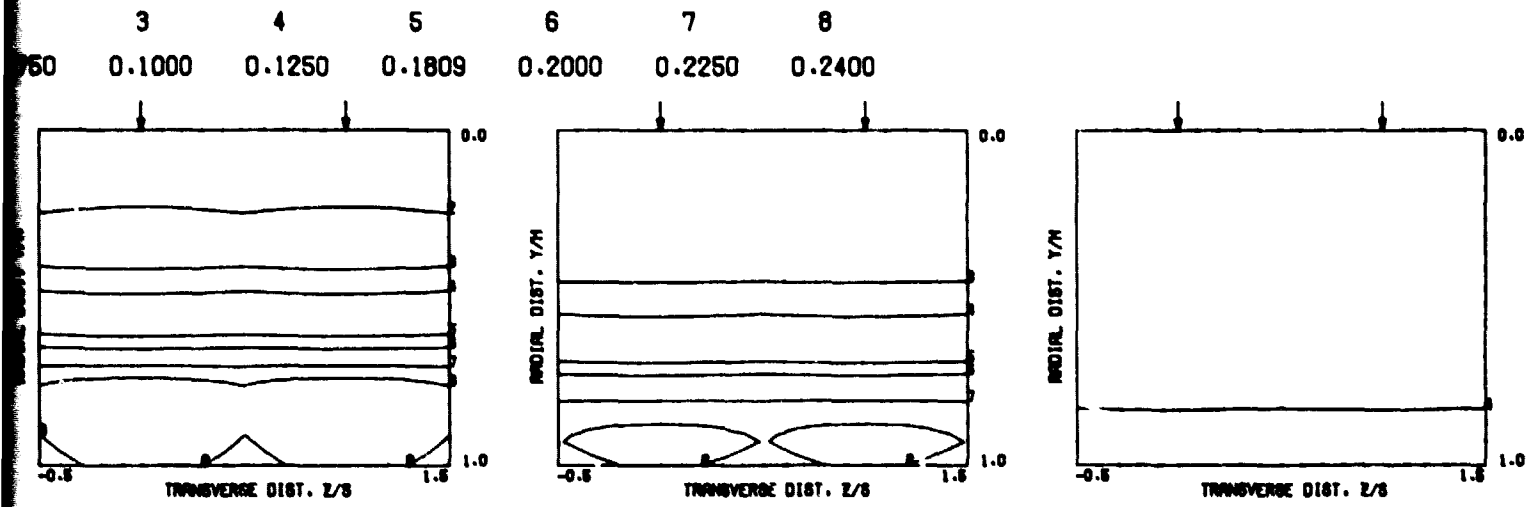

FOR TEST NO.8. TMAIN=CONST. J=109.0. S/D=4.0. H/D=8.0

TIO = 0.460 DENRATIO=2.303 TMAIN = 649.2 K TJET = 298.7 K THEB = 0.181

X/H = 1.00 X/DJ =10.29 X/H = 1.25 X/DJ =12.86 X/H = 2.00 X/DJ =20.57

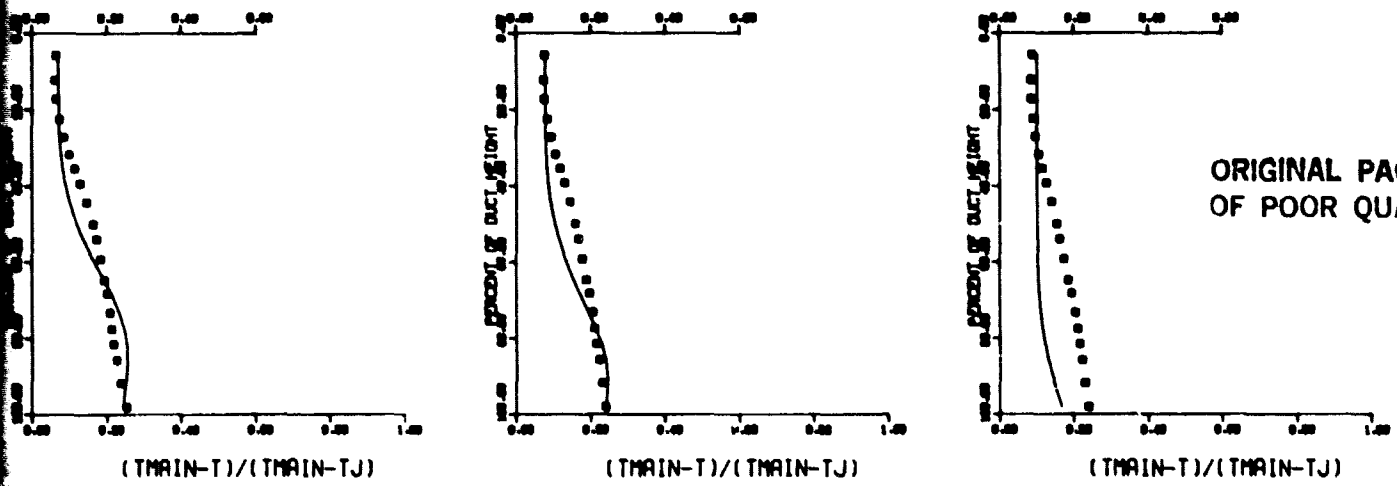

ORIGINAL PAGE IS
OF POOR QUALITY

NO. 8. TEST SECTION I .UNIFORM TMAIN. J = 108.97 . S/D =4.00 . H/D =8.00

Figure 27

2 FOLDOUT FRAME

S = 0.0508 METERS S/DJ = 2.561 HO/DJ = 5.121 VMAIN = 15.4 M/SEC VJET = 109.4 M/SEC TMAIN = 3

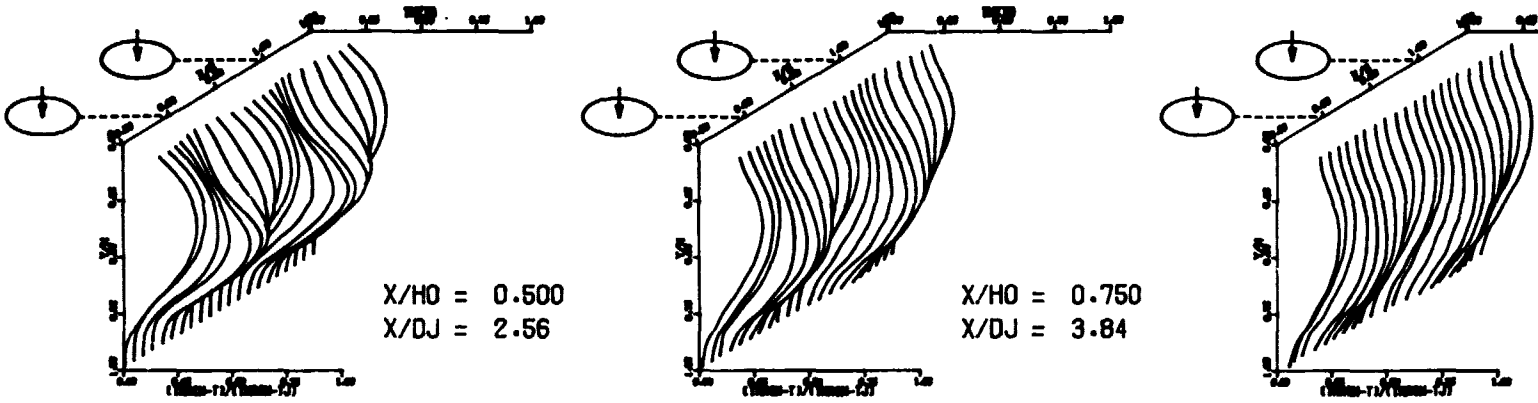

MEASURED THETA PROFILES FOR TEST NO. 9, TEST SECTION I, TMAIN=CONS

CONTOUR	1	2	3	4	5	6
VALUE	0.0500	0.1000	0.1500	0.1830	0.2000	0.2

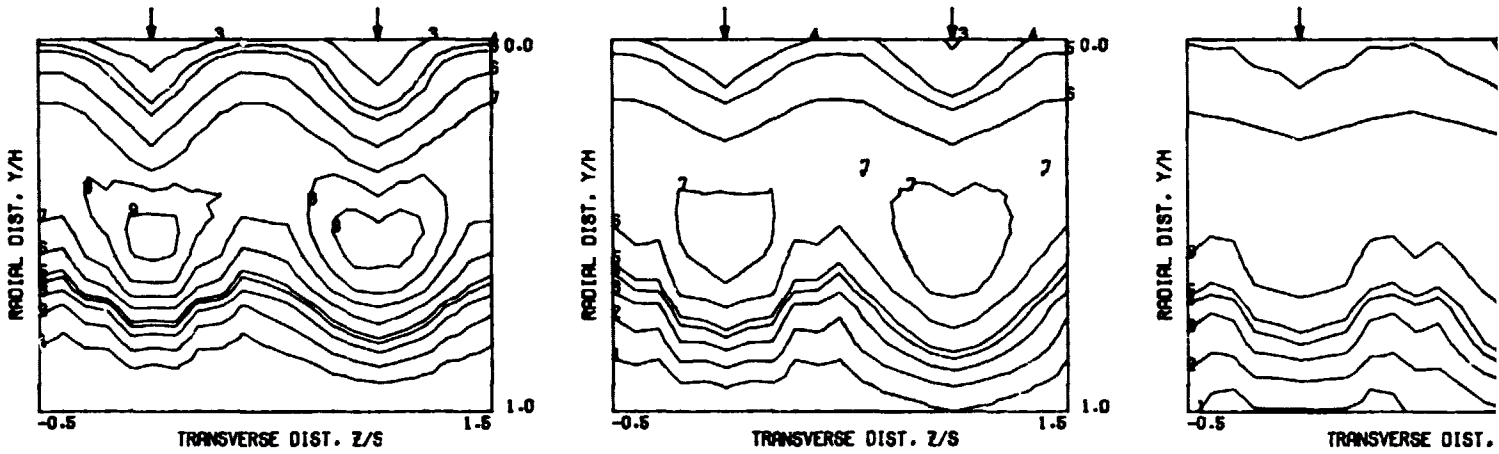

MEASURED THETA CONTOURS FOR TEST NO. 9, TMAI

ORIGINAL PAGE IS
OF POOR QUALITY

FOLDOUT FRAME

TMAIN = 305.8 K TJET = 511.5 K THEB = 0.1830 RLORAT= 3.765 DENRATIO= 0.617 TRATIO= 1.673

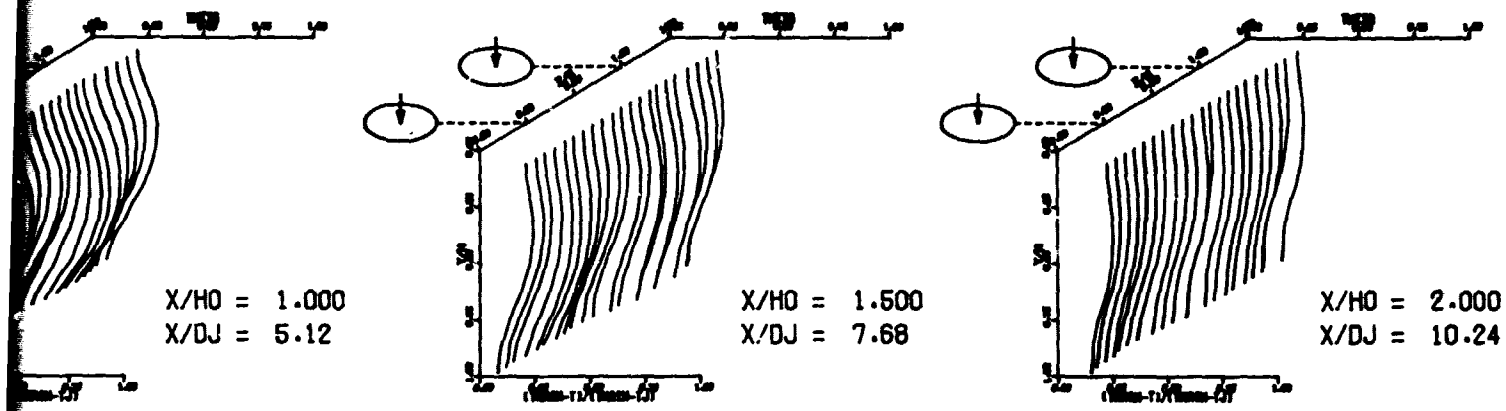

AIN=CONST. , J = 31.00 , S/D = 2.00 , H/D = 4.00

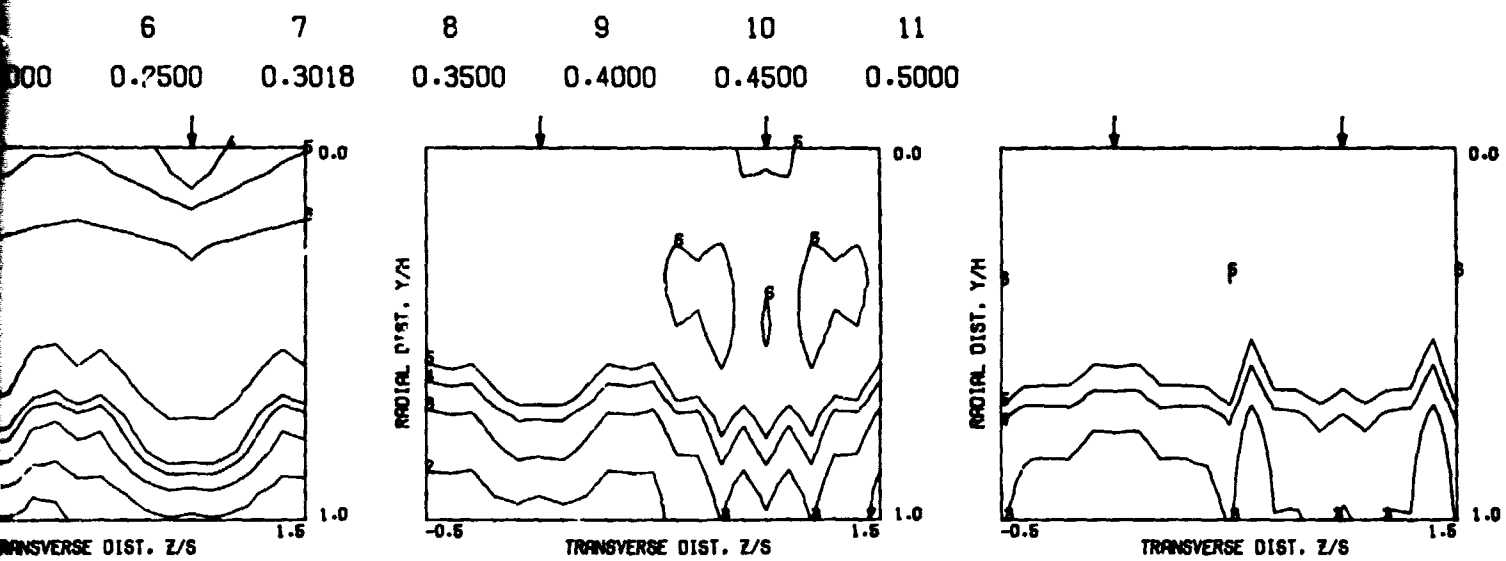

. 9, TMAIN=CONST, J=31.0, S/D=2.0, H/D=4.0

ORIGINAL PAGE IS
OF POOR QUALITY

2 FOLDOUT FRAME

Figure 28

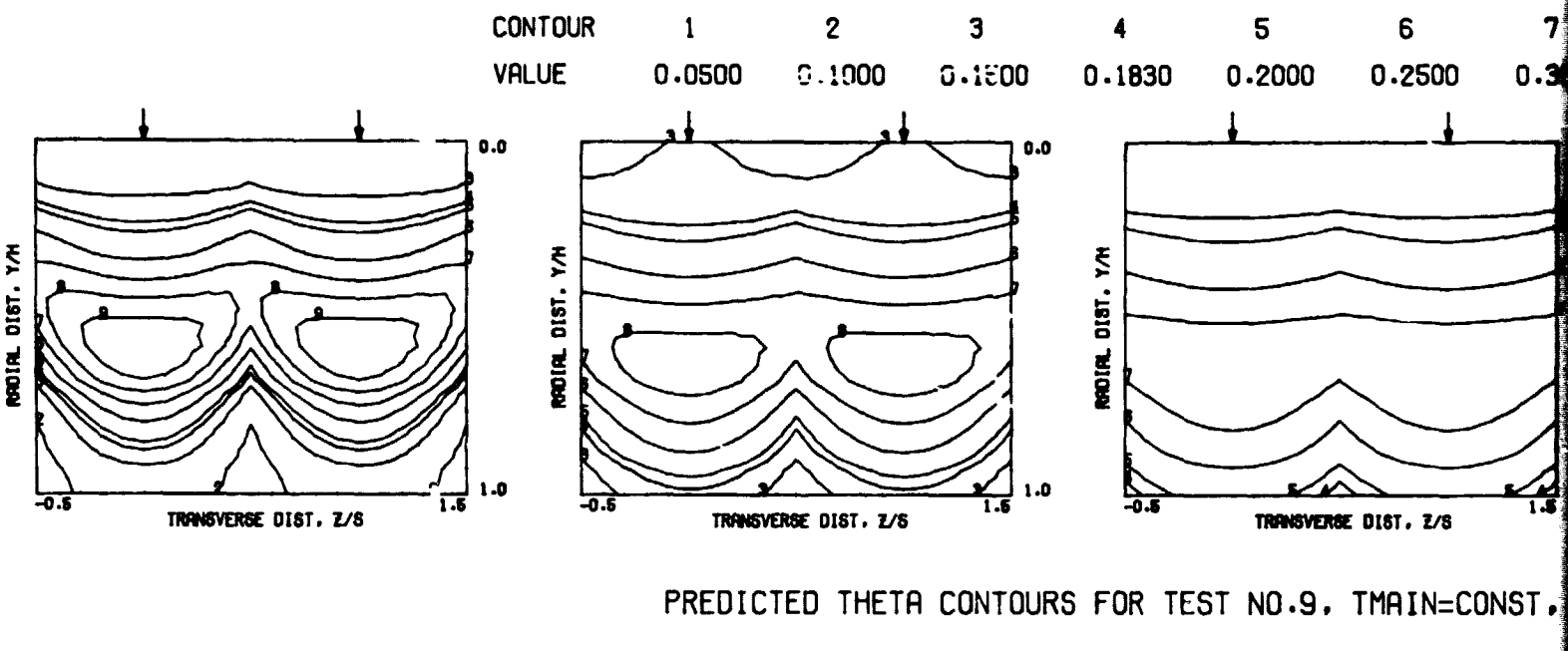

PREDICTED THETA CONTOURS FOR TEST NO.9, TMAIN=CONST,

S/DJ = 2.56 HO/DJ = 5.12 VRATIO = 7.09 TRATIO = 1.673 DENRATIO=0.617

X/H = 0.50 X/DJ =2.56 X/H = 0.75 X/DJ =3.84 X/H = 1.00 X/DJ =5.12

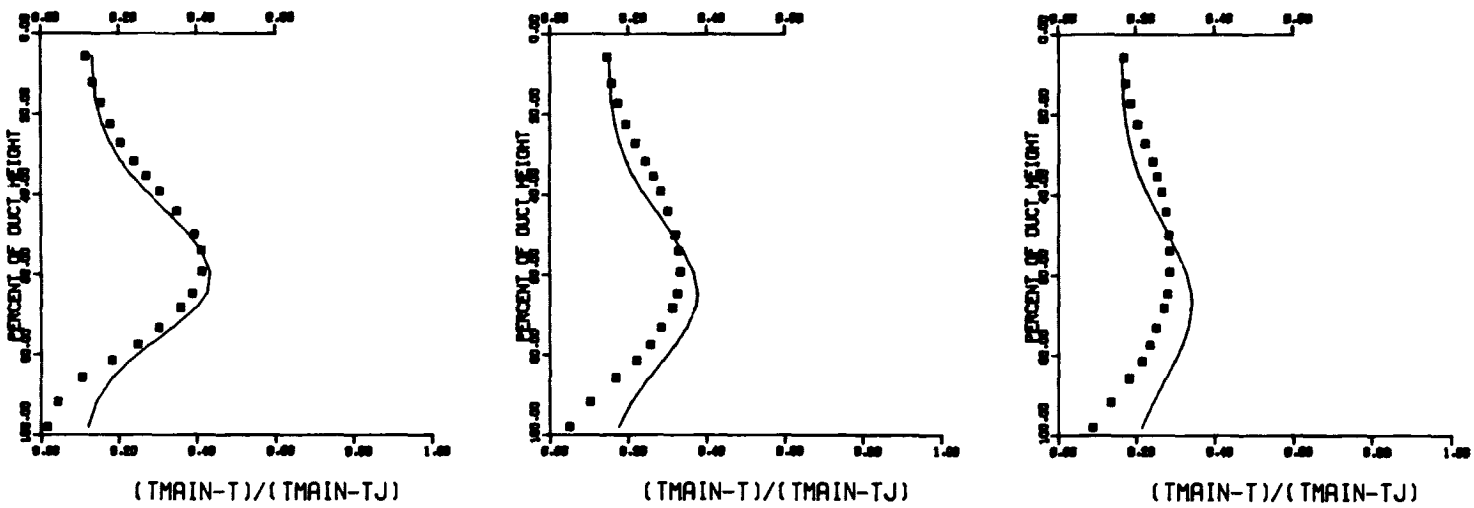

COMPARISON BETWEEN DATA AND CORRELATIONS FOR TEST NO. 9, TEST SECTION I ,UNI

FOLDOUT FRAME

ORIGINAL PAGE IS
OF POOR QUALITY

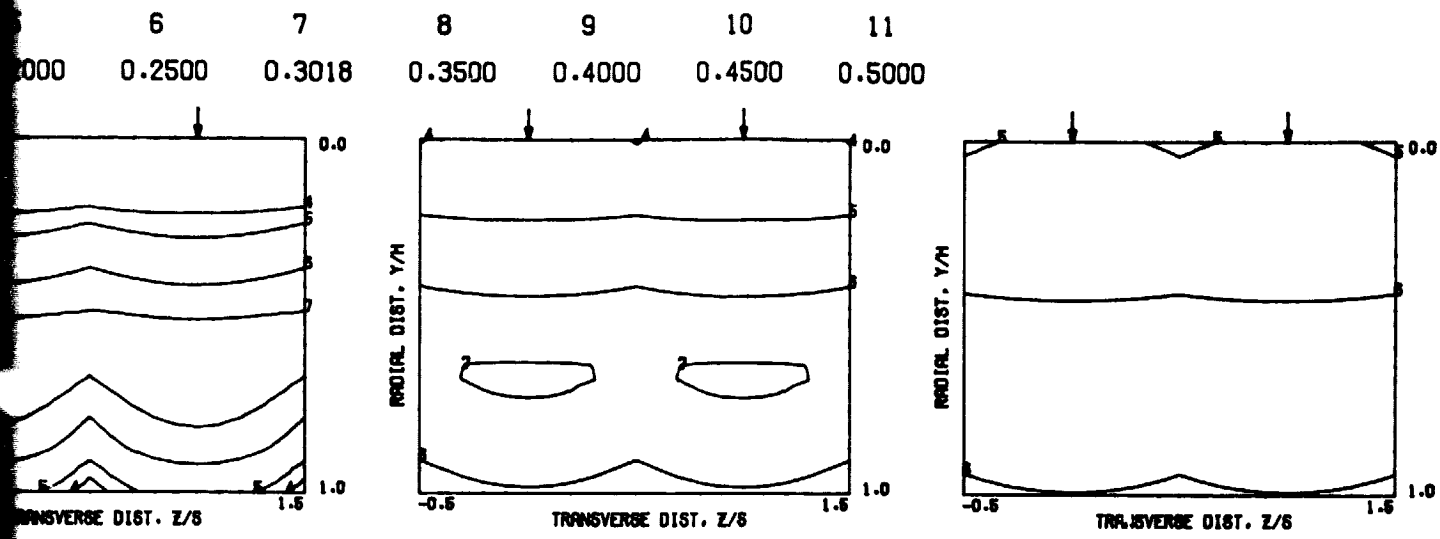

0.9, TMAIN=CONST, J=31.0, S/D=2.0, H/D=4.0

DENRATIO=0.617 TMAIN = 305.8 K TJET = 511.5 K THEB = 0.183

X/DJ =5.12 X/H = 1.50 X/DJ =7.68 X/H = 2.00 X/DJ =10.24

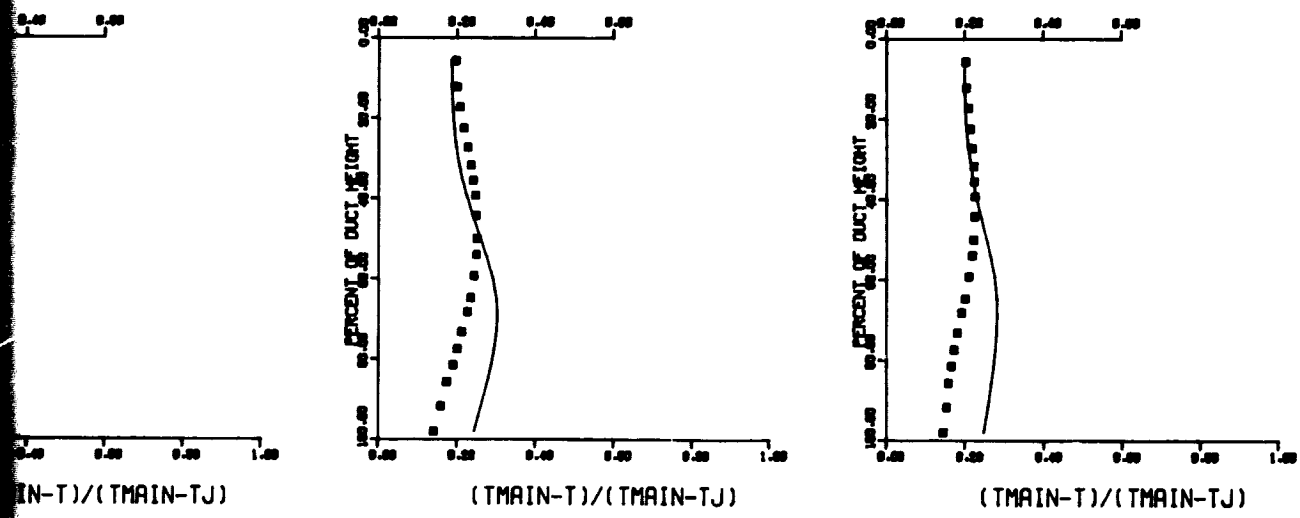

ST SECTION I ,UNIFORM TMAIN, J = 31.00 , S/D =2.00 , H/D =4.00

ORIGINAL PAGE IS
OF POOR QUALITY

Figure 29

2 FOLDOUT FRAME

S = 0.1016 METERS S/DJ = 5.165 HO/DJ = 5.165 VMAIN = 15.2 M/SEC VJET = 103.3 M/SEC TMAIN = 293.5 K TJE

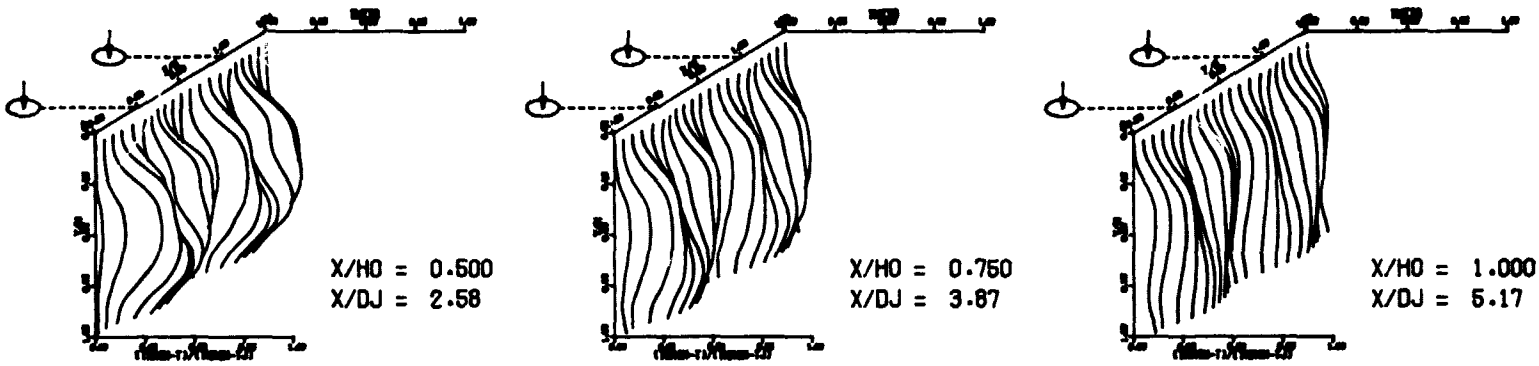

MEASURED THETA PROFILES FOR TEST NO. 10, TEST SECTION I, TMAIN=CONST., J =

CONTOUR	1	2	3	4	5	6	7
VALUE	0.0500	0.1024	0.1500	0.2000	0.2500	0.3018	0.3500

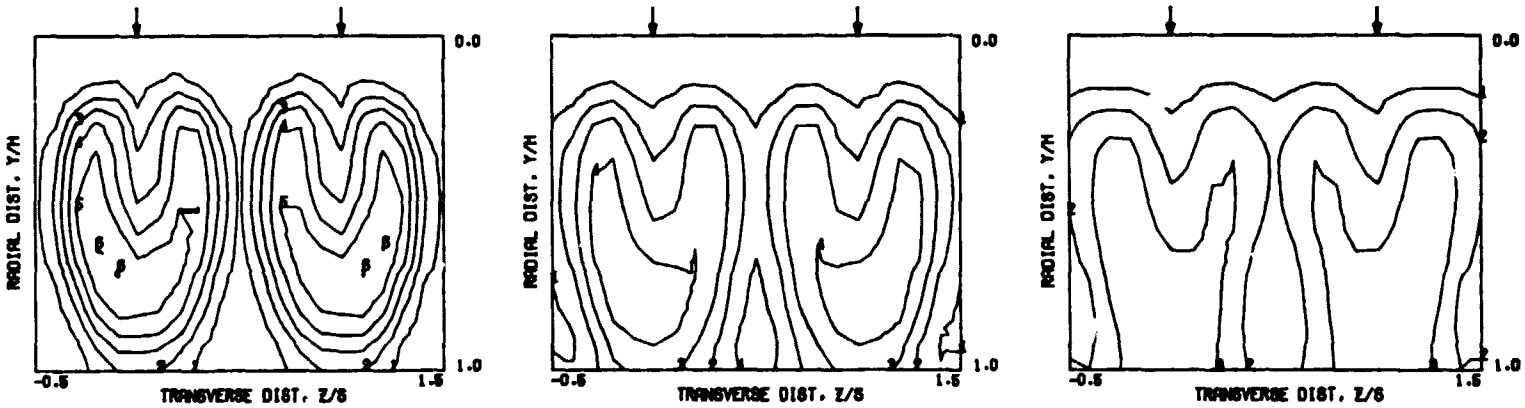

MEASURED THETA CONTOURS FOR TEST NO.10, TMAIN=CONST, J:

FOLDOUT FRAME

ORIGINAL PAGE IS
OF POOR QUALITY

M/SEC TMAIN = 293.5 K TJET = 408.1 K THEB = 0.1024 BLORAT= 3.873 DENRATIO= 0.663 TRATIO= 1.560

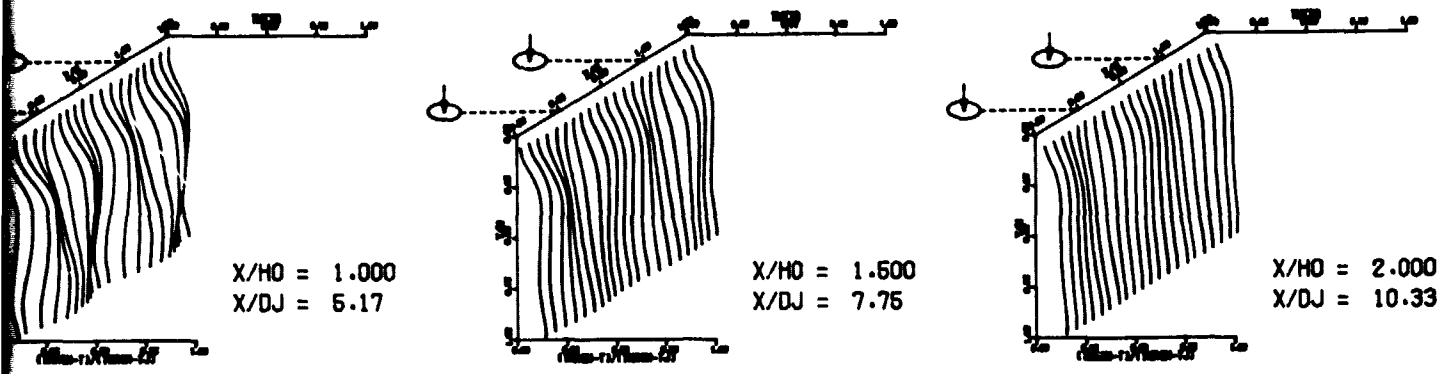

I, TMAIN=CONST., J = 30.64 , S/D = 4.00 , H/D = 4.00

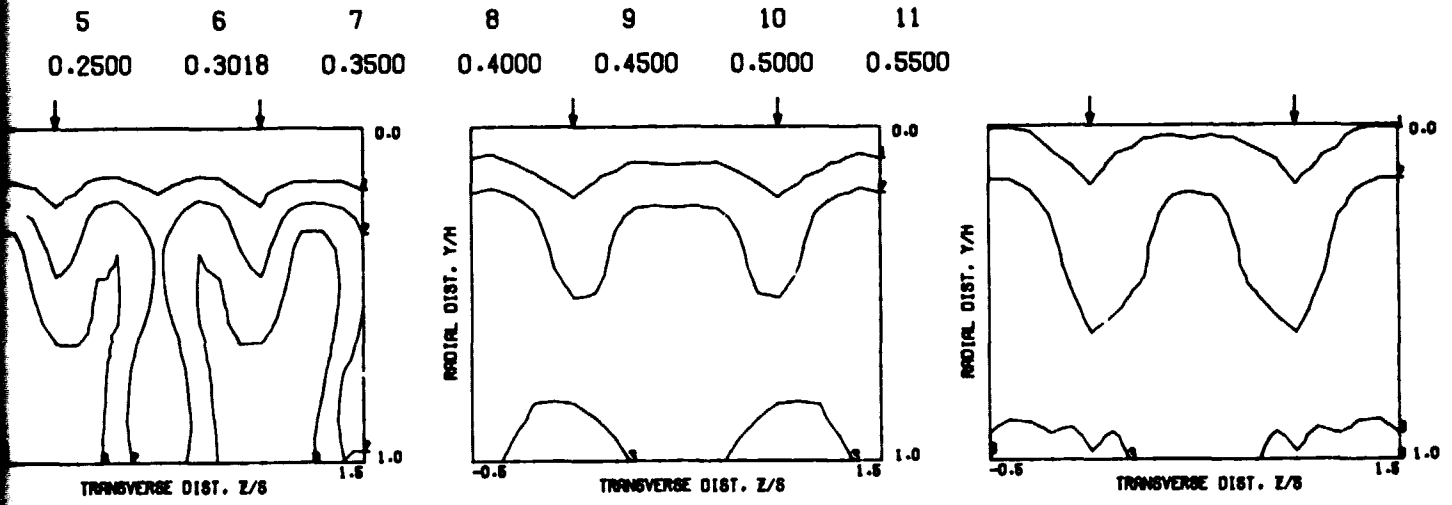

ST NO.10, TMAIN=CONST, J=30.64, S/D=4.0, H/D=4.0

ORIGINAL PAGE IS
OF POOR QUALITY

Figure 30

2 FOLDOUT FRAME

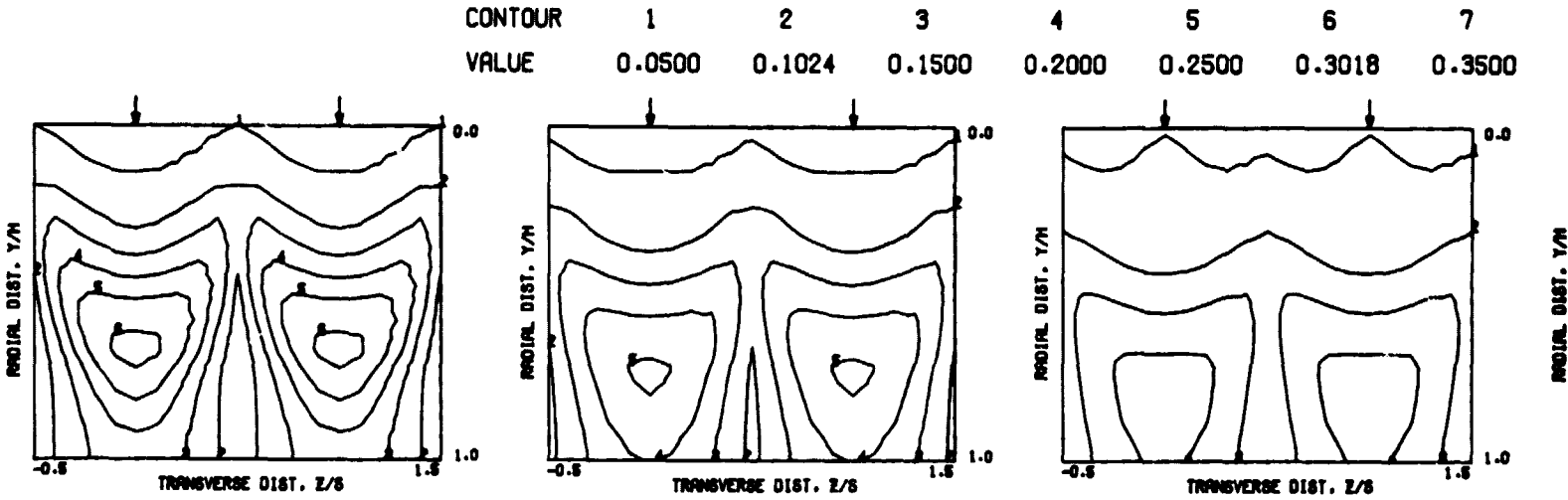

PREDICTED THETA CONTOURS FOR TEST NO.10. TMAIN=CONST. J=30

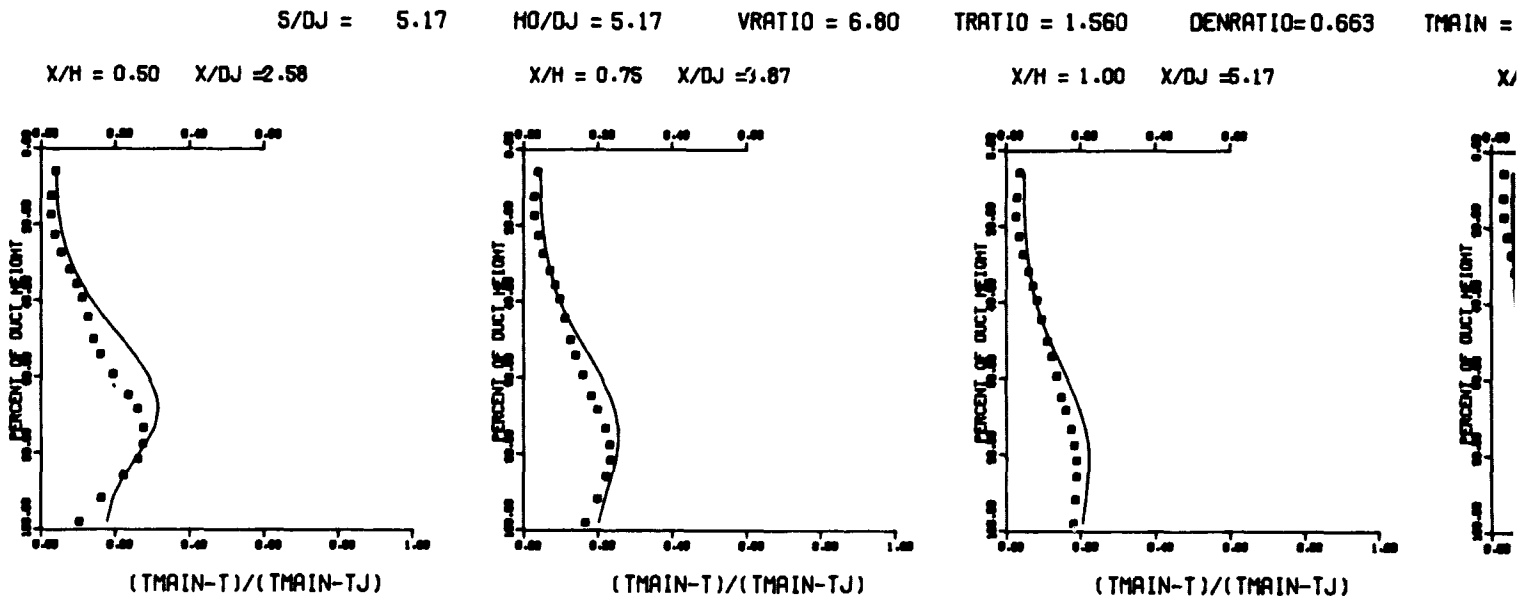

COMPARISON BETWEEN DATA AND CORRELATIONS FOR TEST NO. 10. TEST SECTION I .UNIFORM

FOLDOUT FRAME

ORIGINAL PAGE IS
OF POOR QUALITY

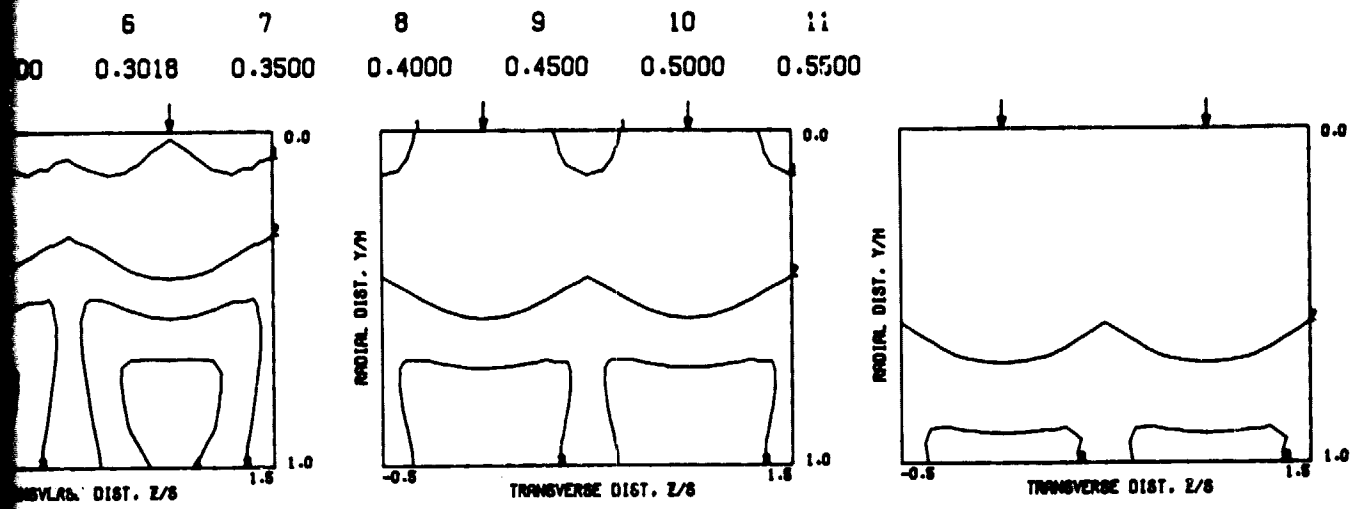

.10. TMAIN=CONST. J=30.6. S/D=4.0. H/D=4.0

DENRATIO=0.663 TMAIN = 293.0 K TJET = 457.2 K THEB = 0.102

X/DJ =5.17 X/H = 1.50 X/DJ =7.75 X/H = 2.00 X/DJ =10.33

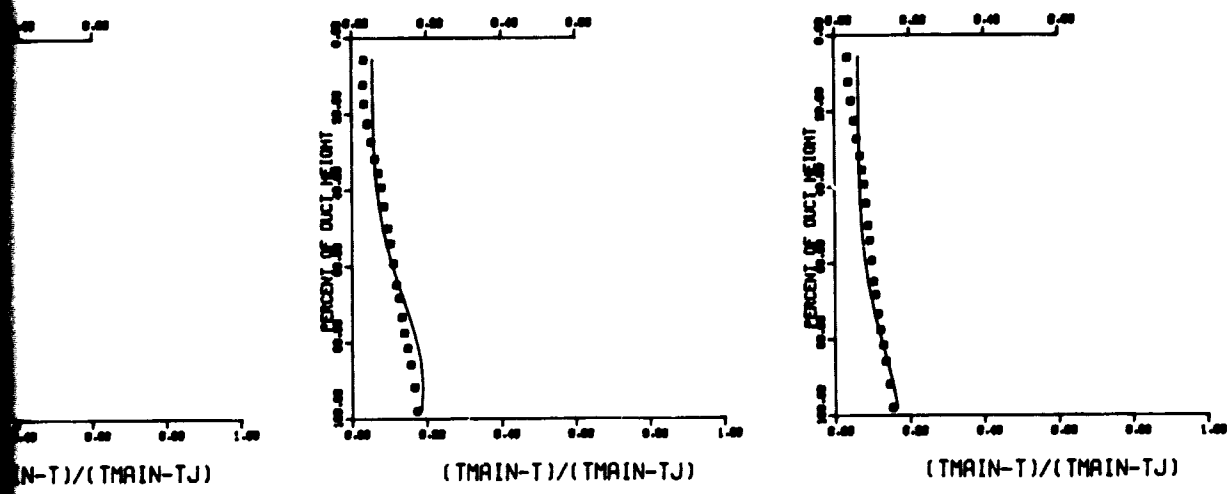

EST SECTION I .UNIFORM TMAIN. J = 30.64 , S/D =4.00 , H/D =4.00

Figure 31

ORIGINAL PAGE IS
OF POOR QUALITY FOLDOUT FRAME

S = 0.0254 METERS S/DJ = 2.582 HO/DJ = 10.327 VMAIN = 15.2 M/SEC VJET = 102.2 M/SEC TMAIN = 290.3 K TJET

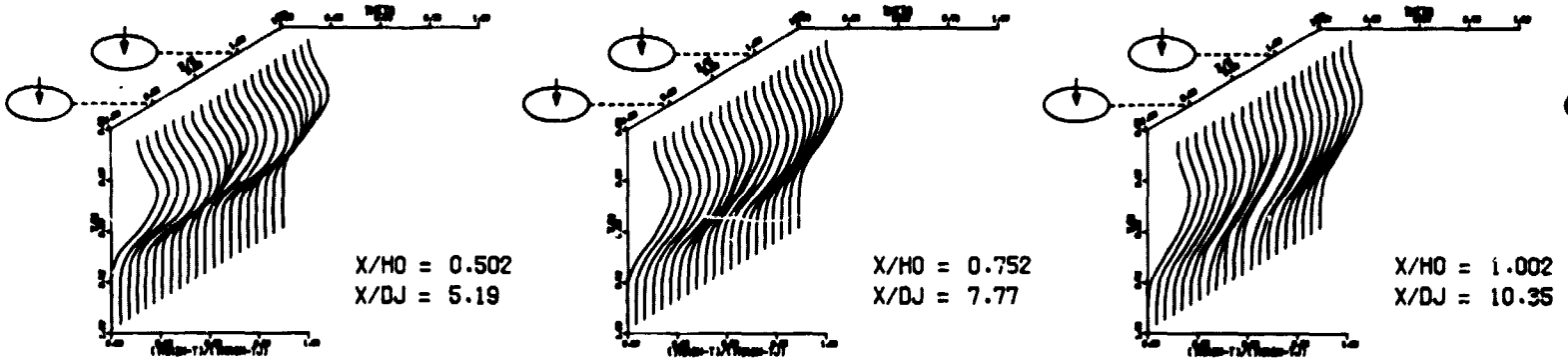

MEASURED THETA PROFILES FOR TEST NO. 11, TEST SECTION I, TMAIN=CONST, J = 3

CONTOUR	1	2	3	4	5	6	7
VALUE	0.0500	0.1025	0.1500	0.2000	0.2500	0.3000	0.3500

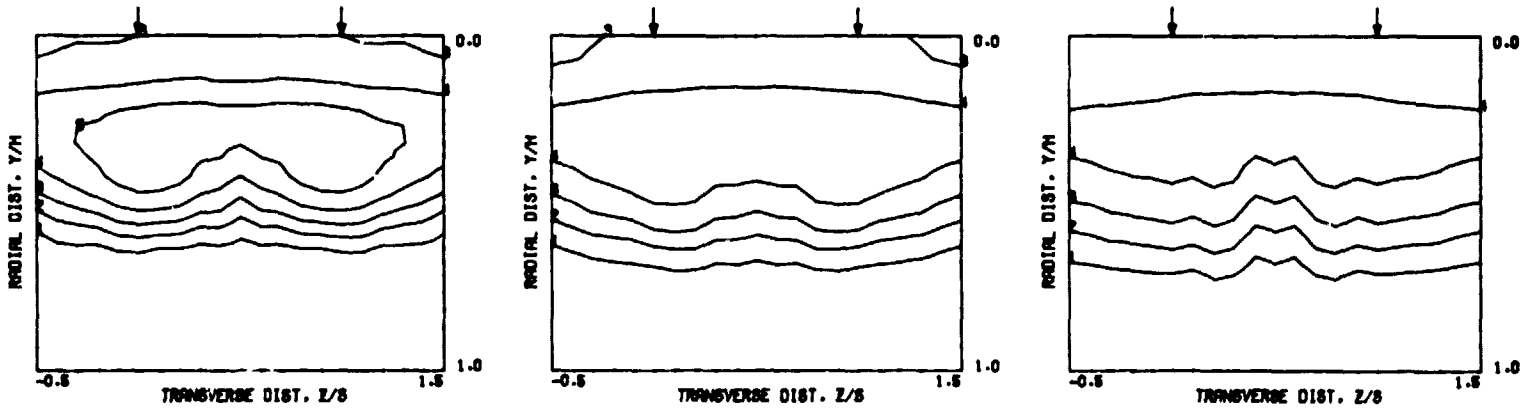

MEASURED THETA CONTOURS FOR TEST NO.11, TMAIN=CONST, J=

FOLDOUT FRAME

ORIGINAL PAGE IS
OF POOR QUALITY

TMAIN = 290.3 K TJET = 444.8 K THEB = 0.1025 BLORAT= 3.875 DENRATIO= 0.672 TRATIO= 1.532

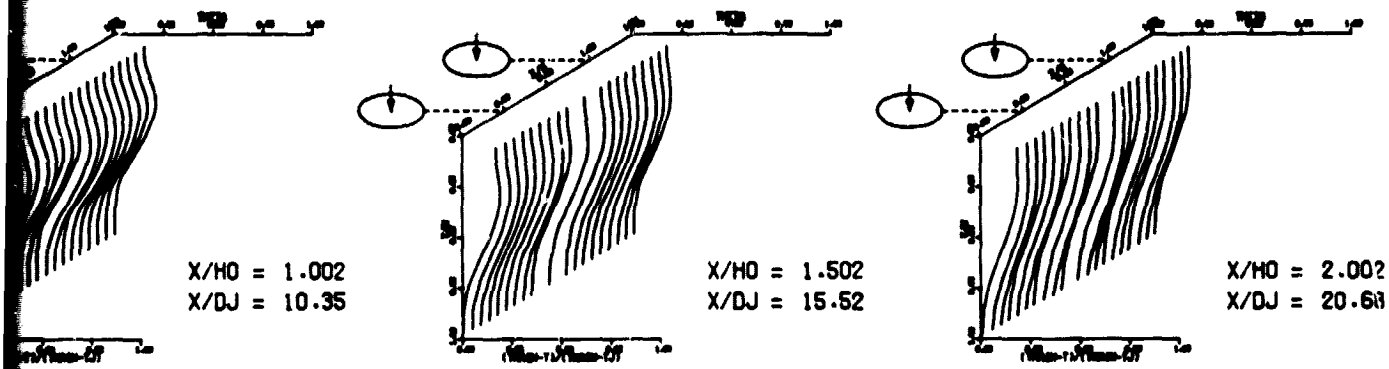

, TMAIN=CONST , J = 30.19 , S/D = 2.00 , H/D = 8.00

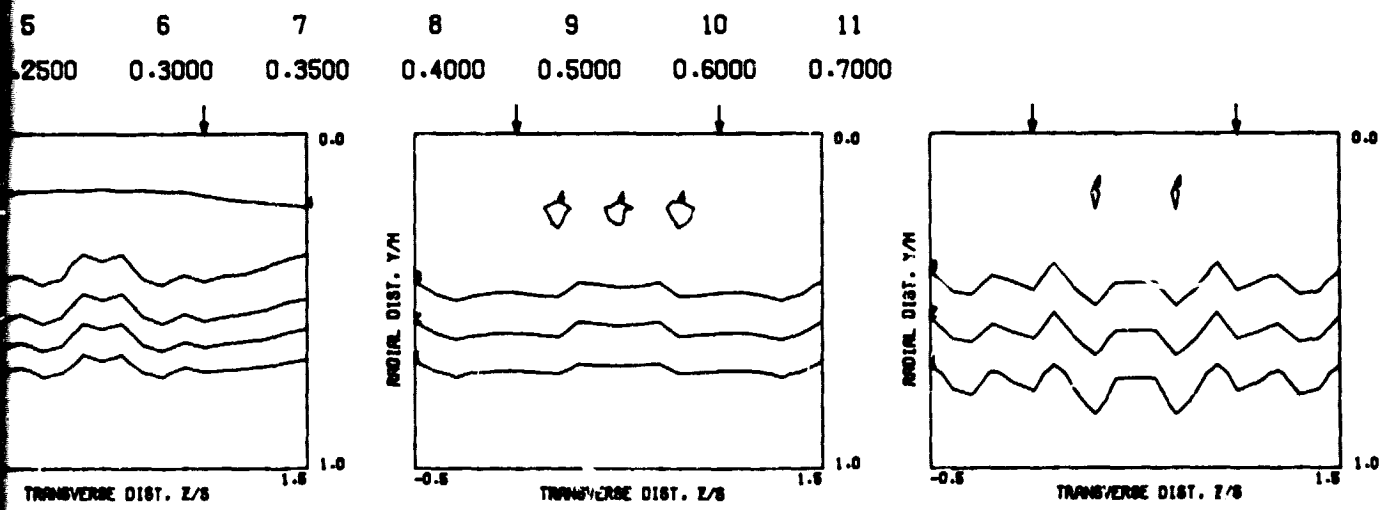

0.11, TMAIN=CONST, J=30.19, S/D=2.0, H/D=8.0

ORIGINAL PAGE IS
OF POOR QUALITY

Figure 32

2 FOLDOUT FRAME

CONTOUR	1	2	3	4	5	6	7
VALUE	0.0500	0.1025	0.1500	0.2000	0.2500	0.3000	0.3500

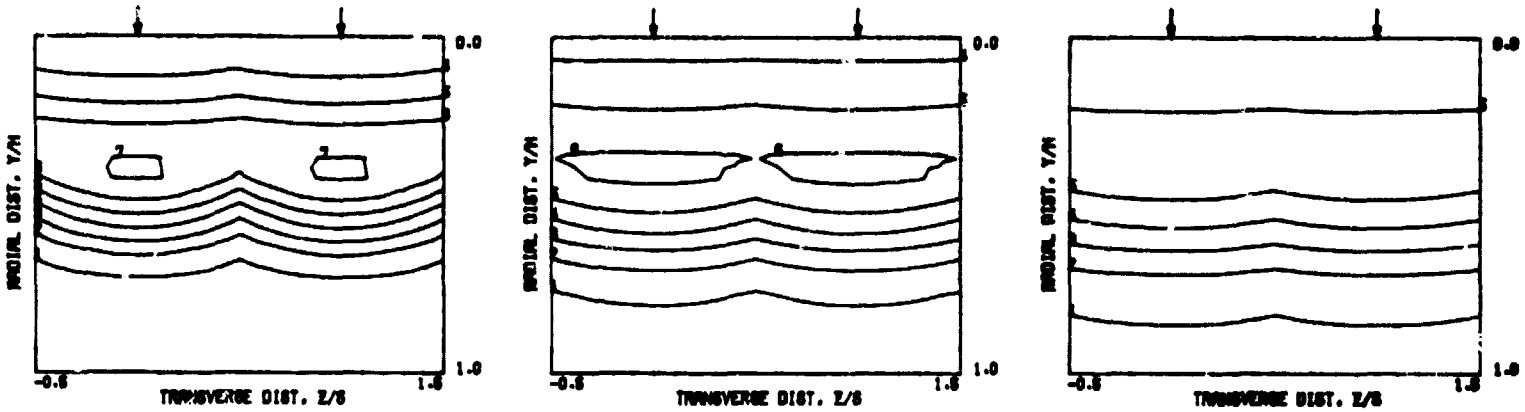

PREDICTED THETA CONTOURS FOR TEST NO. 11. TMAIN=CONST. J=

S/DJ = 2.58 HO/DJ = 10.33 VRATIO = 6.70 TRATIO = 1.532 DENRATIO= 0.672 TMAIN

X/H = 0.50 X/DJ =5.19 X/H = 0.76 X/DJ =7.77 X/H = 1.00 X/DJ =10.36

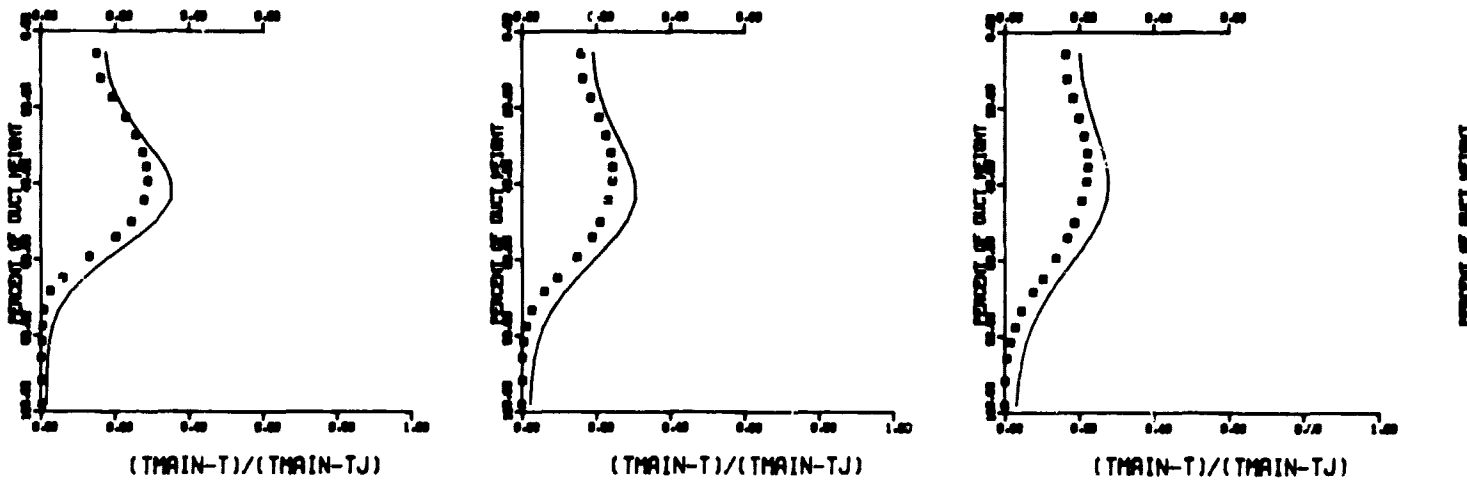

COMPARISON BETWEEN DATA AND CORRELATIONS FOR TEST NO. 11. TEST SECTION I. UNIFOR

FOLDOUT FRAME

ORIGINAL PAGE IS
OF POOR QUALITY

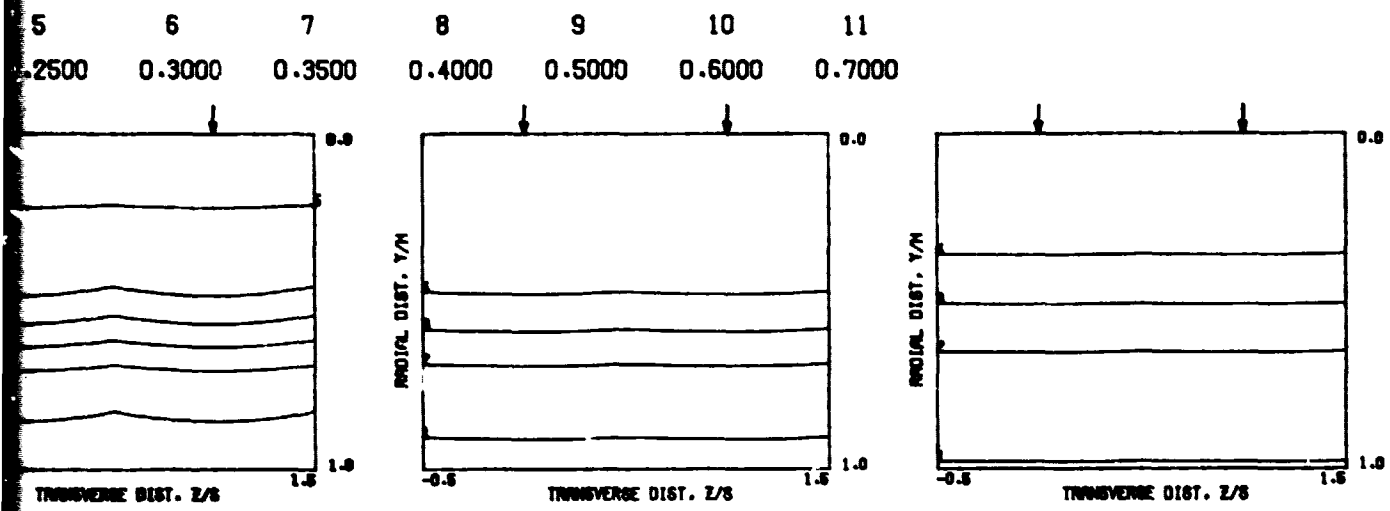

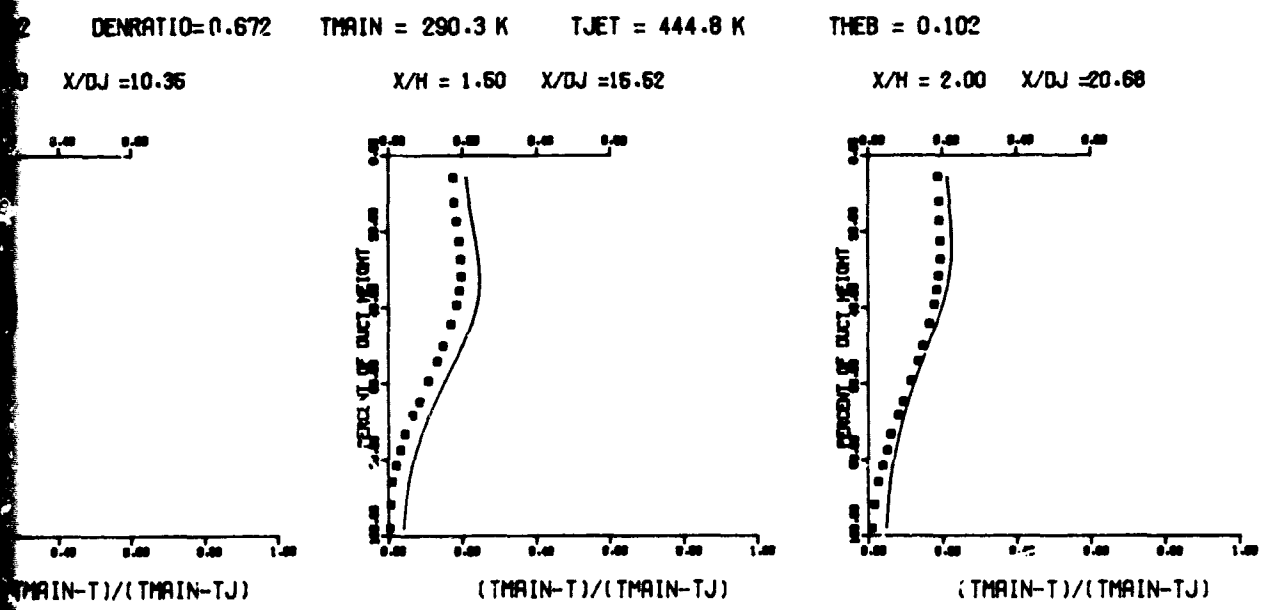

ORIGINAL PAGE IS
OF POOR QUALITY

TEST SECTION I. UNIFORM TMAIN, J = 30.19 , S/D =2.00 , H/D =8.00

Figure 33

2 FOLDOUT FRAME

S = 0.0508 METERS S/DJ = 4.961 HO/DJ = 9.921 VMAIN = 15.3 M/SEC VJET = 97.6 M/SEC TMAIN = 293.0 K T

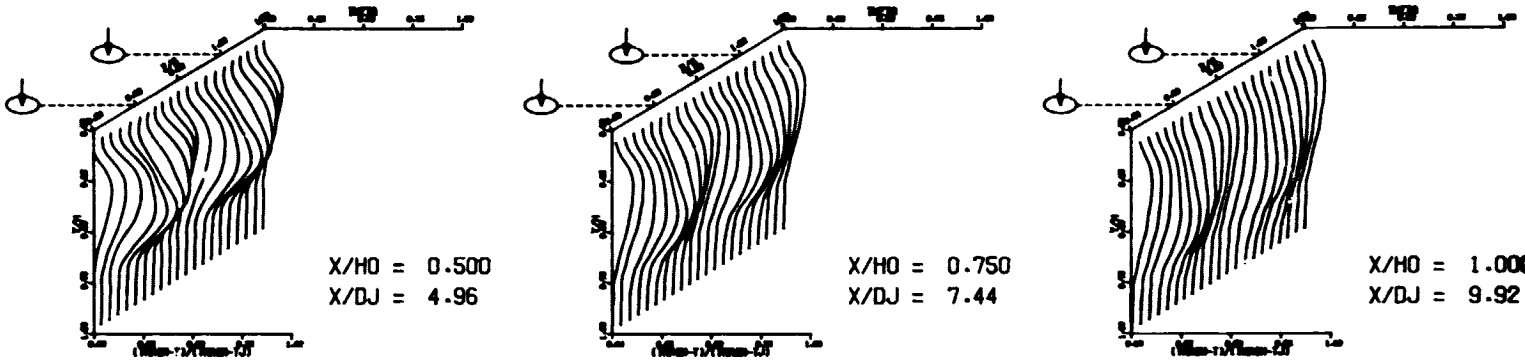

MEASURED THETA PROFILES FOR TEST NO. 12, TEST SECTION I, TMAIN=CONST., J =

CONTOUR	1	2	3	4	5	6	7
VALUE	0.0250	0.0500	0.0617	0.0750	0.1000	0.1250	0.1500

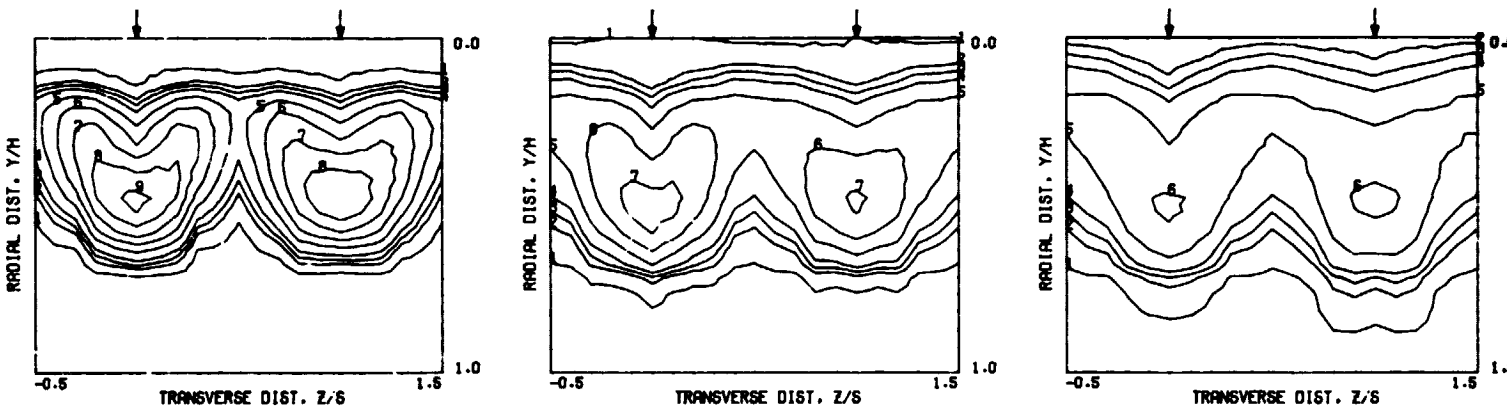

MEASURED THETA CONTOURS FOR TEST NO.12, TMAIN=CONST, J

ORIGINAL PAGE IS
OF POOR QUALITY

FOLDOUT FRAME

M/SEC TMAIN = 293.0 K TJET = 457.2 K THEB = 0.0617 BLORAT= 4.117 DENRATIO= 0.747 TRATIO= 1.391

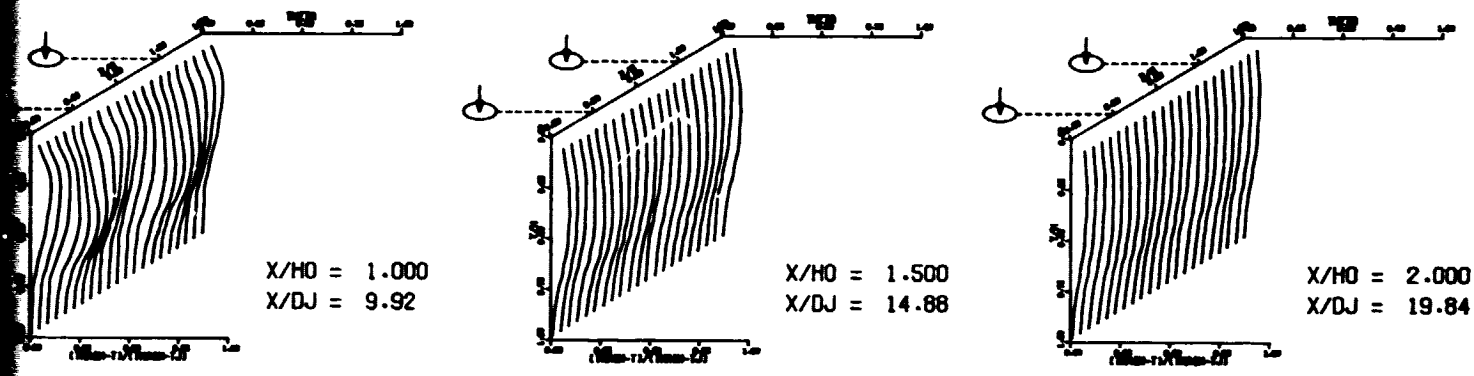

ON I, TMAIN=CONST., J = 30.53 , S/D = 4.00 , H/D = 8.00

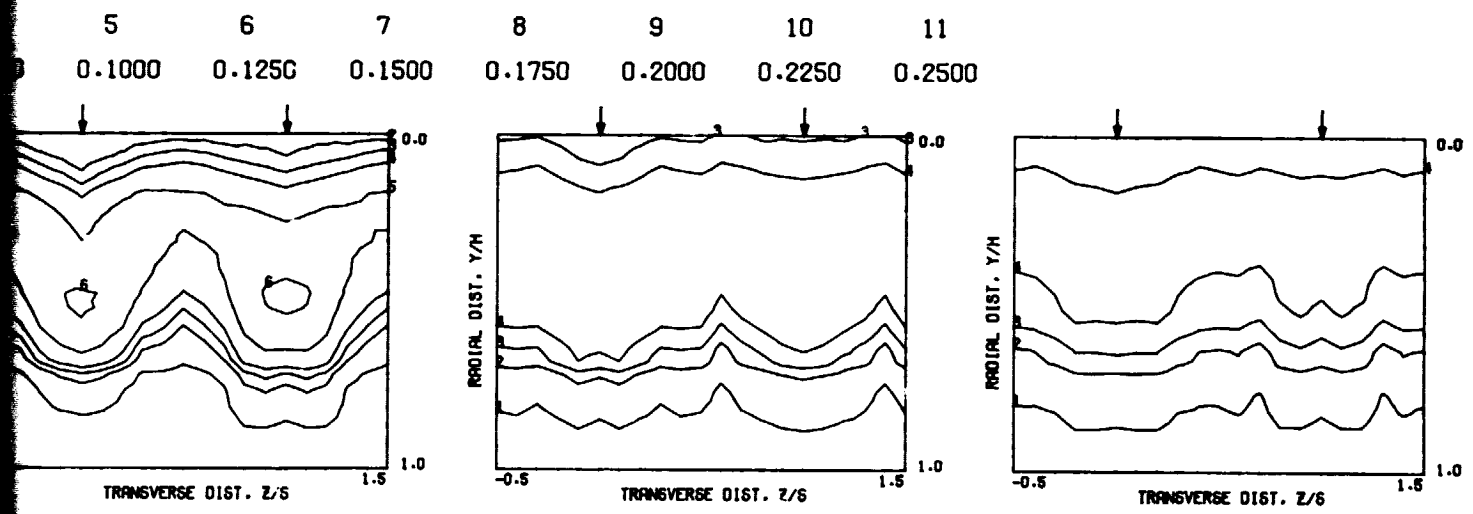

EST NO.12, TMAIN=CONST, J=30.53, S/D=4.0, H/D=8.0

2 FOLDOUT FRAME

Figure 34

ORIGINAL PAGE IS
OF POOR QUALITY

CONTOUR	1	2	3	4	5	6	7
VALUE	0.0250	0.0500	0.0617	0.0750	0.1000	0.1250	0.1500

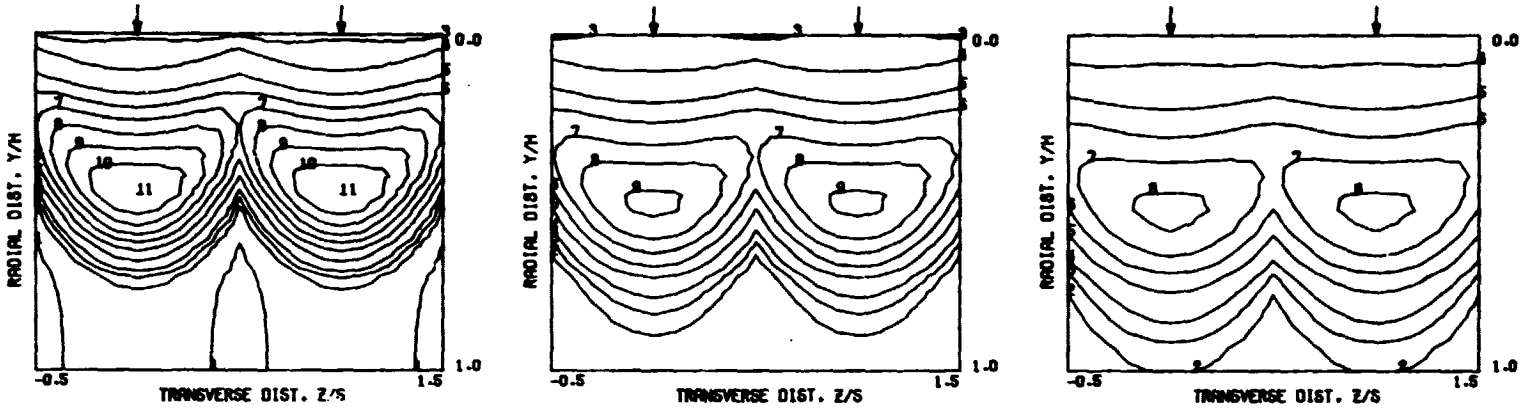

PREDICTED THETA CONTOURS FOR TEST NO.12, TMAIN=CONST, J=3

S/DJ = 4.96 HO/DJ = 9.92 VRATIO = 6.39 TRATIO = 1.391 DENRATIO=0.747 TMAIN

X/H = 0.50 X/DJ =4.96 X/H = 0.75 X/DJ =7.44 X/H = 1.00 X/DJ =9.92

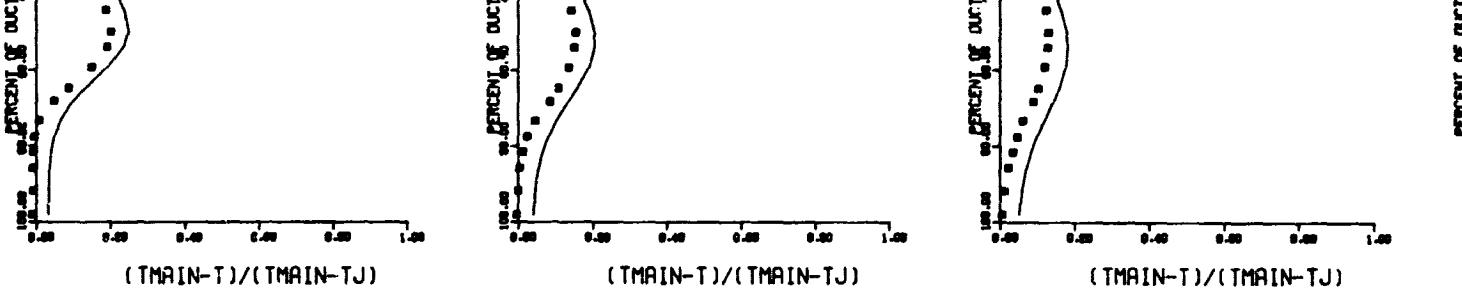

COMPARISON BETWEEN DATA AND CORRELATIONS FOR TEST NO. 12, TEST SECTION I ,UNIFORM

ORIGINAL PAGE IS
OF POOR QUALITY

FOLDOUT FRAME

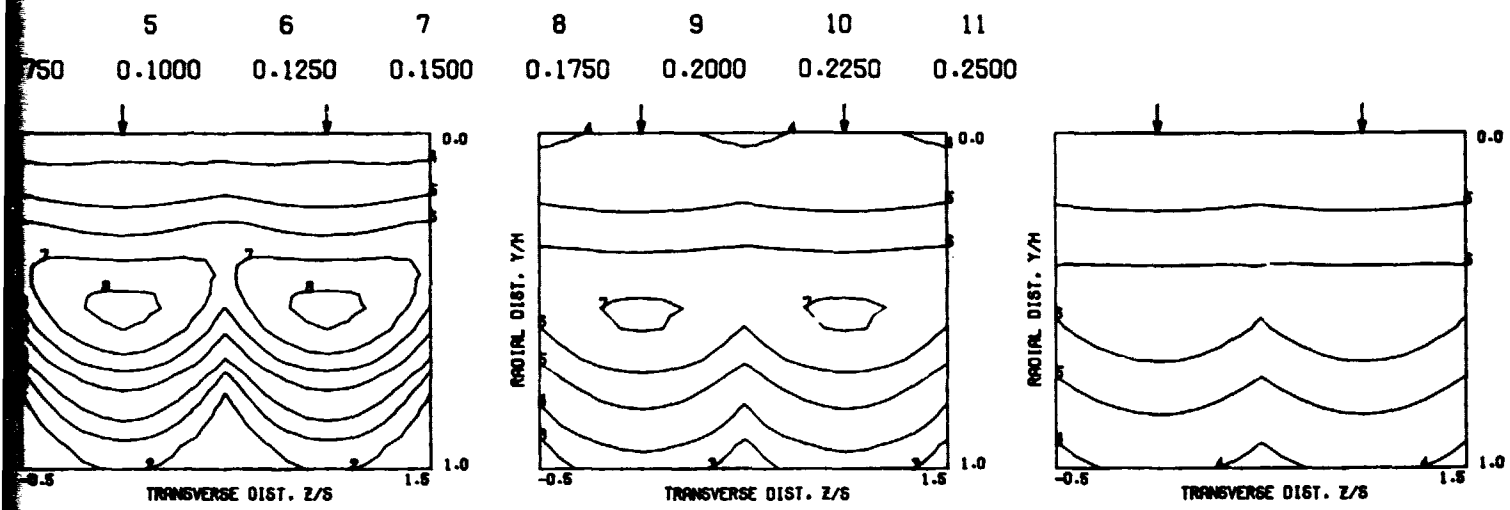

R TEST NO.12. TMAIN=CONST. J=30.5. S/D=4.0. H/D=8.0

IO = 1.391 DENRATIO=0.747 TMAIN = 293.5 K TJET = 408.1 K THEB = 0.062

X/H = 1.00 X/DJ =9.92 X/H = 1.50 X/DJ =14.88 X/H = 2.00 X/DJ =19.84

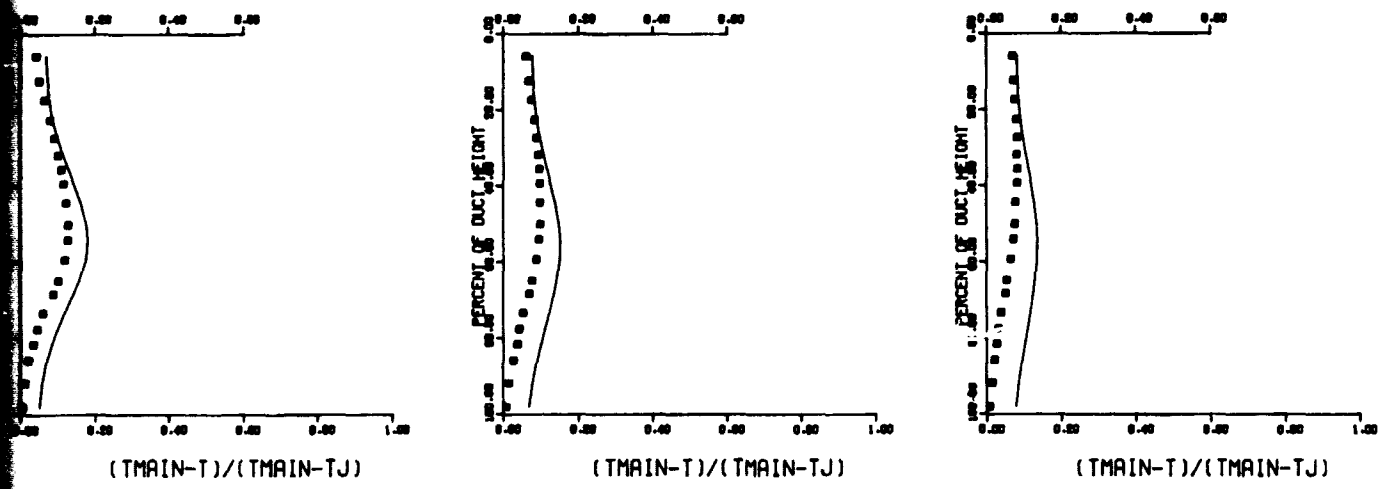

NO. 12. TEST SECTION I ,UNIFORM TMAIN. J = 30.53 , S/D =4.00 , H/D =8.00

Figure 35

2 FOLDOUT FRAME

ORIGINAL PAGE IS
OF POOR QUALITY

ORIGINAL PAGE IS
OF POOR QUALITY

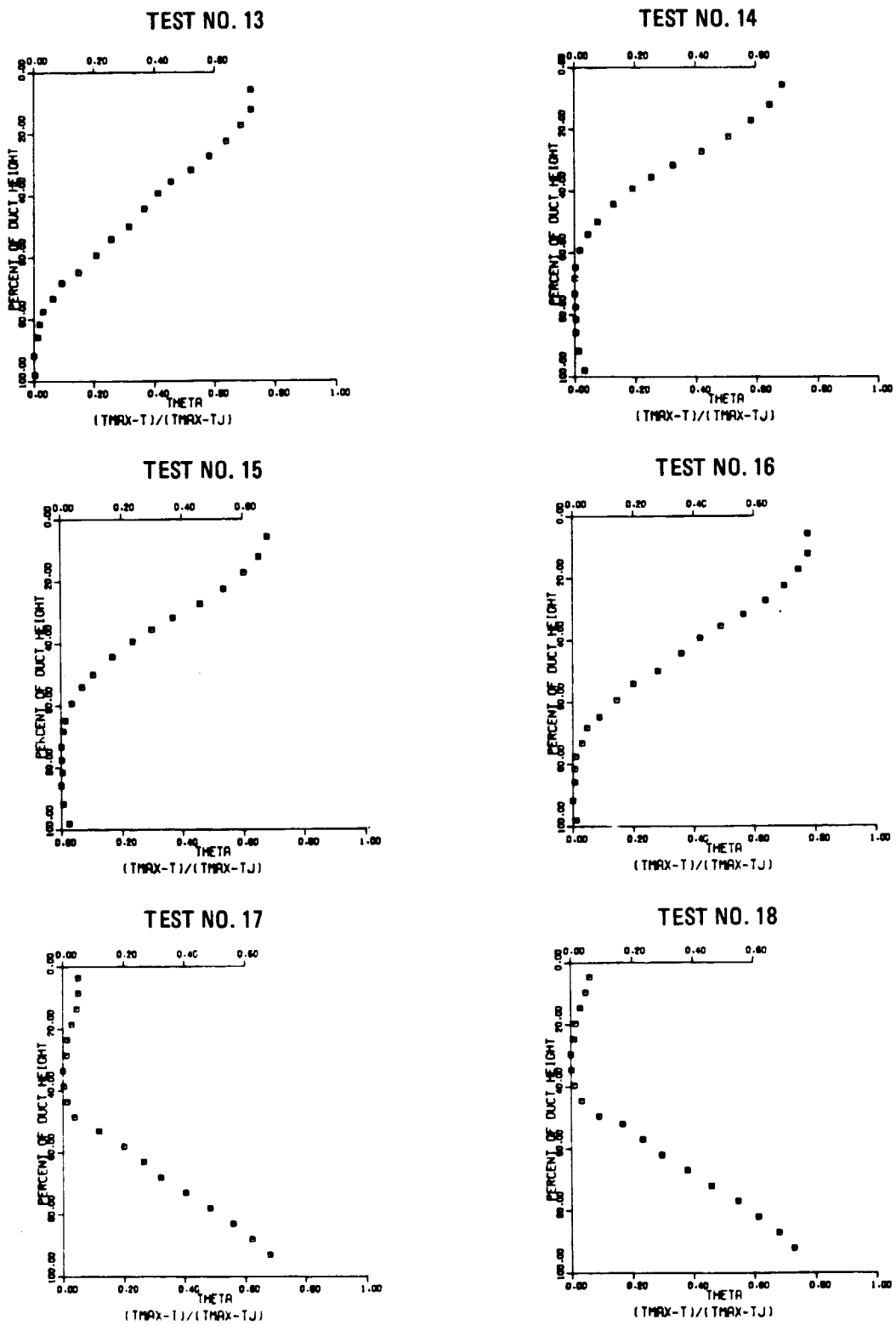

Figure 36. Profiled Mainstream Theta Distributions Used in Series 2 Test Cases.

S = 0.0508 METERS S/DJ = 2.561 HO/DJ = 5.122 VMAIN = 16.9 M/SEC VJET = 59.7 M/SEC TMAIN = 524.4 K TJE

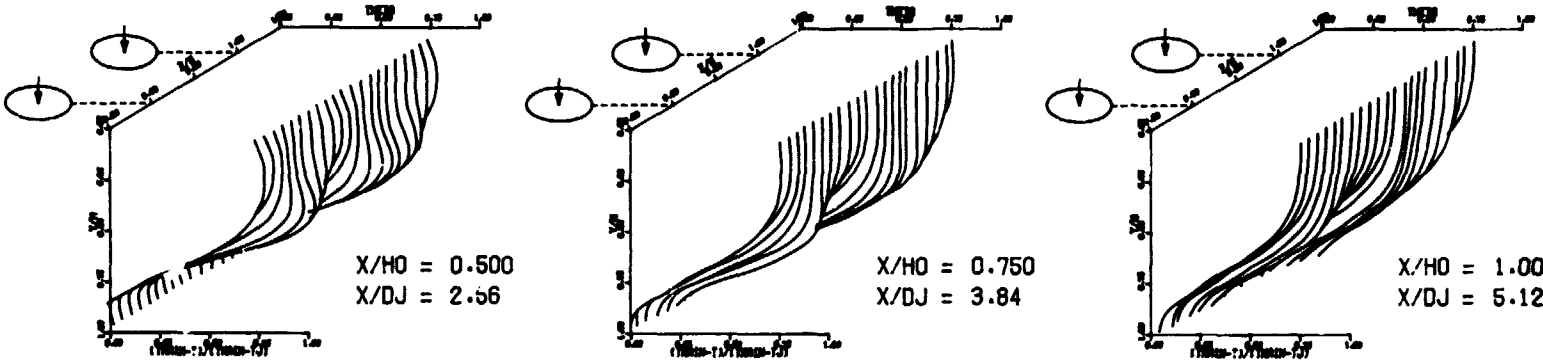

MEASURED THETA PROFILES FOR TEST NO. 13, TEST SECTION II, TOP COLD , J =

CONTOUR	1	2	3	4	5	6	7
VALUE	0.0500	0.1000	0.1500	0.2000	0.2500	0.3120	0.3500

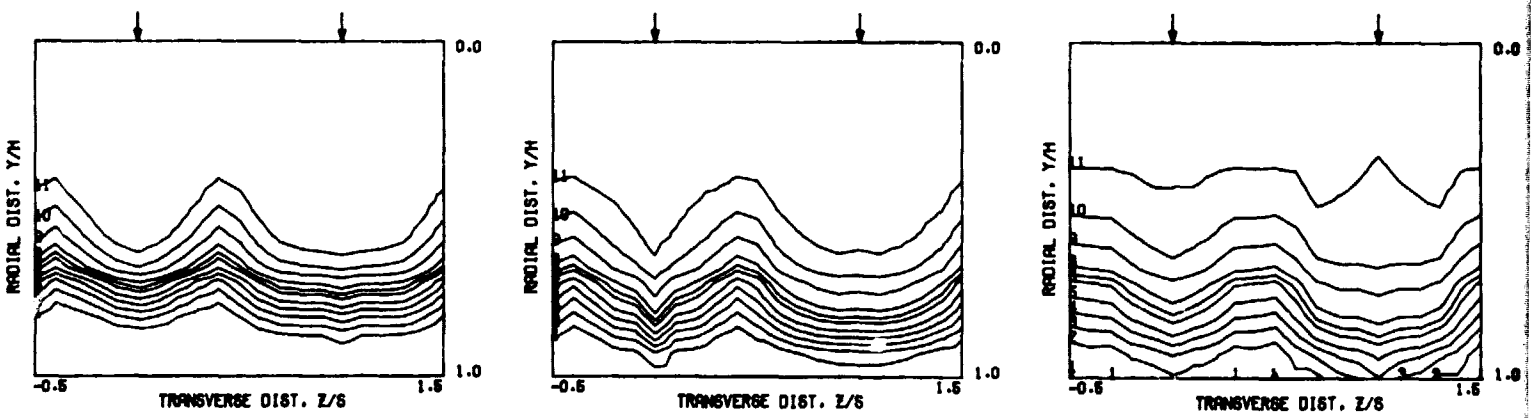

MEASURED THETA CONTOURS FOR TEST NO.13, TOP COLD, J=22

FOLDOUT FRAME

ORIGINAL PAGE IS
OF POOR QUALITY

7 M/SEC TMAIN = 524.4 K TJET = 293.5 K THEB = 0.3120 BLORAT= 7.626 DENRATIO= 1.805 TRATIO= 0.560

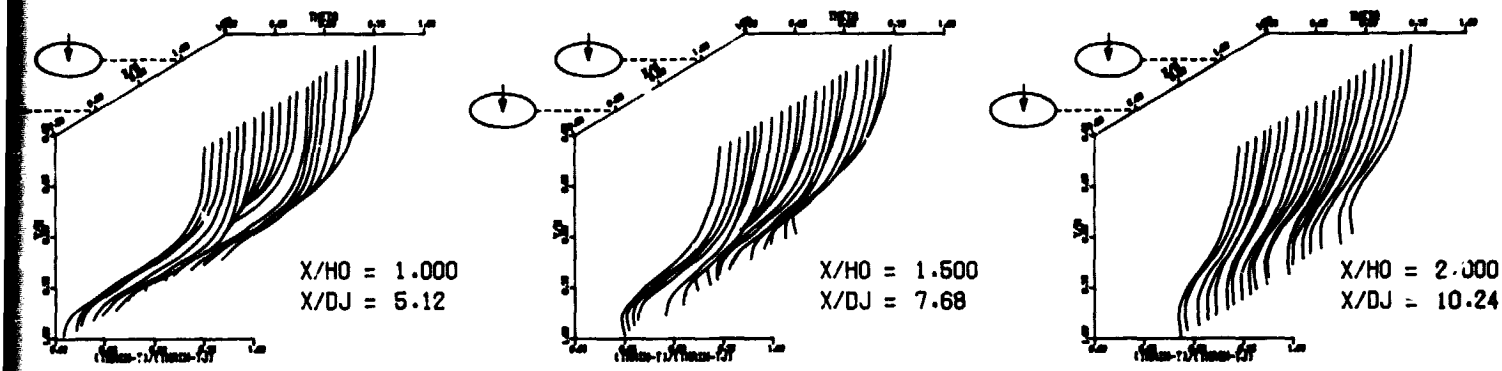

ION II, TOP COLD , J = 22.63 , S/D = 2.00 , H/D = 4.00

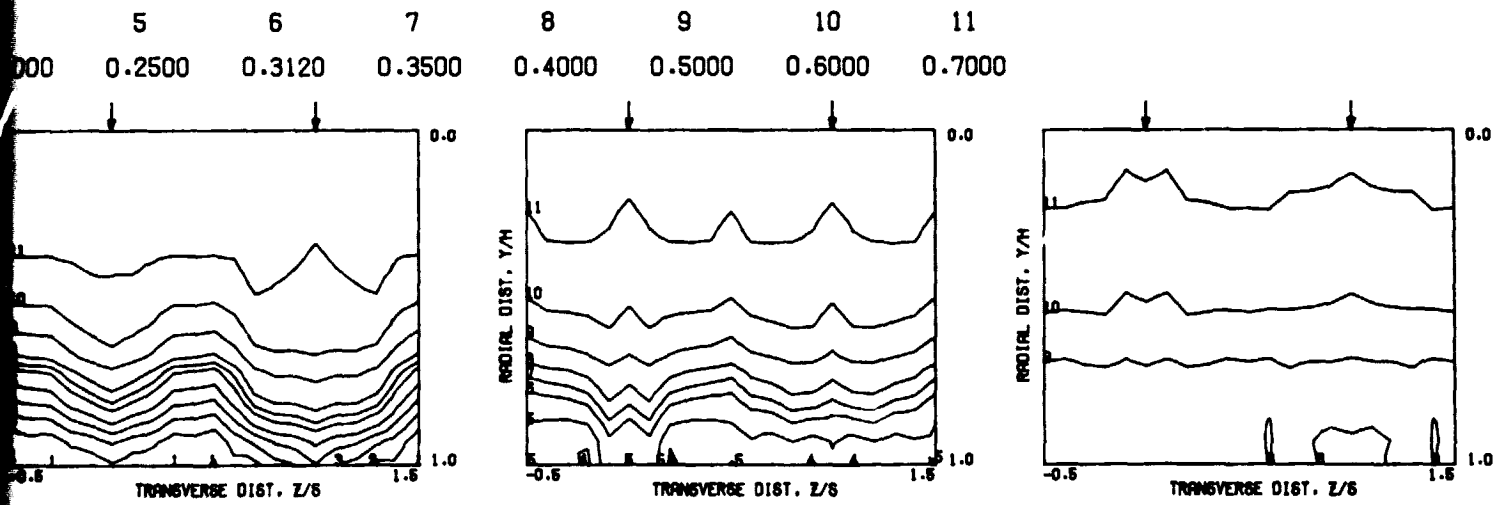

TEST NO.13, TOP COLD, J=22.63, S/D=2.0, H/D=4.0

2 FOLDOUT FRAME

Figure 37

ORIGINAL PAGE IS
OF POOR QUALITY

CONTOUR	1	2	3	4	5	6	7
VALUE	0.0500	0.1000	0.1500	0.2000	0.2500	0.3120	0.3500

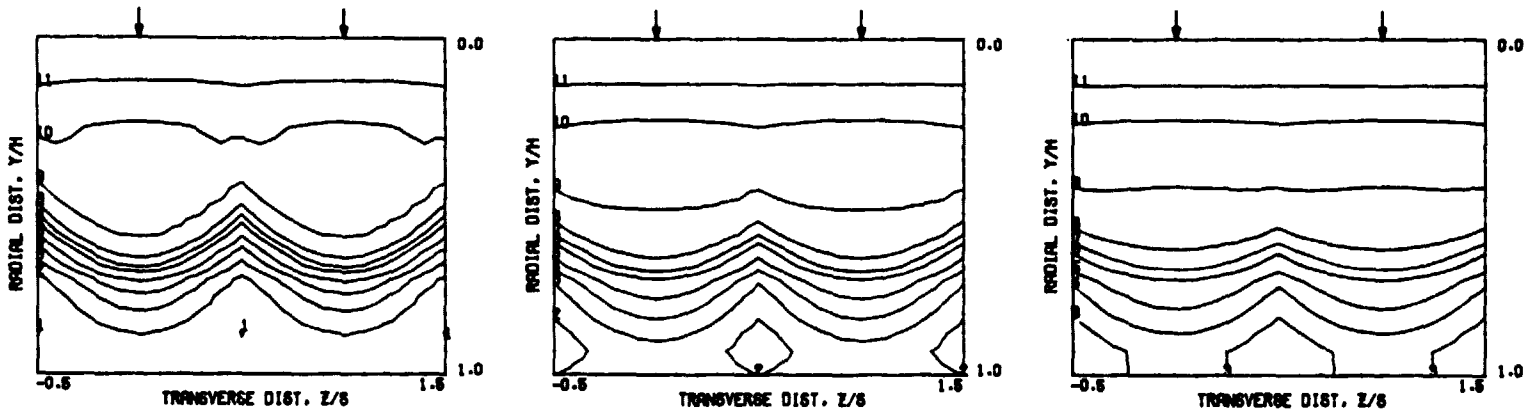

PREDICTED THETA CONTOURS FOR TEST NO. 13, TOP COLD, J=22

S/DJ = 2.56 HO/DJ = 5.12 VRATIO = 3.54 TRATIO = 0.560 DENRATIO= 1.805 TMAIN

X/H = 0.50 X/DJ =2.56 X/H = 0.75 X/DJ =3.84 X/H = 1.00 X/DJ =5.12

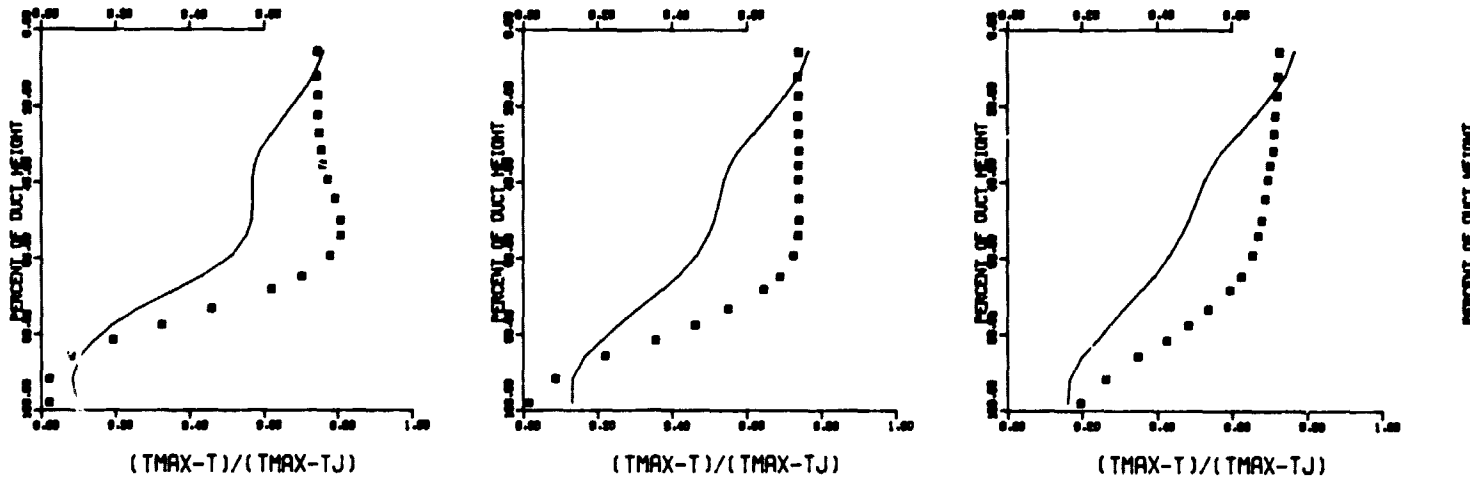

COMPARISON BETWEEN DATA AND CORRELATIONS FOR TEST NO. 13, TEST SECTION II, TOP

FOLDOUT FRAME

ORIGINAL PAGE IS
OF POOR QUALITY

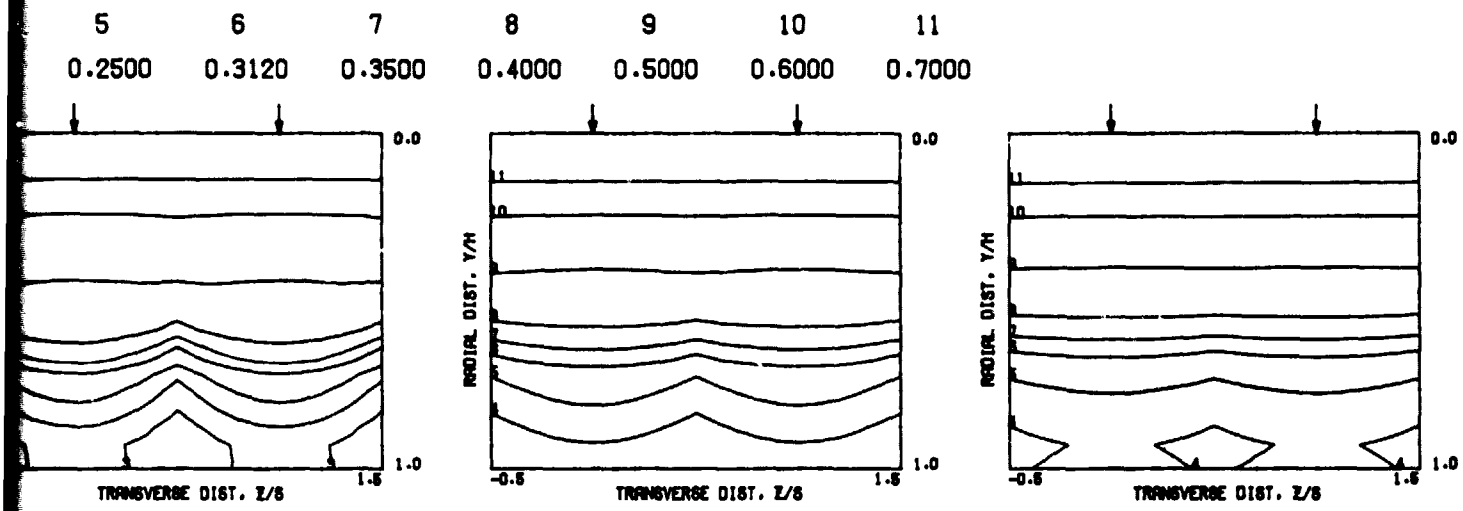

EST NO. 13, TOP COLD, J=22.63, S/D=2.0, H/D=4.0

0.560 DENRATIO=1.805 TMAIN = 524.4 K TJET = 293.5 K THEB = 0.156

= 1.00 X/DJ =5.12 X/H = 1.50 X/DJ =7.68 X/H = 2.00 X/DJ =10.24

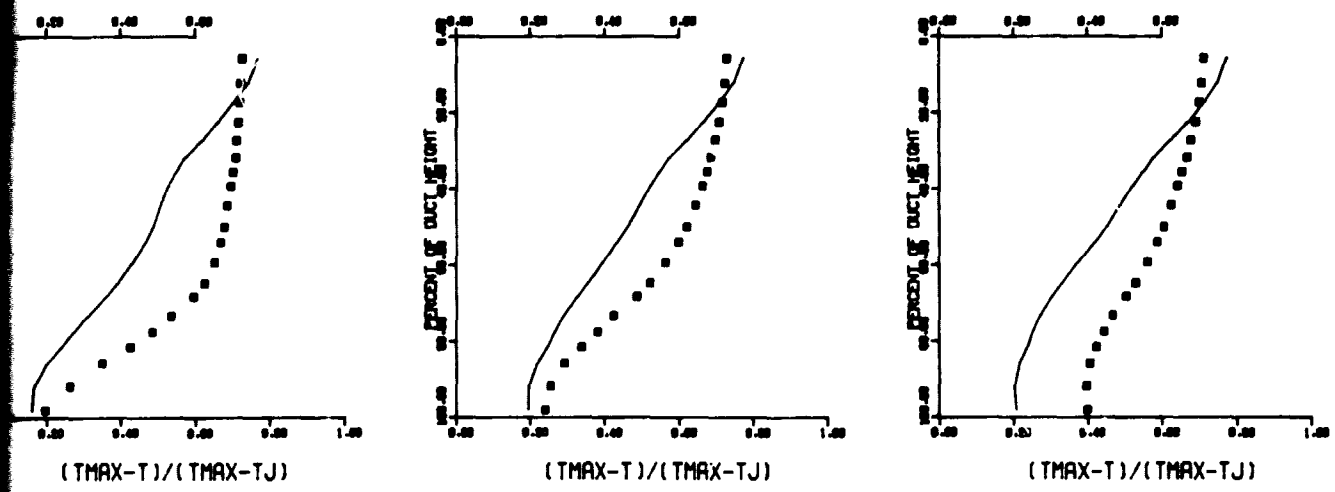

ORIGINAL PAGE IS
OF POOR QUALITY

13, TEST SECTION II, TOP COLD , J = 22.63 , S/D =2.00 , H/D =4.00

Figure 38

2 FOLDOUT FRAME

S = 0.1016 METERS S/DJ = 4.845 HO/DJ = 4.845 VMAIN = 15.4 M/SEC VJET = 28.4 M/SEC TMAIN = 672.3 K TJET

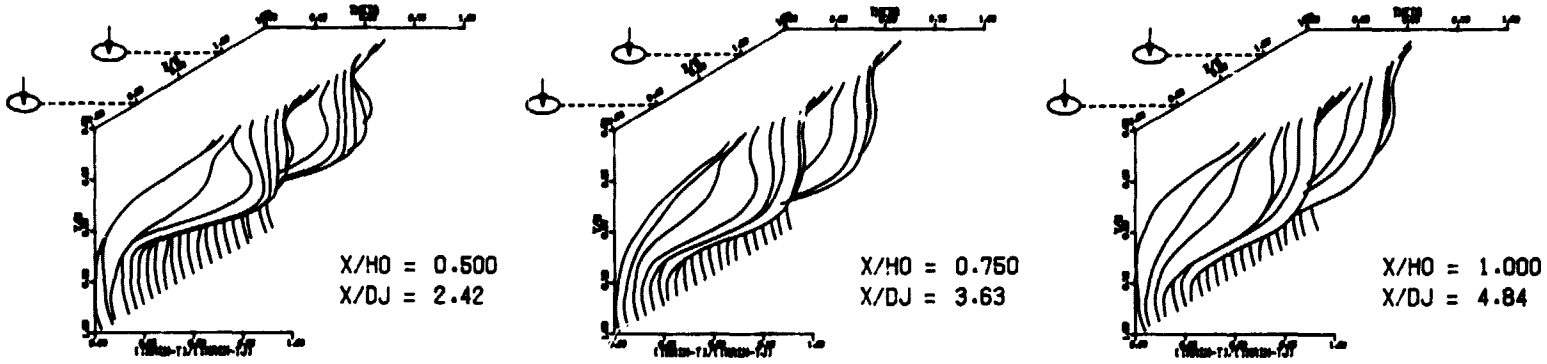

MEASURED THETA PROFILES FOR TEST NO. 14, TEST SECTION I, TOP COLD , J = 7

CONTOUR	1	2	3	4	5	6	7
VALUE	0.0500	0.1140	0.1500	0.2000	0.2500	0.3000	0.3500

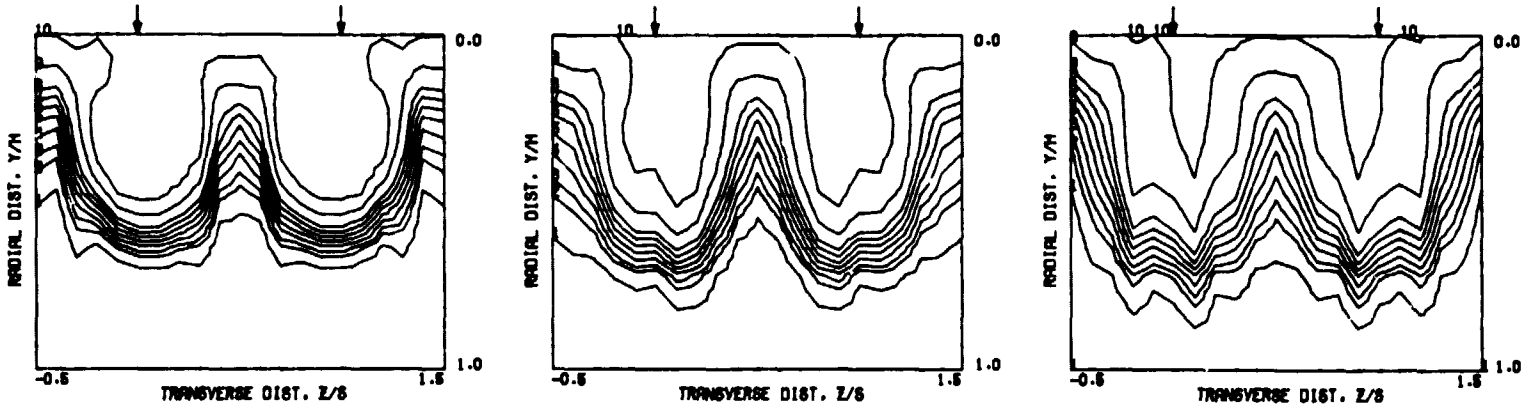

MEASURED THETA CONTOURS FOR TEST NO.14, TOP COLD, J=7.5

FOLDOUT FRAME

ORIGINAL PAGE IS
OF POOR QUALITY

M/SEC TMAIN = 672.3 K TJET = 304.7 K THEB = 0.1140 BLORAT= 3.847 DENRATIO= 2.210 TRATIO=0.453

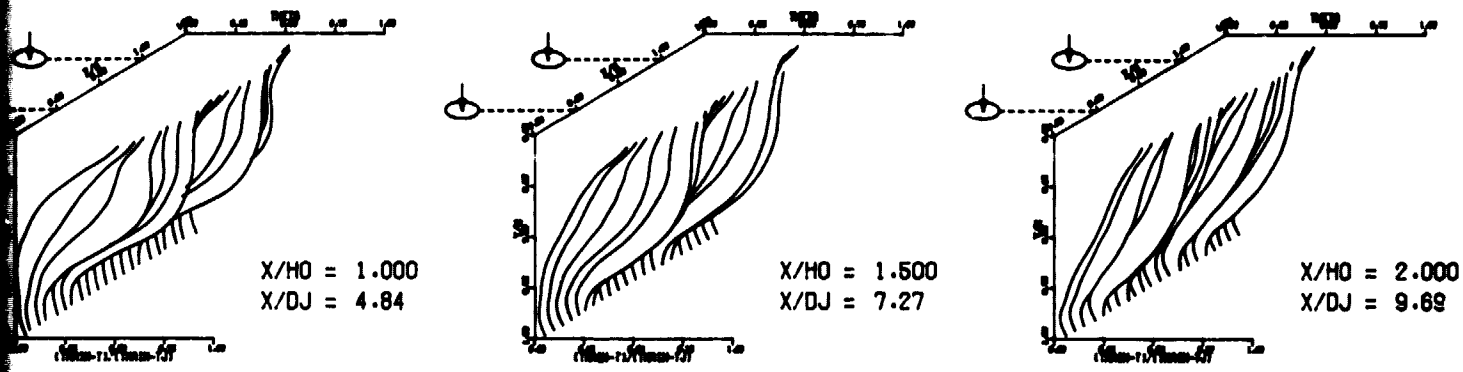

ON I. TOP COLD , J = 7.50 , S/D = 4.00 , H/D = 4.00

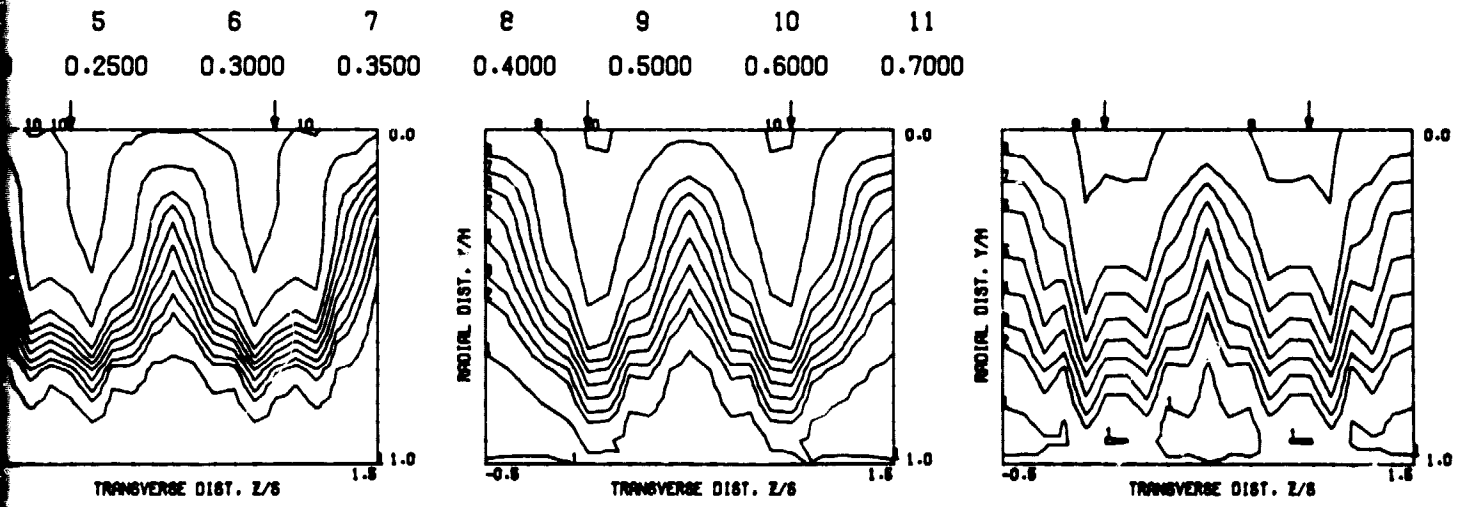

EST NO.14. TOP COLD. J=7.50. S/D=4.0. H/D=4.0

ORIGINAL PAGE IS
OF POOR QUALITY

Figure 39

2 FOLDOUT FRAME

CONTOUR	1	2	3	4	5	6	7
VALUE	0.0500	0.1140	0.1500	0.2000	0.2500	0.3000	0.3500

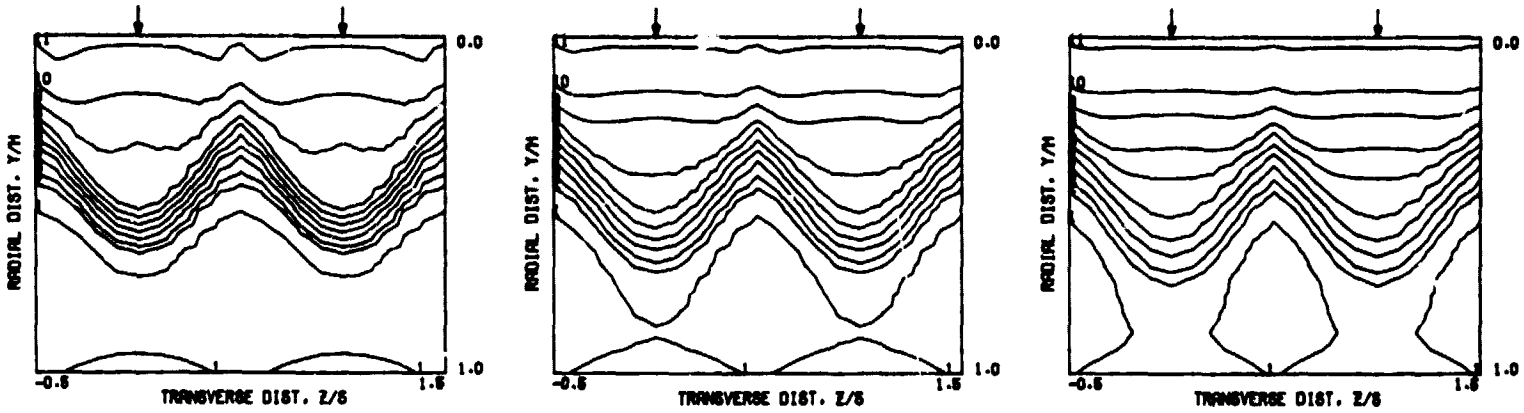

PREDICTED THETA CONTOURS FOR TEST NO. 14, TOP COLD, J=7

S/DJ = 4.84 HO/DJ = 4.84 VRATIO = 1.84 TRATIO = 0.453 DENRATIO=2.210 TMAI

X/H = 0.50 X/DJ =2.42 X/H = 0.75 X/DJ =3.63 X/H = 1.0 X/DJ =4.84

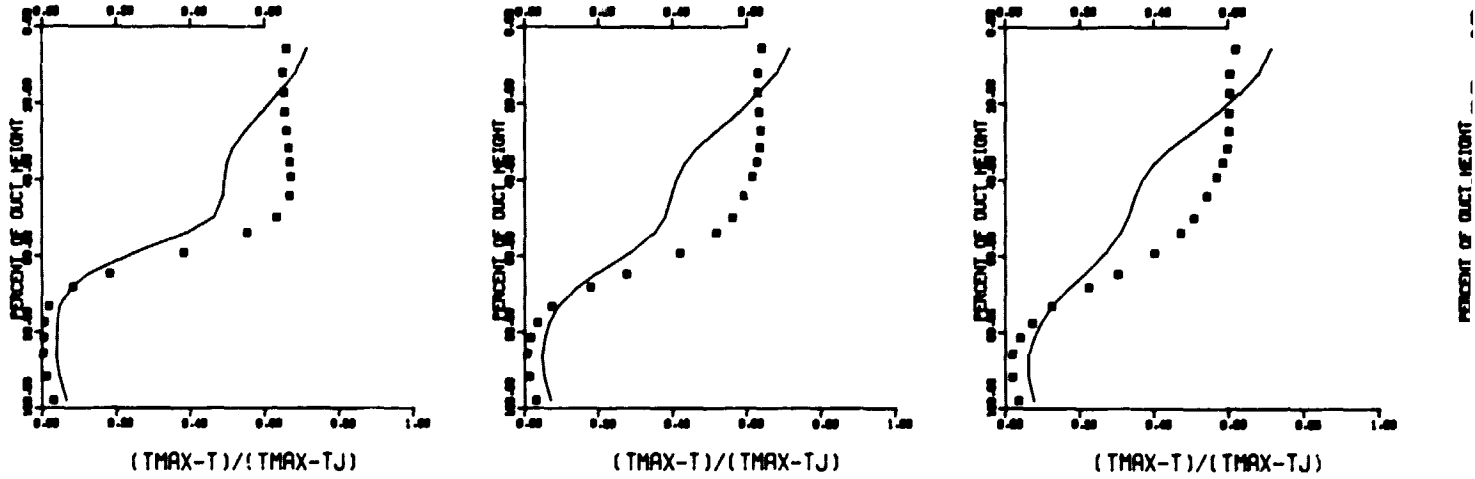

COMPARISON BETWEEN DATA AND CORRELATIONS FOR TEST NO. 14, TEST SECTION I, TOP

ORIGINAL PAGE IS
OF POOR QUALITY

FOLDOUT FRAME

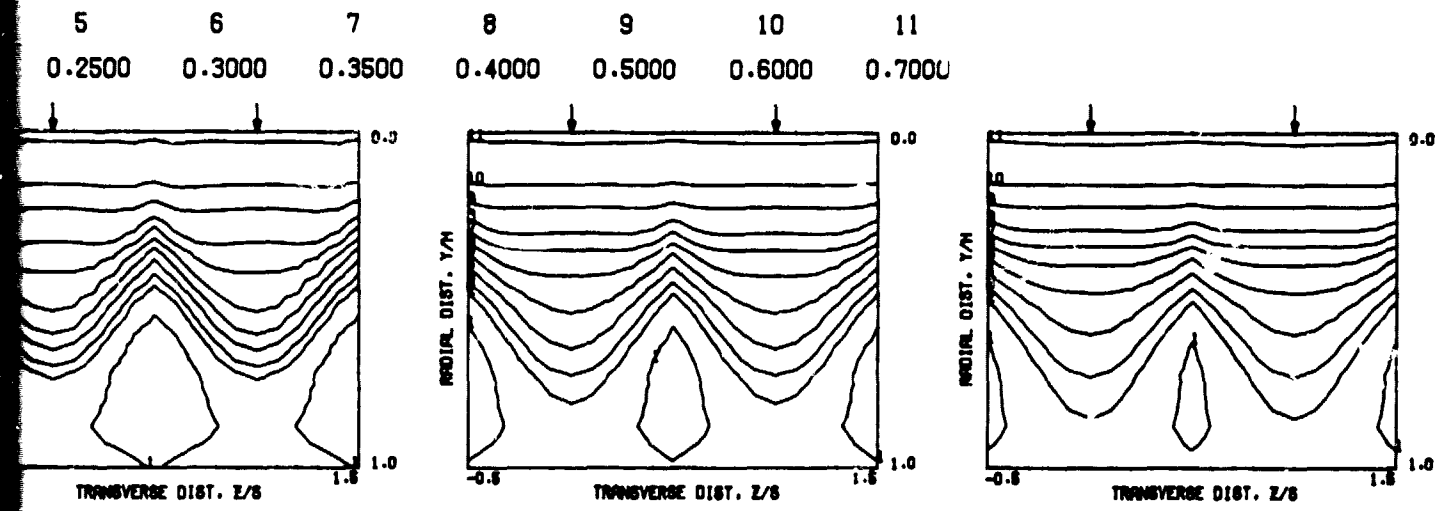

ST NO. 14, TOP COLD, J=7.50, S/D=4.0, H/D=4.0

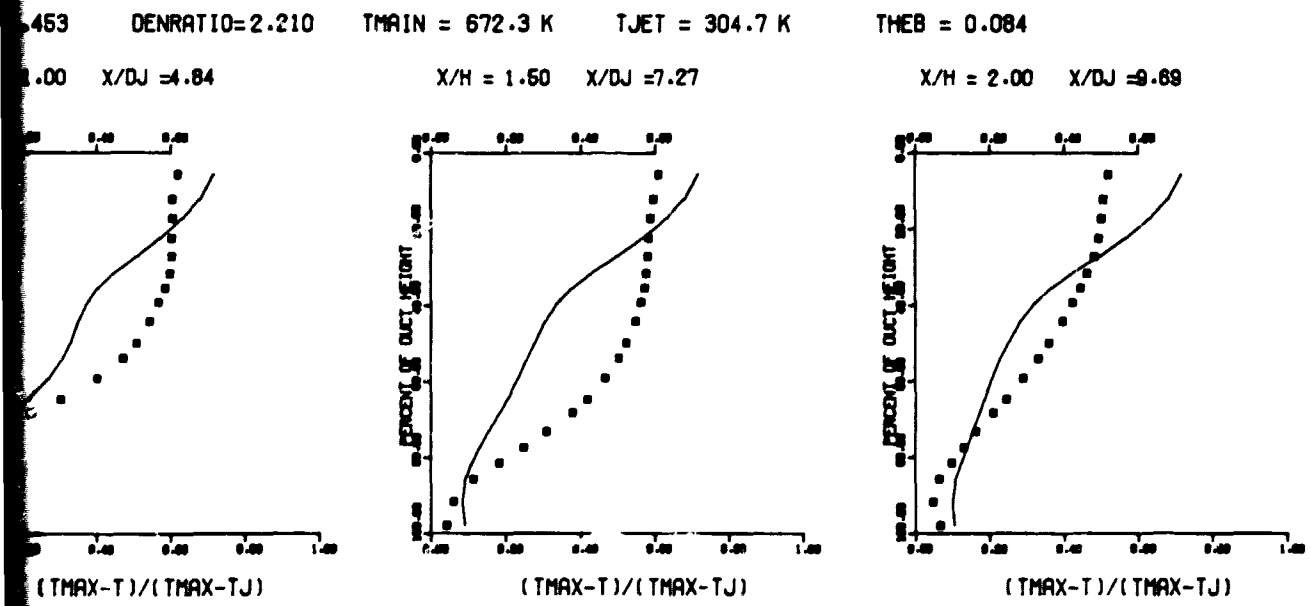

2 FOLDOUT FRAME

4, TEST SECTION I, TOP COLD , J = 7.50 , S/D =4.00 , H/D =4.00

Figure 40

ORIGINAL PAGE IS
OF POOR QUALITY

S = 0.0254 METERS S/DJ = 2.588 HO/DJ = 10.353 VMAIN = 15.5 M/SEC VJET = 109.3 M/SEC TMAIN = 616.1 K TJE

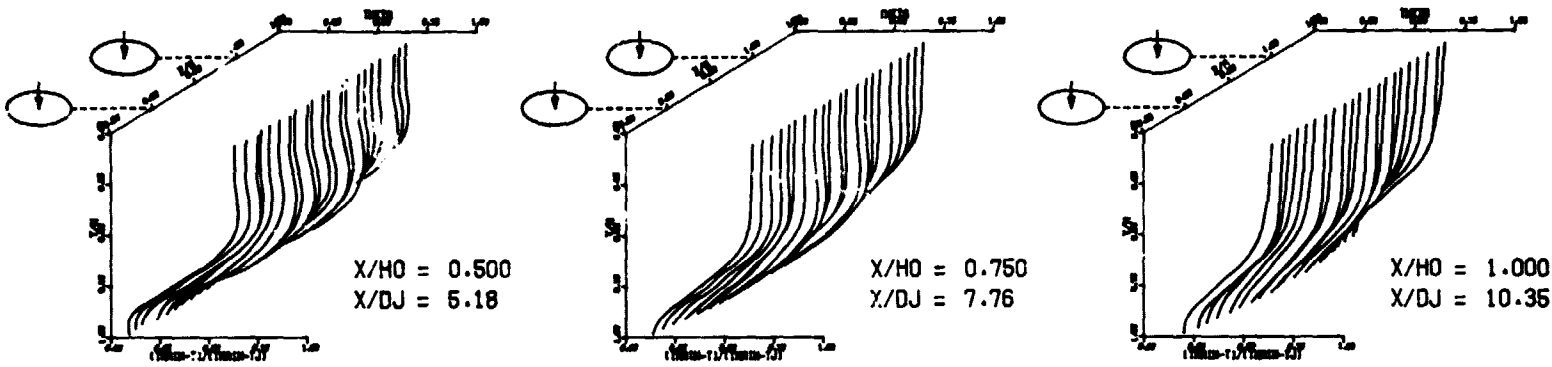

MEASURED THETA PROFILES FOR TEST NO. 15, TEST SECTION I, TOP COLD , J =

CONTOUR	1	2	3	4	5	6	7
VALUE	0.0500	0.1000	0.1500	0.2000	0.2500	0.3029	0.3500

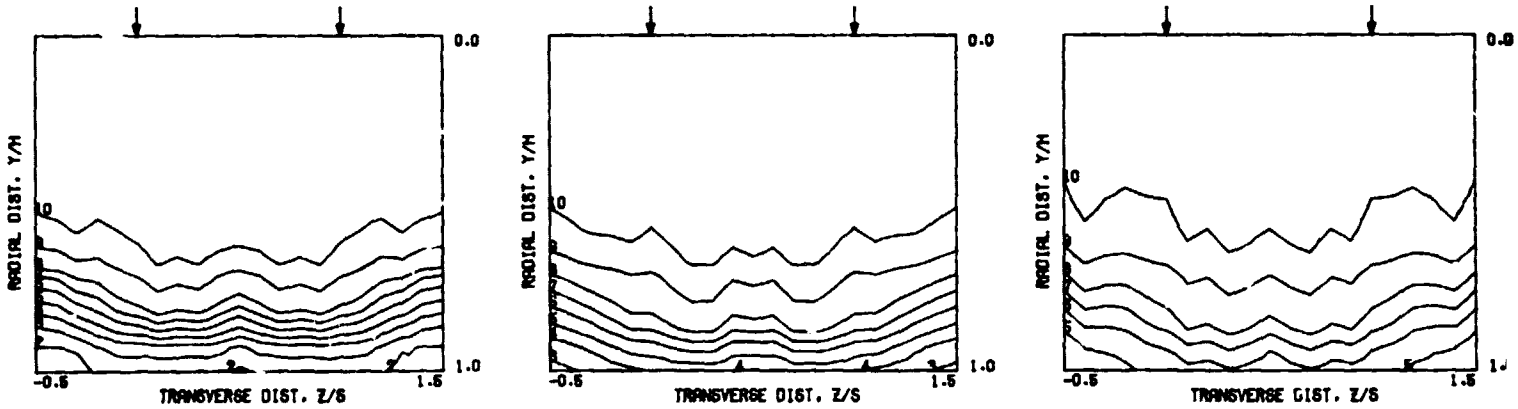

MEASURED THETA CONTOURS FOR TEST NO.15, TOP COLD, J=1(

FOLDOUT FRAME

ORIGINAL PAGE IS
OF POOR QUALITY

SEC TMAIN = 616.1 K TJET = 297.2 K THEB = 0.3029 BLORAT= 14.821 DENRATIO= 2.215 TRATIO=0.482

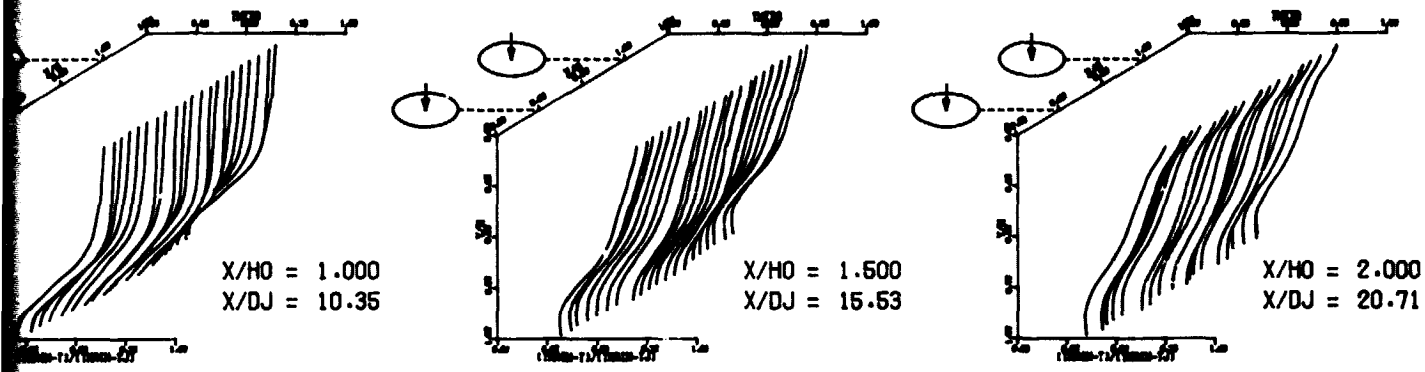

I, TOP COLD , J = 109.85 , S/D = 2.00 , H/D = 8.00

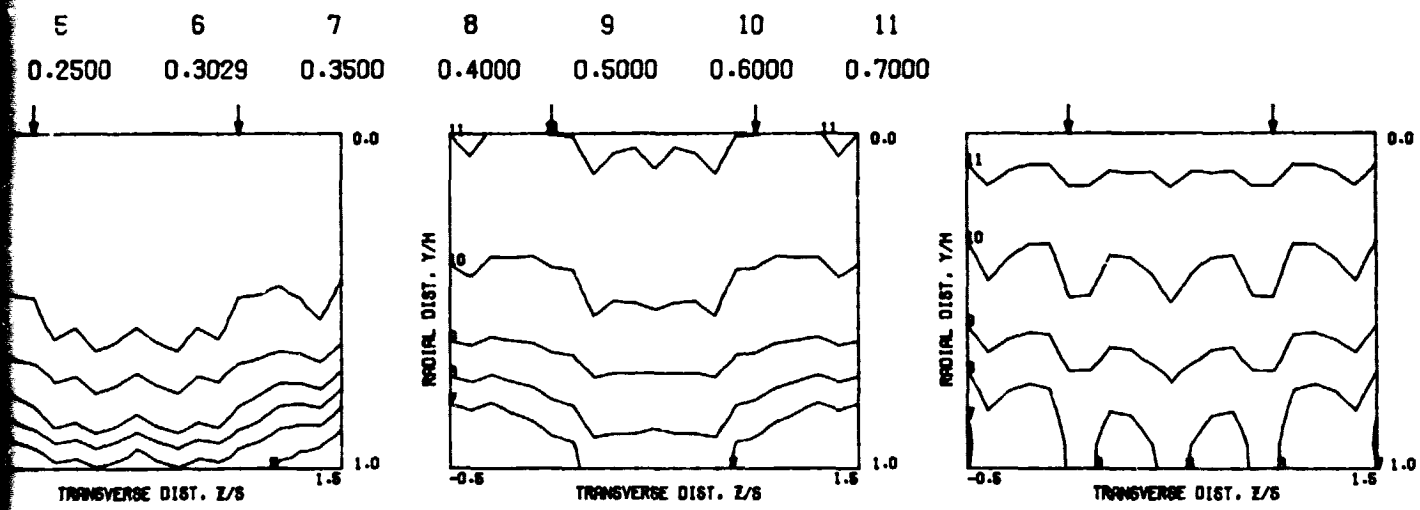

NO.15, TOP COLD, J=109.9, S/D=2.0, H/D=8.0

2 FOLDOUT FRAME

Figure 41

ORIGINAL PAGE IS
OF POOR QUALITY

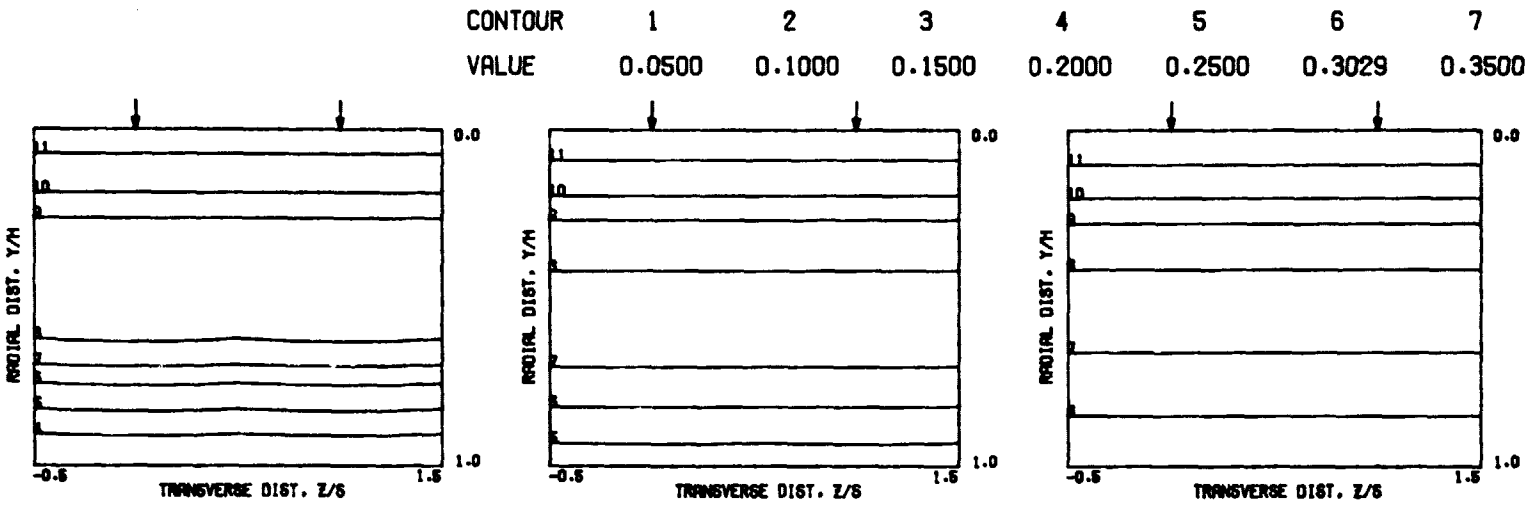

PREDICTED THETA CONTOURS FOR TEST NO. 15, TOP COLD, J=109

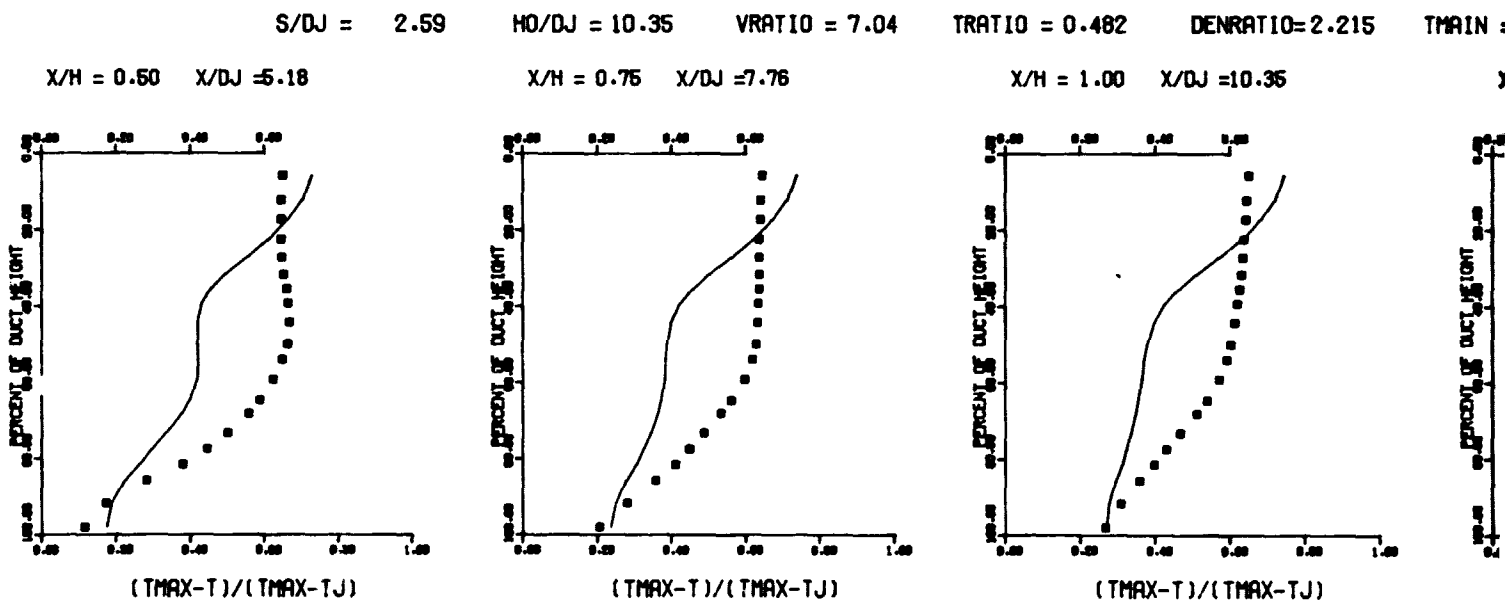

COMPARISON BETWEEN DATA AND CORRELATIONS FOR TEST NO. 15, TEST SECTION I, TOP C

FOLDOUT FRAME

ORIGINAL PAGE IS
OF POOR QUALITY

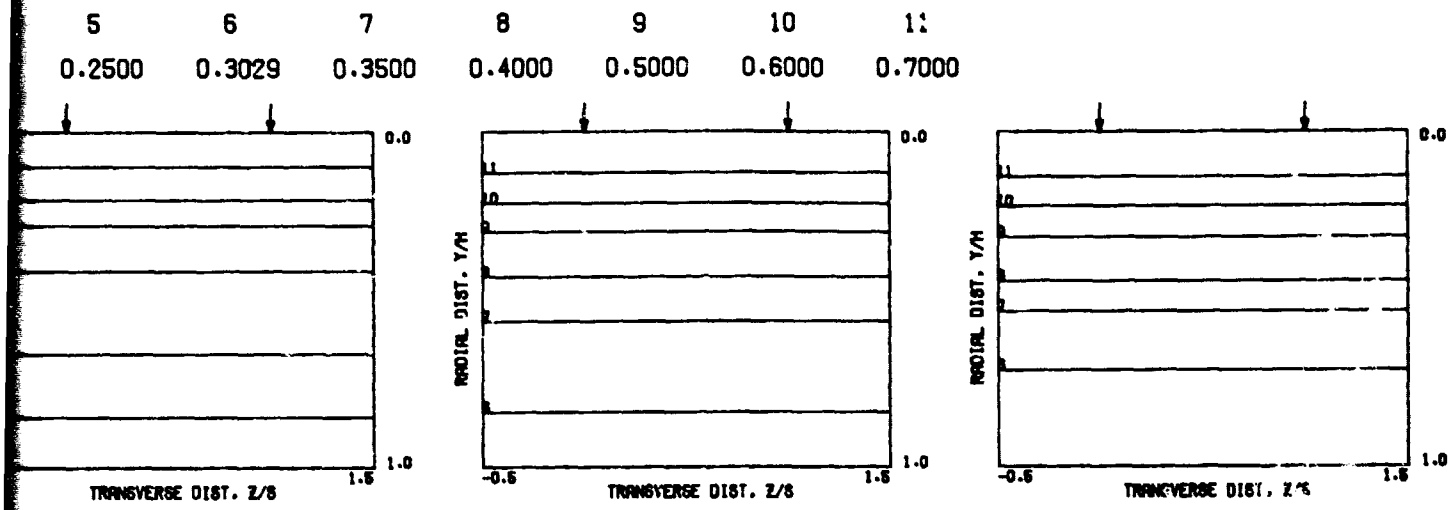

EST NO. 15, TOP COLD, J=109.9, S/D=2.0 H/D=8.0

0.482 DENRATIO=2.215 TMAIN = 616.1 K TJET = 297.2 K THEB = 0.223

= 1.00 X/DJ =10.35 X/H = 1.50 X/DJ =15.53 X/H = 2.00 X/DJ =20.71

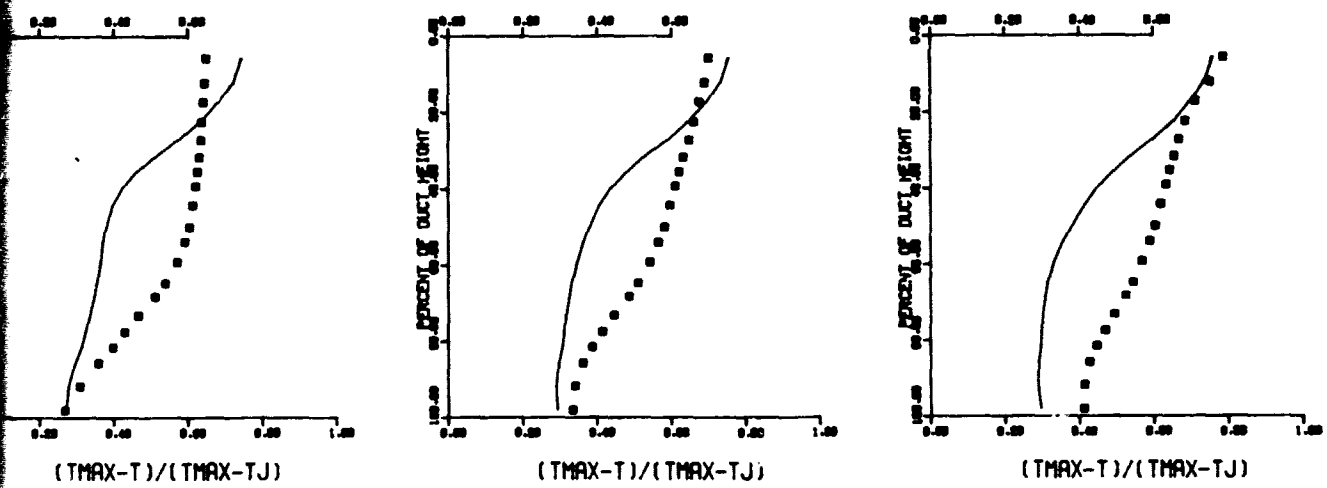

ORIGINAL PAGE IS
OF POOR QUALITY

. 15, TEST SECTION I, TOP COLD , J = 109.85 , S/D =2.00 , H/D =8.00

Figure 42

FOLDOUT FRAME

ORIGINAL PAGE IS
OF POOR QUALITY

S = 0.0508 METERS S/DJ = 4.888 HO/DJ = 9.776 VMAIN = 18.1 M/SEC VJET = 63.0 M/SEC TMAIN = 567.1 K TJE

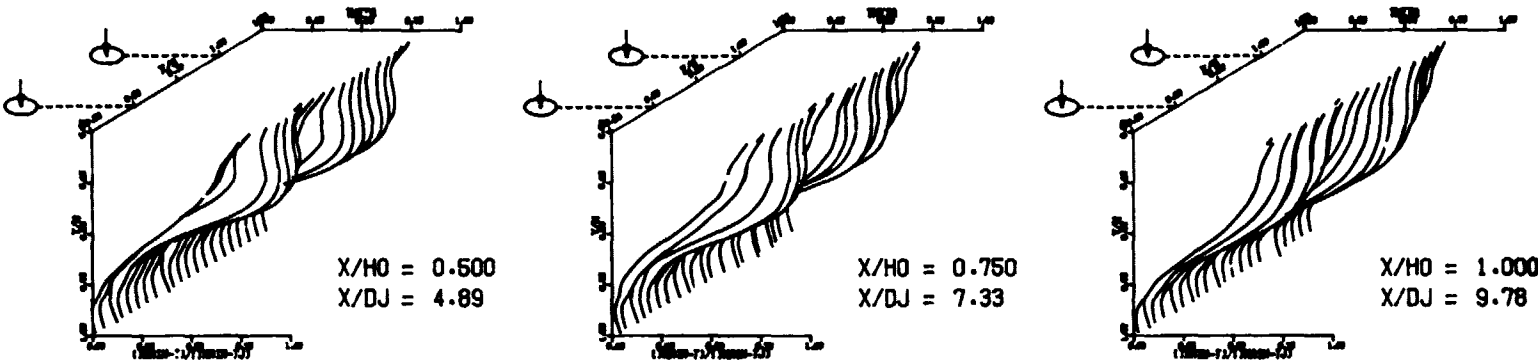

MEASURED THETA PROFILES FOR TEST NO. 16, TEST SECTION I, TOP COLD , J =

CONTOUR	1	2	3	4	5	6	7
VALUE	0.0500	0.0996	0.1500	0.2000	0.2500	0.3000	0.3500

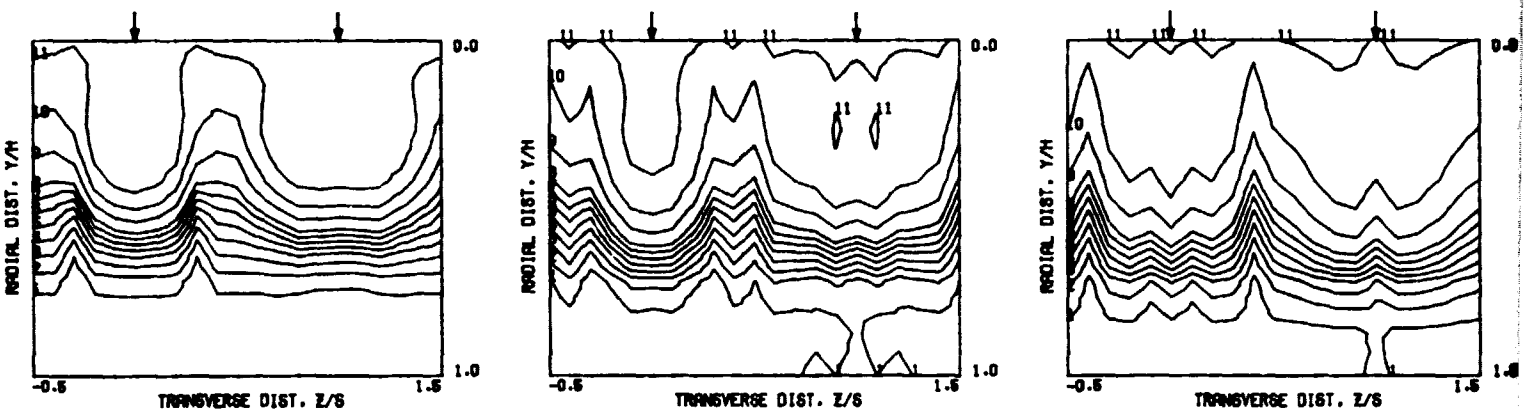

MEASURED THETA CONTOURS FOR TEST NO.16, TOP COLD, J=22

FOLDOUT FRAME

ORIGINAL PAGE IS
OF POOR QUALITY

M/SEC TMAIN = 567.1 K TJET = 310.6 K THEB = 0.0996 BLORAT= 6.908 DENRATIO= 1.856 TRATIO= 0.548

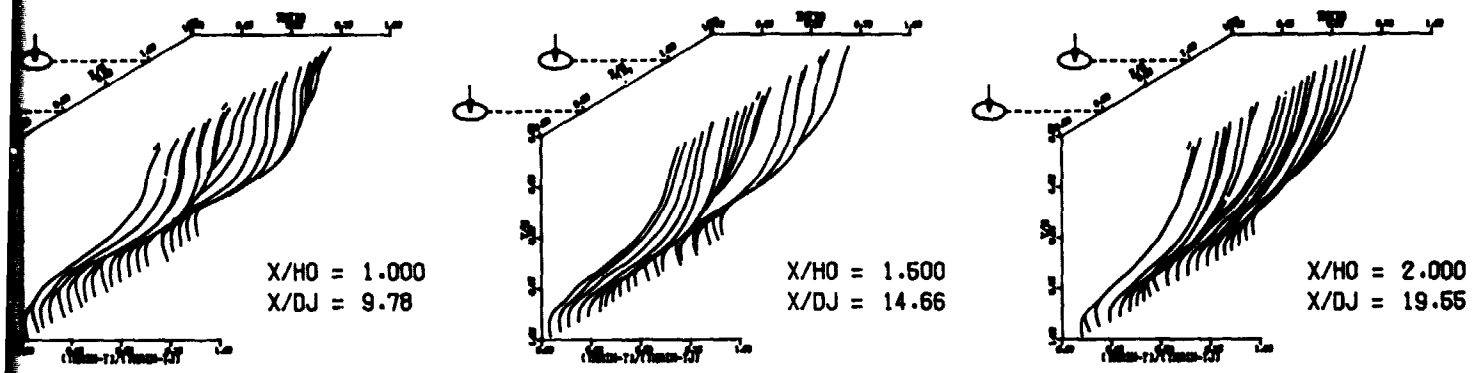

DN I. TOP COLD , J = 22.55 , S/D = 4.00 , H/D = 8.00

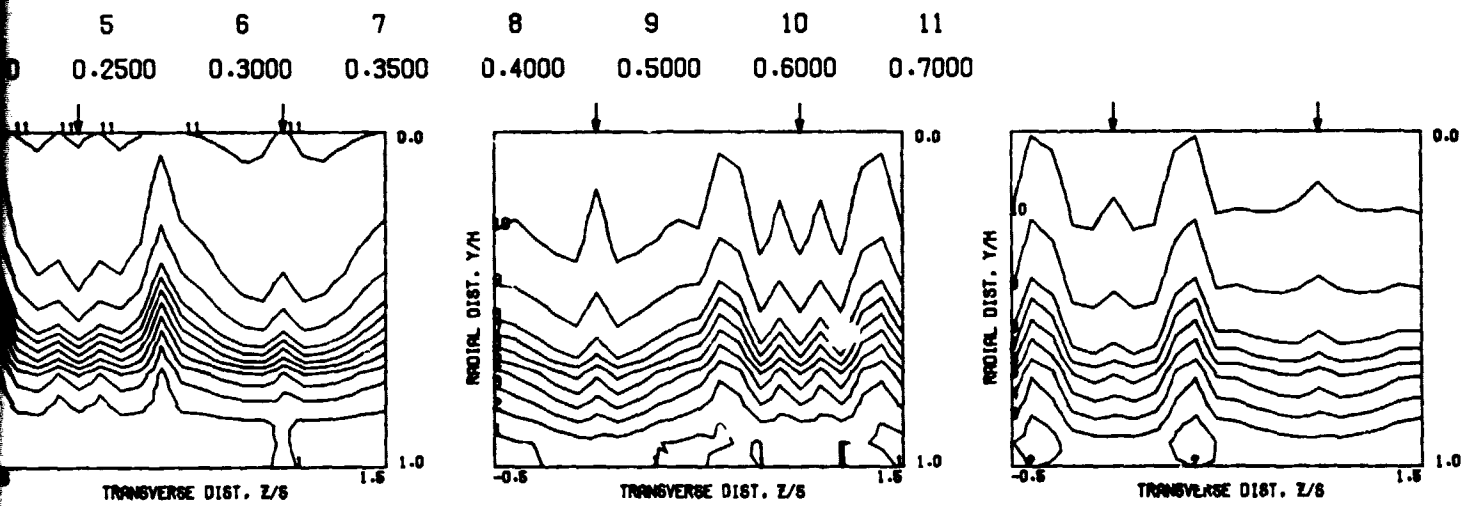

TEST NO.16. TOP COLD. J=22.55. S/D=4.0. H/D=8.0

Figure 43

FOLDOUT FRAME

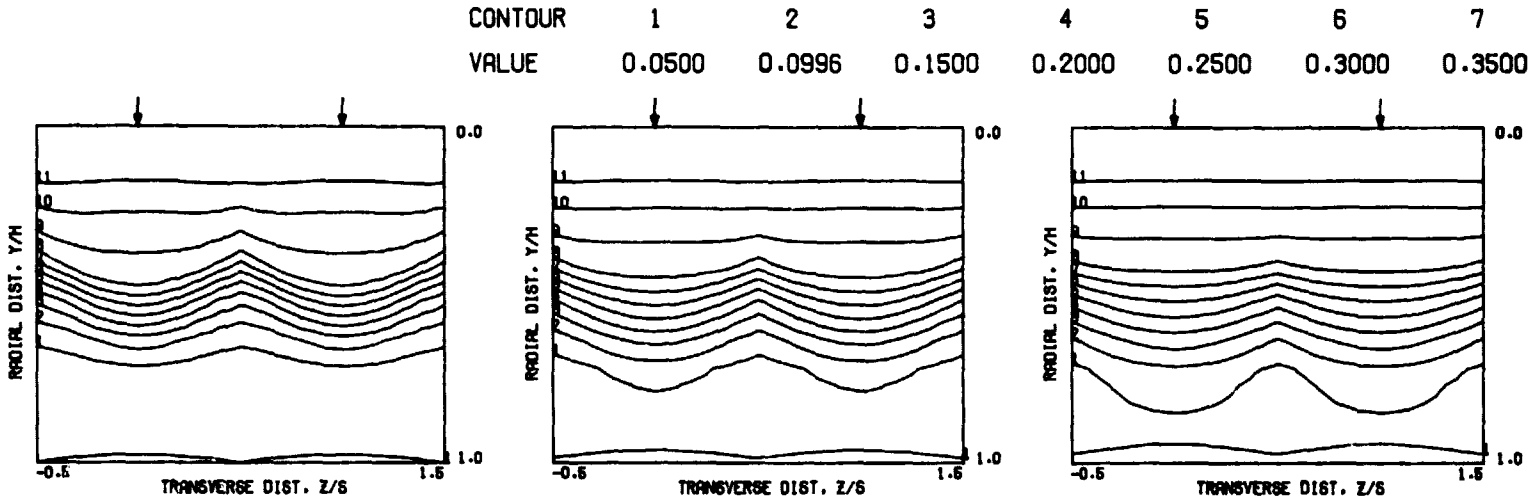

PREDICTED THETA CONTOURS FOR TEST NO. 16, TOP COLD, J=2

S/DJ = 4.89 HO/DJ = 9.78 VRATIO = 3.49 TRATIO = 0.548 DENRATIO=1.856 TMAI

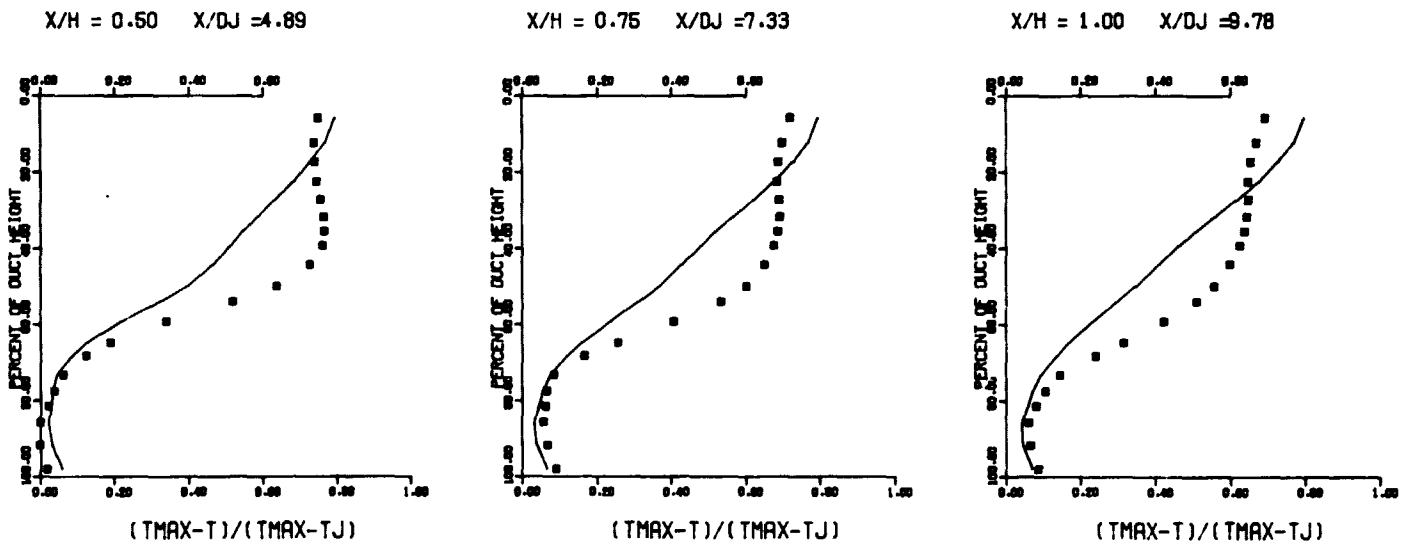

FOLDOUT FRAME

COMPARISON BETWEEN DATA AND CORRELATIONS FOR TEST NO. 16, TEST SECTION I, TOP

ORIGINAL PAGE IS
OF POOR QUALITY

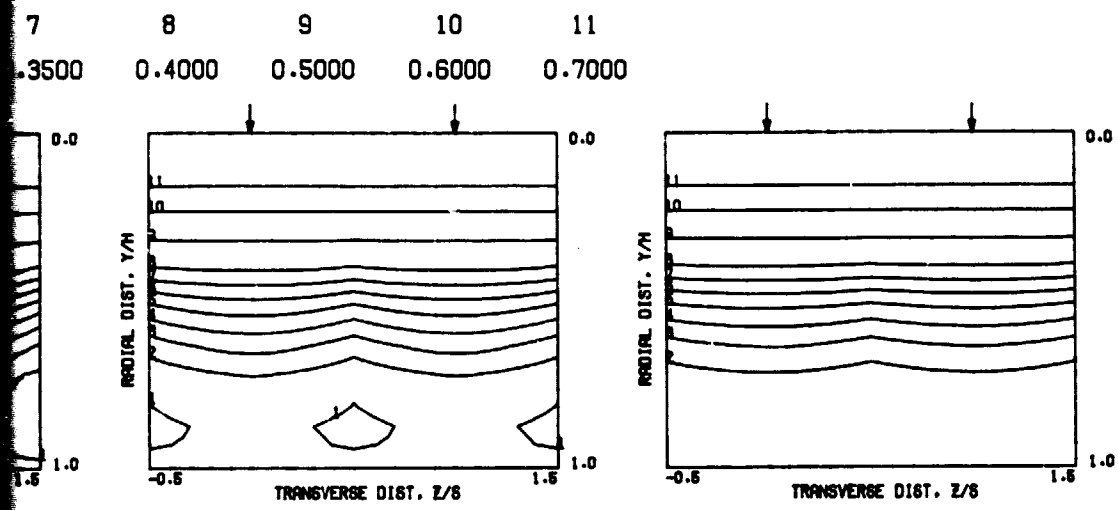

, J=22.55, S/D=4.0 H/D=8.0

TMAIN = 567.1 K TJET = 310.6 K THEB = 0.053

X/H = 1.50 X/DJ =14.66 X/H = 2.00 X/DJ =19.55

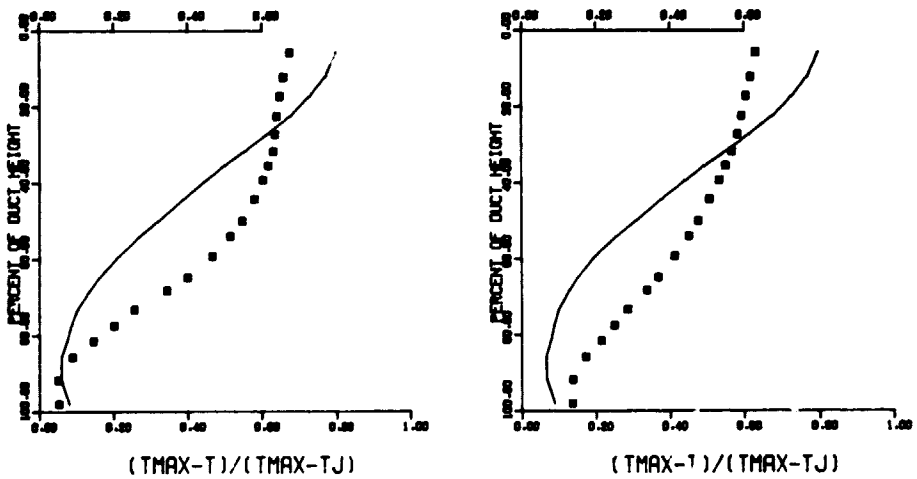

2 FOLDOUT FRAME

TOP COLD , J = 22.55 , S/D =4.00 , H/D =8.00

Figure 44

ORIGINAL PAGE IS
OF POOR QUALITY

S = 0.0508 METERS S/DJ = 2.434 HO/DJ = 4.869 VMAIN = 16.5 M/SEC VJET = 57.9 M/SEC TMAIN = 538.2 K T

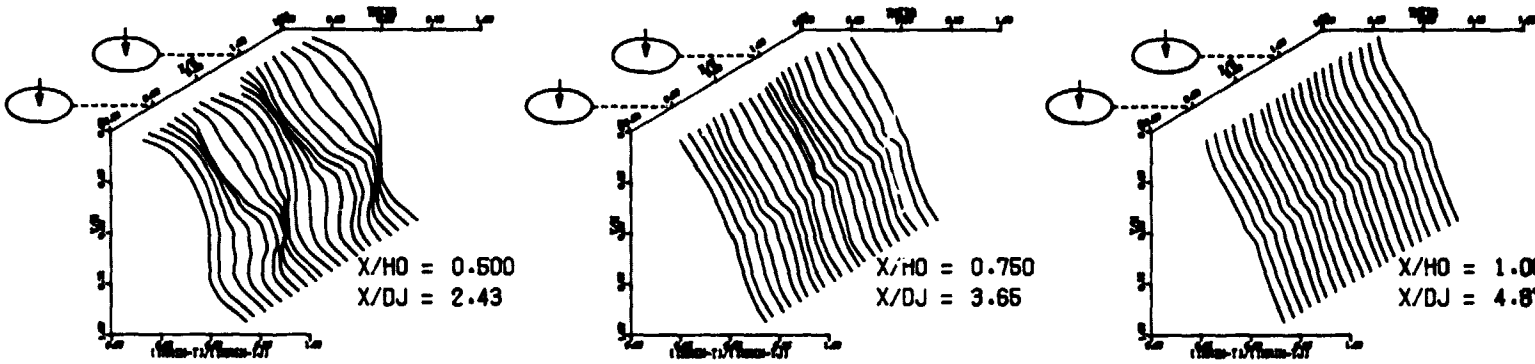

MEASURED THETA PROFILES FOR TEST NO. 17, TEST SECTION I, TOP HOT , J

CONTOUR	1	2	3	4	5	6	7
VALUE	0.0500	0.1000	0.1500	0.2000	0.2500	0.3052	0.35

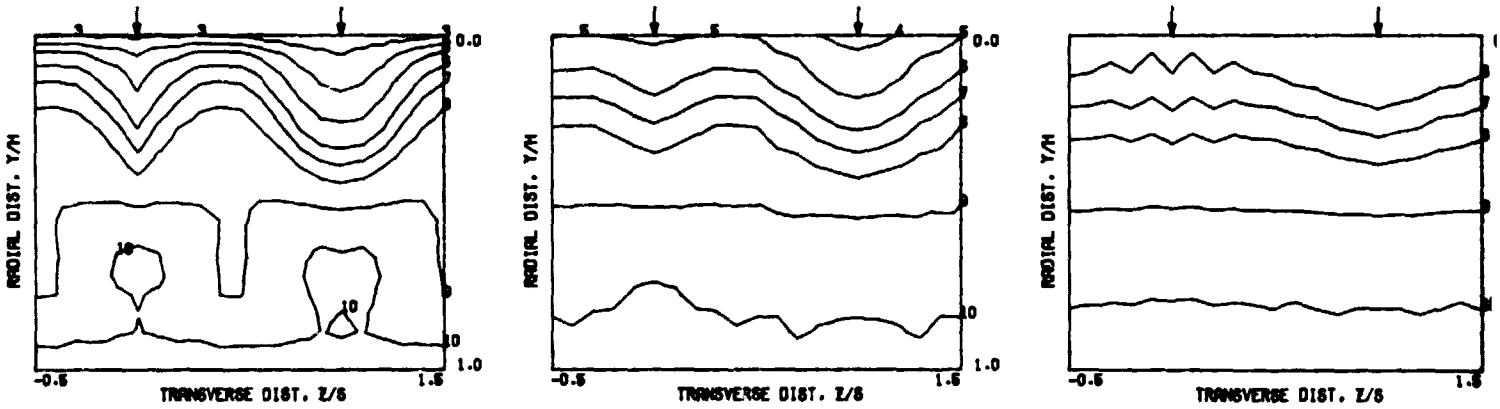

MEASURED THETA CONTOURS FOR TEST NO.17, TOP HOT, J=

FOLDOUT FRAME

ORIGINAL PAGE IS
OF POOR QUALITY

/SEC TMAIN = 538.2 K TJET = 303.3 K THEB = 0.3052 BLORAT= 6.629 DENRATIO= 1.798 TRATIO=0.564

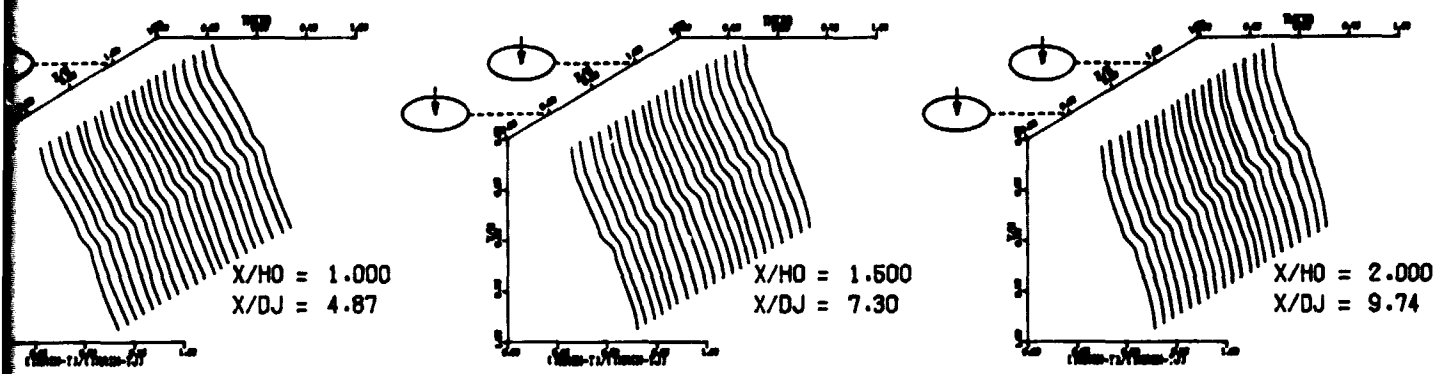

I. TOP HOT , J = 22.14 , S/D = 2.00 , H/D = 4.00

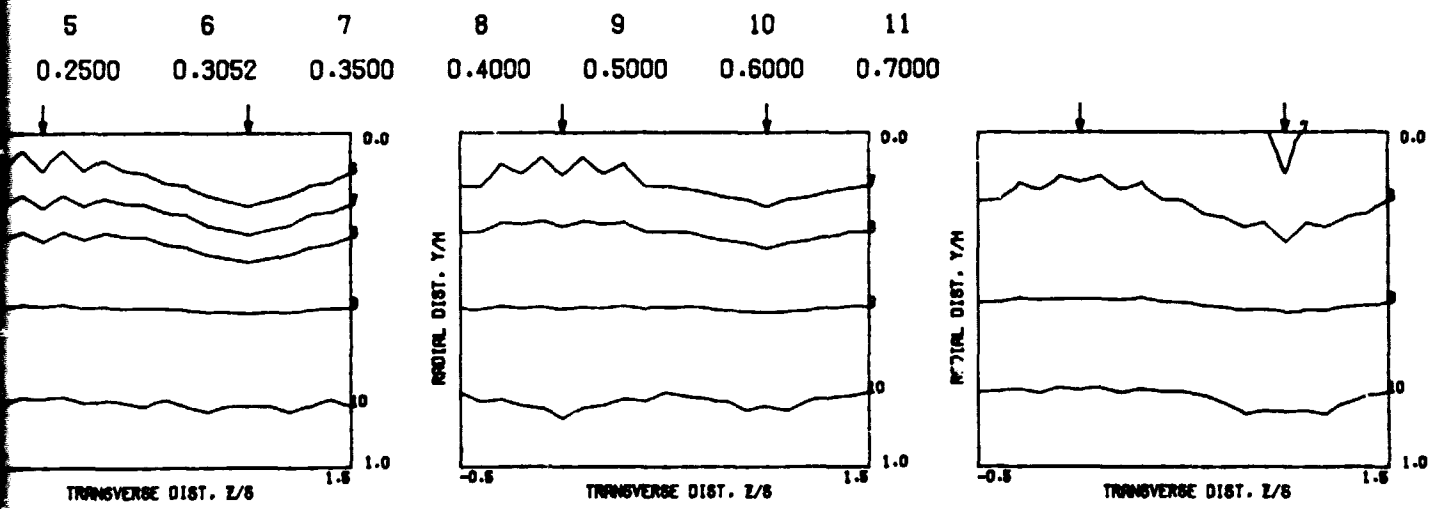

T NO.17, TOP HOT, J=22.14, S/D=2.0, H/D=4.0

ORIGINAL PAGE IS
OF POOR QUALITY

Figure 45

2 FOLDOUT FRAME

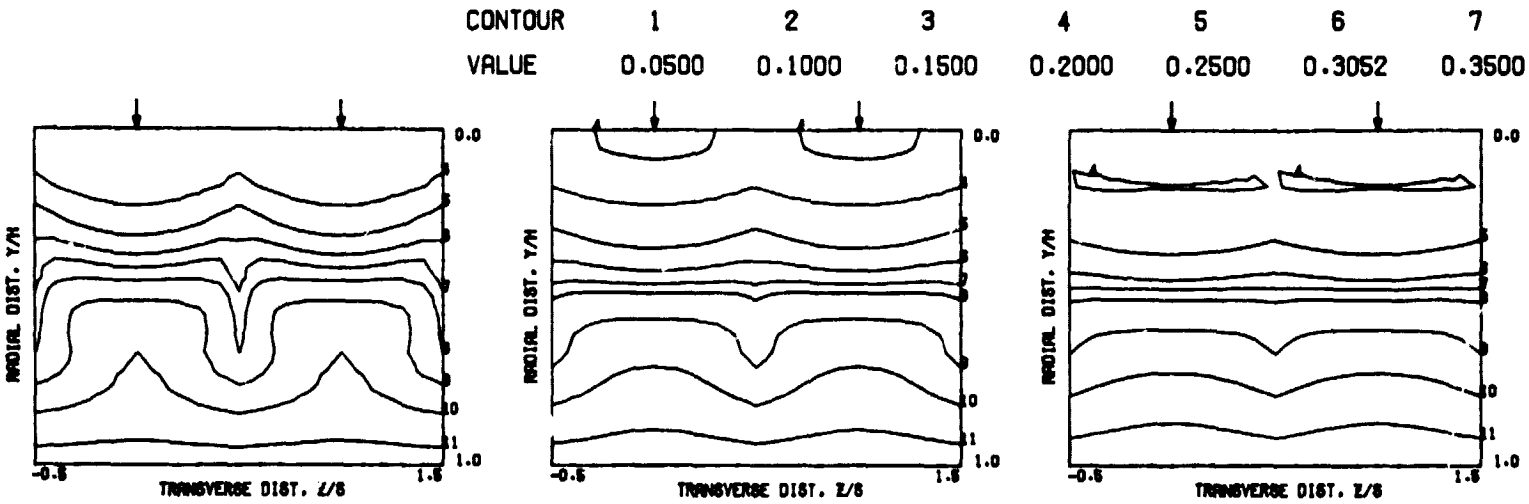

PREDICTED THETA CONTOURS FOR TEST NO. 17, TOP HOT, J=22.1

S/DJ = 2.43 HO/DJ = 4.87 VRATIO = 3.51 TRATIO = 0.564 DENRATIO= 1.798 TMAIN =

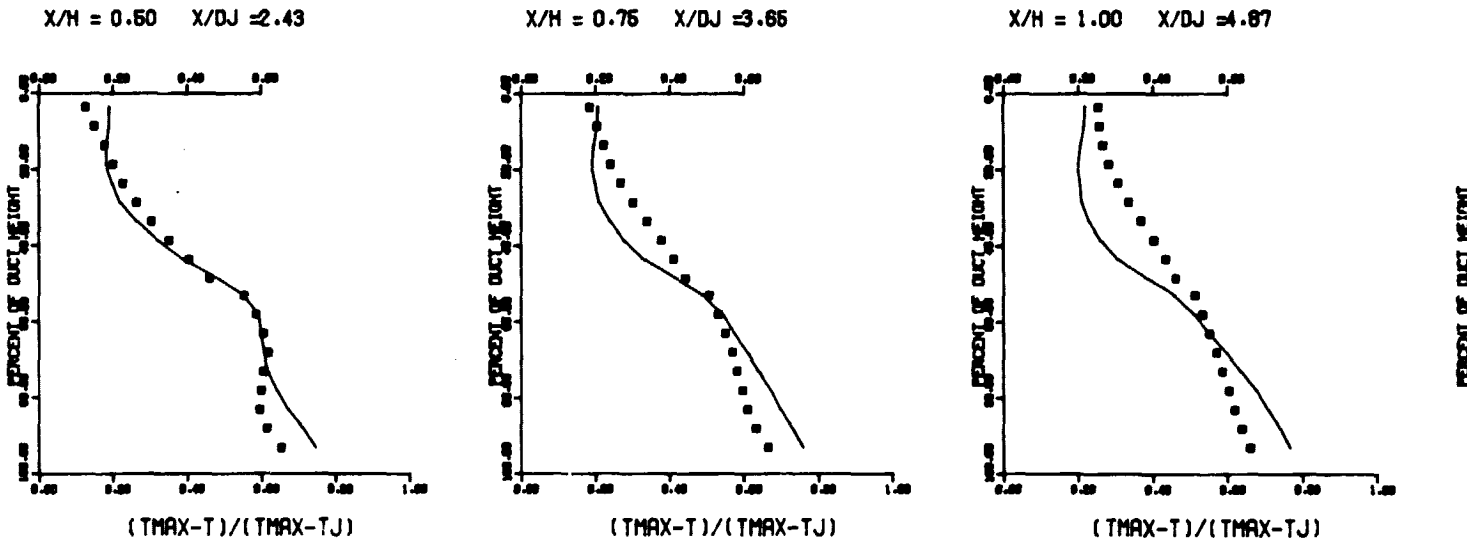

COMPARISON BETWEEN DATA AND CORRELATIONS FOR TEST NO. 17, TEST SECTION I, TOP H

ORIGINAL PAGE IS
OF POOR QUALITY

FOLDOUT FRAME

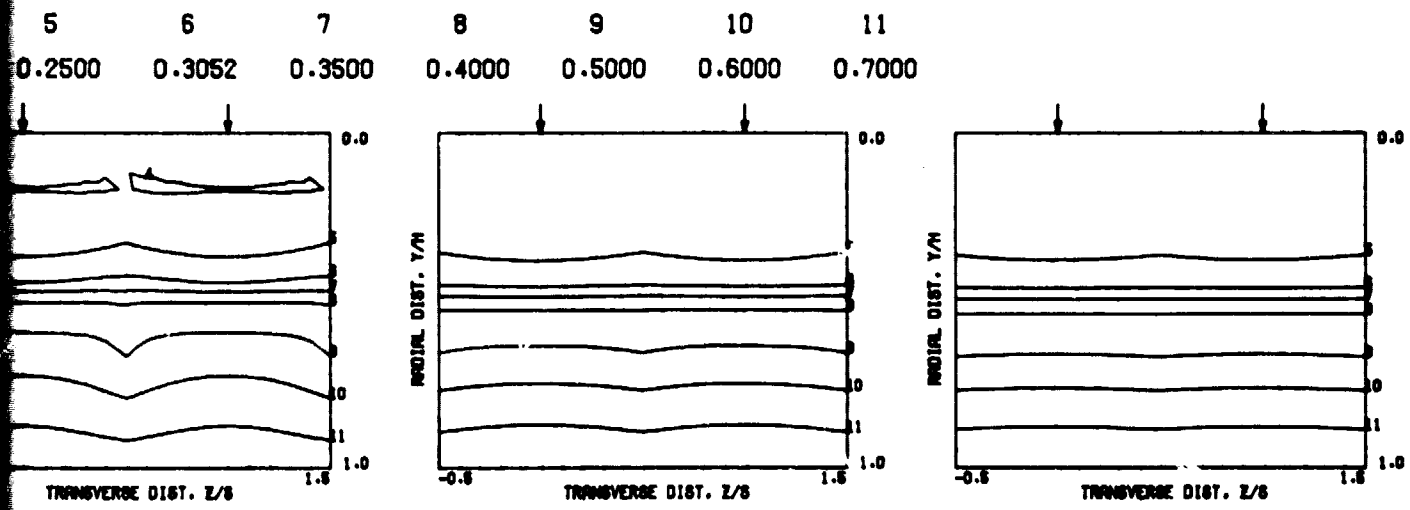

NO. 17, TOP HOT, J=22.14, S/D=2.0 H/D=4.0

DENRATIO=1.798 TMAIN = 538.2 K TJET = 303.3 K THEB = 0.153

X/DJ =4.87 X/H = 1.60 X/DJ =7.30 X/H = 2.00 X/DJ =9.74

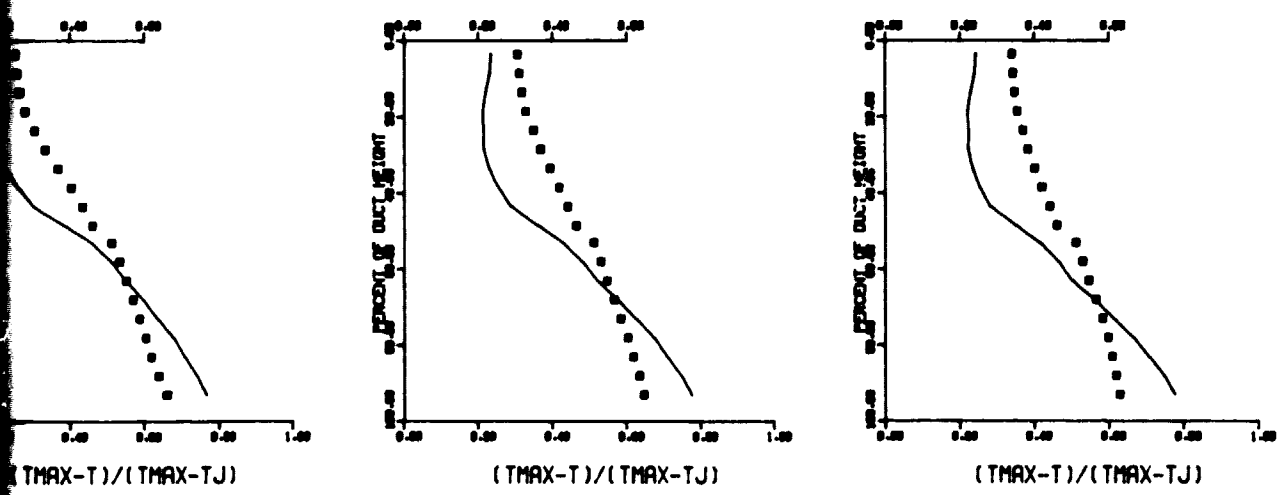

2 FOLDOUT FRAME

, TEST SECTION I, TOP HOT , J = 22.14 , S/D =2.00 , H/D =4.00

Figure 46

ORIGINAL PAGE IS
OF POOR QUALITY

S = 0.0508 METERS S/DJ = 4.869 HO/DJ = 9.737 VMAIN = 18.2 M/SEC VJET = 72.2 M/SEC TMAIN = 545.0 K TJET

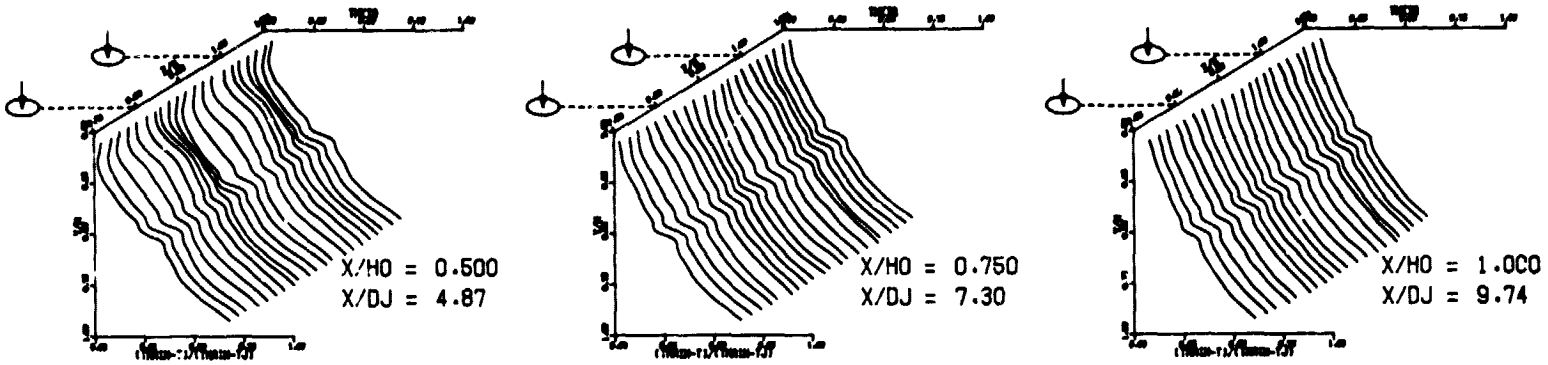

MEASURED THETA PROFILES FOR TEST NO. 18, TEST SECTION I, TOP HOT , J = 2

CONTOUR	1	2	3	4	5	6	7
VALUE	0.0500	0.1066	0.1500	0.2000	0.2500	0.3000	0.3500

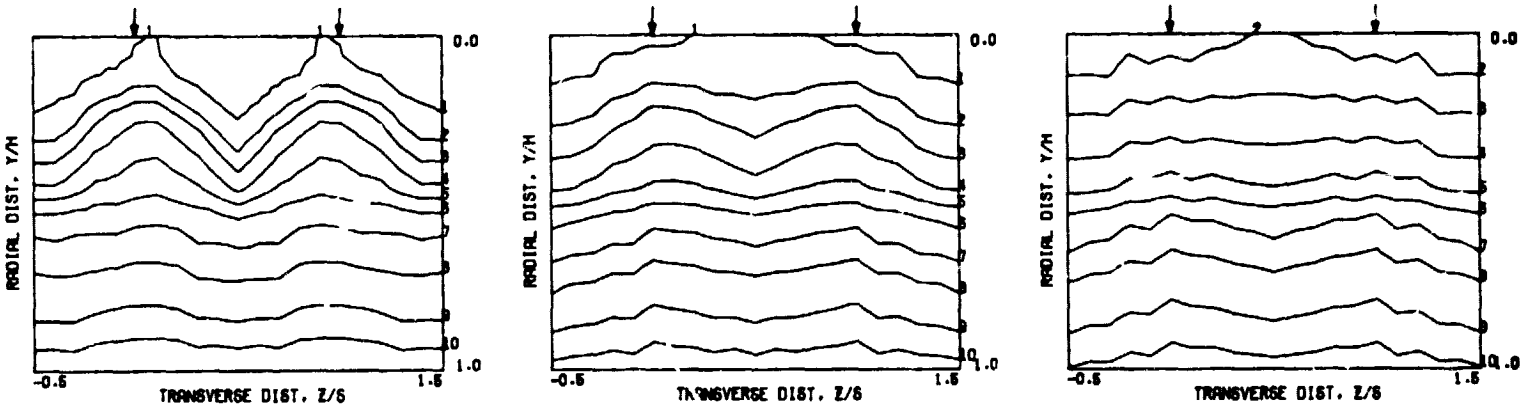

MEASURED THETA CONTOURS FOR TEST NO.18, TOP HOT, J=27

FOLDOUT FRAME

ORIGINAL PAGE IS
OF POOR QUALITY

M/SEC TMAIN = 545.0 K TJET = 316.8 K THEB = 0.1066 BLORAT= 7.207 DENRATIO= 1.757 TRATIO=0.581

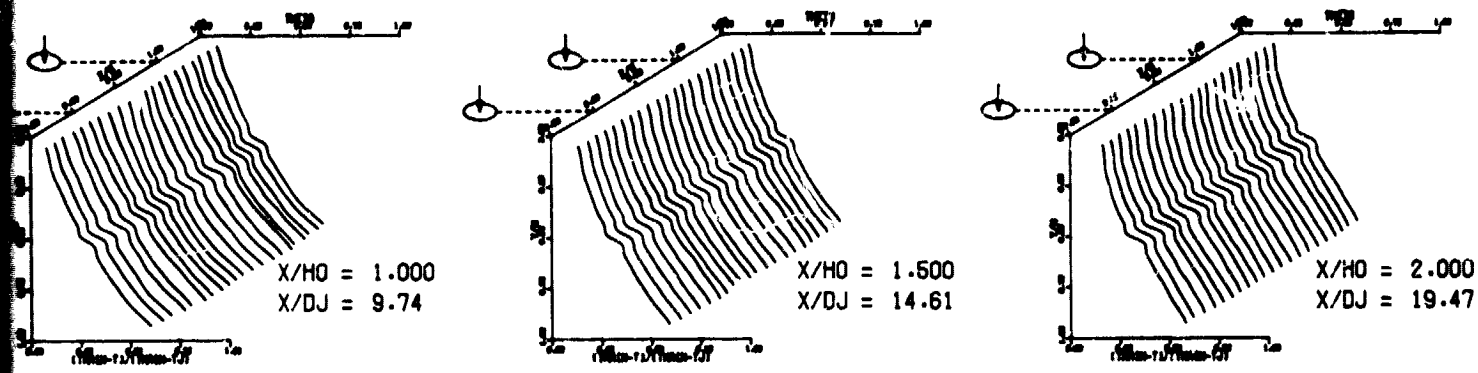

ON I, TOP HOT , J = 27.69 , S/D = 4.00 , H/D = 8.00

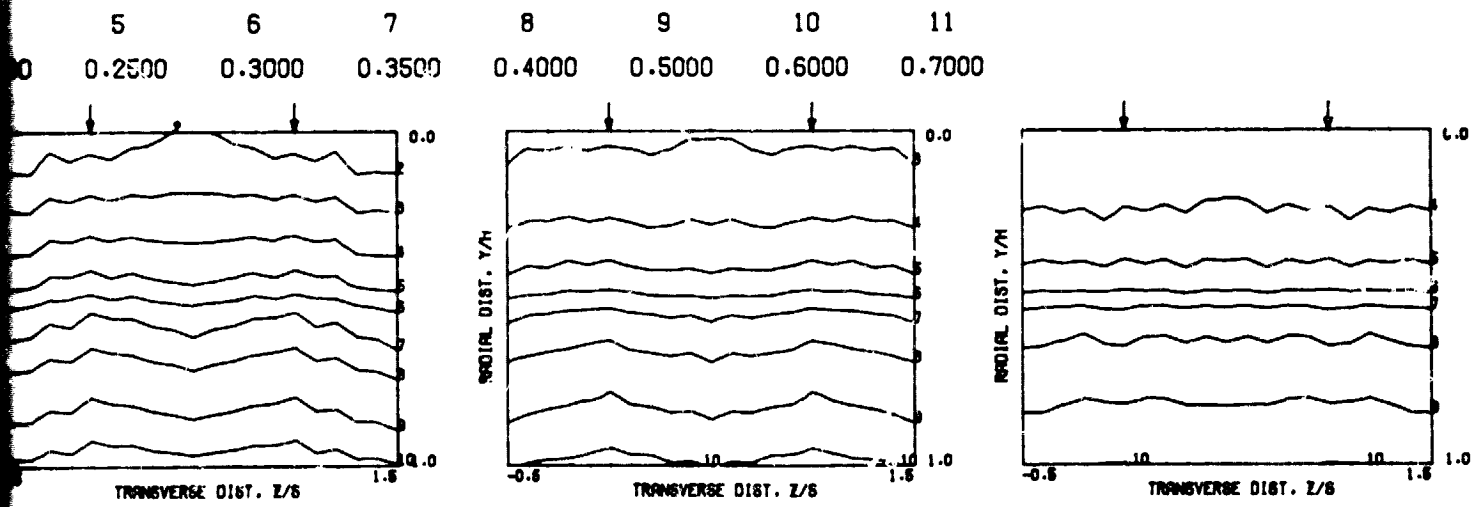

TEST NO.18, TOP HOT, J=27.63, S/D=4.0, H/D=8.0

2 FOLDOUT FRAME

Figure 47

ORIGINAL PAGE IS
OF POOR QUALITY

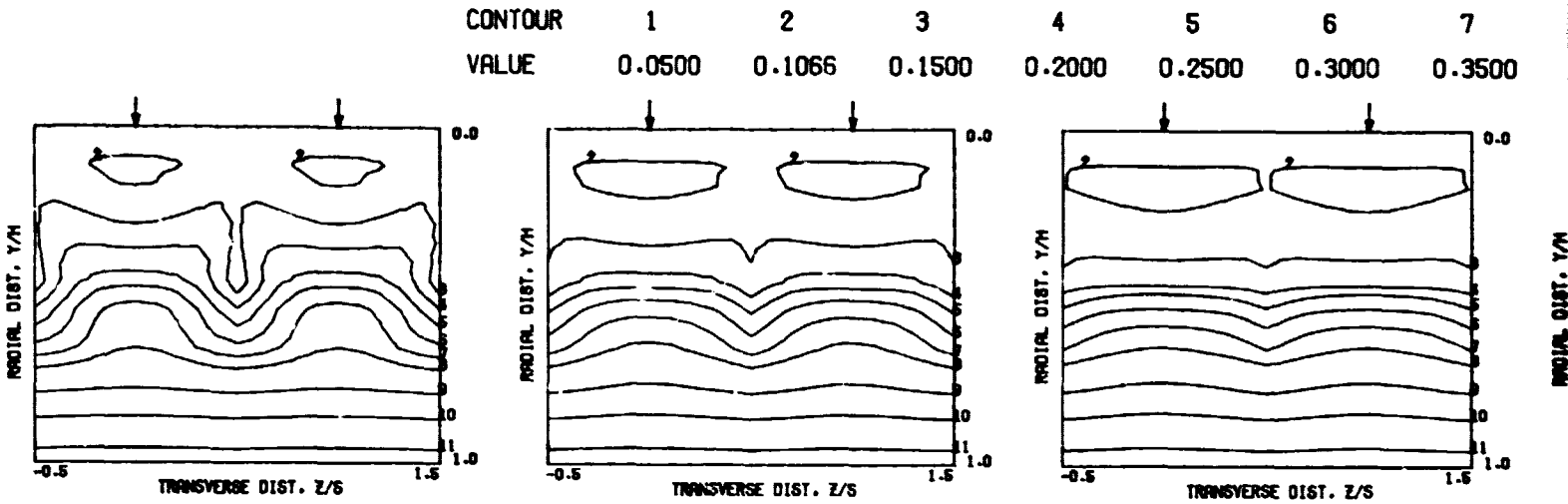

PREDICTED THETA CONTOURS FOR TEST NO. 18. TOP HOT. J=27.6

S/DJ = 4.87 HO/DJ = 9.74 VRATIO = 3.97 TRATIO = 0.581 DENRATIO= 1.757 TMAIN =

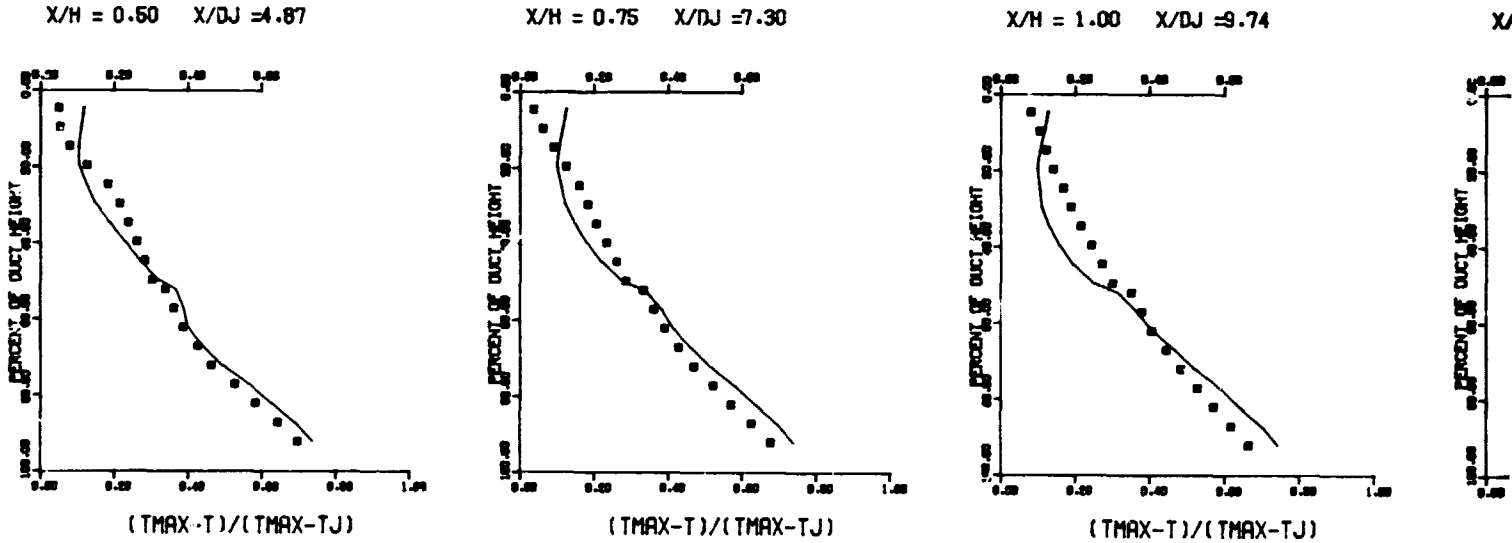

COMPARISON BETWEEN DATA AND CORRELATIONS FOR TEST NO. 18. TEST SECTION I. TOP H

ORIGINAL PAGE IS
OF POOR QUALITY

FOLDOUT FRAME

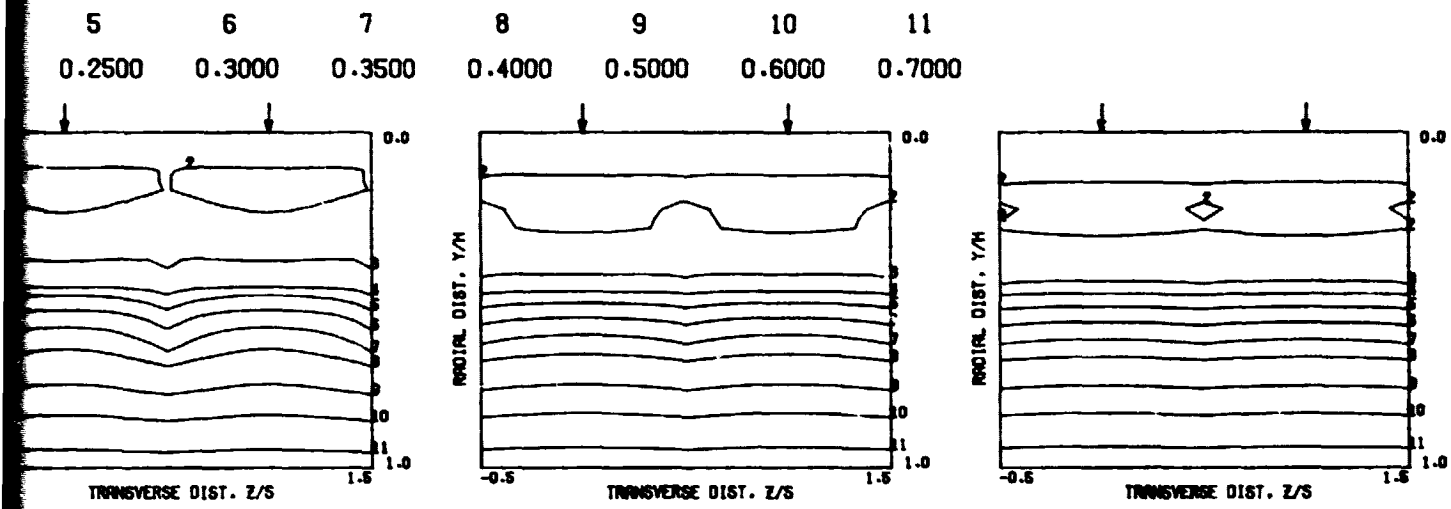

EST NO. 18. TOP HOT. J=27.69. S/D=4.0 H/D=8.0

0.581 DENRATIO=1.757 TMAIN = 545.0 K TJET = 316.8 K THEB = 0.053

= 1.00 X/DJ =9.74 X/H = 1.50 X/DJ =14.61 X/H = 2.00 X/DJ =19.47

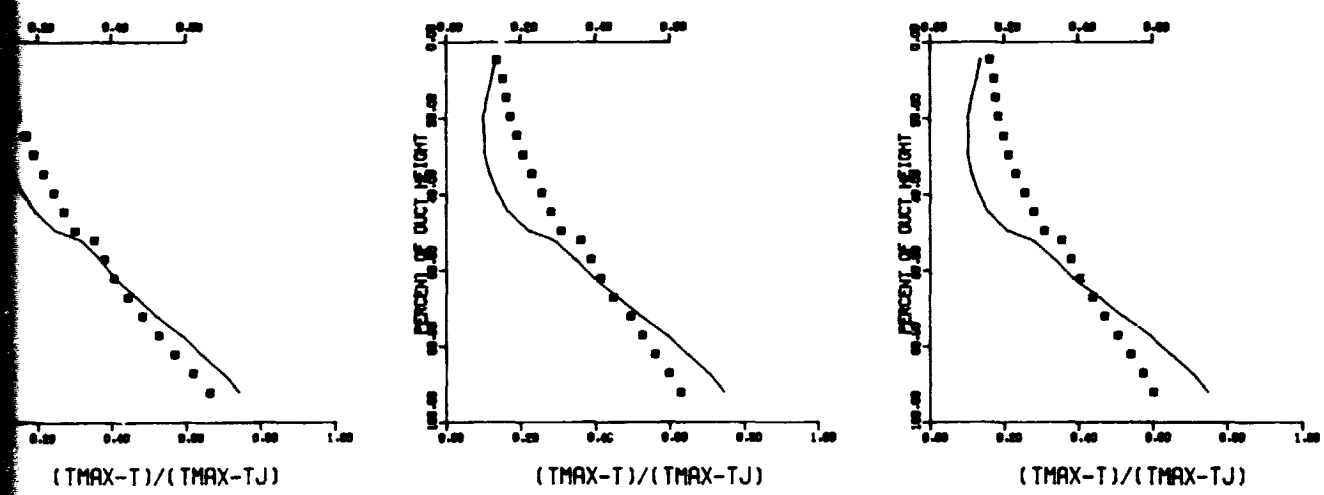

2 FOLDOUT FRAME

18. TEST SECTION 1. TOP HOT , J = 27.69 , S/D =4.00 , H/D =8.00

Figure 48

ORIGINAL PAGE IS
OF POOR QUALITY

S = 0.0508 METERS S/DJ = 4.961 HO/DJ = 9.921 VMAIN = 15.9 M/SEC VJET = 58.1 M/SEC TMAIN = 656.2 K TJET

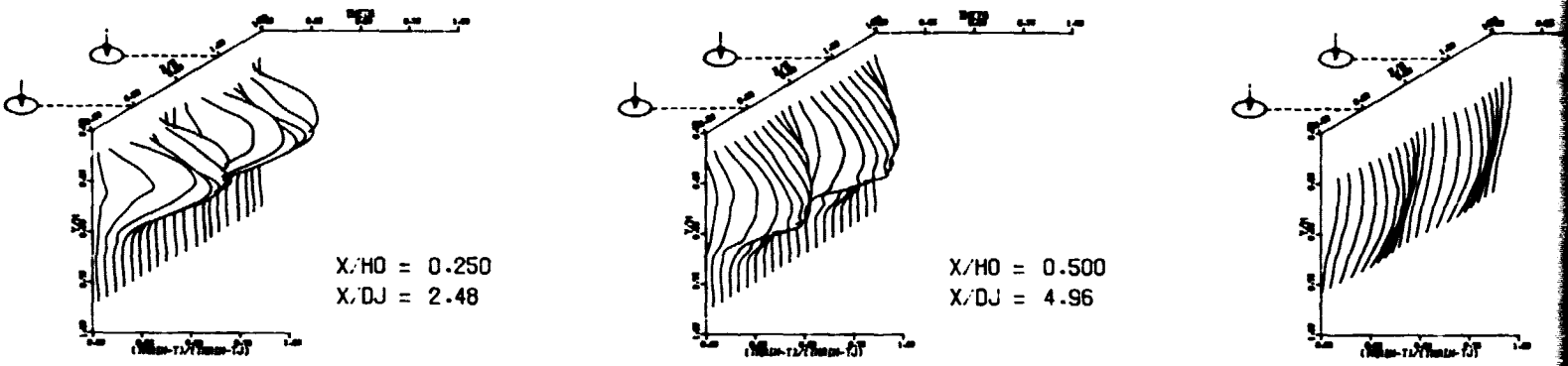

MEASURED THETA PROFILES FOR TEST NO. 19, TEST SECTION II, TMAIN=CONST., J = 27

CONTOUR	1	2	3	4	5	6
VALUE	0.0500	0.1055	0.1500	0.2000	0.2500	0.3000

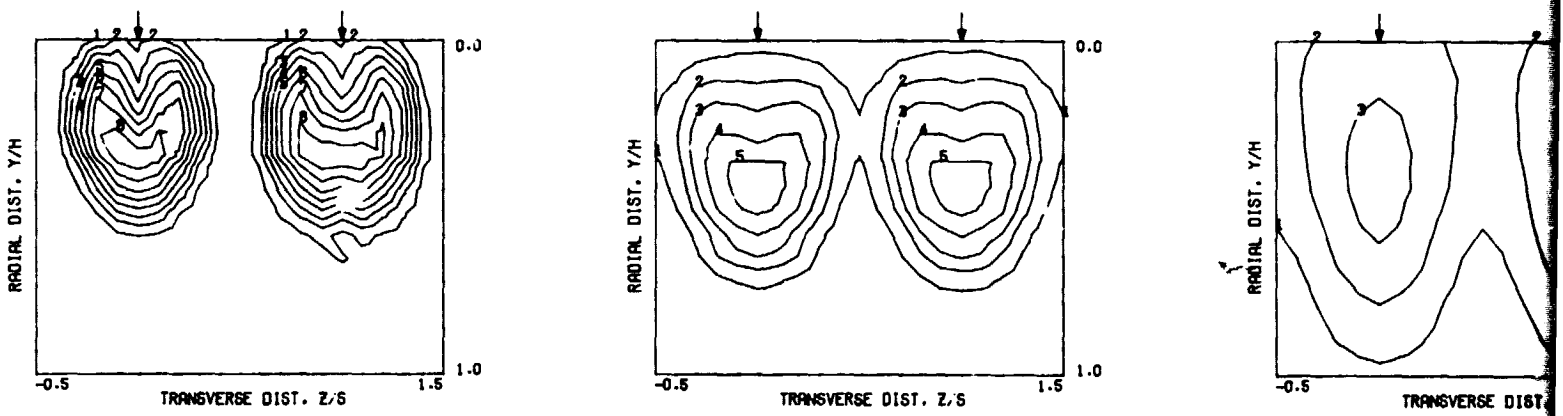

MEASURED THETA CONTOURS FOR TEST NO.19, TMAIN=CONS

ORIGINAL PAGE IS
OF POOR QUALITY

FOLDOUT FRAME

.1 M/SEC TMAIN = 656.2 K TJET = 330.4 K THEB = 0.1055 BLORAT= 7.395 DENRATIO= 2.020 TRATIO= 0.504

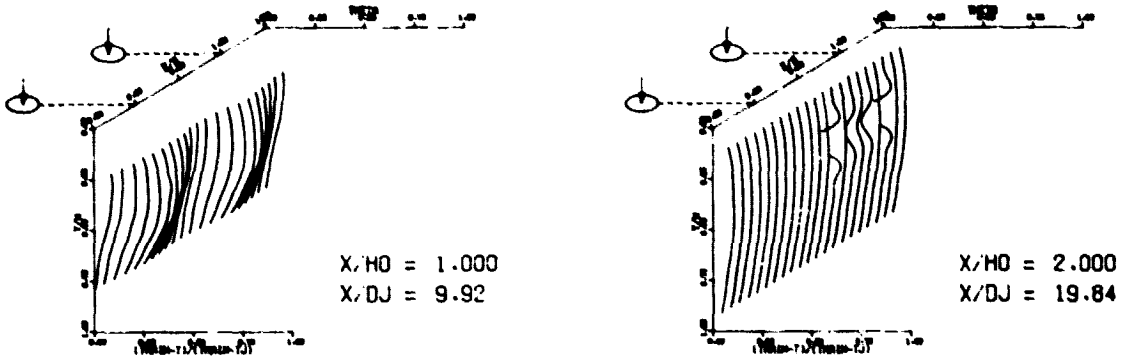

TION II. TMAIN=CONST., J = 27.09 , S/D = 4.00 , H/D = 8.00

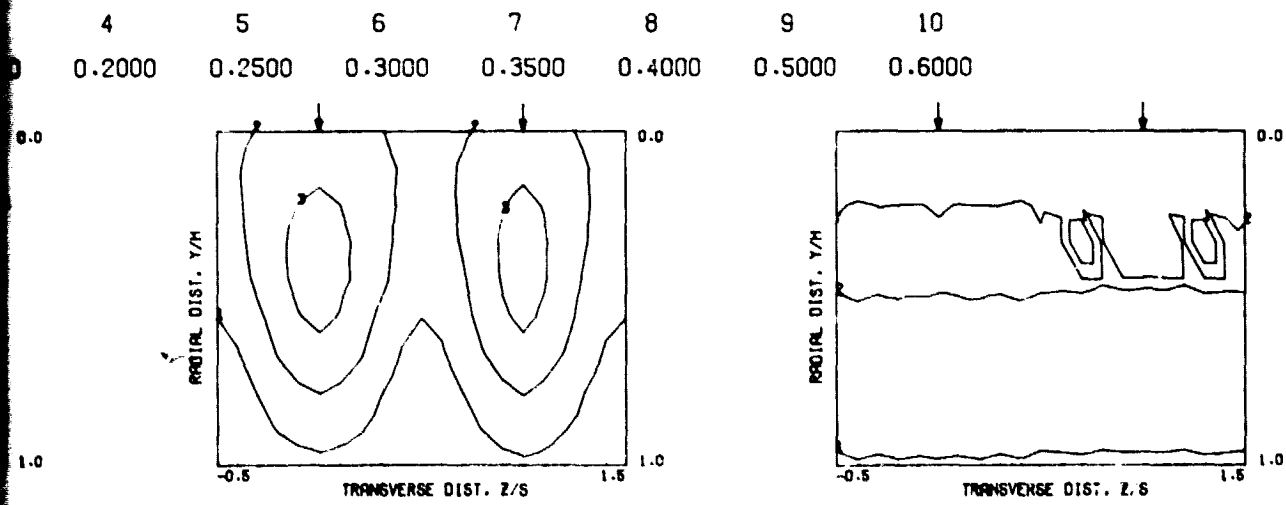

URS FOR TEST NO.19, TMAIN=CONST, J=27.09, S/D=4.0, H/D=8.0

ORIGINAL PAGE IS
OF POOR QUALITY

Figure 49

FOLDOUT FRAME

CONTOUR	1	2	3	4	5	6
VALUE	0.0500	0.1055	0.1500	0.2000	0.2500	0.3000

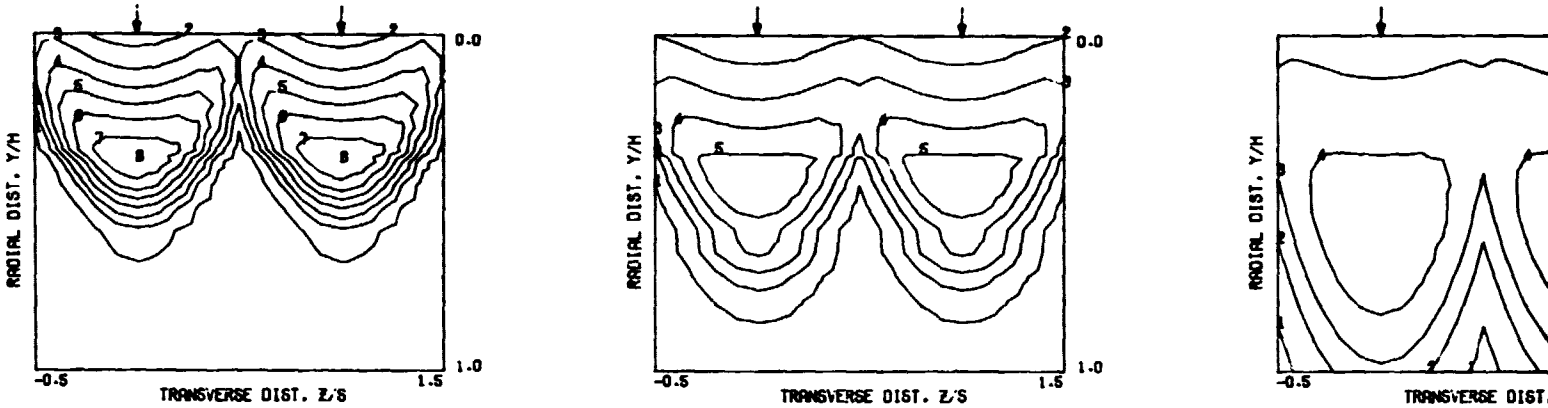

PREDICTED THETA CONTOURS FOR TEST NO.19. TMAIN=CON

S/DJ = 4.96 HO/DJ = 9.92 VRATIO = 3.66 TRATIO = 0.504 DENRATIO=2.020 TMAIN

X/H = 0.25 X/DJ =2.48 X/H = 0.50 X/DJ =4.96 X/H = 1.00 X/DJ =9.92

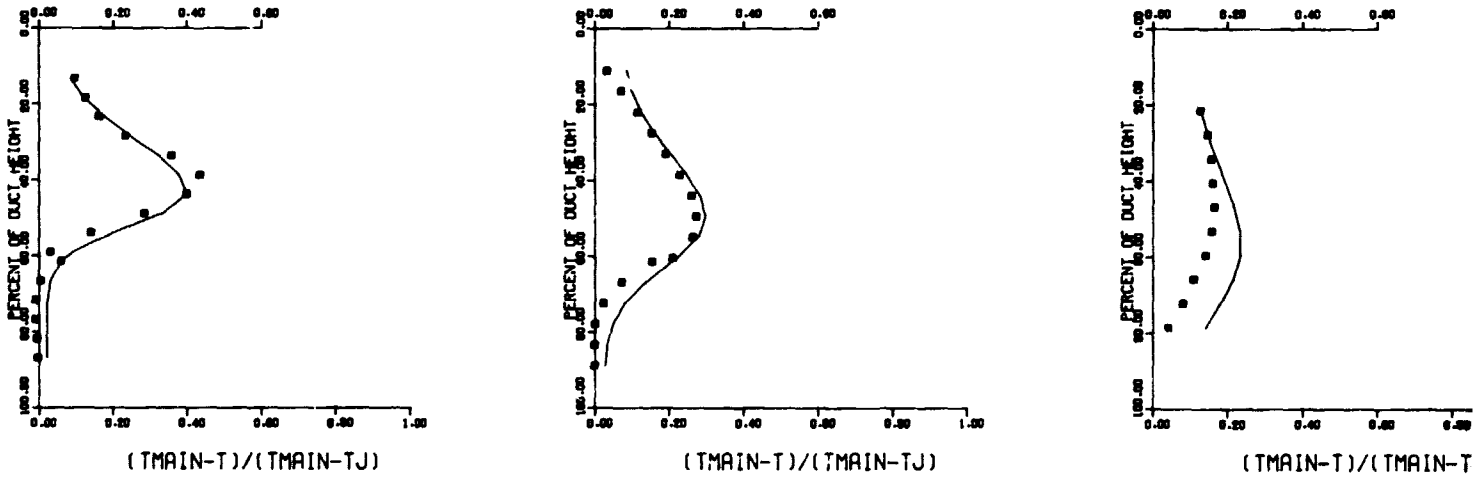

COMPARISON BETWEEN DATA AND CORRELATIONS FOR TEST NO. 19, TEST SECTION II,UNIFO

ORIGINAL PAGE IS
OF POOR QUALITY

FOLDOUT FRAME

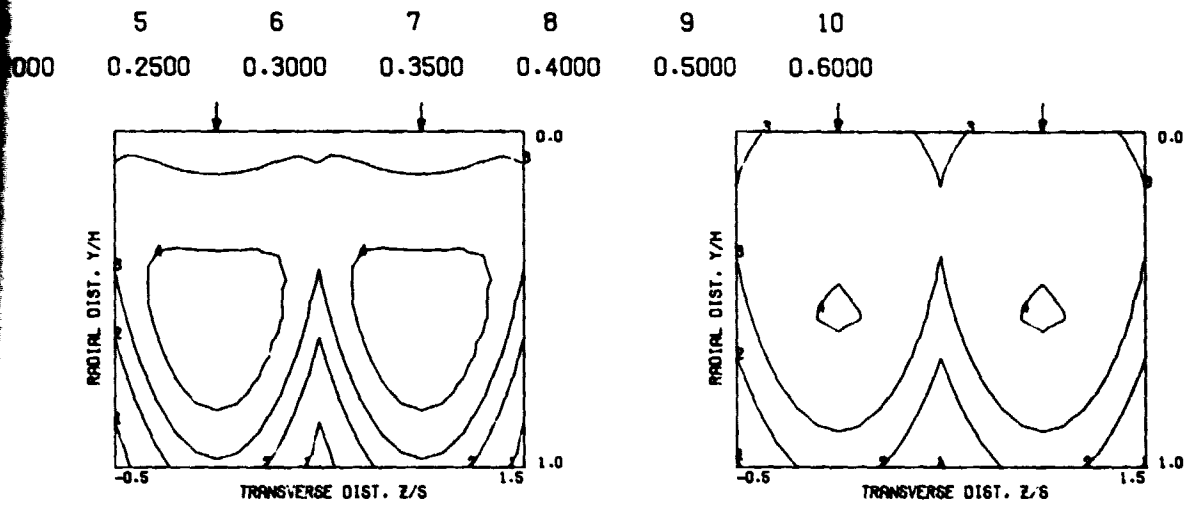

OR TEST NO.19. TMAIN=CONST. J=27.09. S/D=4.0. H/D=8.0

504 DENRATIO=2.020 TMAIN = 656.2 K TJET = 330.4 K THEB = 0.106

X/H = 1.00 X/DJ =9.92 X/H = 2.00 X/DJ =19.84

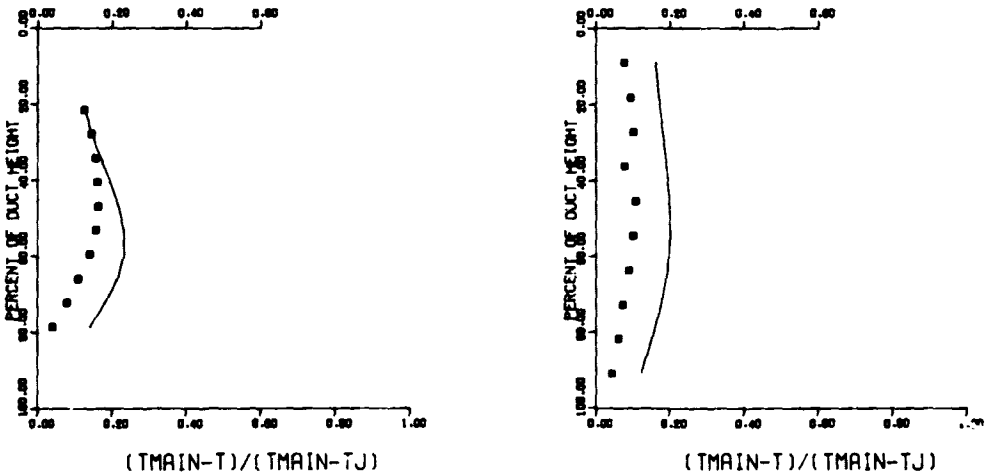

2 FOLDOUT FRAME

19. TEST SECTION II.UNIFORM TMAIN. J = 27.09 . S/D =4.00 . H/D =8.00

Figure 50

ORIGINAL PAGE IS
OF POOR QUALITY

S = 0.0508 METERS S/DJ = 5.037 HO/DJ = 10.074 VMAIN = 15.5 M/SEC VJET = 106.4 M/SEC TMAIN = 644.6 K

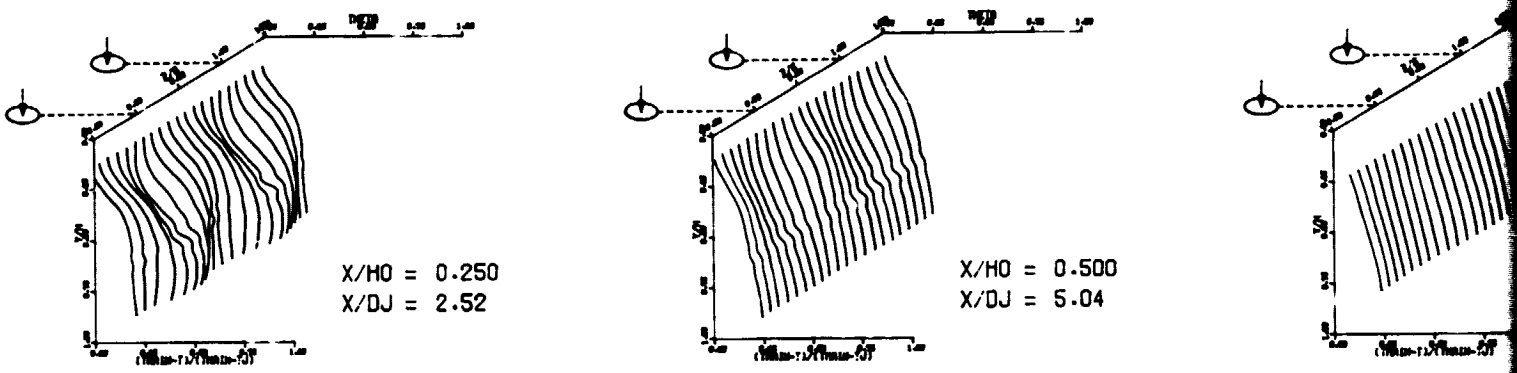

MEASURED THETA PROFILES FOR TEST NO. 20, TEST SECTION II, TMAIN=CONST., J

CONTOUR	1	2	3	4	5	6
VALUE	0.0500	0.1000	0.1500	0.1881	0.2000	0.2500

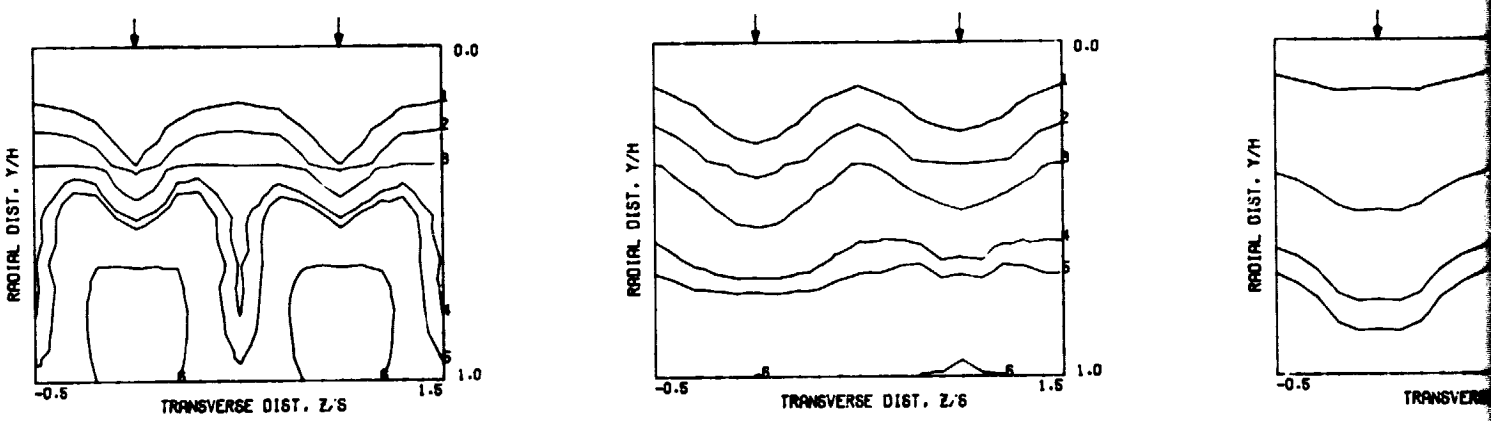

MEASURED THETA CONTOURS FOR TEST NO.20, TMAIN=

FOLDOUT FRAME

ORIGINAL PAGE IS
OF POOR QUALITY

106.4 M/SEC TMAIN = 644.6 K TJET = 313.9 K THEB = 0.1881 BLORAT= 15.278 DENRATIO= 2.185 TRATIO= 0.487

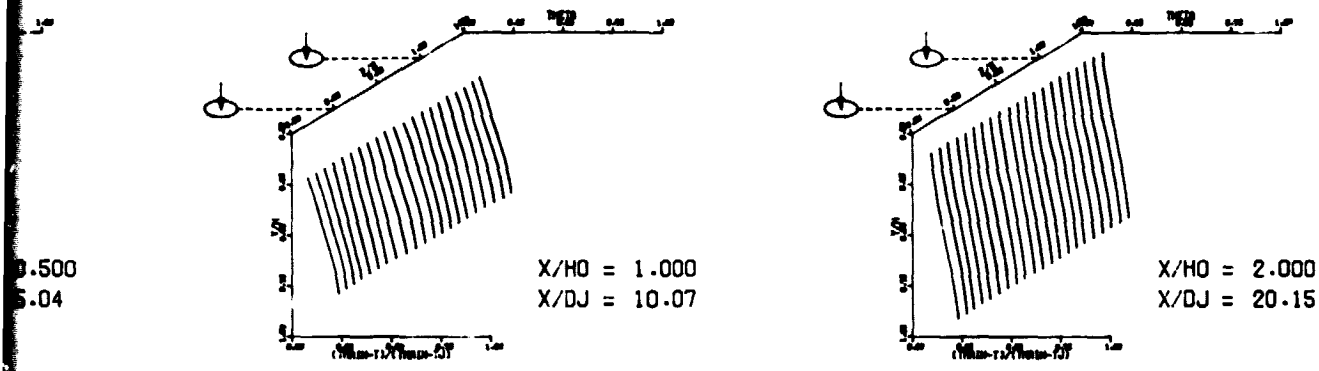

ECTION II, TMAIN=CONST., J = 102.50 , S/D = 4.00 , H/D = 8.00

	4	5	6	7	8	9	10
500	0.1881	0.2000	0.2500	0.3000	0.3500	0.4000	0.5000

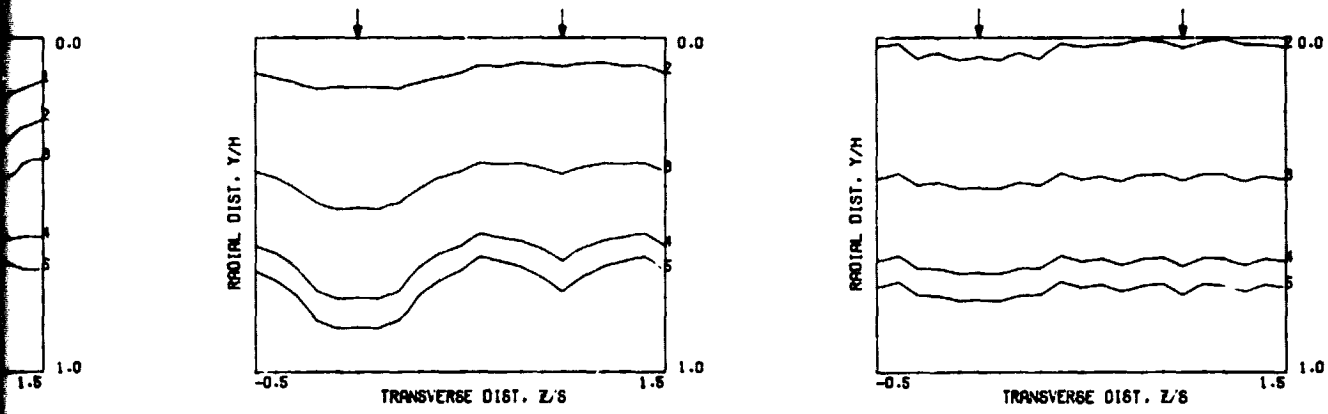

TOURS FOR TEST NO.20, TMAIN=CONST, J=102.5, S/D=4.0, H/D=8.0

ORIGINAL PAGE IS
OF POOR QUALITY

Figure 51

FOLDOUT FRAME

CONTOUR	1	2	3	4	5	6
VALUE	0.0500	0.1000	0.1500	0.1881	0.2000	0.2500

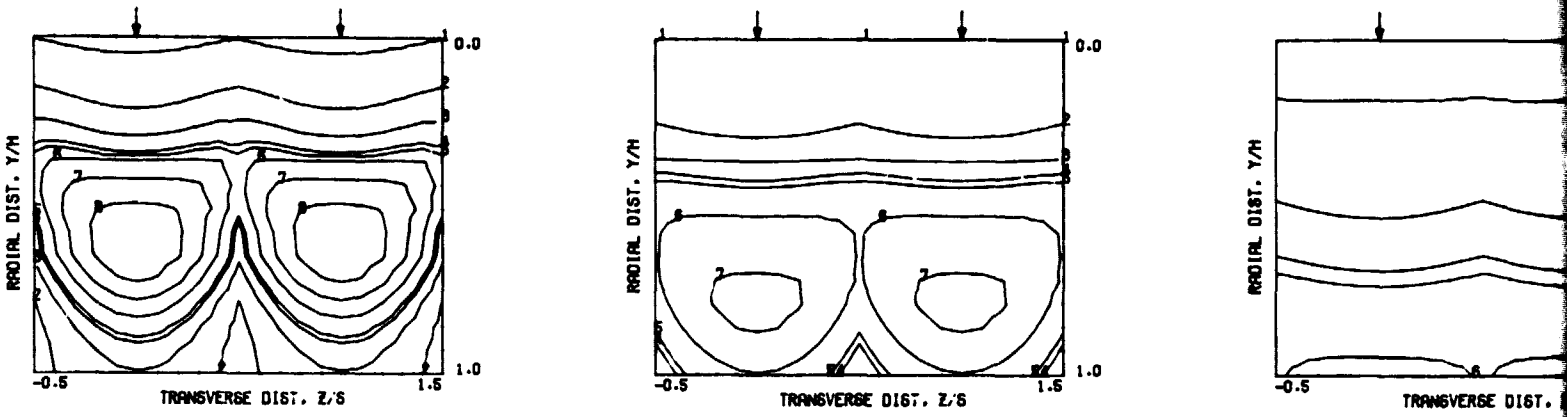

PREDICTED THETA CONTOURS FOR TEST NO.20, TMAIN=CONS

S/DJ = 5.04 HO/DJ = 10.07 VRATIO = 6.85 TRATIO = 0.487 DENRATIO= 2.185 TMAIN

X/H = 0.25 X/DJ =2.52 X/H = 0.50 X/DJ =5.04 X/H = 1.00 X/DJ =10.07

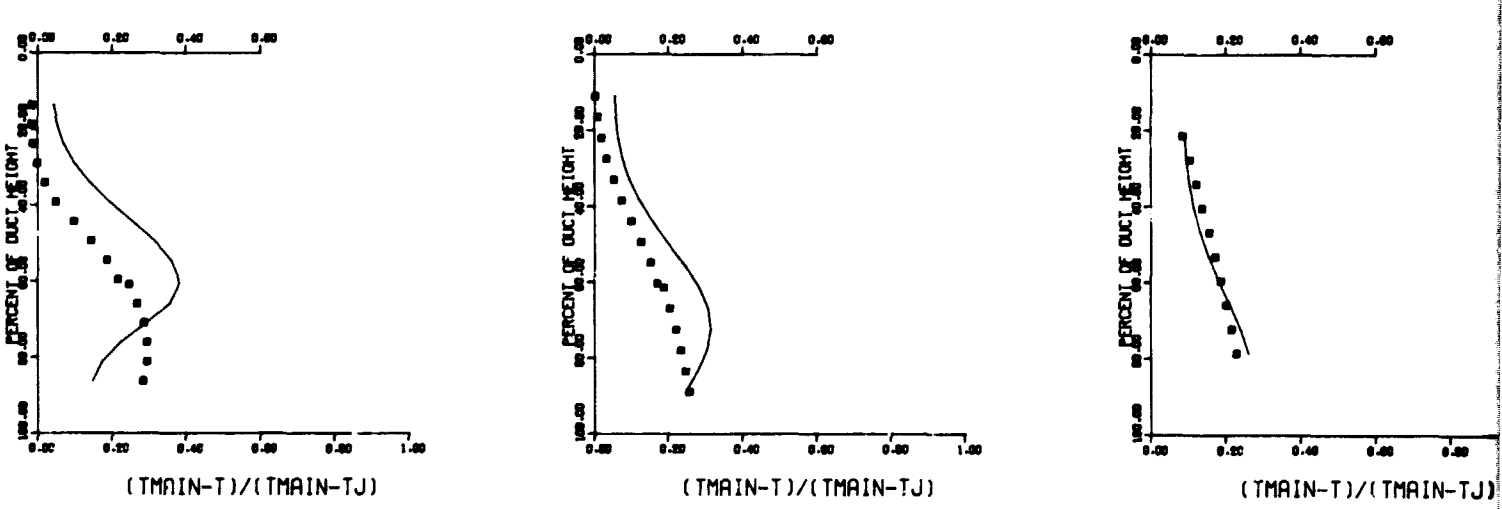

COMPARISON BETWEEN DATA AND CORRELATIONS FOR TEST NO. 20, TEST SECTION II ,UNIFORM

FOLDOUT FRAME

ORIGINAL PAGE IS
OF POOR QUALITY

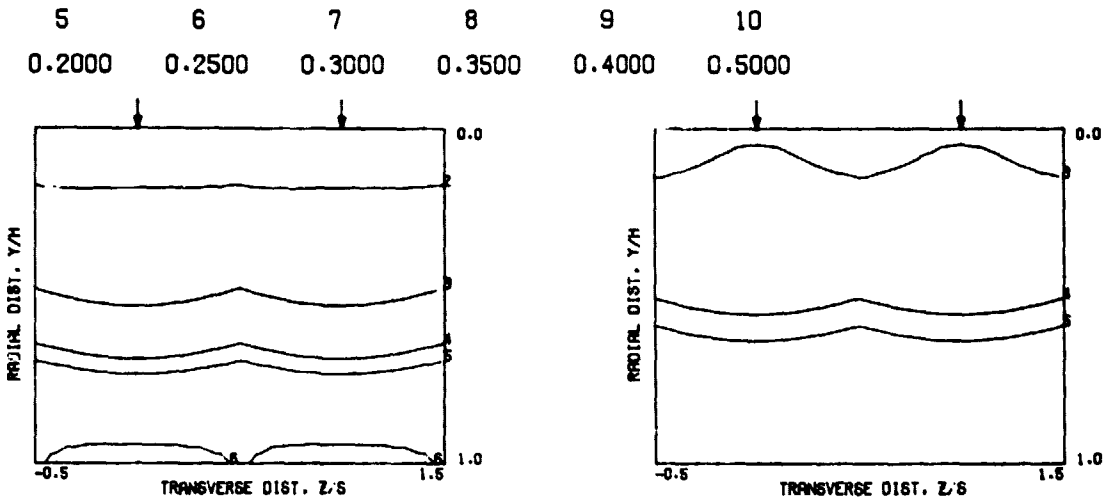

R TEST NO.20. TMAIN=CONST. J=102.5. S/D=4.0. H/D=8.0

7 DENRATIO=2.185 TMAIN = 644.6 K TJET = 313.9 K THEB = 0.188

X/H = 1.00 X/DJ =10.07 X/H = 2.00 X/DJ =20.15

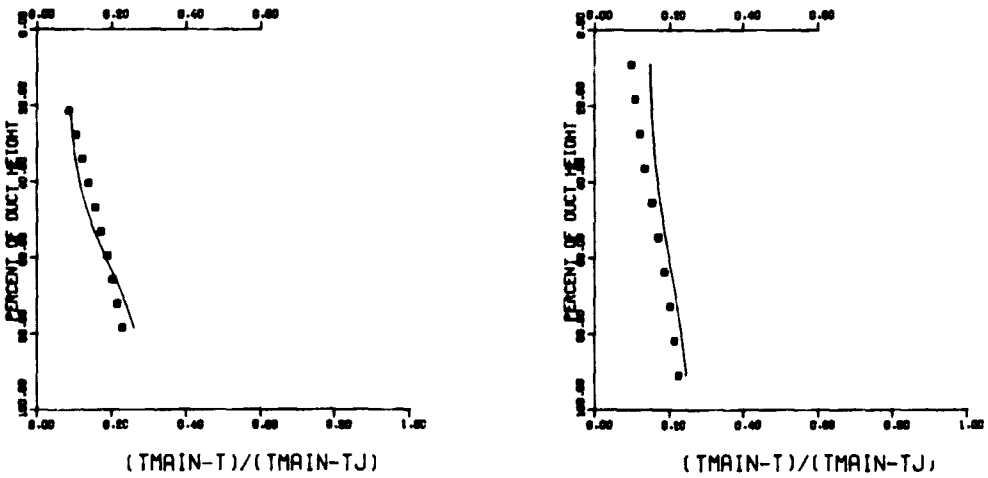

2 FOLDOUT FRAME

. TEST SECTION II .UNIFORM TMAIN. J = 102.50 . S/D =4.00 . H/D =8.00

Figure 52

ORIGINAL PAGE IS
OF POOR QUALITY

S = 0.0508 METERS S/DJ = 2.462 HO/DJ = 4.923 VMAIN = 15.8 M/SEC VJET = 28.1 M/SEC TMAIN = 653.7 K TJE

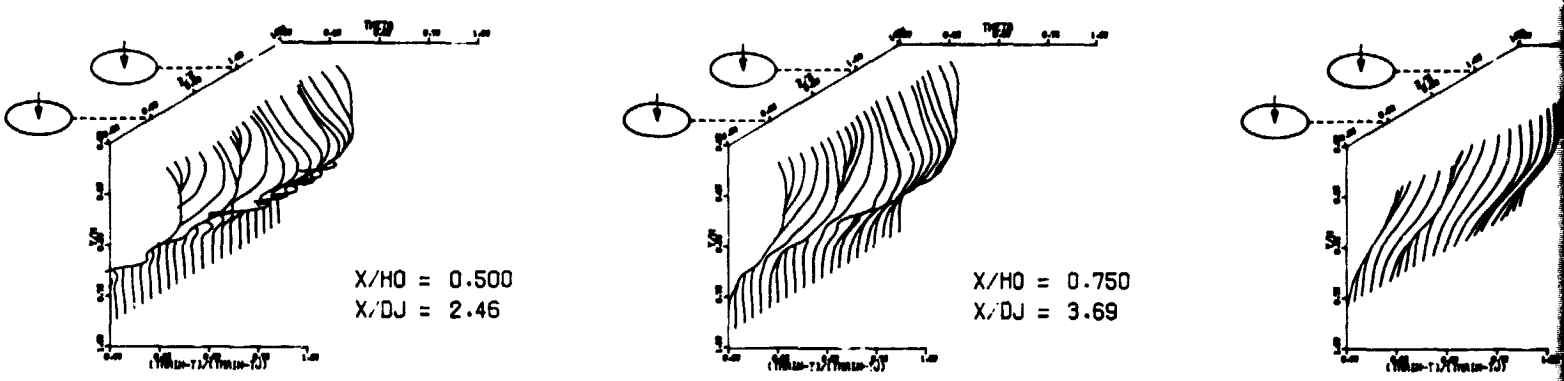

MEASURED THETA PROFILES FOR TEST NO. 21, TEST SECTION II, TMAIN=CONST., J =

CONTOUR	1	2	3	4	5	6
VALUE	0.0500	0.1000	0.1500	0.1973	0.2000	0.2500

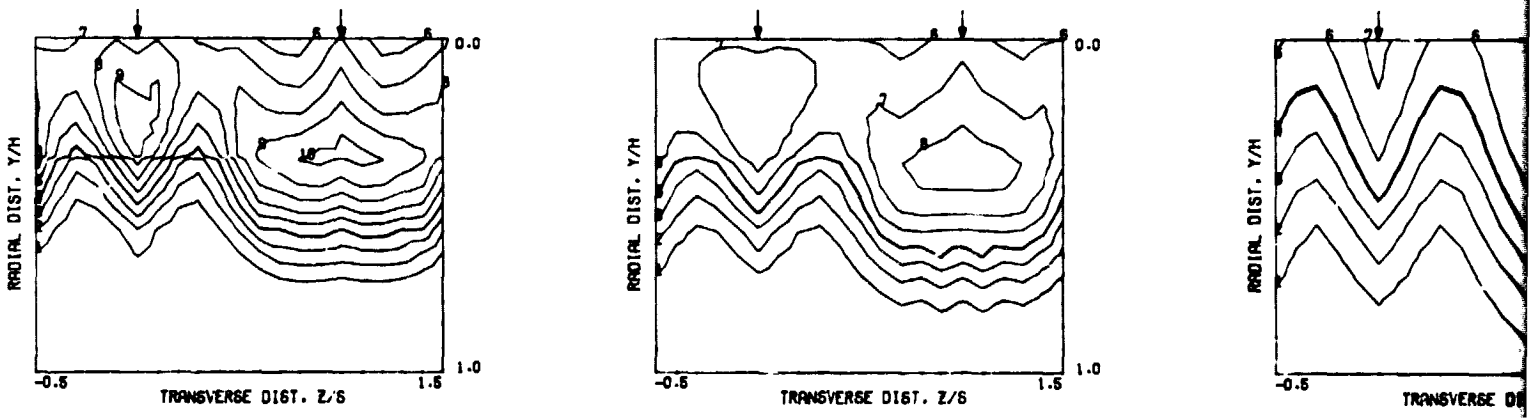

MEASURED THETA CONTOURS FOR TEST NO.21, TMAIN=CO

FOLDOUT FRAME

ORIGINAL PAGE IS
OF POOR QUALITY

/SEC TMAIN = 653.7 K TJET = 307.9 K THEB = 0.1973 BLORAT= 3.794 DENRATIO= 2.129 TRATIO=0.471

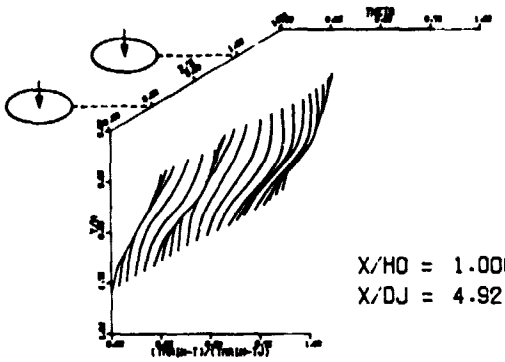

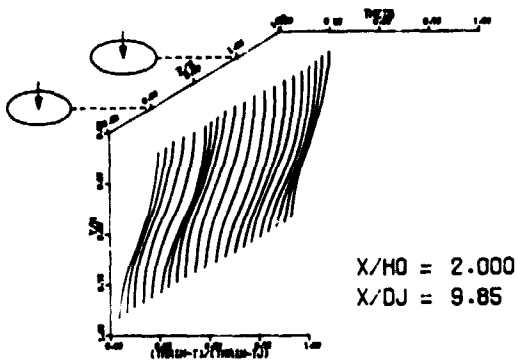

II, TMAIN=CONST., J = 6.76 , S/D = 2.00 , H/D = 4.00

4	5	6	7	8	9	10
0.1973	0.2000	0.2500	0.3000	0.3500	0.4000	0.4500

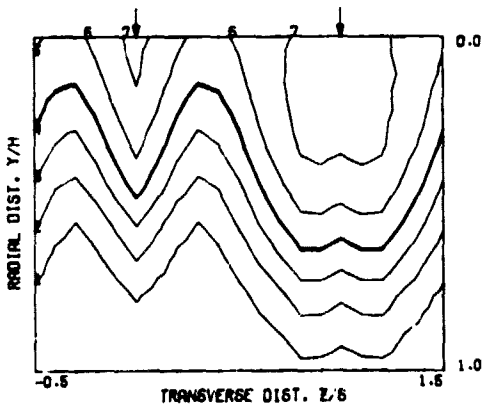

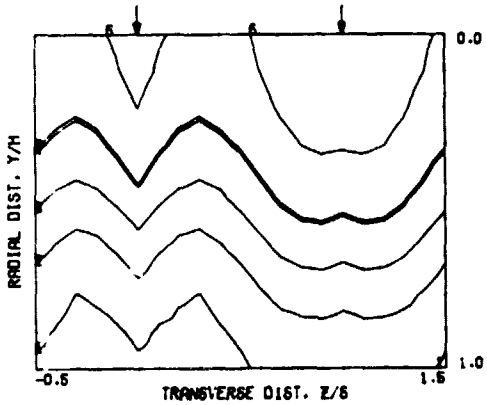

FOR TEST NO.21, TMAIN=CONST, J=6.76, S/D=2.0, H/D=4.0

2 FOLDOUT FRAME

Figure 53

ORIGINAL PAGE IS
OF POOR QUALITY

CONTOUR	1	2	3	4	5	6
VALUE	0.0500	0.1000	0.1500	0.1973	0.2000	0.2500

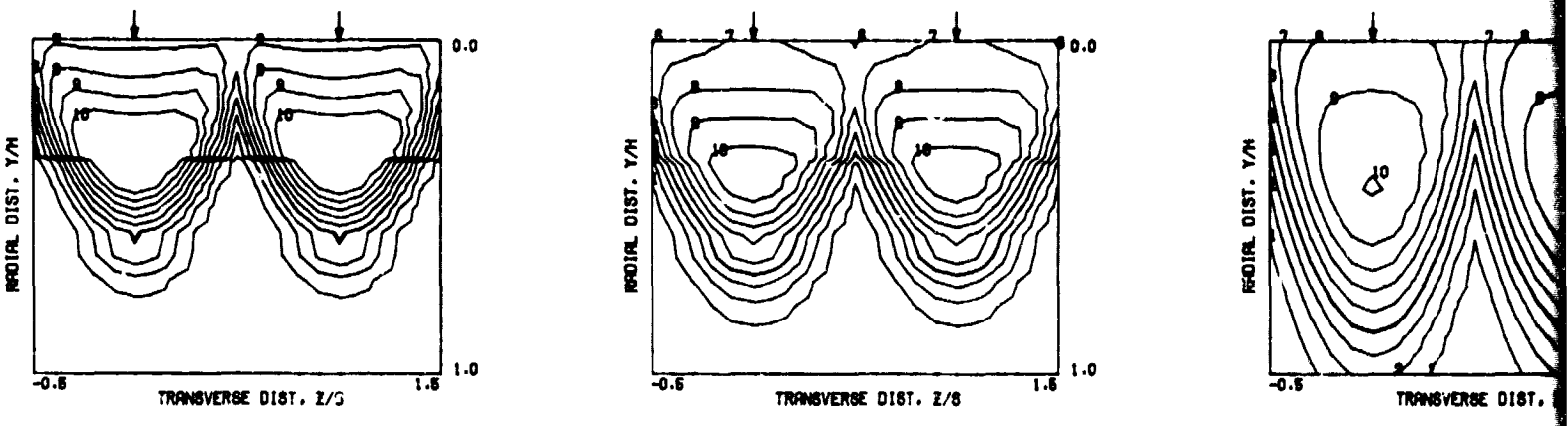

PREDICTED THETA CONTOURS FOR TEST NO.21. TMAIN=CONS

S/DJ = 2.46 HO/DJ = 4.92 VRATIO = 1.78 TRATIO = 0.471 DENRATIO=2.129 TMAIN

X/H = 0.50 X/DJ =2.46 X/H = 0.75 X/DJ =3.69 X/H = 1.00 X/DJ =4.92

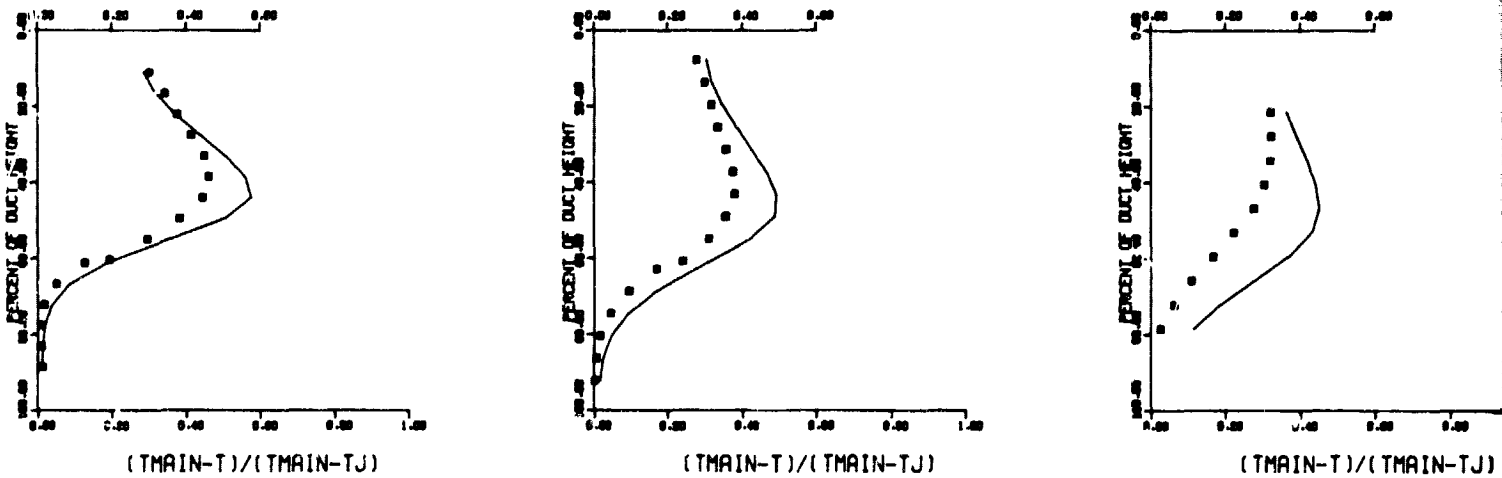

COMPARISON BETWEEN DATA AND CORRELATIONS FOR TEST NO. 21. TEST SECTION II.UNIFORM

ORIGINAL PAGE IS
OF POOR QUALITY

FOLDOUT FRAME

4	5	6	7	8	9	10
0.1973	0.2000	0.2500	0.3000	0.3500	0.4000	0.4500

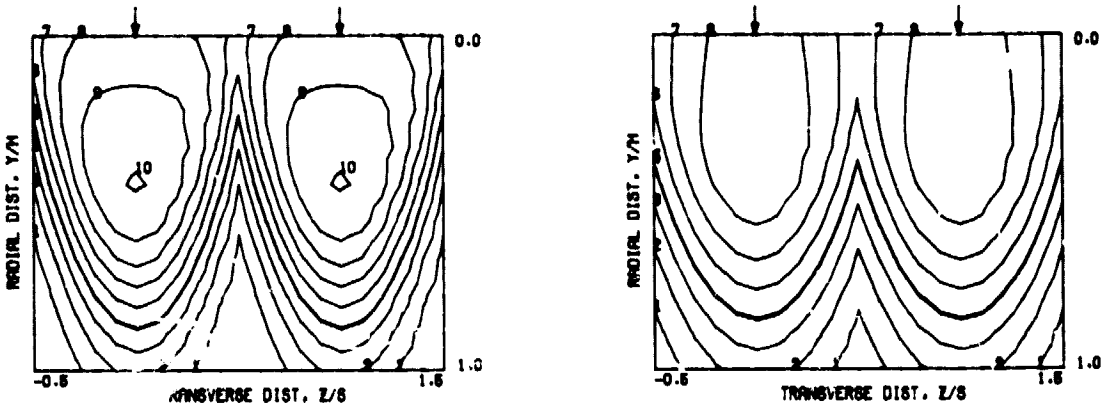

RS FOR TEST NO.21, TMAIN=CONST, J=6.76, S/D=2.0, H/D=4.0

= 0.471 DENRATIO=2.129 TMAIN = 653.7 K TJET = 307.9 K THEB = 0.197

X/H = 1.00 X/DJ =4.92 X/H = 2.00 X/DJ =9.85

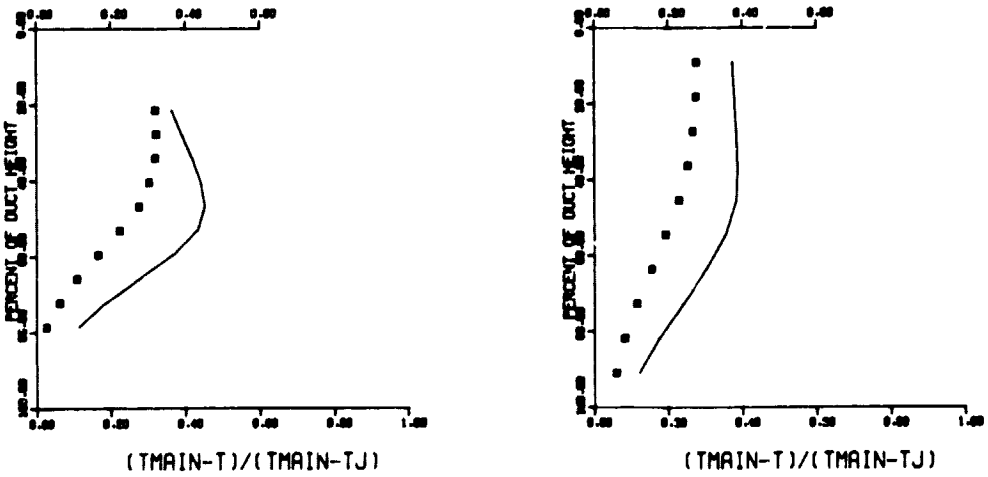

FOLDOUT FRAME 2

. 21, TEST SECTION II,UNIFORM TMAIN, J = 6.76 , S/D =2.00 , H/D =4.00

Figure 54

ORIGINAL PAGE IS
OF POOR QUALITY

S = 0.0508 METERS S/DJ = 2.582 HO/DJ = 5.164 VMAIN = 15.8 M/SEC VJET = 54.5 M/SEC TMAIN = 653.7 K TJE

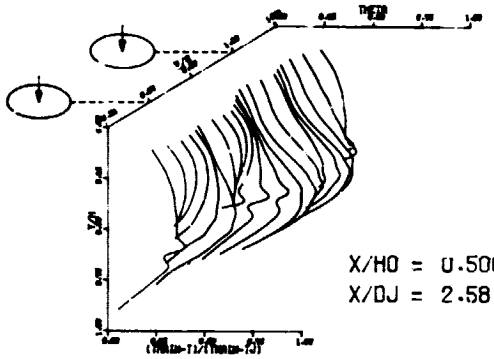

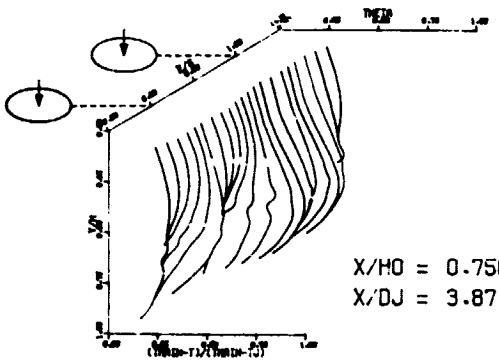

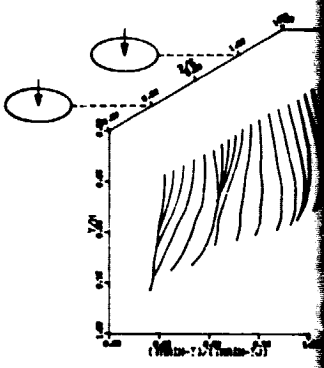

MEASURED THETA PROFILES FOR TEST NO. 22, TEST SECTION II, TMAIN=CONST., J =

CONTOUR	1	2	3	4	5	6
VALUE	0.0500	0.1000	0.1500	0.2000	0.2500	0.3074

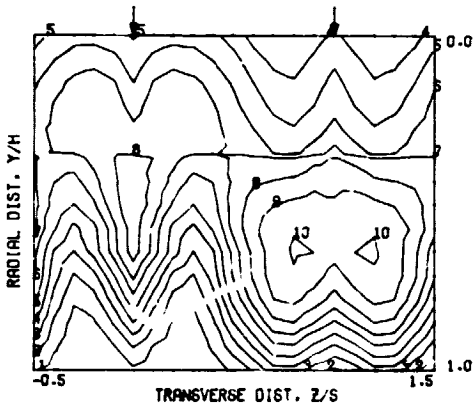

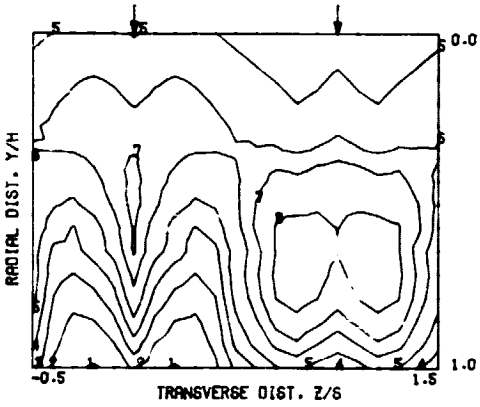

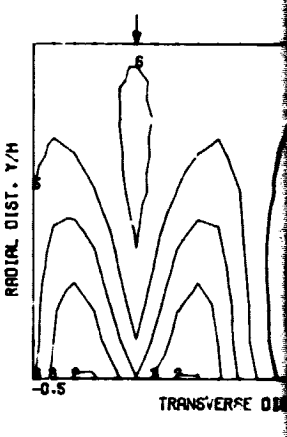

MEASURED THETA CONTOURS FOR TEST NO.22, TMAIN=CO

FOLDOUT FRAME

ORIGINAL PAGE IS
OF POOR QUALITY

SEC TMAIN = 653.7 K TJET = 303.8 K THEB = 0.3074 BLORAT= 7.538 DENRATIO= 2.179 TRATIO=0.465

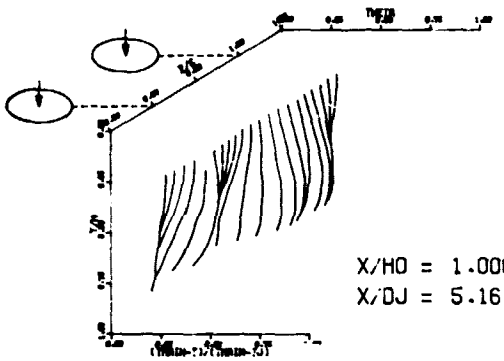

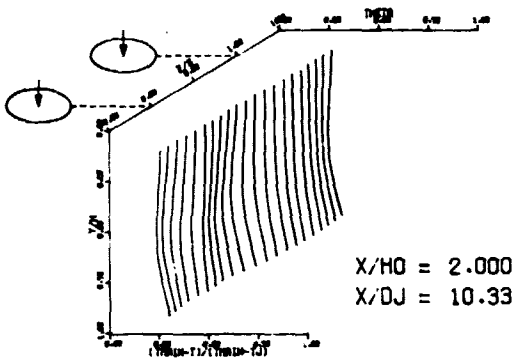

II, TMAIN=CONST., J = 26.07 , S/D = 2.00 , H/D = 4.00

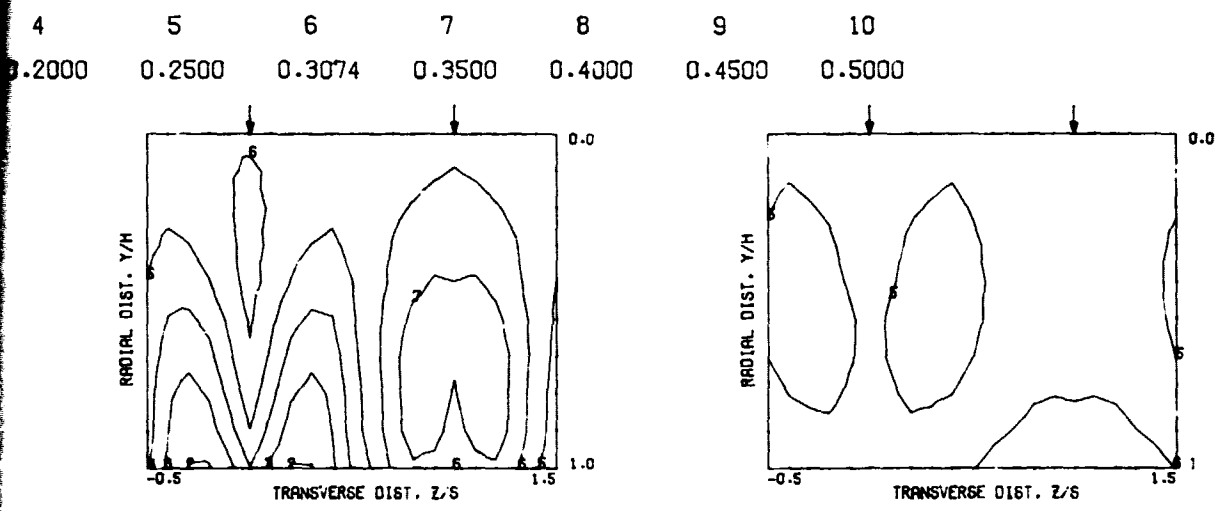

FOR TEST NO.22, TMAIN=CONST, J=26.07, S/D=2.0, H/D=4.0

2 FOLDOUT FRAME

ORIGINAL PAGE IS OF POOR QUALITY

Figure 55

CONTOUR	1	2	3	4	5	6
VALUE	0.0500	0.1000	0.1500	0.2000	0.2500	0.3074

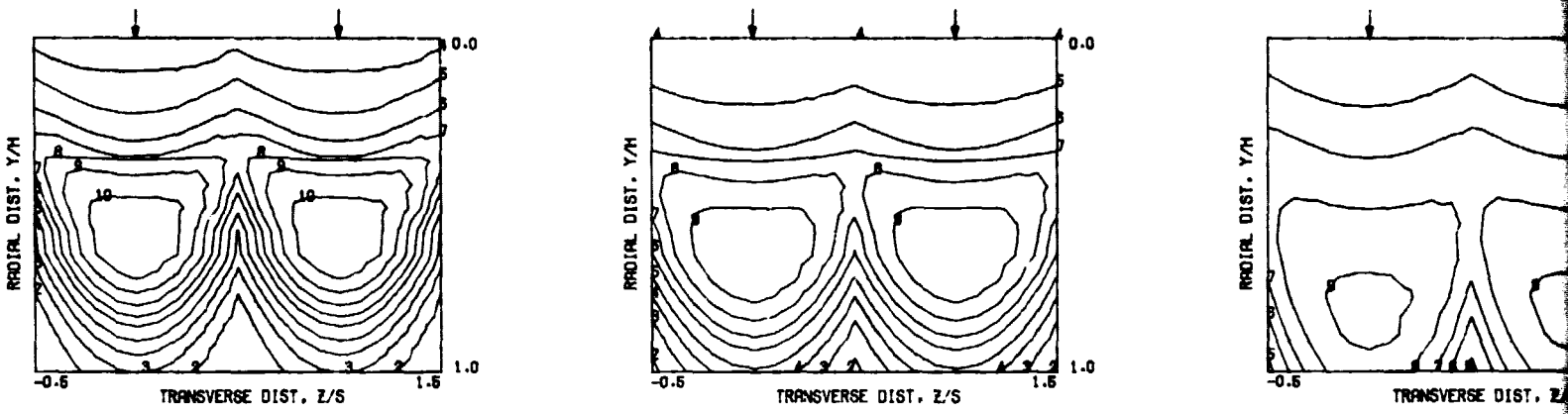

PREDICTED THETA CONTOURS FOR TEST NO.22, TMAIN=CONS

S/DJ = 2.58 HO/DJ = 5.16 VRATIO = 3.46 TRATIO = 0.465 DENRATIO=2.179 TMAIN =

X/H = 0.50 X/DJ =2.58 X/H = 0.75 X/DJ =3.87 X/H = 1.00 X/DJ =5.16

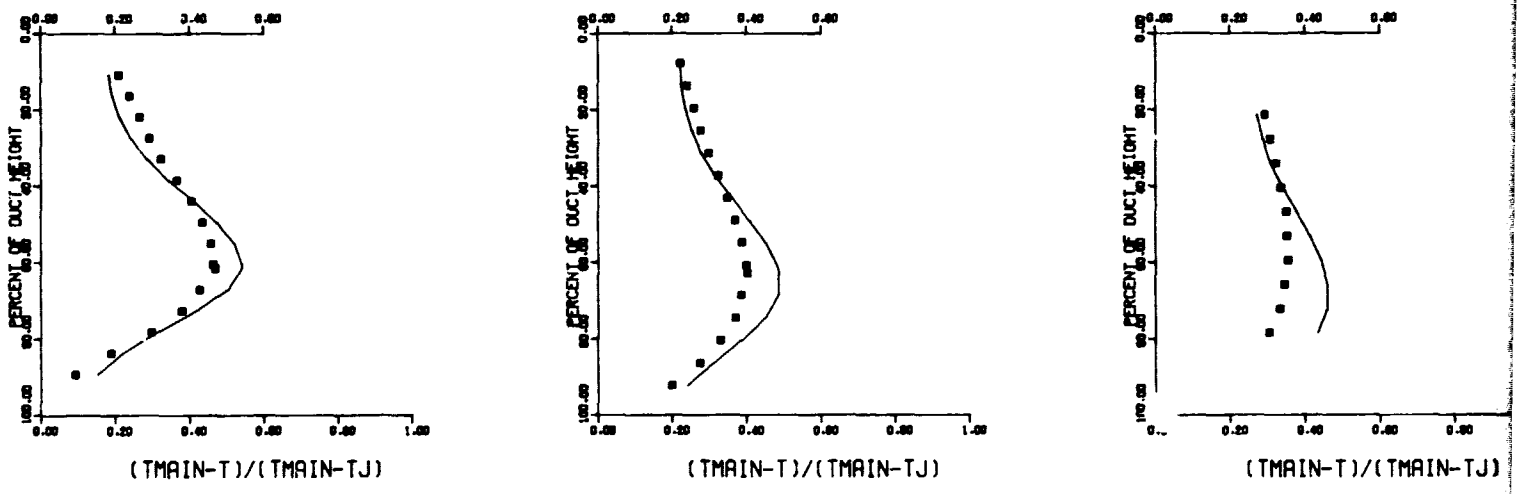

COMPARISON BETWEEN DATA AND CORRELATIONS FOR TEST NO. 22, TEST SECTION II,UNIFORM

FOLDOUT FRAME

ORIGINAL PAGE IS
OF POOR QUALITY

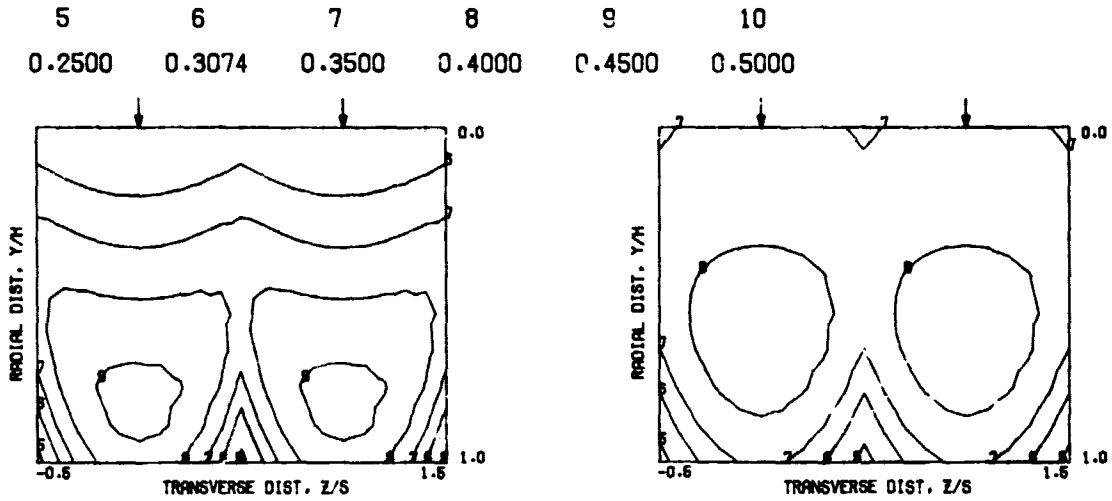

TEST NO.22, TMAIN=CONST, J=26.07, S/D=2.0, H/D=4.0

DENRATIO=2.179 TMAIN = 653.7 K TJET = 303.8 K THEB = 0.307

X/H = 1.00 X/DJ =5.16 X/H = 2.00 X/DJ =10.33

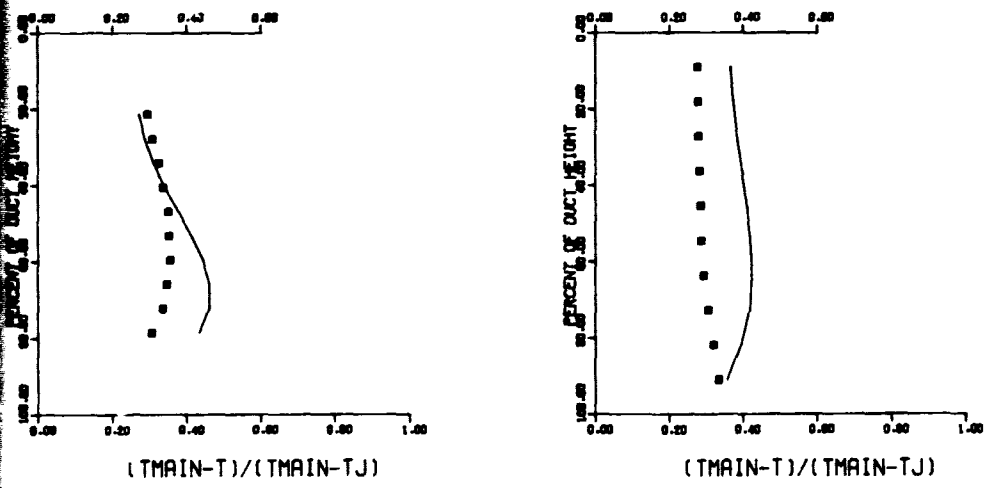

FOLDOUT FRAME

TEST SECTION II,UNIFORM TMAIN, J = 26.07 , S/D =2.00 , H/D =4.00

Figure 56

ORIGINAL PAGE IS
OF POOR QUALITY

ORIGINAL PAGE IS
OF POOR QUALITY

S = 0.0508 METERS S/DJ = 4.925 HO/DJ = 9.851 VMAIN = 17.0 M/SEC VJET = 53.9 M/SEC TMAIN = 645.5 K TJET

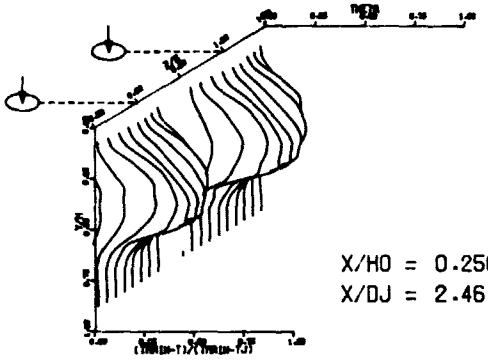

X/HO = 0.250
X/DJ = 2.46

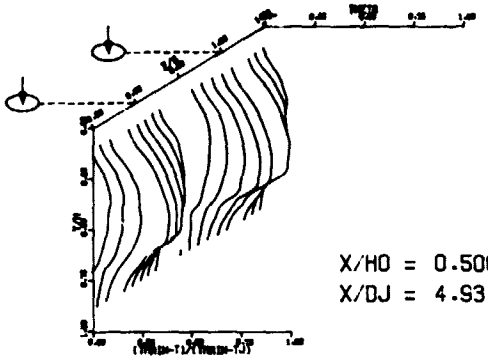

X/HO = 0.500
X/DJ = 4.93

MEASURED THETA PROFILES FOR TEST NO. 23, TEST SECTION IV, TMAIN=CONST, J = 21

CONTOUR	1	2	3	4	5	6	7	8	9
VALUE	0.0500	0.0972	0.1500	0.2000	0.2500	0.3000	0.3500	0.4000	0.5

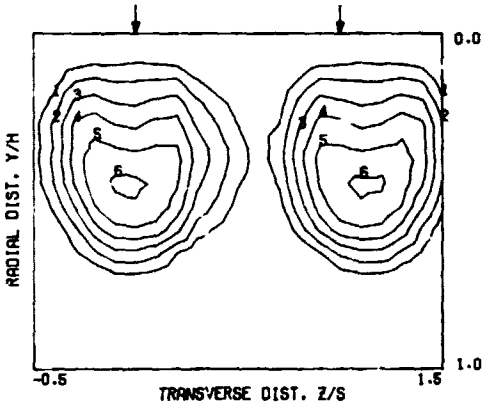

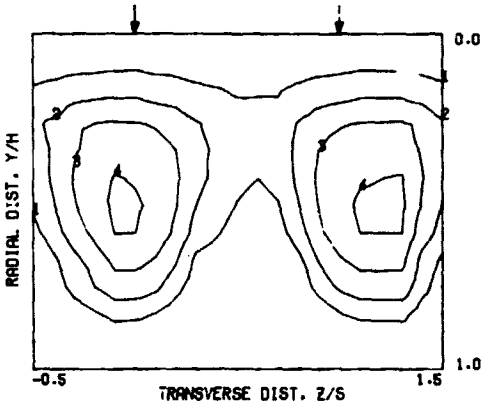

MEASURED THETA CONTOURS FOR TEST NO.23, TMAIN=CONST, J=21.07, S/D=4.

FOLDOUT FRAME

ORIGINAL PAGE IS
OF POOR QUALITY

.8 M/SEC TMAIN = 645.5 K TJET = 312.2 K THEB = 0.0972 BLORAT= 6.653 DENRATIO= 2.102 TRATIO=0.484

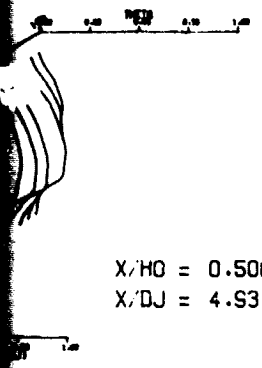

X/HO = 0.500
X/DJ = 4.S3

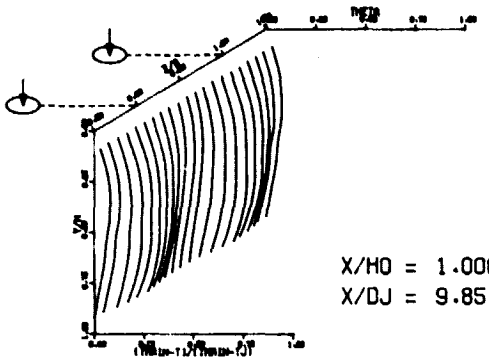

X/HO = 1.000
X/DJ = 9.85

TION IV, TMAIN=CONST , J = 21.07 , S/D = 4.00 , H/D = 8.00

6	7	8	9	10	11
0.3000	0.3500	0.4000	0.5000	0.6000	0.7000

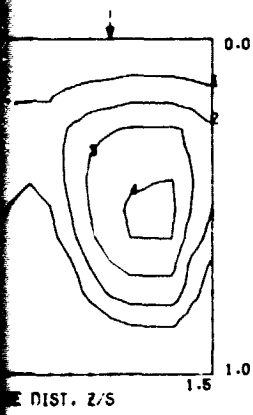

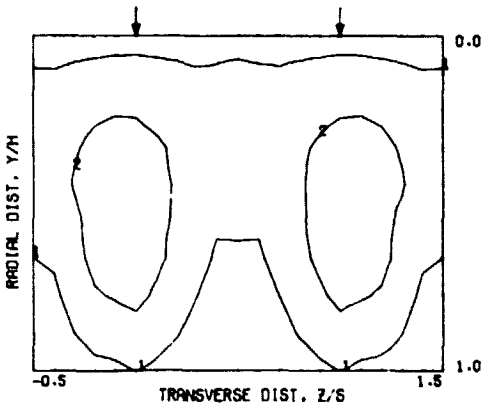

TMAIN=CONST, J=21.07, S/D=4.0, H/D=8.0

FOLDOUT FRAME

Figure 57

CONTOUR	1	2	3	4	5	6	7	8	9
VALUE	0.0500	0.0972	0.1500	0.2000	0.2500	0.3000	0.3500	0.4000	0.500

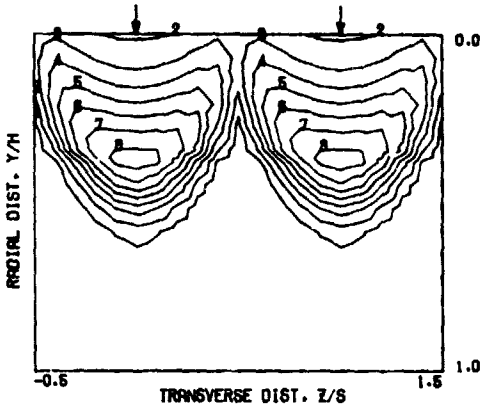

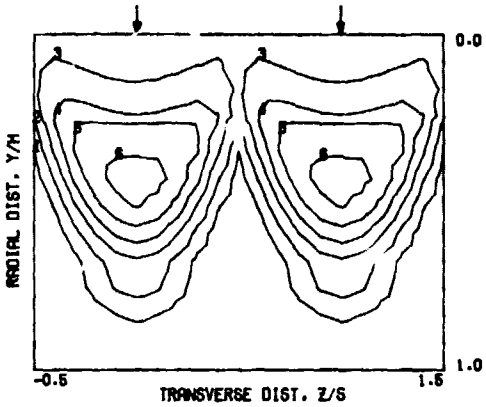

PREDICTED THETA CONTOURS FOR TEST NO. 23, TMAIN=CONST, J=21.07, S/D=4.

S/DJ = 4.93 HO/DJ = 9.85 VRATIO = 3.17 TRATIO = 0.484 DENRATIO=2.102 TMAIN =

X/H = 0.25 X/DJ =2.46

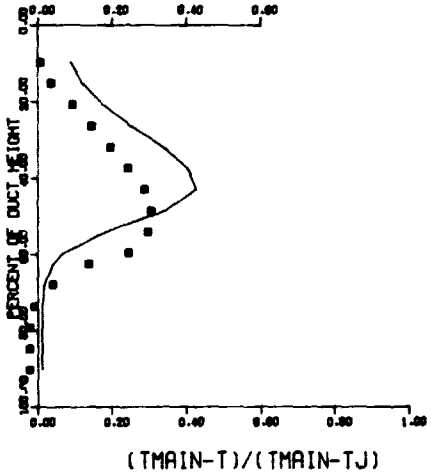

X/H = 0.50 X/DJ =4.93

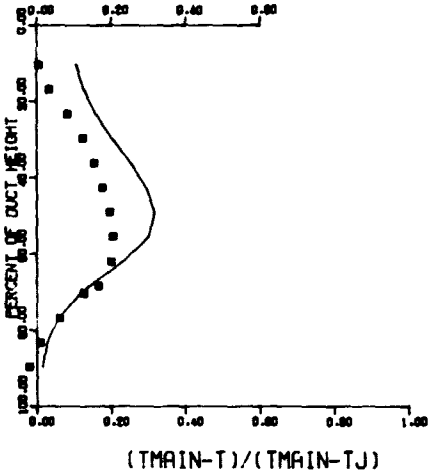

COMPARISON BETWEEN DATA AND CORRELATIONS FOR TEST NO. 23, TEST SECTION IV, TMAI

ORIGINAL PAGE IS
OF POOR QUALITY

FOLDOUT FRAME

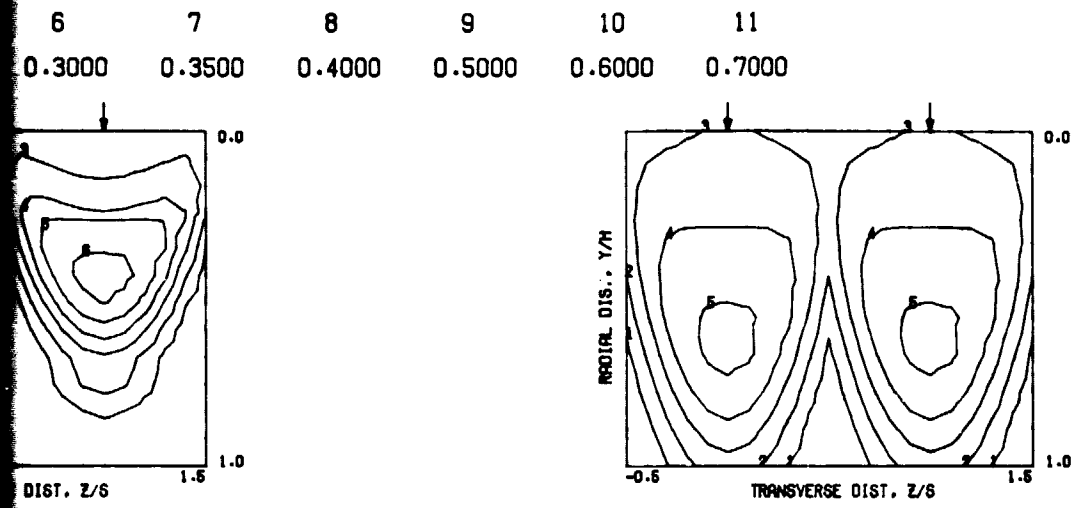

TMAIN=CONST, J=21.07, S/D=4.0 H/D=8.0

= 0.484 DENRATIO=2.102 TMAIN = 645.5 K TJET = 312.2 K THEB = 0.097

DJ =4.93 X/H = 1.00 X/DJ =9.85

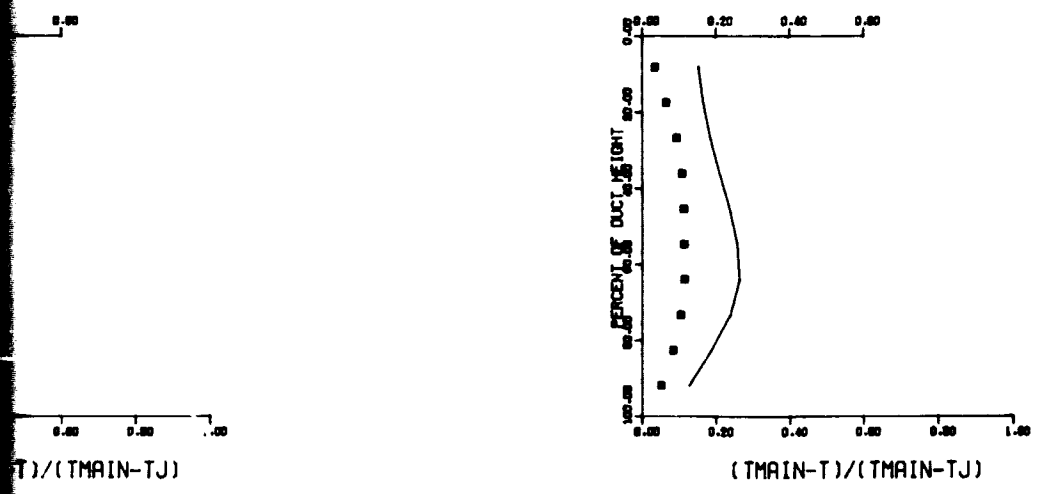

FOLDOUT FRAME

0. 23, TEST SECTION IV, TMAIN=CONST, J = 21.07 , S/D =4.00 , H/D =8.00

Figure 58

ORIGINAL PAGE IS
OF POOR QUALITY

S = 0.0508 METERS S/DJ = 5.000 HO/DJ = 10.000 VMAIN = 16.9 M/SEC VJET = 105.1 M/SEC TMAIN = 642.8 K TJE

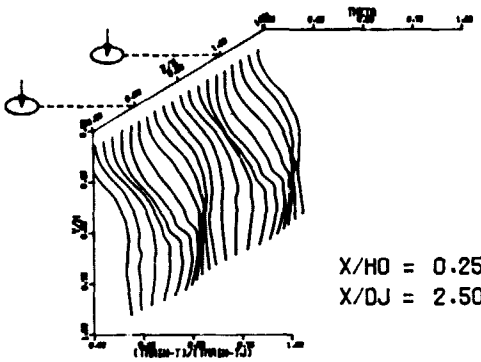

X/HO = 0.250
X/DJ = 2.50

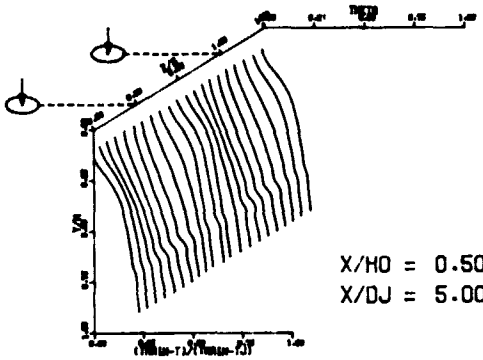

X/HO = 0.500
X/DJ = 5.00

MEASURED THETA PROFILES FOR TEST NO. 24, TEST SECTION IV, TMAIN=CONST , J =

CONTOUR	1	2	3	4	5	6	7	8
VALUE	0.0500	0.1000	0.1500	0.1781	0.2000	0.2500	0.3000	0.3500

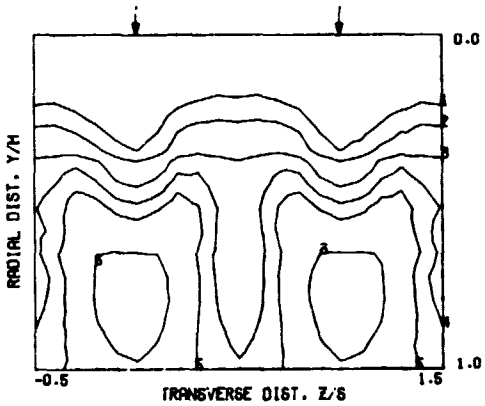

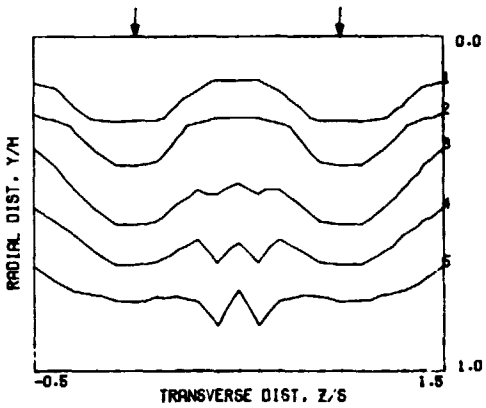

MEASURED THETA CONTOURS FOR TEST NO.24, TMAIN=CONST, J=85.84, S/D=4

ORIGINAL PAGE IS
OF POOR QUALITY

FOLDOUT FRAME

M/SEC TMAIN = 642.8 K TJET = 311.0 K THEB = 0.1781 BLORAT= 13.792 DENRATIO= 2.217 TRATIO= 0.484

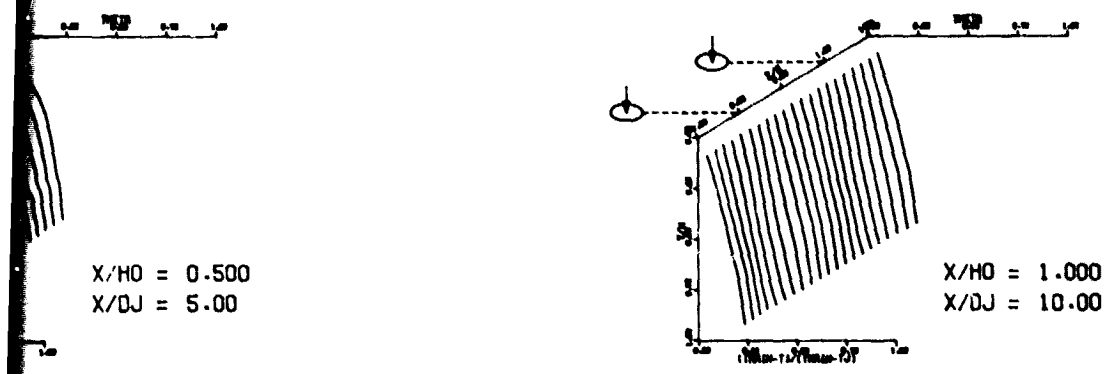

ON IV, TMAIN=CONST , J = 85.84 , S/D = 4.00 , H/D = 8.00

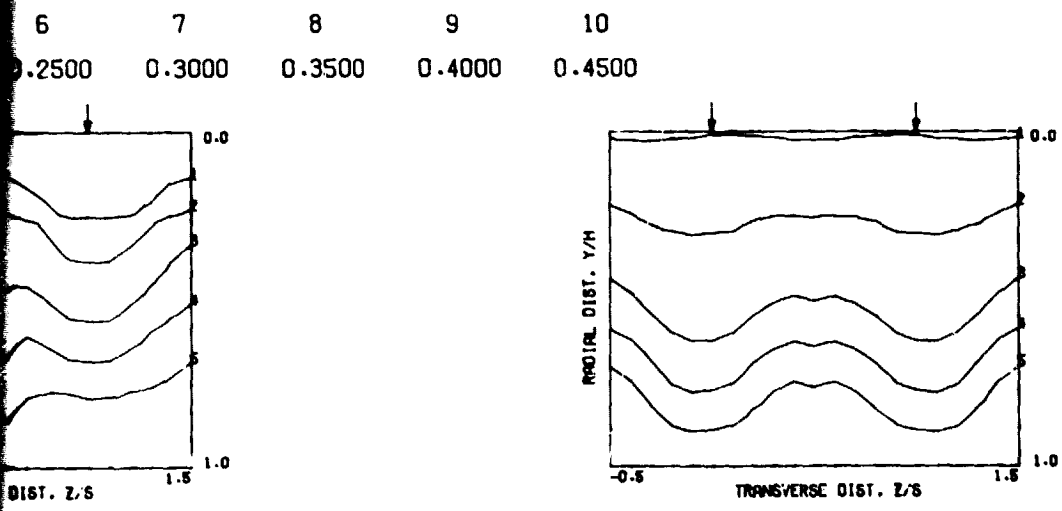

TMAIN=CONST, J=85.84, S/D=4.0, H/D=8.0

2 FOLDOUT FRAME

Figure 59

ORIGINAL PAGE IS
OF POOR QUALITY

CONTOUR	1	2	3	4	5	6	7	8	9
VALUE	0.0500	0.1000	0.1500	0.1781	0.2000	0.2500	0.3000	0.3500	0.4000

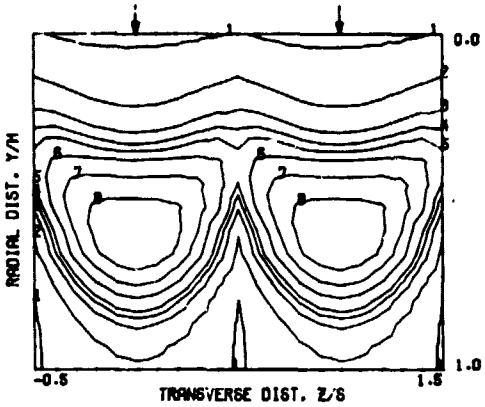

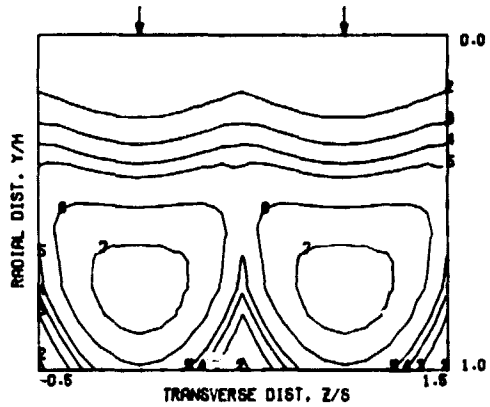

PREDICTED THETA CONTOURS FOR TEST NO.24. TMAIN=CONST. J=85.84. S/D=4.0.

S/DJ = 5.00 HO/DJ = 10.00 VRATIO = 6.22 TRATIO = 0.484 DENRATIO=2.217 TMAIN =

X/H = 0.25 X/DJ =2.50

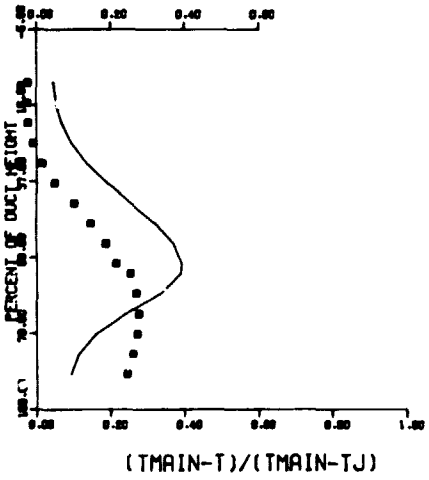

X/H = 0.50 X/DJ =5.00

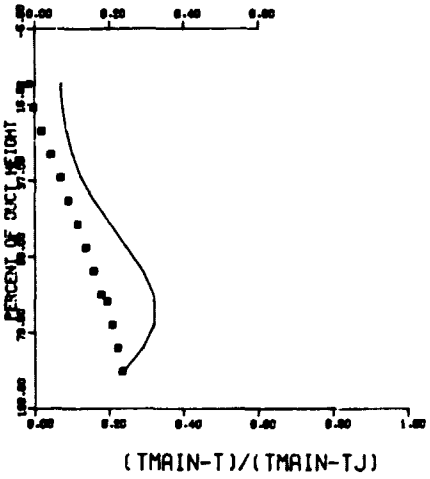

COMPARISON BETWEEN DATA AND CORRELATIONS FOR TEST NO. 24. TEST SECTION IV.UNIFORM

ORIGINAL PAGE IS
OF POOR QUALITY

FOLDOUT FRAME

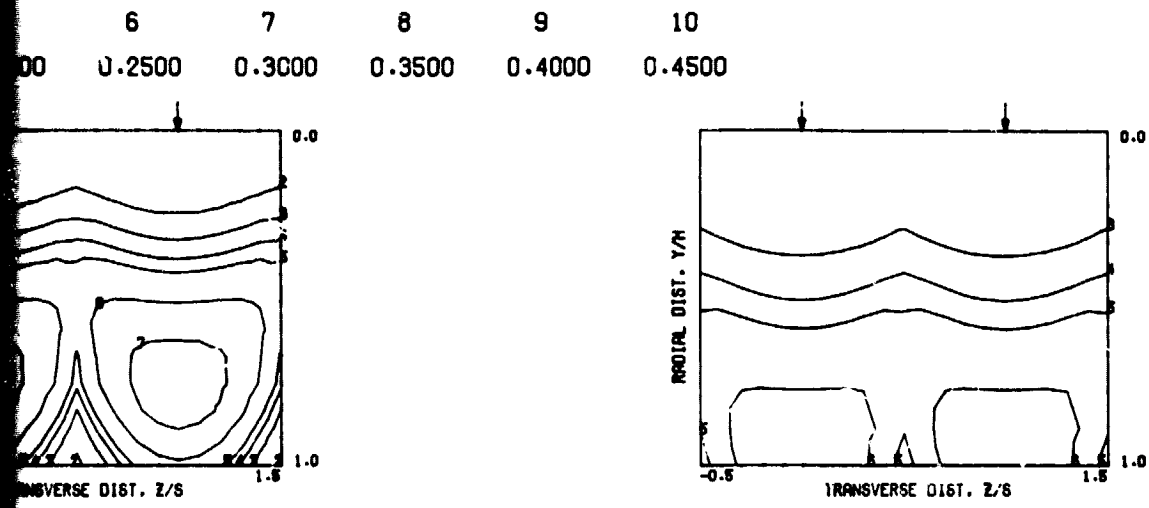

.24, TMAIN=CONST, J=85.84, S/D=4.0, H/D=8.0

TRATIO = 0.484 DENRATIO=2.217 TMAIN = 642.8 K TJET = 311.0 K THEB = 0.178

0 X/DJ =5.00 X/H = 1.00 X/DJ =10.00

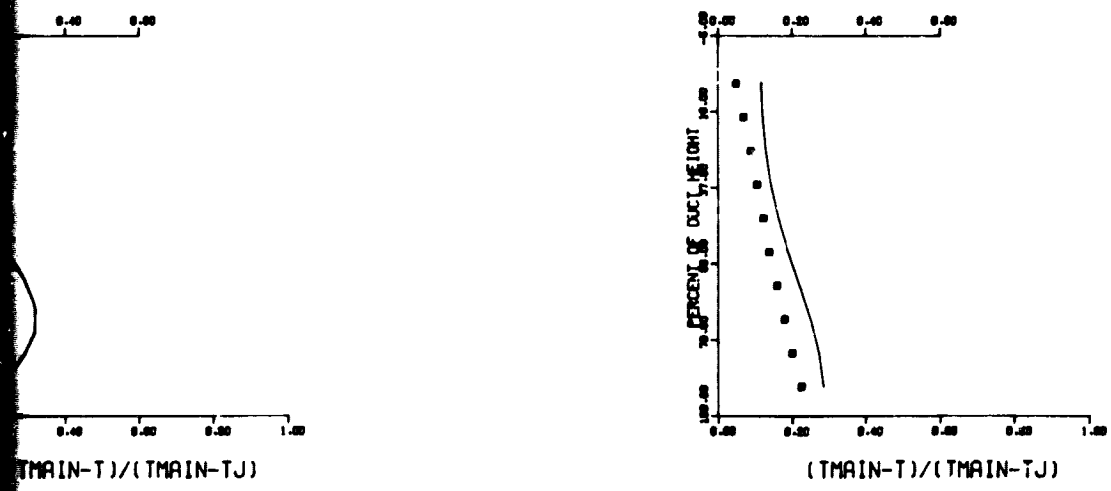

FOLDOUT FRAME

T NO. 24, TEST SECTION IV.UNIFORM TMAIN, J = 85.84 , S/D =4.00 , H/D =8.00

Figure 60

ORIGINAL PAGE IS
OF POOR QUALITY

S = 0.0508 METERS S/DJ = 2.538 HO/DJ = 5.075 VMAIN = 15.1 M/SEC VJET = 27.7 M/SEC TMAIN = 643.4 K TJE

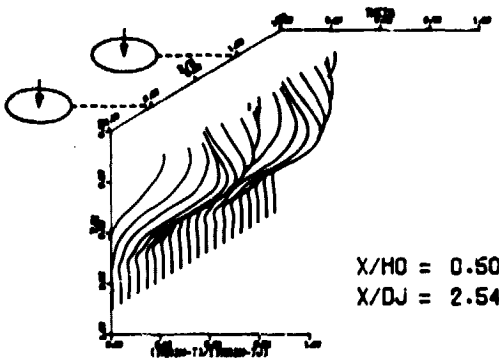

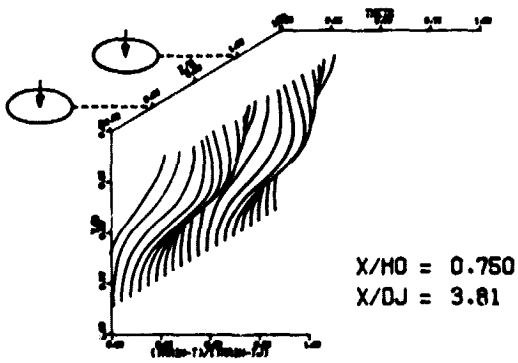

MEASURED THETA PROFILES FOR TEST NO. 25, TEST SECTION IV, TMAIN=CONST , J =

CONTOUR	1	2	3	4	5	6	7	8
VALUE	0.0500	0.1000	0.1500	0.1830	0.2000	0.2500	0.3000	0.3500

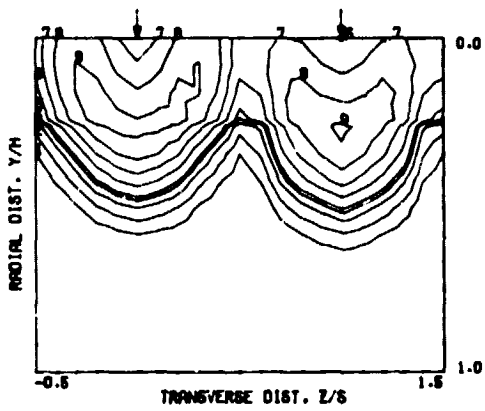

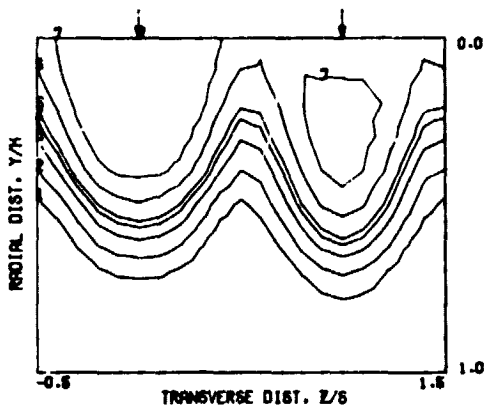

MEASURED THETA CONTOURS FOR TEST NO.25, TMAIN=CONST, J=6.73, S/D=2.

FOLDOUT FRAME

ORIGINAL PAGE IS
OF POOR QUALITY

7 M/SEC TMAIN = 643.4 K TJET = 321.6 K THEB = 0.1830 BLORAT= 3.672 DENRATIO= 2.003 TRATIO= 0.500

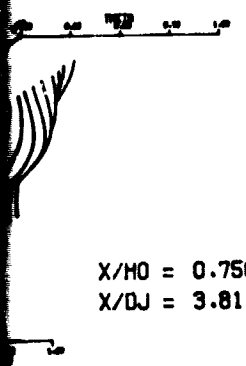

X/HO = 0.750
X/DJ = 3.81

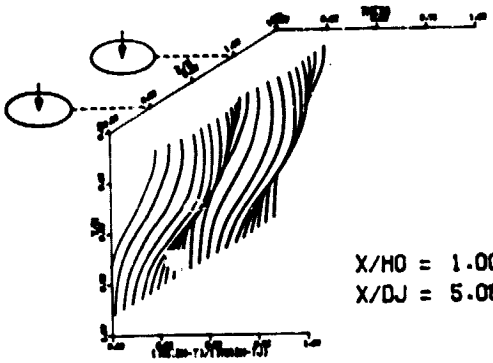

X/HO = 1.000
X/DJ = 5.08

ION IV, TMAIN=CONST , J = 6.73 , S/D = 2.00 , H/D = 4.00

6	7	8	9	10
0.2500	0.3000	0.3500	0.4000	0.4500

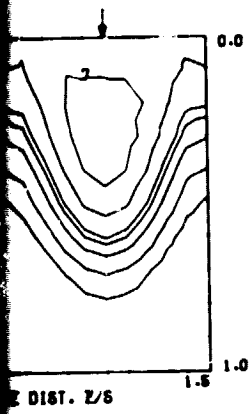

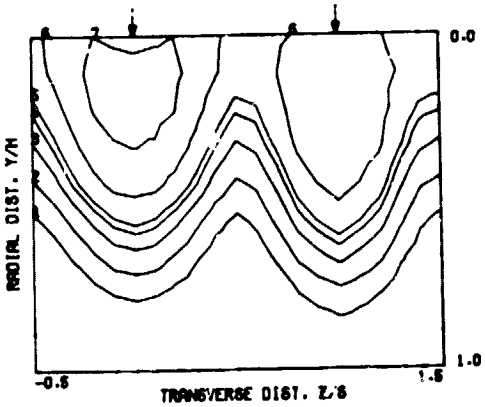

TMAIN=CONST, J=6.73, S/D=2.0, H/D=4.0

FOLDOUT FRAME

Figure 61

ORIGINAL PAGE IS
OF POOR QUALITY

CONTOUR	1	2	3	4	5	6	7	8
VALUE	0.0500	0.1000	0.1500	0.1830	0.2000	0.2500	0.3000	0.3500

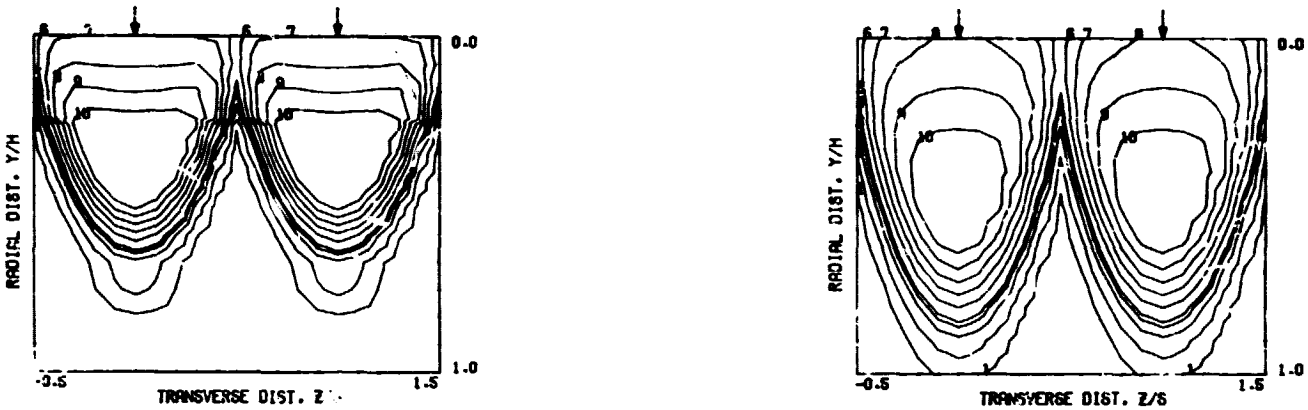

PREDICTED THETA CONTOURS FOR TEST NO.25, TMAIN=CONST, J=6.73, S/D=2

S/DJ = 2.54 HO/DJ = 5.08 VRATIO = 1.83 TRATIO = 0.500 DENRATIO=2.003 TMA

X/H = 0.50 X/DJ =2.54

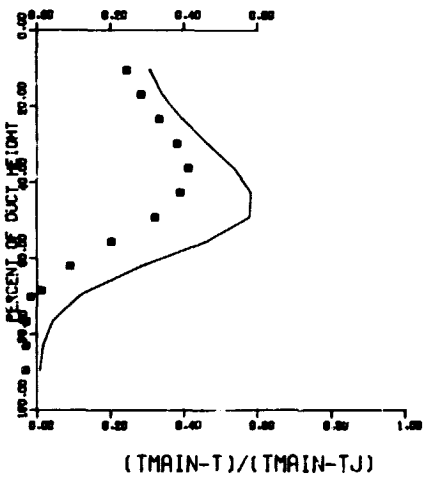

X/H = 0.75 X/DJ =3.81

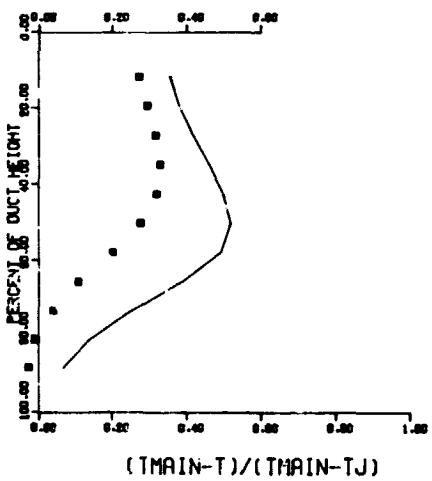

COMPARISON BETWEEN DATA AND CORRELATIONS FOR TEST NO. 25, TEST SECTION IV,UNIF

ORIGINAL PAGE IS
OF POOR QUALITY

FOLDOUT FRAME

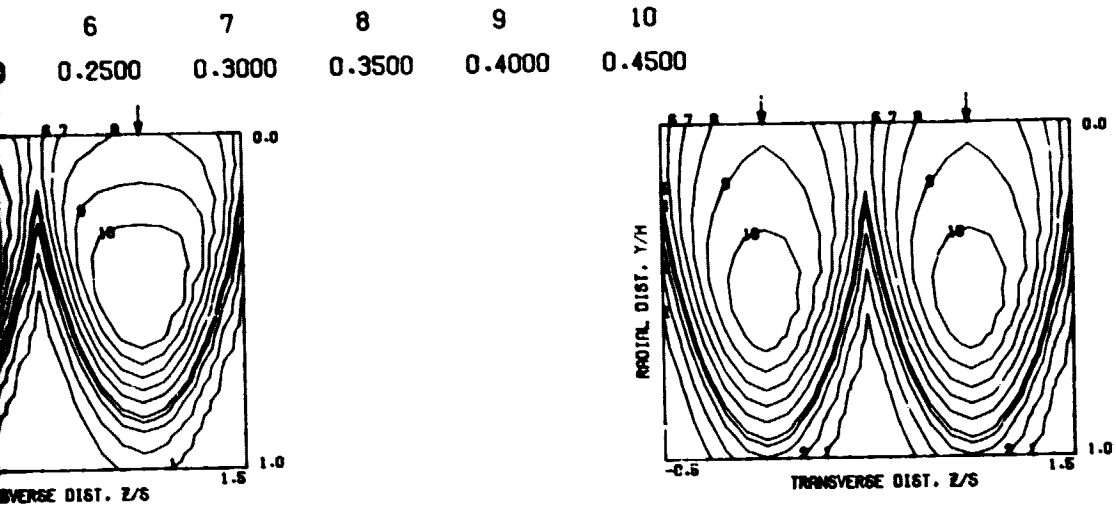

25. TMAIN=CONST. J=6.73. S/D=2.0. H/D=4.0

TRATIO = 0.500 DENRATIO=2.003 TMAIN = 643.4 K TJET = 321.6 K THEB = 0.183

X/DJ =3.81 X/H = 1.00 X/DJ =5.08

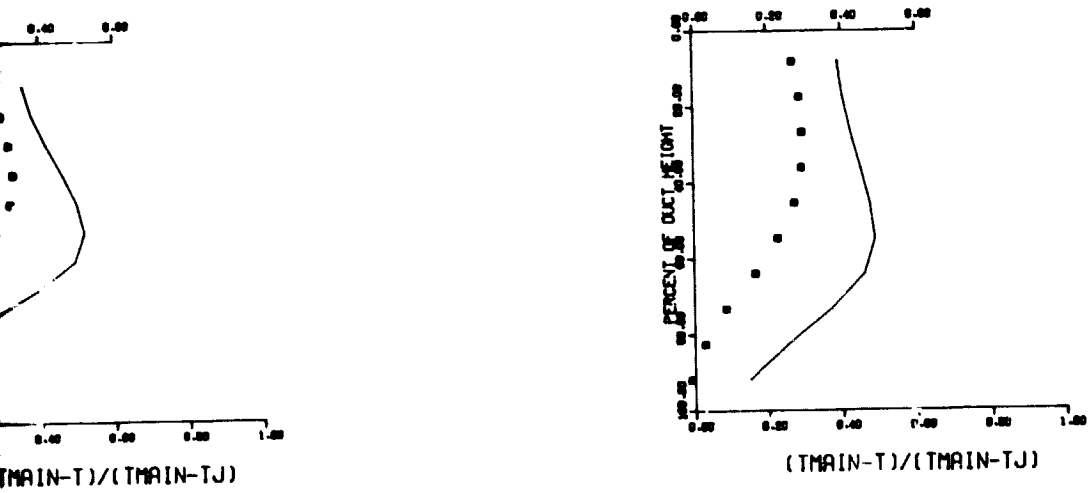

FOLDOUT FRAME

T NO. 25. TEST SECTION IV.UNIFORM TMAIN. J = 6.73 . S/D =2.00 . H/D =4.00

Figure 62

ORIGINAL PAGE IS
OF POOR QUALITY

S = 0.0508 METERS S/DJ = 2.582 HO/DJ = 5.164 VMAIN = 14.9 M/SEC VJET = 55.1 M/SEC TMAIN = 640.7 K TJET

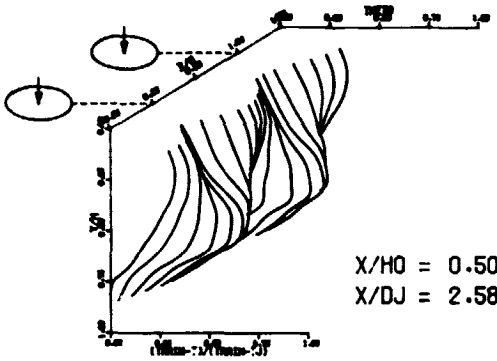

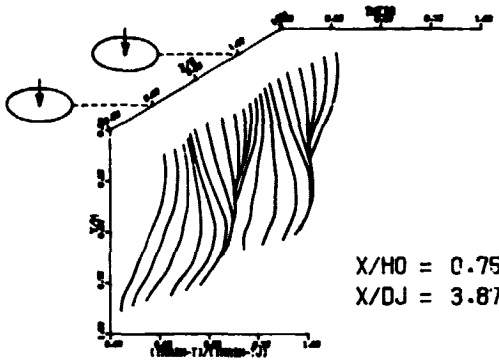

MEASURED THETA PROFILES FOR TEST NO. 26, TEST SECTION IV, TMAIN=CONST , J = 26

CONTOUR	1	2	3	4	5	6	7	8	9
VALUE	0.0500	0.1000	0.1500	0.2000	0.2500	0.2988	0.3500	0.4000	0.45

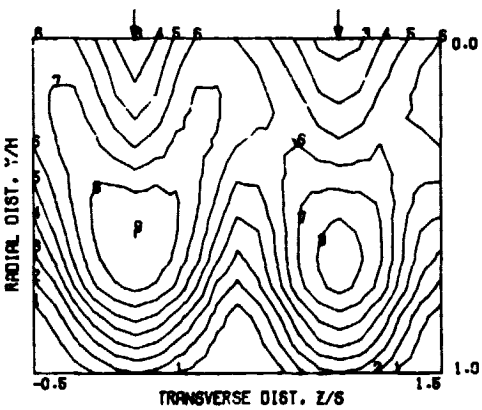

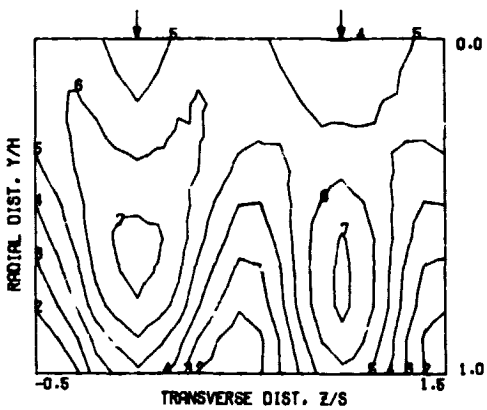

MEASURED THETA CONTOURS FOR TEST NO.26, TMAIN=CONST, J=26.73, S/D=2.0

ORIGINAL PAGE IS
OF POOR QUALITY

FOLDOUT FRAME

55.1 M/SEC TMAIN = 640.7 K TJET = 329.8 K THEB = 0.2988 BLORAT= 7.233 DENRATIO= 1.958 TRATIO=0.515

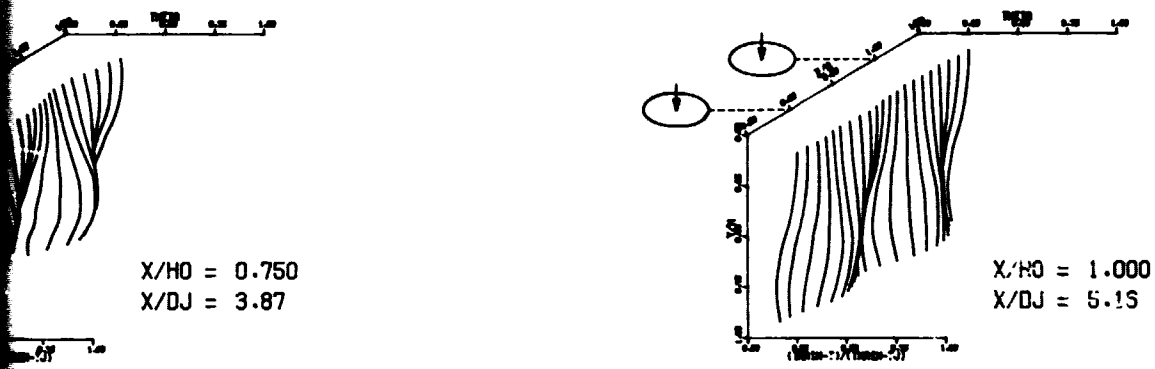

ECTION IV. TMAIN=CONST , J = 26.73 , S/D = 2.00 , H/D = 4.00

6	7	8	9	10
0.2988	0.3500	0.4000	0.4500	0.5000

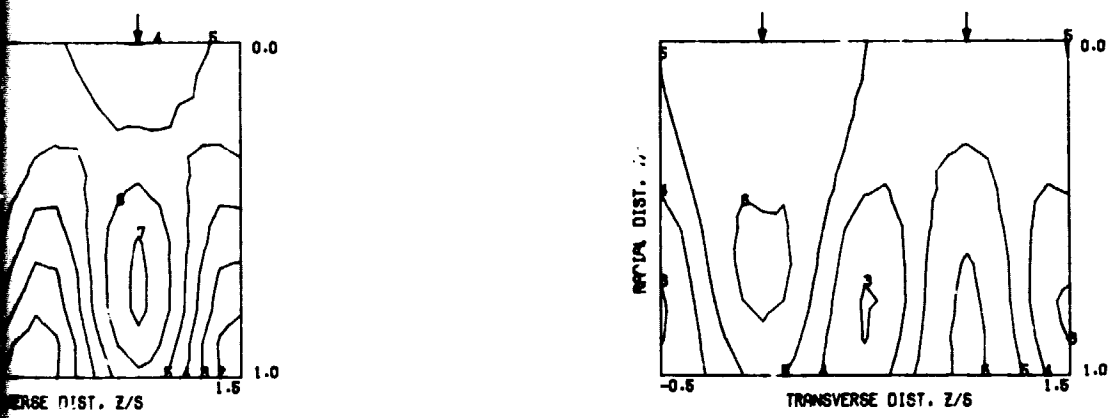

FOLDOUT FRAME

ORIGINAL PAGE IS OF POOR QUALITY

, TMAIN=CONST. J=26.73. S/D=2.0. H/D=4.0

Figure 63

CONTOUR	1	2	3	4	5	6	7	8	9
VALUE	0.0500	0.1000	0.1500	0.2000	0.2500	0.2988	0.3500	0.4000	0.45

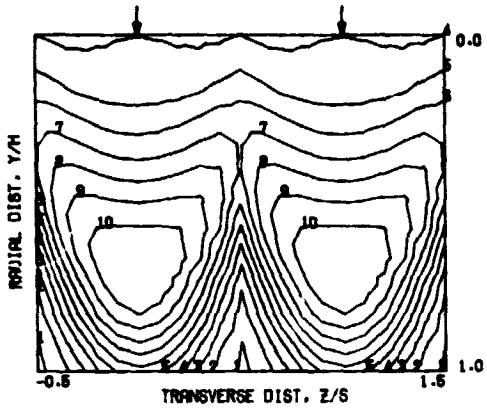

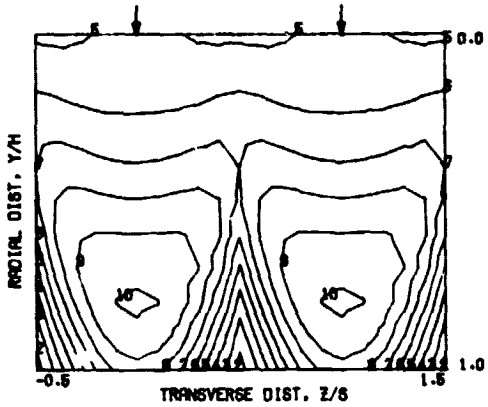

PREDICTED THETA CONTOURS FOR TEST NO.26, TMAIN=CONST. H=26.73, S/D=2.0

S/DJ = 2.58 HO/DJ = 5.16 VRATIO = 3.70 TRATIO = 0.515 DENRATIO= 1.958 TMAIN

X/H = 0.50 X/DJ =2.58

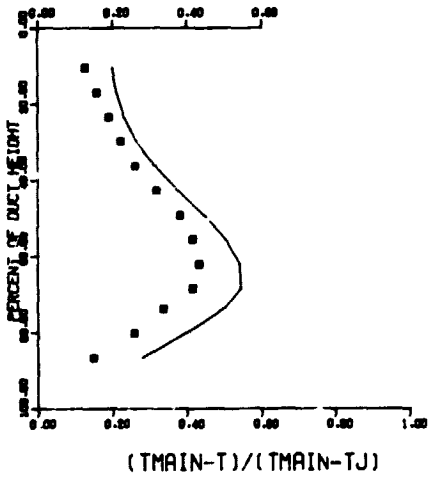

X/H = 0.75 X/DJ =3.87

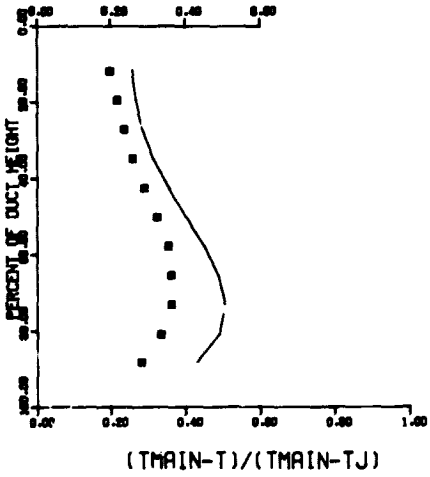

COMPARISON BETWEEN DATA AND CORRELATIONS FOR TEST NO. 26, TEST SECTION V,UNIFOR

ORIGINAL PAGE IS
OF POOR QUALITY

FOLDOUT FRAME

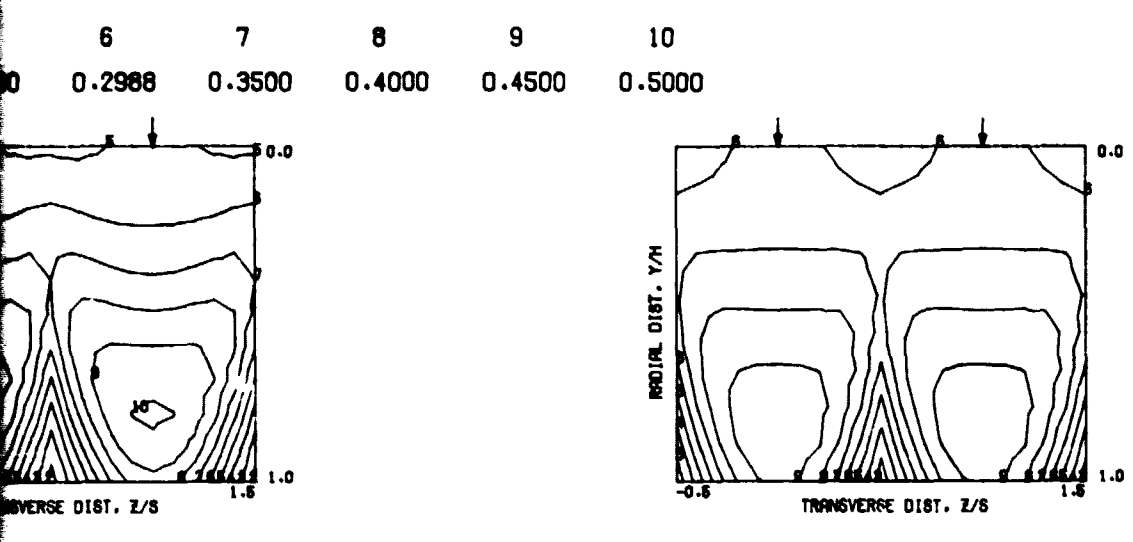

26, TMAIN=CONST, J=26.73, S/D=2.0, H/D=4.0

RATIO = 0.515 DENRATIO=1.958 TMAIN = 640.7 K TJET = 329.8 K THEB = 0.299

X/DJ =2.97 X/H = 1.00 X/DJ =5.16

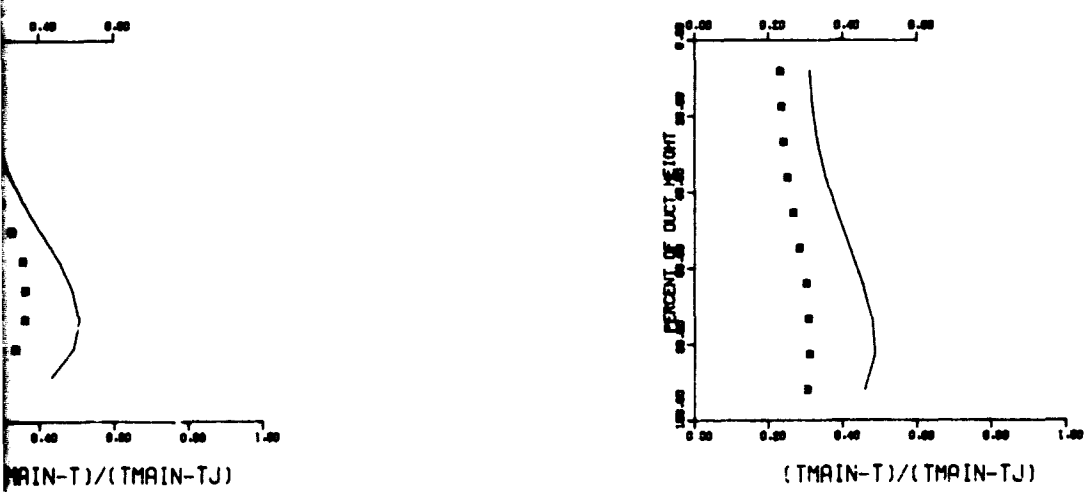

FOLDOUT FRAME

NO. 26, TEST SECTION IV,UNIFORM TMAIN, J = 26.73 , S/D =2.00 , H/D =4.00

Figure 64

ORIGINAL PAGE IS
OF POOR QUALITY

S = 0.0508 METERS S/DJ = 4.961 HO/DJ = 9.921 VMAIN = 16.1 M/SEC VJET = 58.7 M/SEC TMAIN = 646.4 K 1

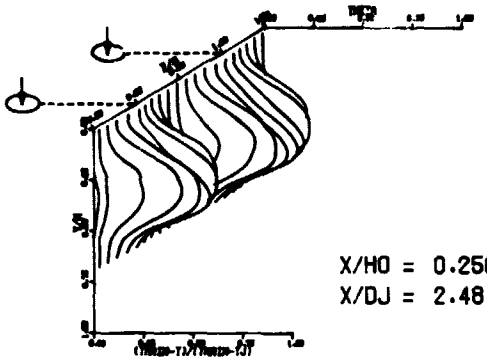

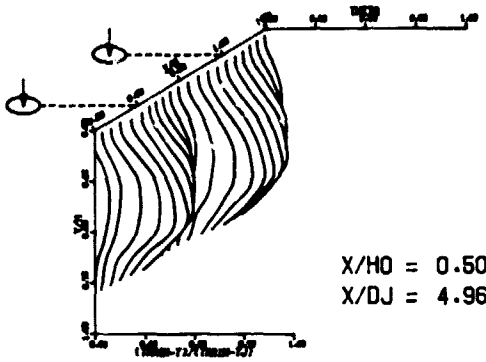

MEASURED THETA PROFILES FOR TEST NO. 27, TEST SECTION V, TMAIN=CONST , J

CONTOUR	1	2	3	4	5	6	7	8
VALUE	0.0500	0.1065	0.1500	0.2000	0.2500	0.3000	0.3500	0.4000

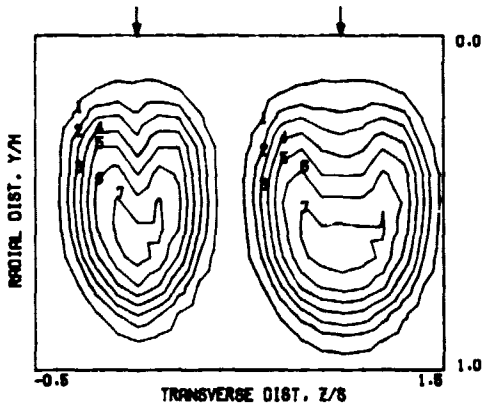

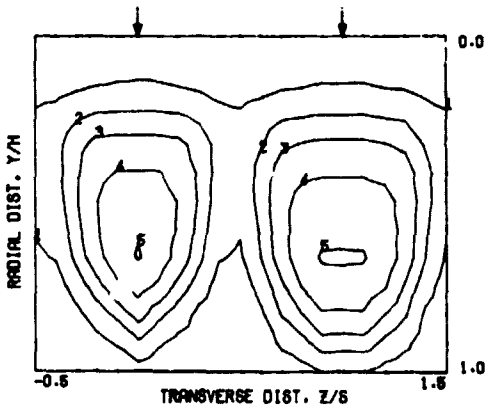

MEASURED THETA CONTOURS FOR TEST NO.27, TMAIN=CONST, J=27.18, S/D

ORIGINAL PAGE IS
OF POOR QUALITY
FOLDOUT FRAME

58.7 M/SEC TMAIN = 646.4 K TJET = 320.3 K THEB = 0.1065 BLORAT= 7.470 DENRATIO= 2.053 TRATIO= 0.496

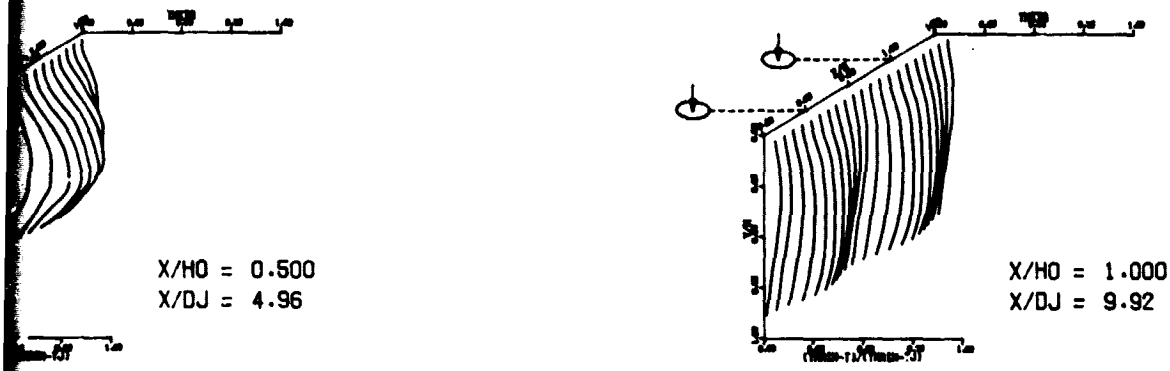

ECTION V, TMAIN=CONST , J = 27.18 , S/D = 4.00 , H/D = 8.00

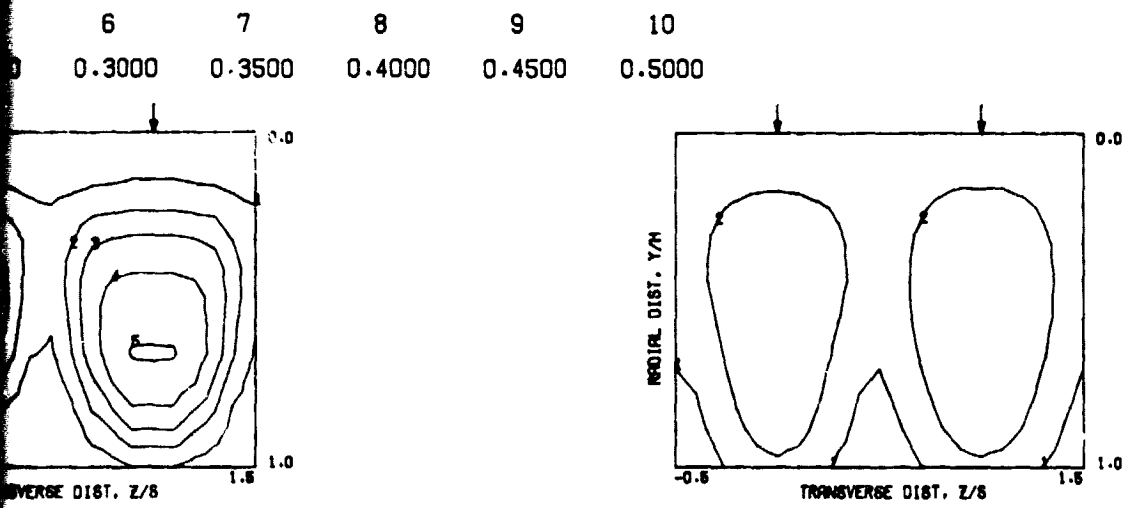

7, TMAIN=CONST, J=27.18, S/D=4.0, H/D=8.0

2 FOLDOUT FRAME

Figure 65

ORIGINAL PAGE IS
OF POOR QUALITY

CONTOUR	1	2	3	4	5	6	7	8	9
VALUE	0.0500	0.1065	0.1500	0.2000	0.2500	0.3000	0.3500	0.4000	0.45

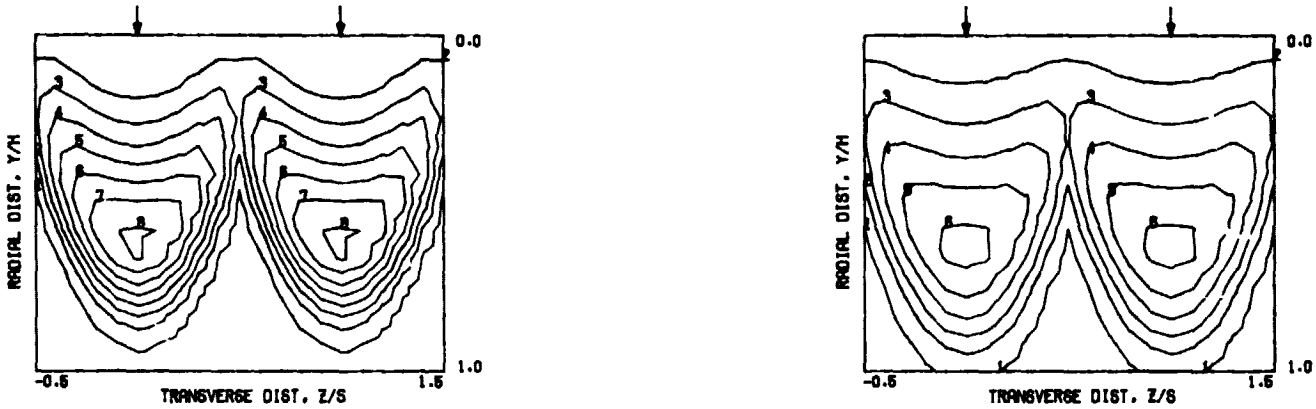

PREDICTED THETA CONTOURS FOR TEST NO.27, TMAIN=CONST, J=27.18, S/D=4.6

S/DJ = 4.96 HO/DJ = 9.92 VRATIO = 3.64 TRATIO = 0.496 DENRATIO= 2.053 TMAIN

X/H = 0.25 X/DJ =2.48 X/H = 0.50 X/DJ =4.96

COMPARRISON BETWEEN DATA AND CORRELATIONS FOR TEST NO. 27, TEST SECTION V,UNIFOR

FOLDOUT FRAME

ORIGINAL PAGE IS
OF POOR QUALITY

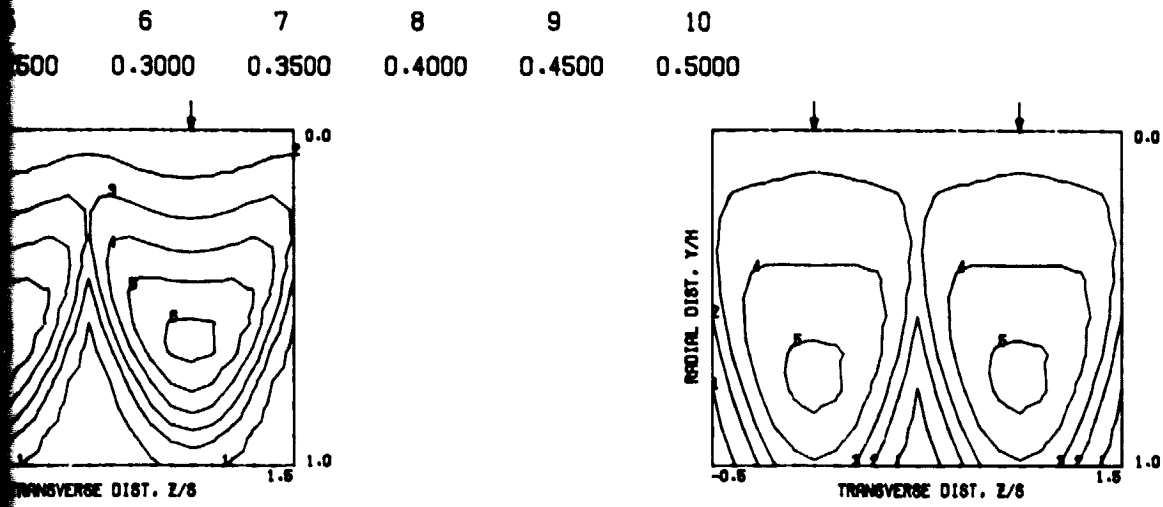

0.27, TMAIN=CONST, J=27.18, S/D=4.0, H/D=8.0

TRATIO = 0.496 DENRATIO=2.053 TMAIN = 646.4 K TJET = 320.3 K THEB = 0.107

.60 X/DJ =4.96 X/H = 1.00 X/DJ =9.92

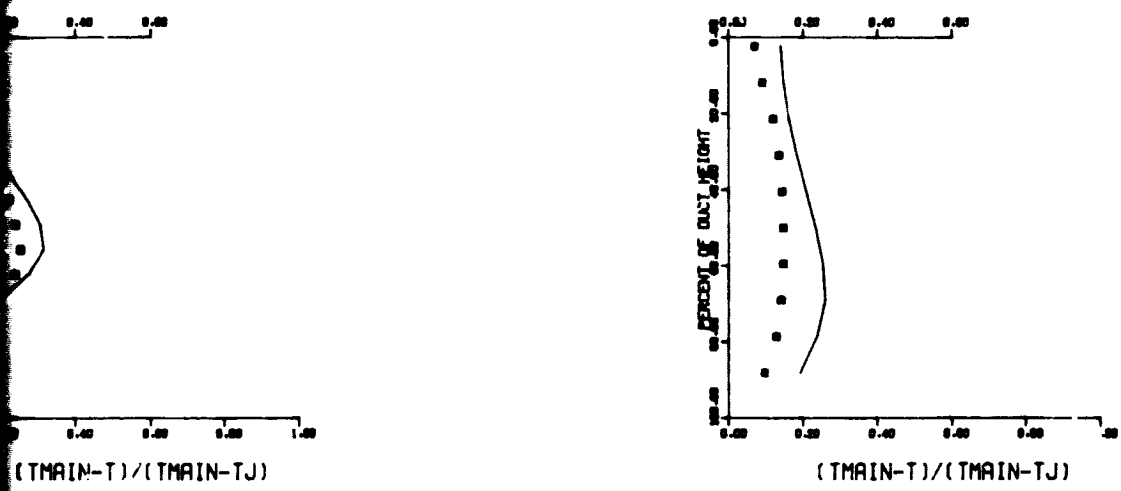

ORIGINAL PAGE IS
OF POOR QUALITY

EST NO. 27, TEST SECTION V,UNIFORM TMAIN, J = 27.18 , S/D =4.00 , H/D =8.00

Figure 66

FOLDOUT FRAME

ORIGINAL PAGE IS
OF POOR QUALITY

S = 0.0508 METERS S/DJ = 5.061 HO/DJ = 10.121 VMAIN = 16.0 M/SEC VJET = 112.5 M/SEC TMAIN = 645.1 K T

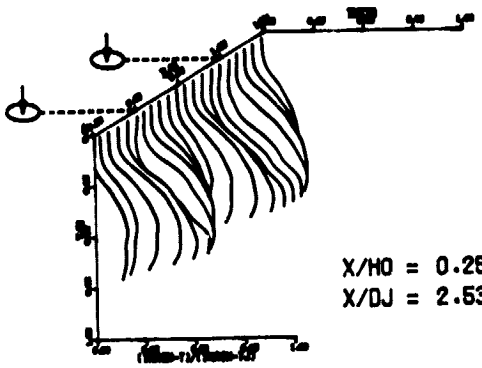

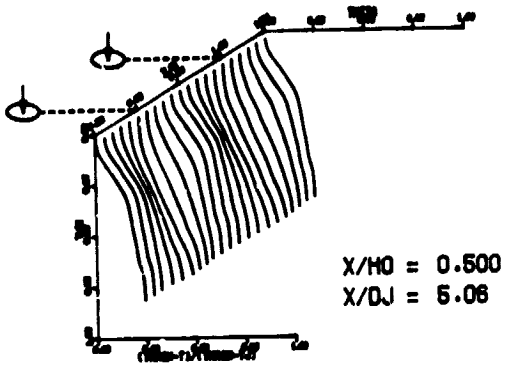

MEASURED THETA PROFILES FOR TEST NO. 28, TEST SECTION V, TMAIN=CONST. , J =

CONTOUR	1	2	3	4	5	6	7	8
VALUE	0.0500	0.1000	0.1500	0.1888	0.2500	0.3000	0.3500	0.4000

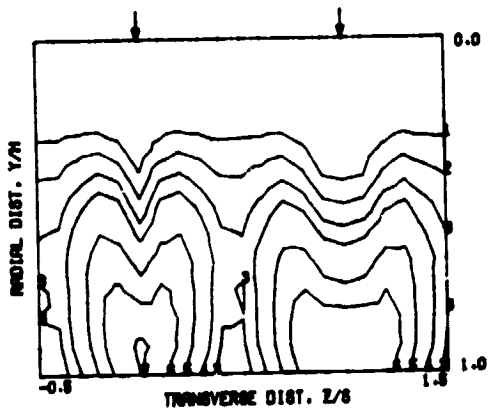

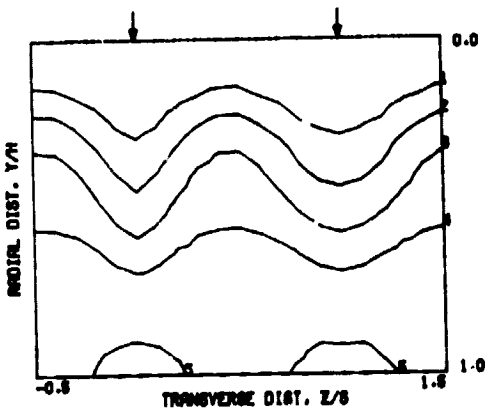

MEASURED THETA CONTOURS FOR TEST NO.28, TMAIN=CONST, J=106.7, S/D=

FOLDOUT FRAME

ORIGINAL PAGE IS
OF POOR QUALITY

.5 M/SEC TMAIN = 645.1 K TJET = 319.1 K THEB = 0.1888 BLORAT= 15.176 DENRATIO= 2.159 TRATIO=0.496

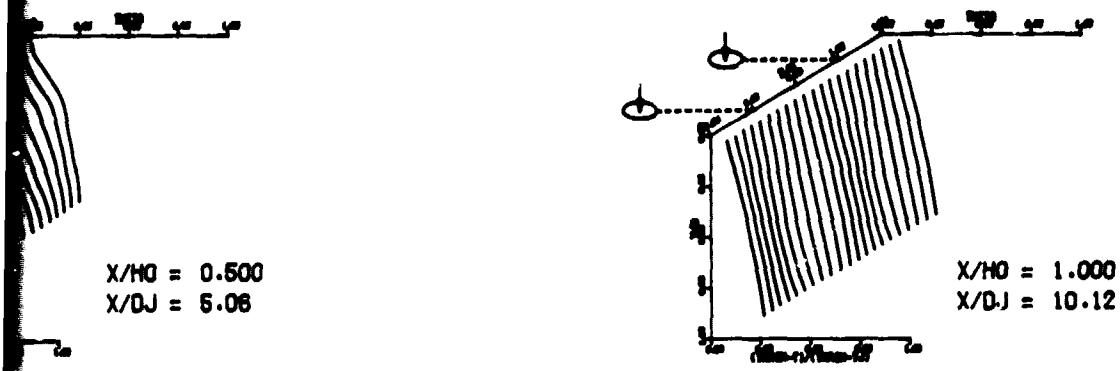

ION V, TMAIN=CONST., J = 106.72 , S/D = 4.00 , H/D = 8.00

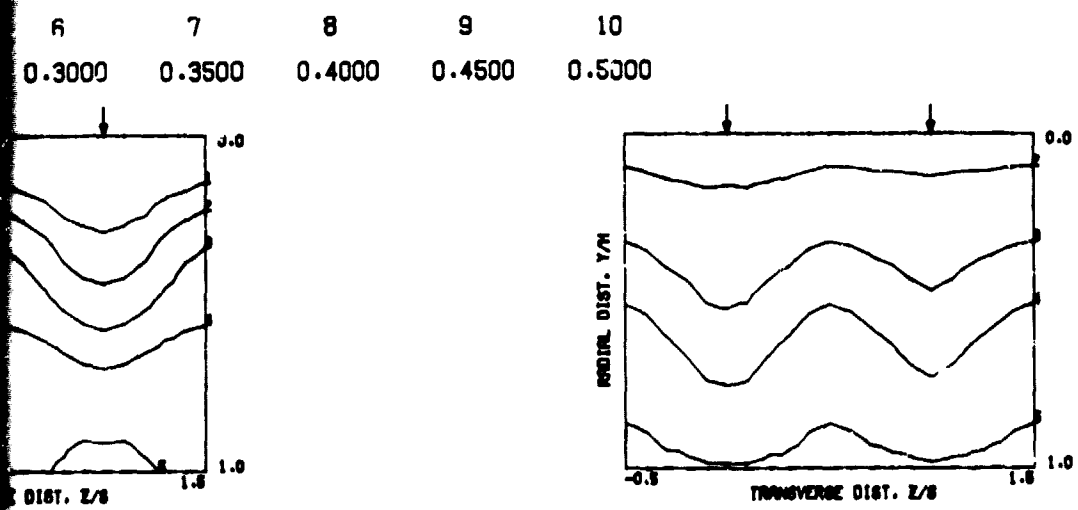

TMAIN=CONST, J=106.7, S/D=4.0, H/D=8.0

Figure 67

FOLDOUT FRAME

CONTOUR	1	2	3	4	5	6	7	8	9
VALUE	0.0500	0.1000	0.1500	0.1888	0.2500	0.3000	0.3500	0.4000	0.4

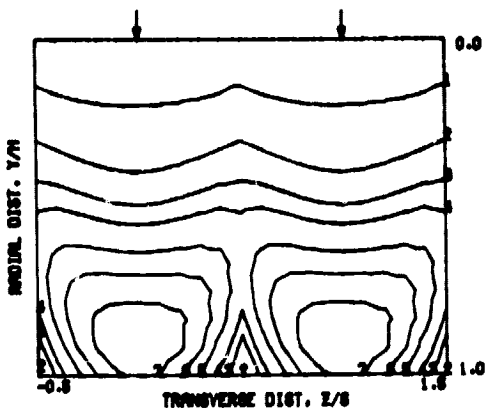

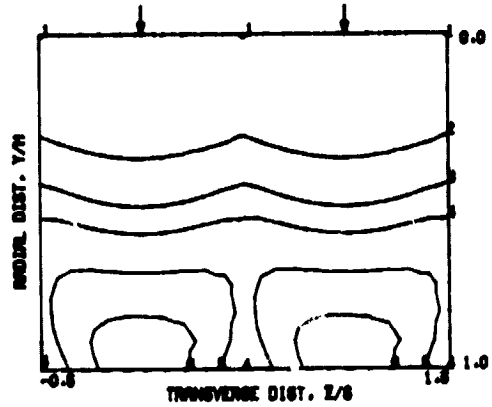

PREDICTED THETA CONTOURS FOR TEST NO.28, TMAIN=CONST, J=106.7, S/D=4.

S/DJ = 5.06 HO/DJ = 10.12 VRATIO = 7.03 TRATIO = 0.495 DENRATIO=2.159 TMAIN

X/H = 0.26 X/DJ =2.53

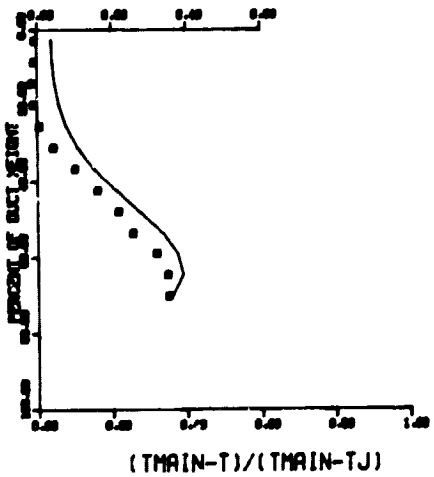

X/H = 0.50 X/DJ =5.06

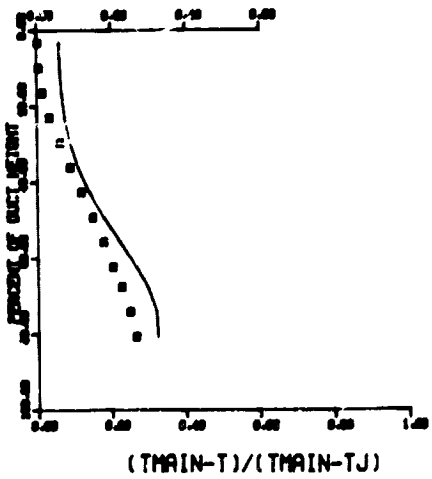

COMPARISON BETWEEN DATA AND CORRELATIONS FOR TEST NO. 28, TEST SECTION V,UNIFORM

ORIGINAL PAGE IS
OF POOR QUALITY

FOLDOUT FRAME

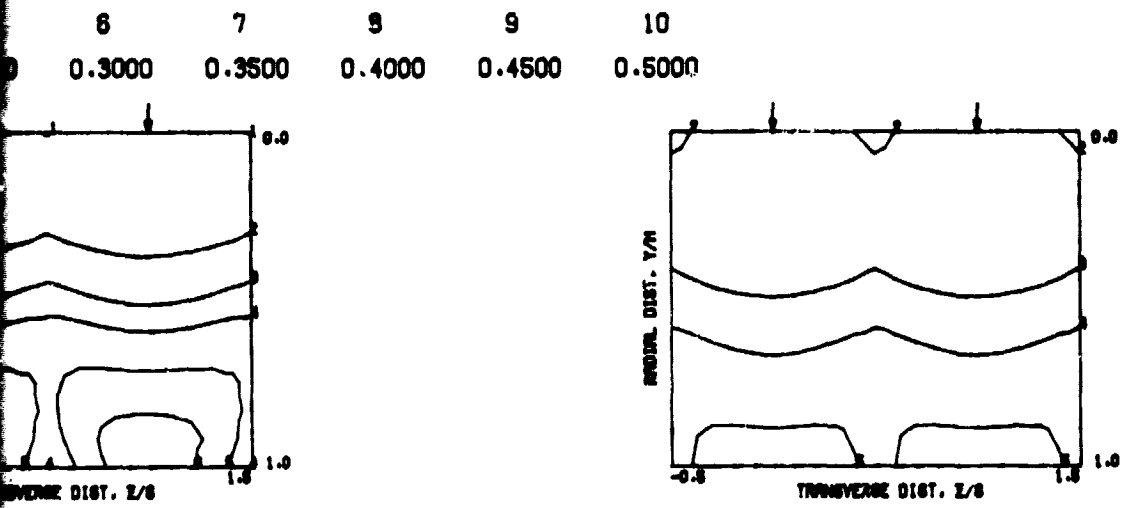

28. TMAIN=CONST. J=106.7. S/D=4.0. H/D=8.0

RATIO = 0.495 DENRATIO=2.159 TMAIN = 645.1 K TJET = 319.1 K THEB = 0.189

X/DJ =5.06 X/H = 1.00 X/DJ =10.12

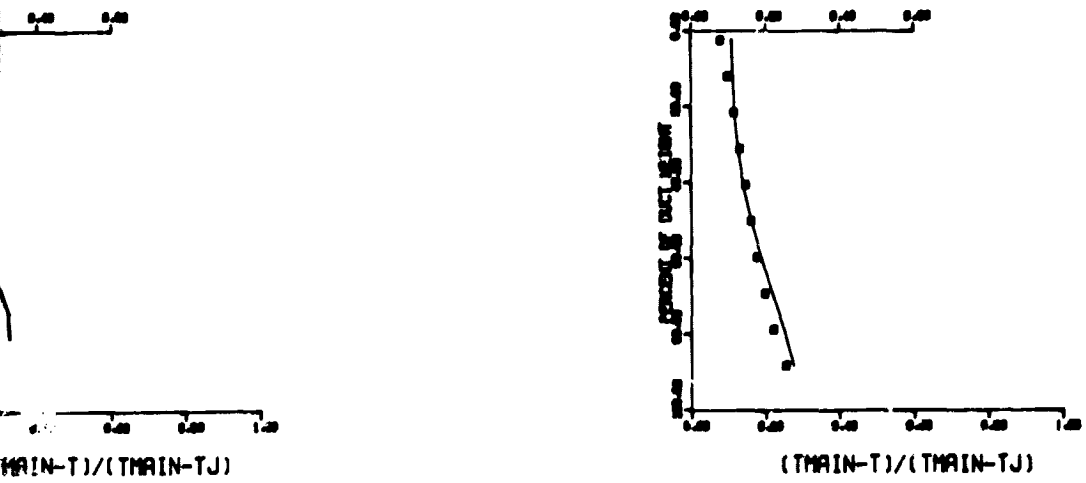

FOLDOUT FRAME

T NO. 28. TEST SECTION V.UNIFORM TMAIN. J = 106.72 . S/D =4.00 . H/D =8.00

Figure 68

ORIGINAL PAGE IS
OF POOR QUALITY

S = 0.0508 METERS S/DJ = 2.462 HO/DJ = 4.924 VMAIN = 15.7 M/SEC VJET = 29.1 M/SEC TMAIN = 645.0 K TJET

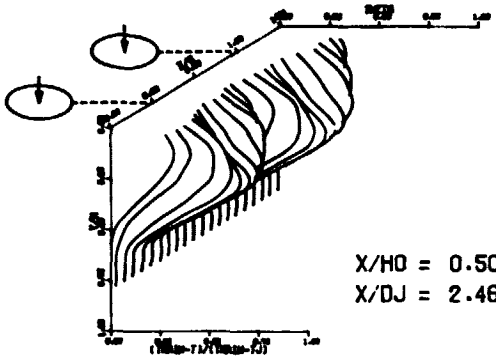

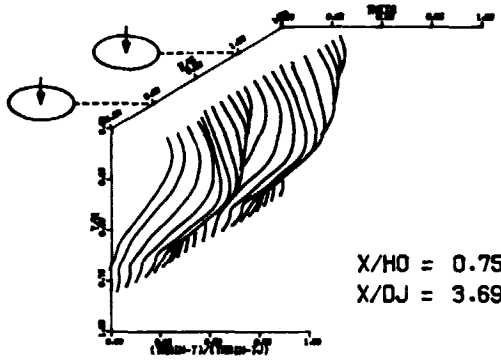

MEASURED THETA PROFILES FOR TEST NO. 29, TEST SECTION V, TMAIN=CONST. , J = 7

CONTOUR	1	2	3	4	5	6	7	8	9
VALUE	0.0500	0.1000	0.1500	0.1984	0.2500	0.3000	0.3500	0.4000	0.4

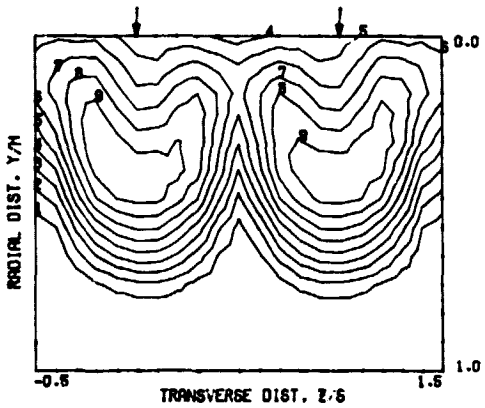

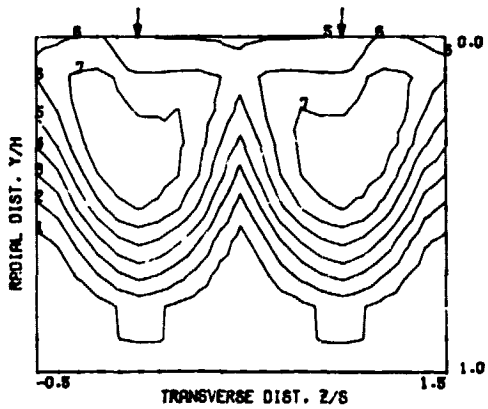

MEASURED THETA CONTOURS FOR TEST NO.29, TMAIN=CONST, J=7.07, S/D=2.0,

ORIGINAL PAGE IS
OF POOR QUALITY

FOLDOUT FRAME

/SEC TMAIN = 645.0 K TJET = 313.5 K THEB = 0.1983 BLORAT= 3.818 DENRATIO= 2.064 TRATIO=0.486

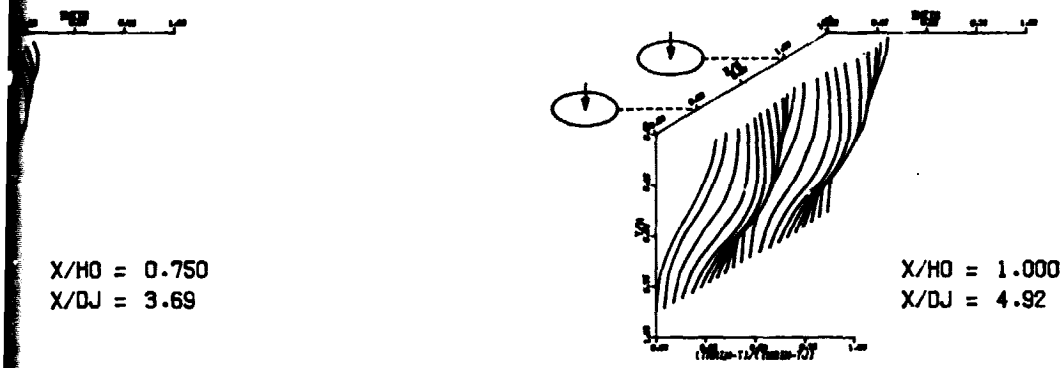

X/HO = 0.750
X/DJ = 3.69

X/HO = 1.000
X/DJ = 4.92

V, TMAIN=CONST., J = 7.07 , S/D = 2.00 , H/D = 4.00

	7	8	9	10
000	0.3500	0.4000	0.4500	0.5000

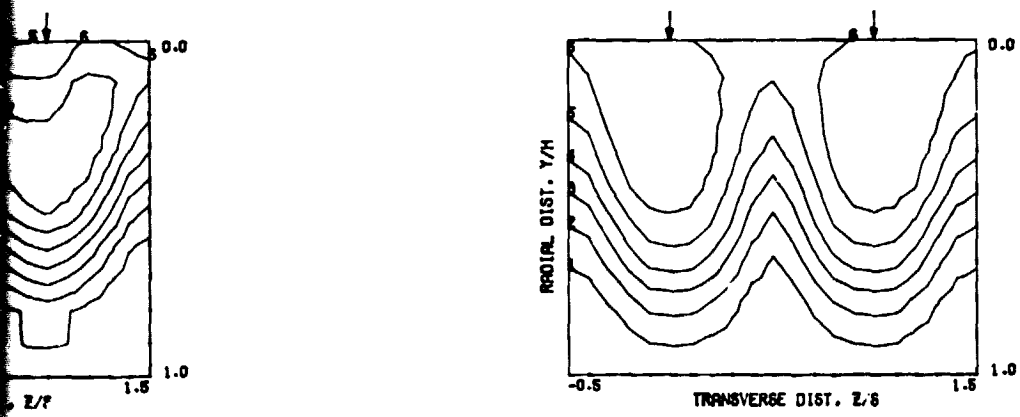

IN=CONST, J=7.07, S/D=2.0, H/D=4.0

FOLDOUT FRAME

Figure 69

ORIGINAL PAGE IS
OF POOR QUALITY

CONTOUR	1	2	3	4	5	6	7	8
VALUE	0.0500	0.1000	0.1500	0.1984	0.2500	0.3000	0.3500	0.4000

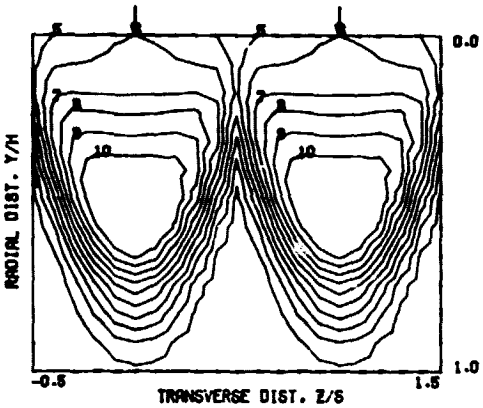

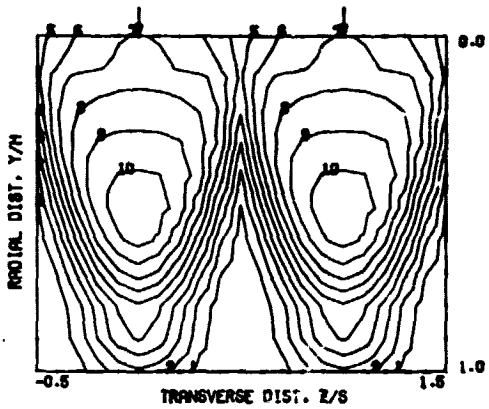

PREDICTED THETA CONTOURS FOR TEST NO.29, TMAIN=CONST, J=7.07, S/D=2.

S/DJ = 2.46 HO/DJ = 4.92 VRATIO = 1.85 TRATIO = 0.486 DENRATIO=2.064 TMAI

X/H = 0.50 X/DJ =2.46

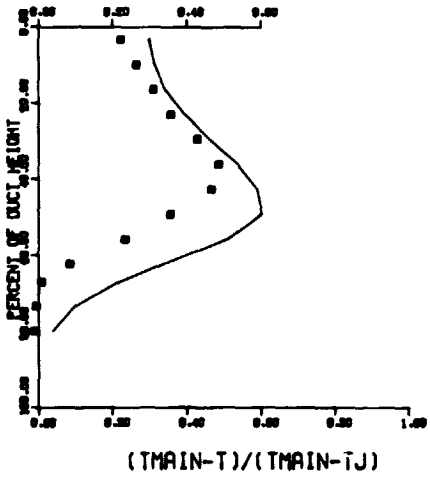

X/H = 0.75 X/DJ =3.69

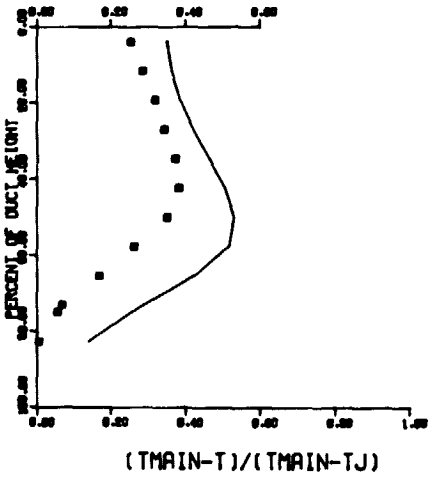

COMPARISON BETWEEN DATA AND CORRELATIONS FOR TEST NO. 29, TEST SECTION V,UNIFO

ORIGINAL PAGE IS
OF POOR QUALITY

FOLDOUT FRAME

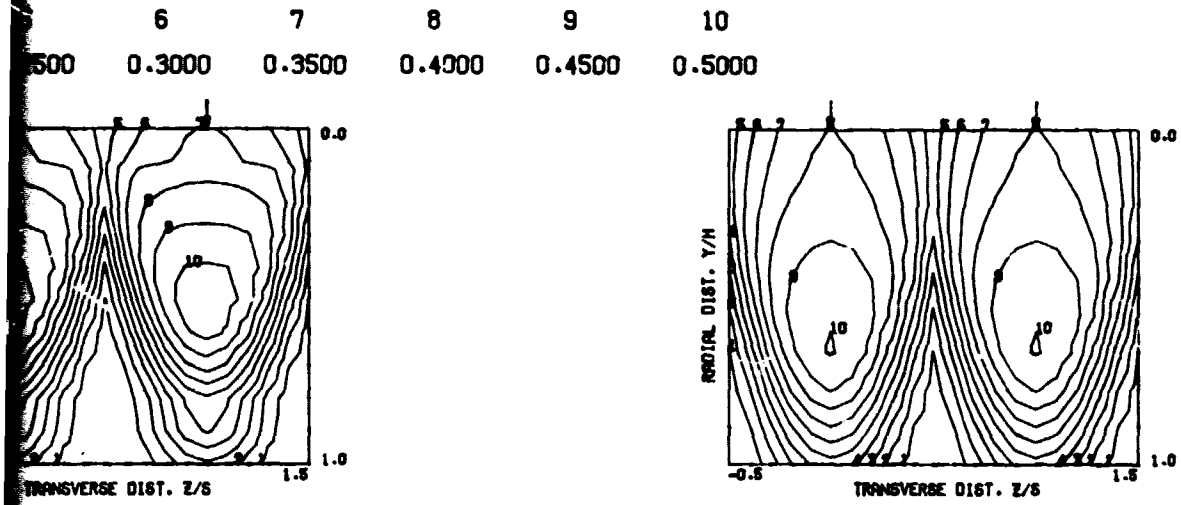

0.29, TMAIN=CONST, J=7.07, S/D=2.0, H/D=4.0

TRATIO = 0.486 DENRATIO=2.064 TMAIN = 645.0 K TJET = 313.5 K THEB = 0.198

0.75 X/DJ =3.69 X/H = 1.00 X/DJ =4.92

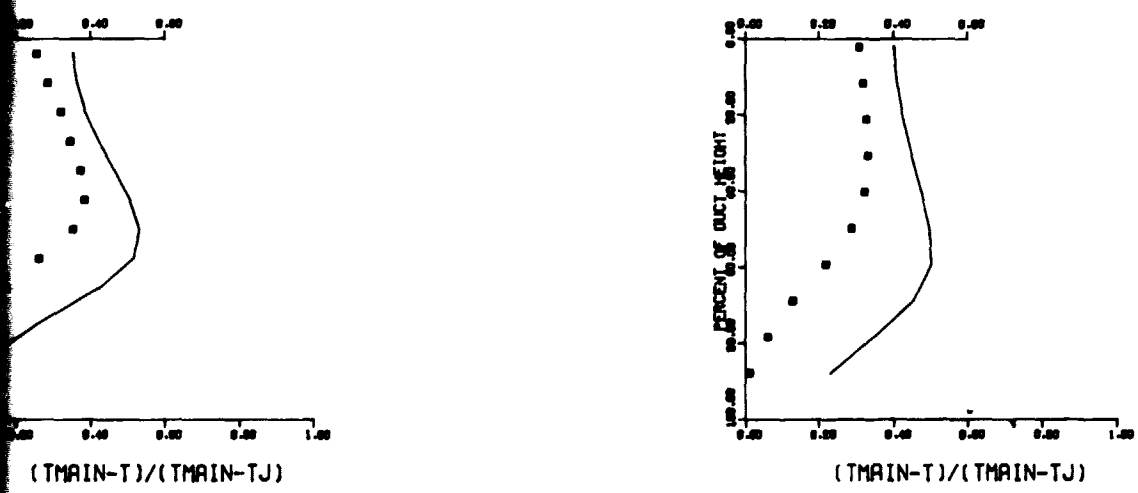

FOLDOUT FRAME

TEST NO. 29, TEST SECTION V,UNIFORM TMAIN, J = 7.07 , S/D =2.00 , H/D =4.00

Figure 70

ORIGINAL PAGE IS
OF POOR QUALITY

S = 0.0508 METERS S/DJ = 2.540 HO/DJ = 5.080 VMAIN = 15.6 M/SEC VJET = 56.4 M/SEC TMAIN = 645.6 K TJ

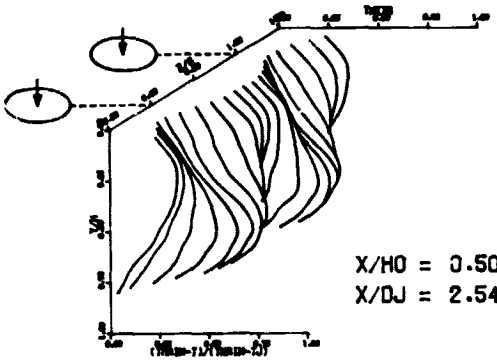

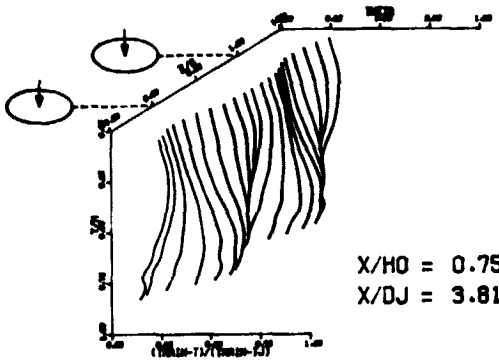

MEASURED THETA PROFILES FOR TEST NO. 30, TEST SECTION V, TMAIN=CONST., J =

CONTOUR	1	2	3	4	5	6	7	8
VALUE	0.0500	0.1000	0.1500	0.2000	0.2500	0.3149	0.3500	0.4000

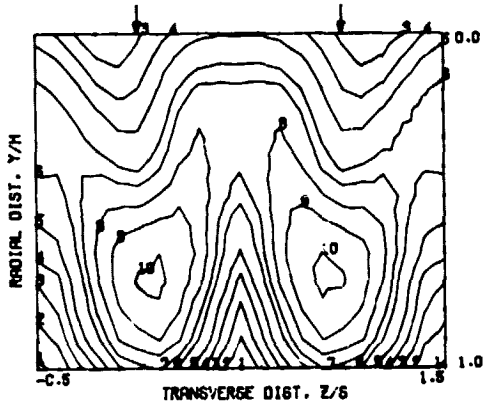

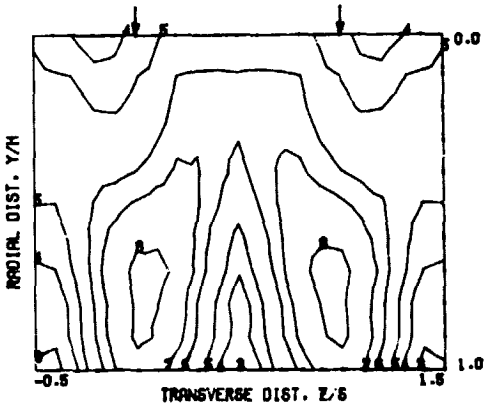

MEASURED THETA CONTOURS FOR TEST NO.30, TMAIN=CONST. J=27.31, S/D=

ORIGINAL PAGE IS
OF POOR QUALITY

FOLDOUT FRAME

3.4 M/SEC TMAIN = 645.6 K TJET = 313.7 K THEB = 0.3149 BLORAT= 7.549 DENRATIO= 2.087 TRATIO= 0.486

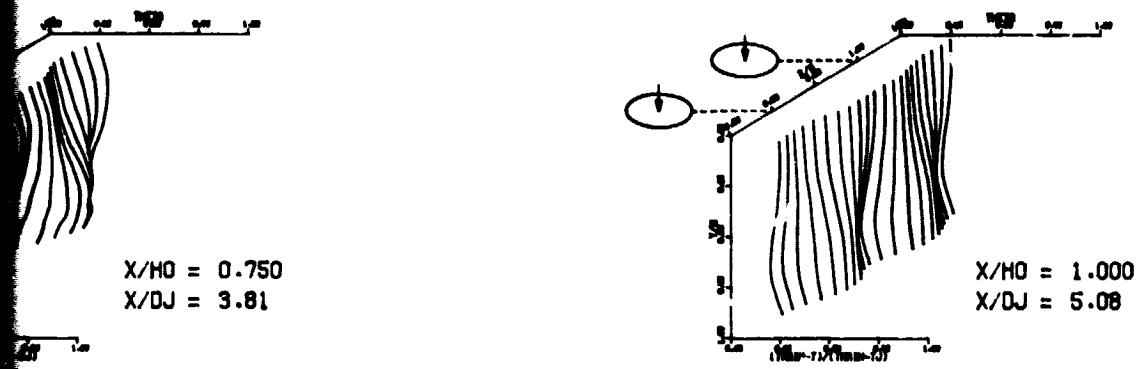

TION V. TMAIN=CONST. , J = 27.31 , S/D = 2.00 , H/D = 4.00

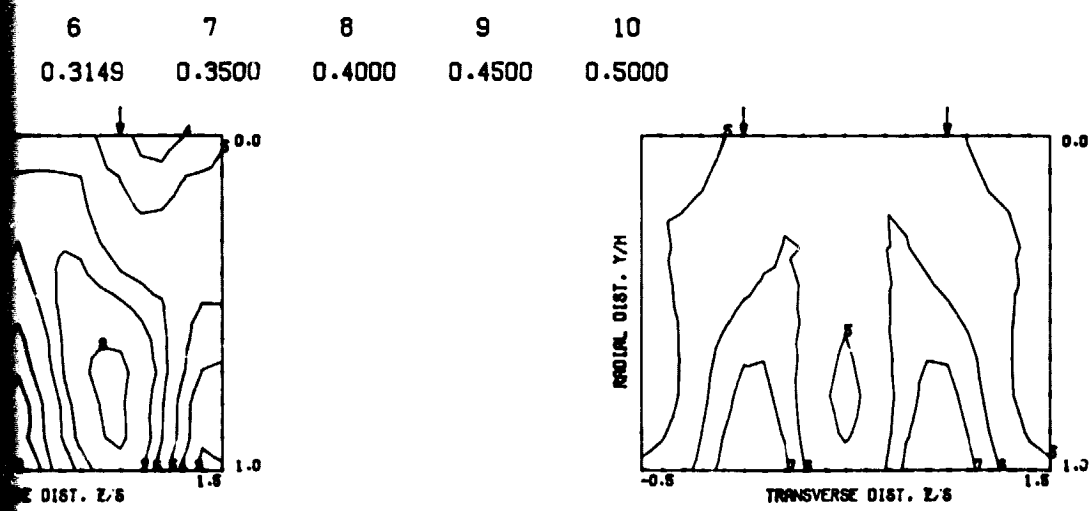

TMAIN=CONST, J=27.31, S/D=2.0, H/D=4.0

ORIGINAL PAGE IS
OF POOR QUALITY

Figure 71

FOLDOUT FRAME

CONTOUR	1	2	3	4	5	6	7	8	9
VALUE	0.0500	0.1000	0.1500	0.2000	0.2500	0.3149	0.3500	0.4000	0.4

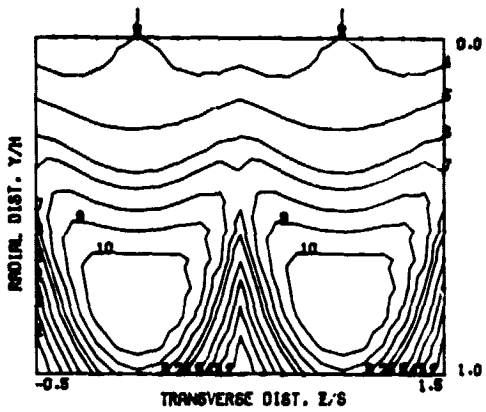

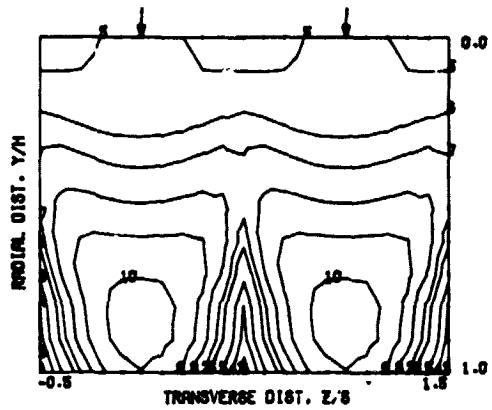

PREDICTED THETA CONTOURS FOR TEST NO.30. TMAIN=CONST. J=27.31. S/D=2.

S/DJ = 2.54 HG/DJ = 5.08 VRATIO = 3.62 TRATIO = 0.486 DENRATIO=2.087 TMAIN

X/H = 0.50 X/DJ =2.54

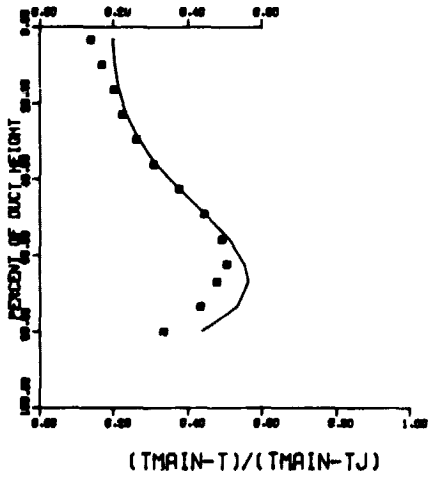

X/H = 0.75 X/DJ =3.81

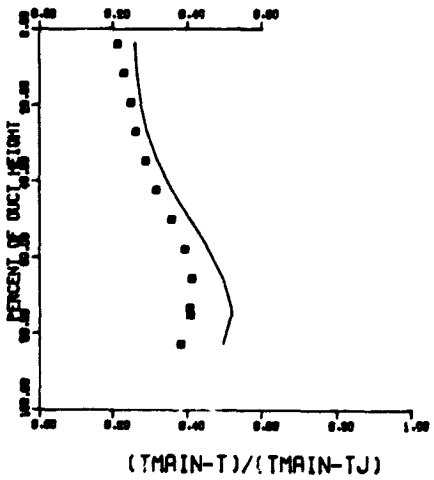

COMPARISON BETWEEN DATA AND CORRELATIONS FOR TEST NO. 30. TEST SECTION V.UNIFORM

FOLDOUT FRAME

ORIGINAL PAGE IS
OF POOR QUALITY

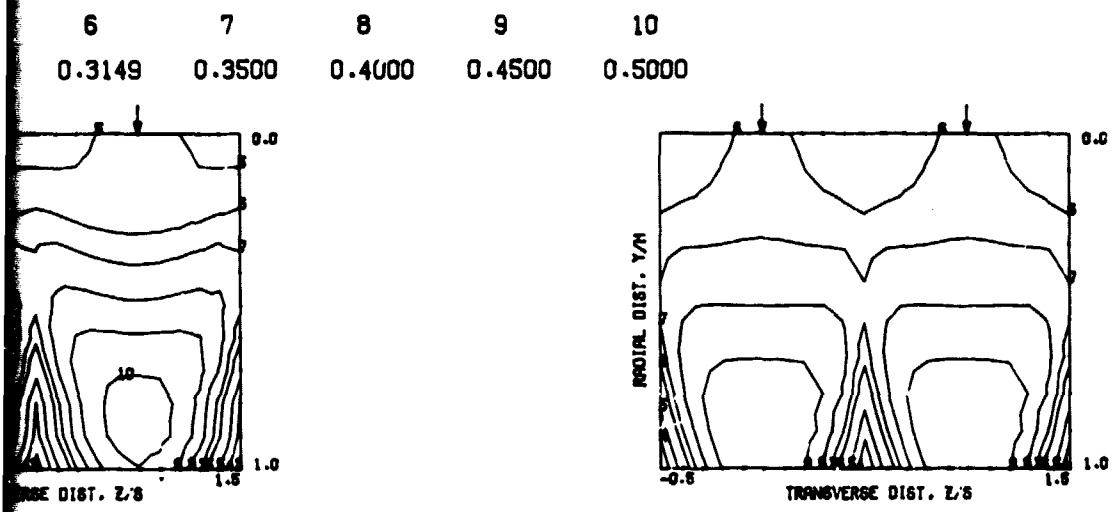

, TMAIN=CONST. J=27.31. S/D=2.0. H/D=4.0

ATIO = 0.486 DENRATIO=2.087 TMAIN = 645.6 K TJET = 313.7 K THEB = 0.315

X/DJ =3.81 X/H = 1.00 X/DJ =5.08

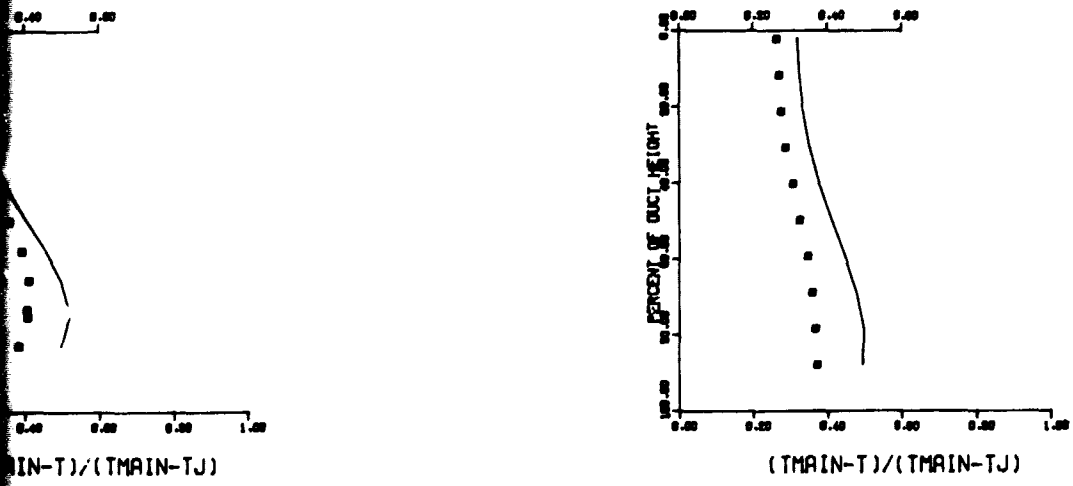

ORIGINAL PAGE IS
OF POOR QUALITY

NO. 30. TEST SECTION V.UNIFORM TMAIN. J = 27.31 . S/D =2.00 . H/D =4.00

Figure 72

FOLDOUT FRAME

S = 0.0508 METERS S/DJ = 4.941 HO/DJ = 9.883 VMAIN = 16.4 M/SEC VJET = 58.6 M/SEC TMAIN = 649.2 K TJE

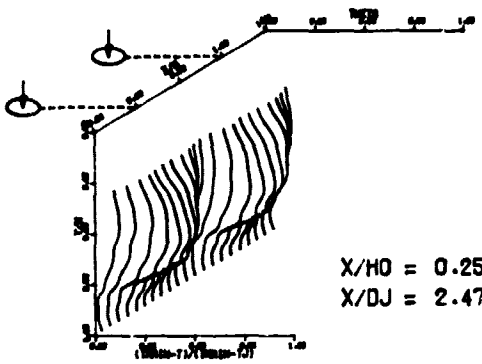

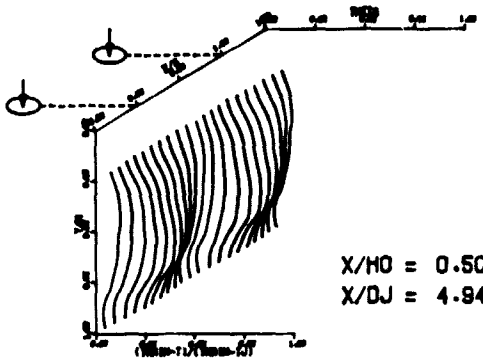

MEASURED THETA PROFILES FOR TEST NO. 31. TEST SECTION VI. TMAIN=CONST . J =

CONTOUR	1	2	3	4	5	6	7	8
VALUE	0.0500	0.1066	0.1250	0.1500	0.2000	0.2500	0.3000	0.3500

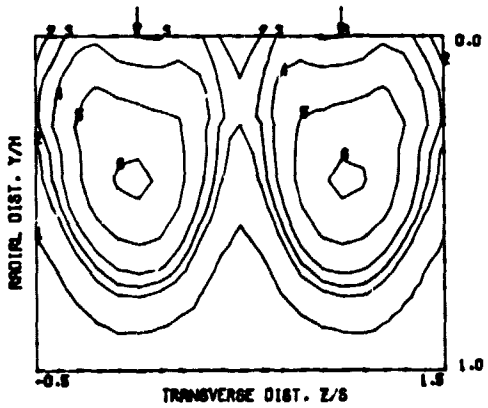

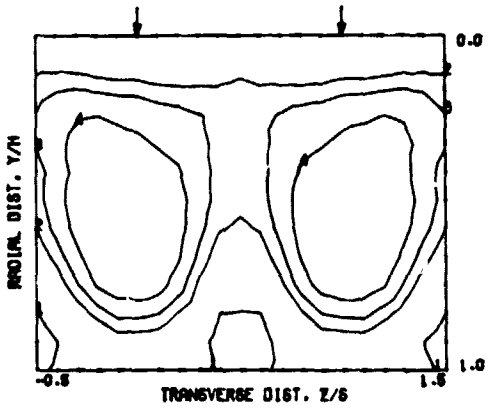

MEASURED THETA CONTOURS FOR TEST NO.31. TMAIN=CONST. J=26.59. S/D=4

ORIGINAL PAGE IS
OF POOR QUALITY

FOLDOUT FRAME

M/SEC TMAIN = 649.2 K TJET = 319.5 K THEB = 0.1066 BLORAT= 7.421 DENRATIO= 2.072 TRATIO= 0.492

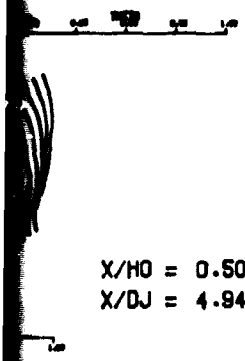

X/HO = 0.500
X/DJ = 4.94

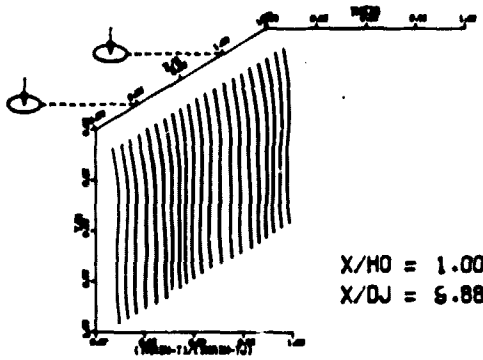

X/HO = 1.000
X/DJ = 5.88

ION VI. TMAIN=CONST . J = 26.59 . S/D = 4.00 . H/D = 8.00

6 7 8 9 10
0.2500 0.3000 0.3500 0.4000 0.4500

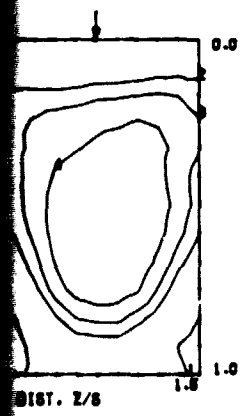

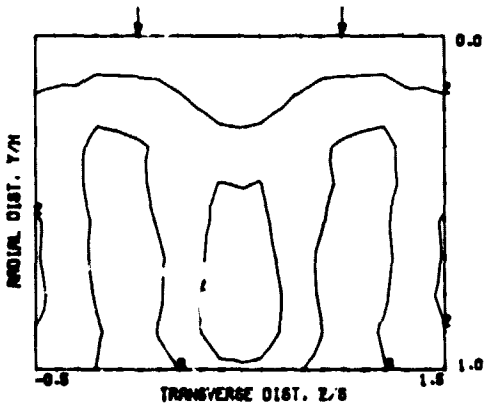

MAIN=CONST. J=26.59. S/D=4.0. H/D=8.0

Figure 73

ORIGINAL PAGE IS
OF POOR QUALITY

FOLDOUT FRAME

CONTOUR	1	2	3	4	5	6	7	8
VALUE	0.0500	0.1066	0.1250	0.1500	0.2000	0.2500	0.3149	0.3500

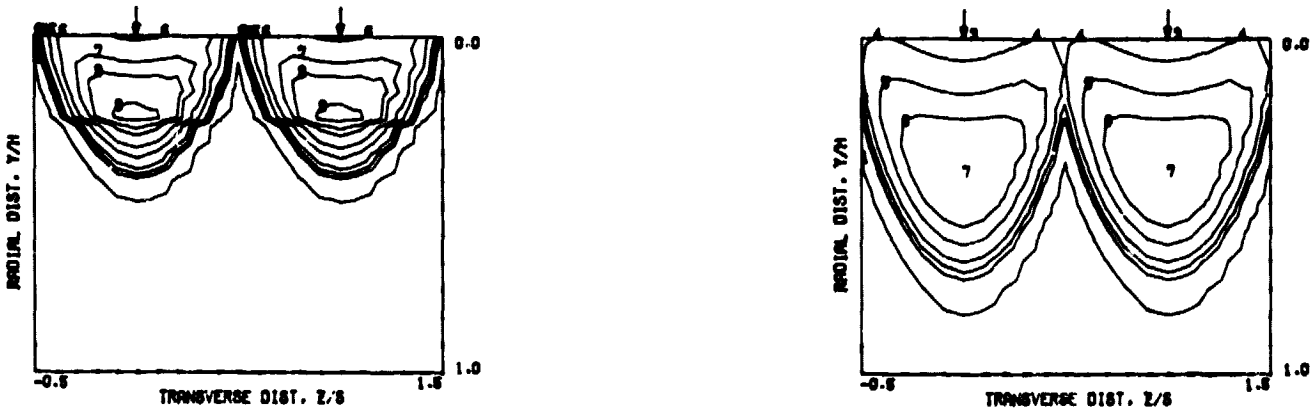

PREDICTED THETA CONTOURS FOR TEST NO.31. TMAIN=CONST. J=26.59. S/D=

S/DJ = 4.94 HO/DJ = 9.88 VRATIO = 3.58 TRATIO = 0.492 DENRATIO=2.072 TM

X/H = 0.25 X/DJ =2.47

X/H = 0.50 X/DJ =4.94

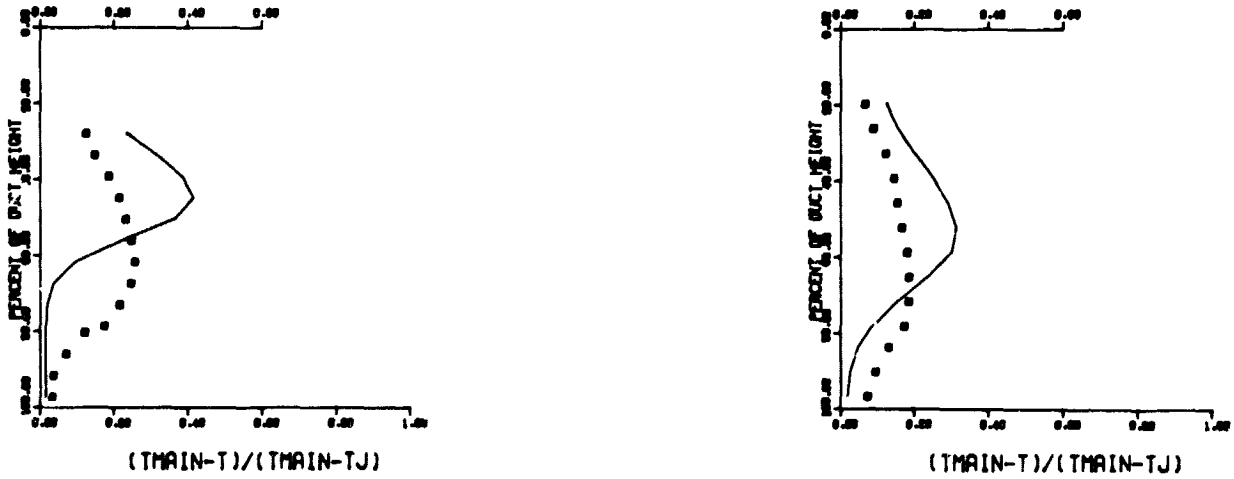

COMPARISON BETWEEN DATA AND CORRELATIONS FOR TEST NO. 31. TEST SECTION VI.UNI

ORIGINAL PAGE IS
OF POOR QUALITY

FOLDOUT FRAME

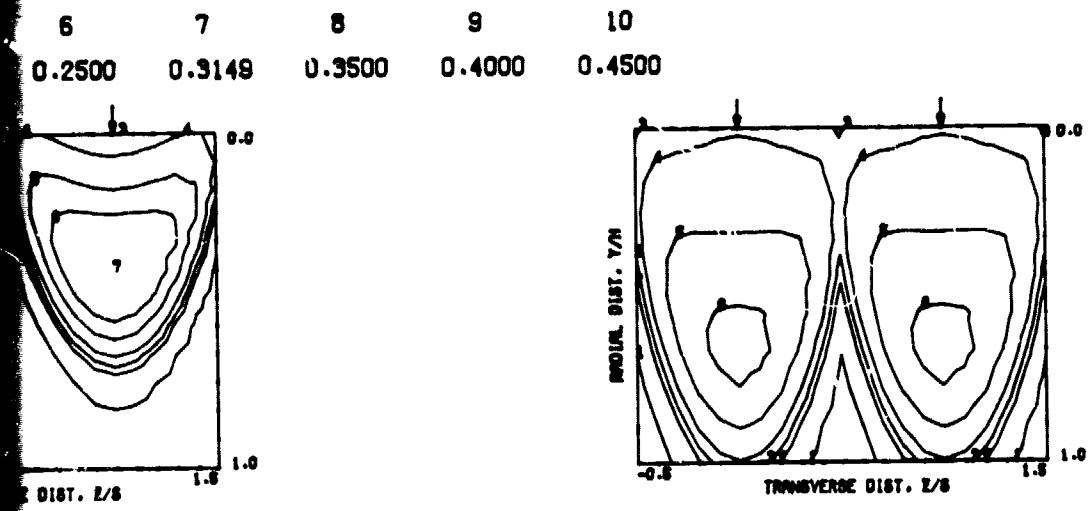

TMAIN=CONST. J=26.59. S/D=4.0. H/D=8.0

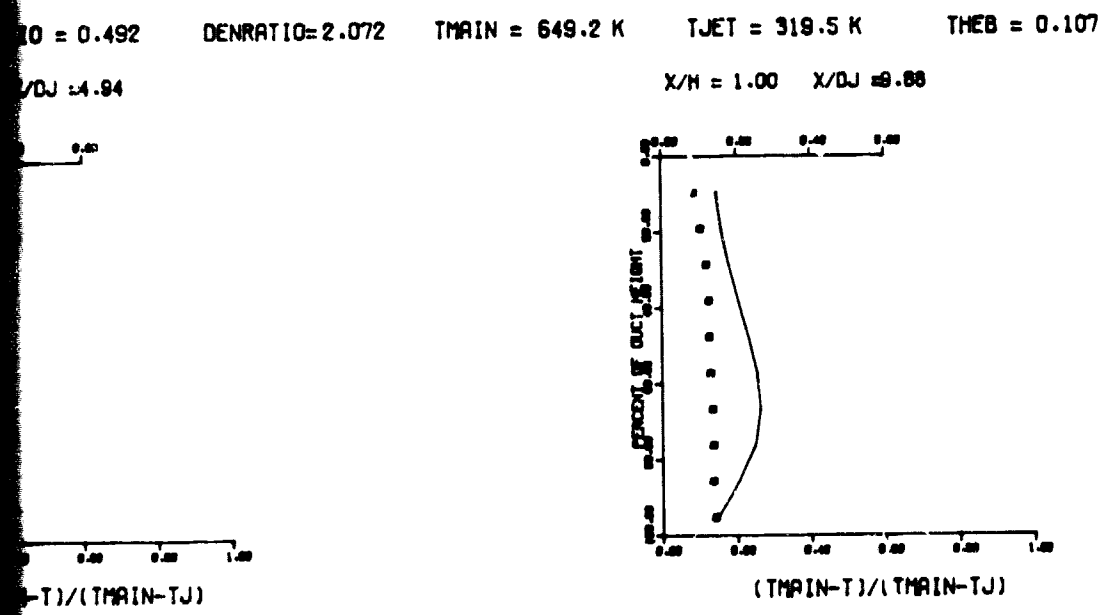

FOLDOUT FRAME

NO. 31. TEST SECTION VI.UNIFORM TMAIN. J = 26.59 . S/D =4.00 . H/D =8.00

Figure 74

ORIGINAL PAGE IS
OF POOR QUALITY

ORIGINAL PAGE IS
OF POOR QUALITY

3 = 0.0508 METERS S/DJ = 5.081 HO/DJ = 10.163 VMAIN = 16.5 M/SEC VJET = 116.0 M/SEC TMAIN = 647.0 K

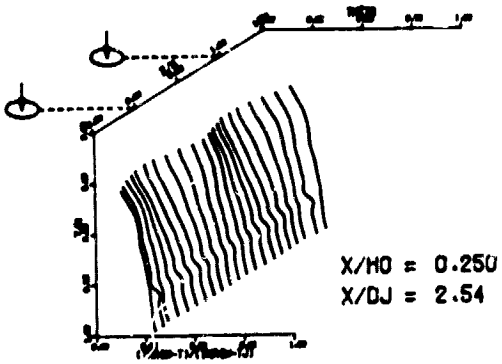

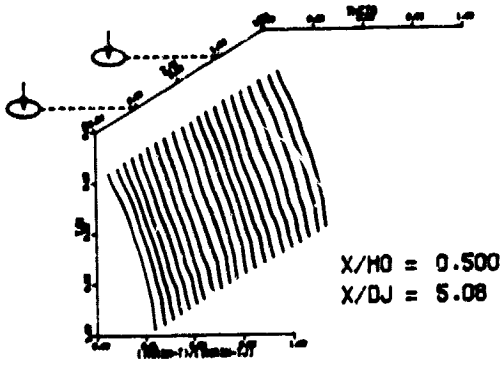

MEASURED THETA PROFILES FOR TEST NO. 32. TEST SECTION VI. TMAIN=CONST .

CONTOUR	1	2	3	4	5	6	7	8
VALUE	0.0500	0.1000	0.1500	0.1888	0.2500	0.3000	0.3500	0.4000

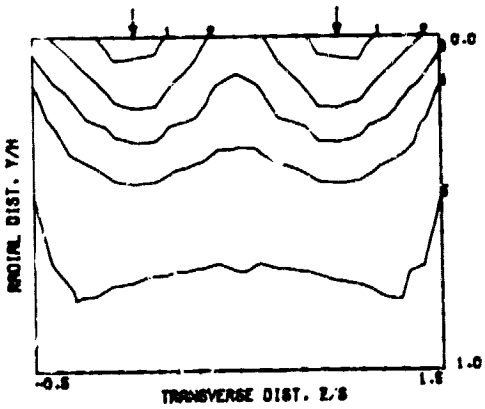

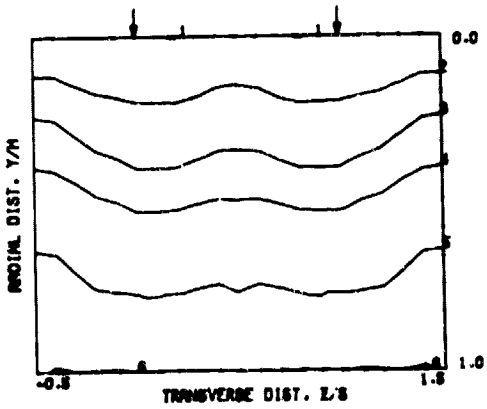

MEASURED THETA CONTOURS FOR TEST NO.32. TMAIN=CONST. U=107.8. S

FOLDOUT FRAME

ORIGINAL PAGE IS
OF POOR QUALITY

M/SEC TMAIN = 647.0 K TJET = 321.2 K THEB = 0.1887 BLORAT= 15.297 DENRATIO= 2.176 TRATIO= 0.496

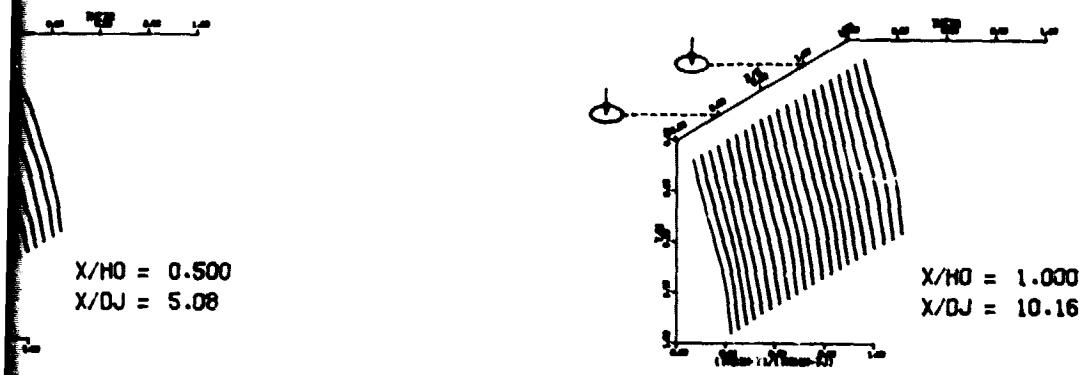

N VI. TMAIN=CONST . J = 107.76 . S/D = 4.00 . H/D = 8.00

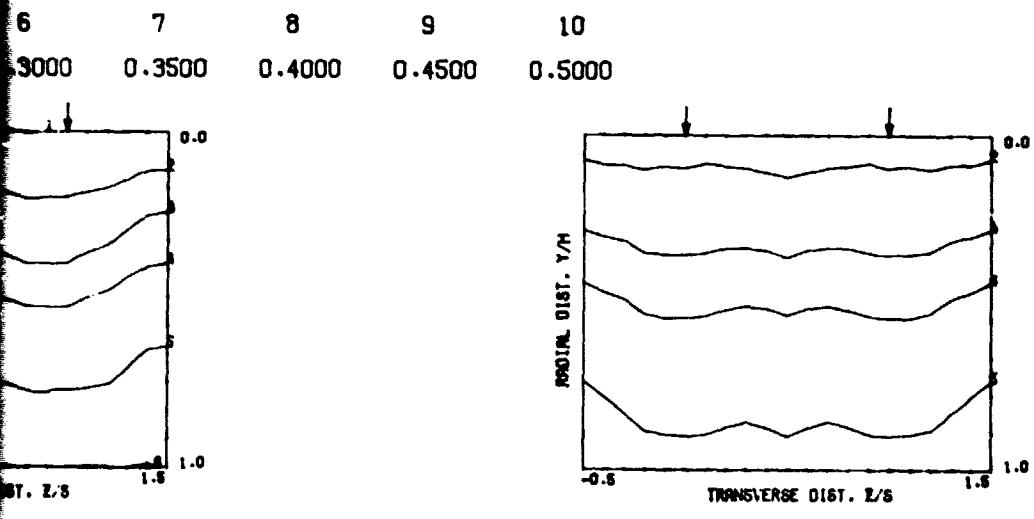

AIN=CONST. J=107.8. S/D=4.0. H/D=8.0

Figure 75

EOLDOUT LEAF

CONTOUR	1	2	3	4	5	6	7	8	
VALUE	0.0500	0.1000	0.1500	0.1888	0.2500	0.3000	0.3500	0.4000	0

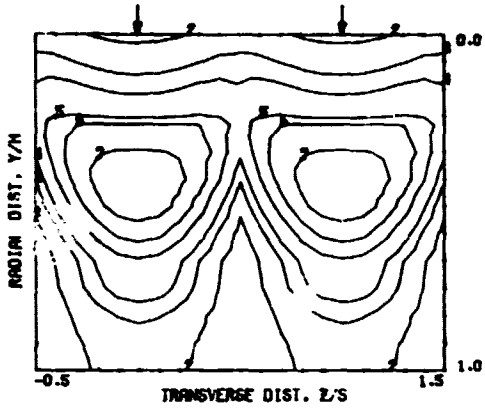

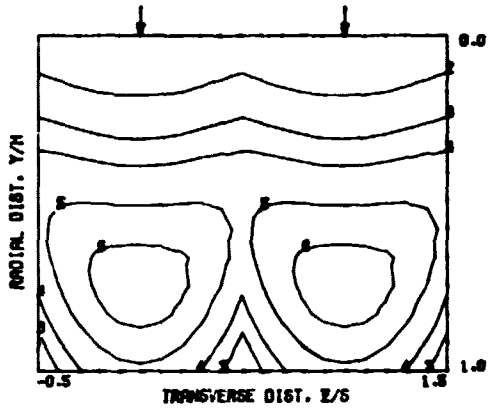

PREDICTED THETA CONTOURS FOR TEST NO.32. TMAIN=CONST. J=107.8. S/D=

S/DJ = 5.08 HO/DJ = 10.16 VRATIO = 7.04 TRATIO = 0.496 DENRATIO=2.176 TM

X/H = 0.25 X/DJ =2.54

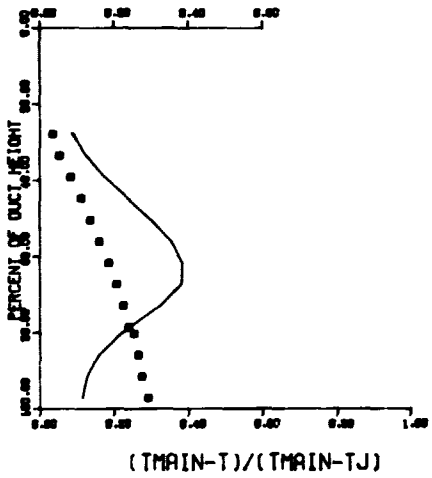

X/H = 0.50 X/DJ =5.08

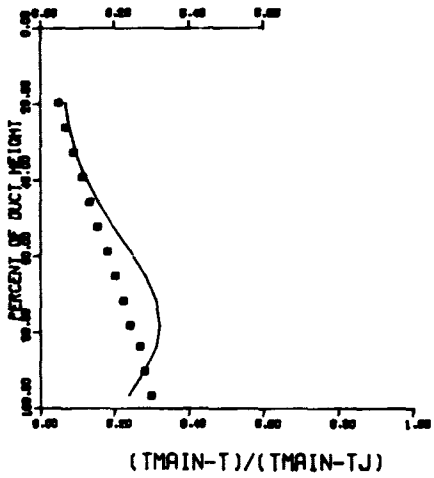

COMPARISON BETWEEN DATA AND CORRELATIONS FOR TEST NO. 32. TEST SECTION VI.UNI

FOLDOUT FRAME

ORIGINAL PAGE IS
OF POOR QUALITY

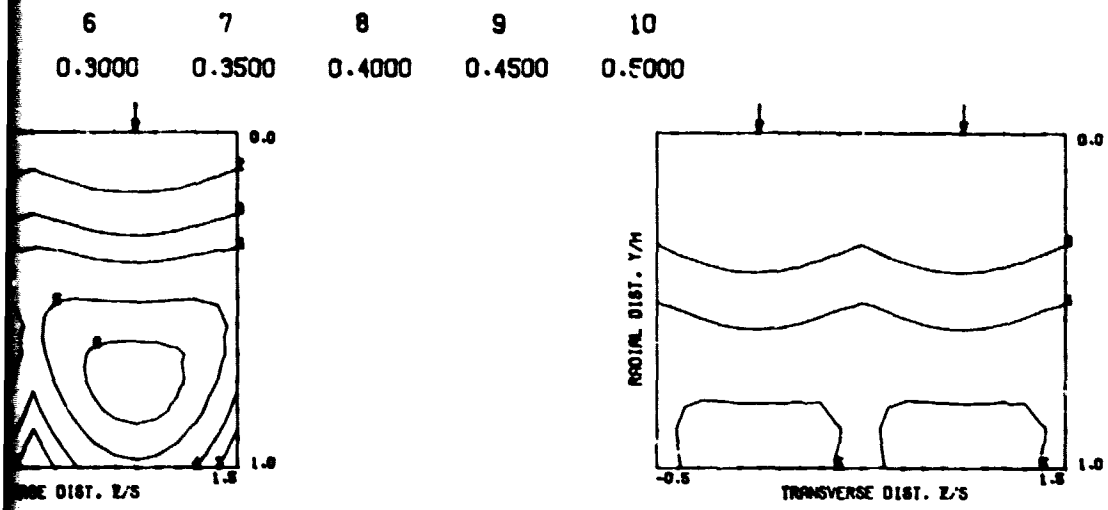

. TMAIN=CONST. J=107.8. S/D=4.0. H/D=8.0

TIO = 0.496 DENRATIO=2.176 TMAIN = 647.0 K TJET = 321.2 K THEB = 0.189

X/DJ =5.08 X/M = 1.00 X/DJ =10.16

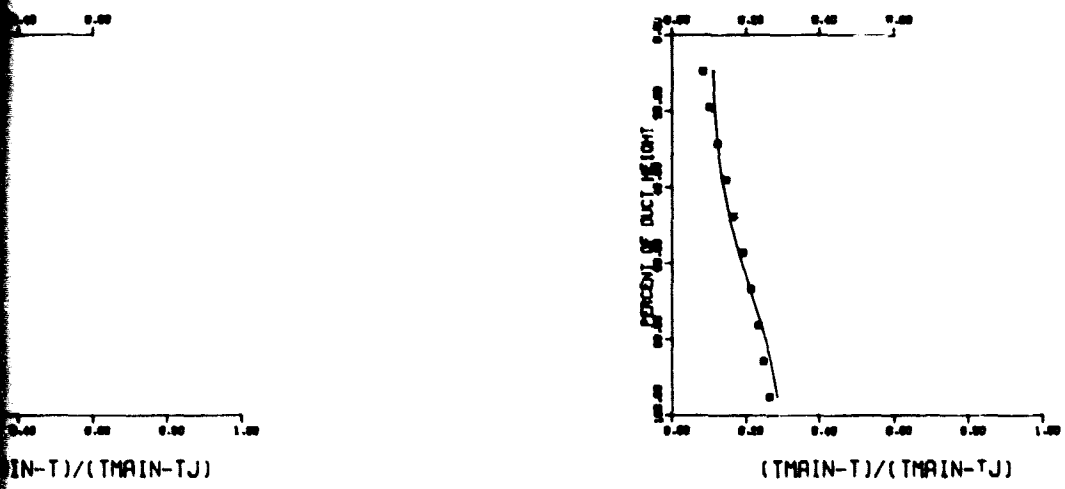

FOLDOUT FRAME

NO. 32. TEST SECTION VI.UNIFORM TMAIN. J = 107.76 . S/D =4.00 . H/D =8.00

Figure 76

ORIGINAL PAGE IS
OF POOR QUALITY

S = 0.0508 METERS S/DJ = 2.500 HO/DJ = 5.001 VMAIN = 16.3 M/SEC VJET = 29.5 M/SEC TMAIN = 649.8 K TJE

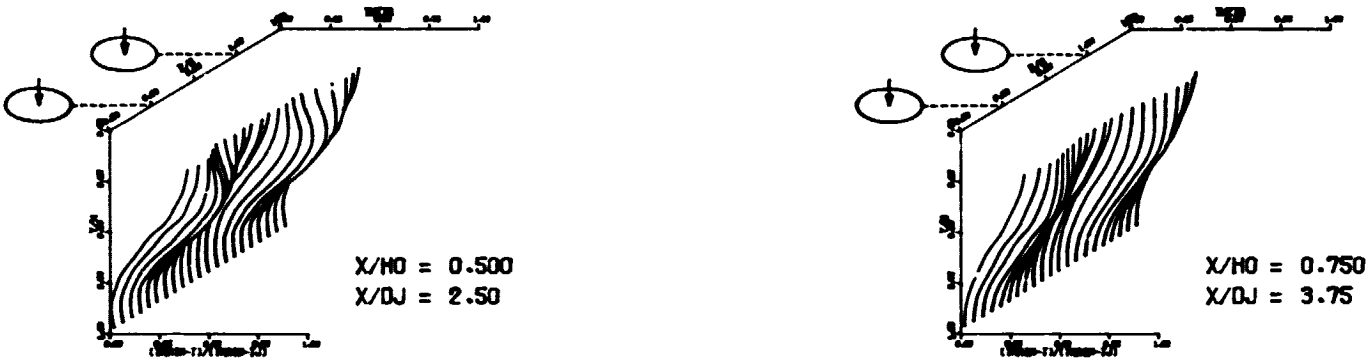

MEASURED THETA PROFILES FOR TEST NO. 33. TEST SECTION VI. TMAIN=CONST . J = 7

CONTOUR	1	2	3	4	5	6	7	8	9
VALUE	0.0500	0.1000	0.1500	0.1969	0.2500	0.3000	0.3500	0.4000	0.4

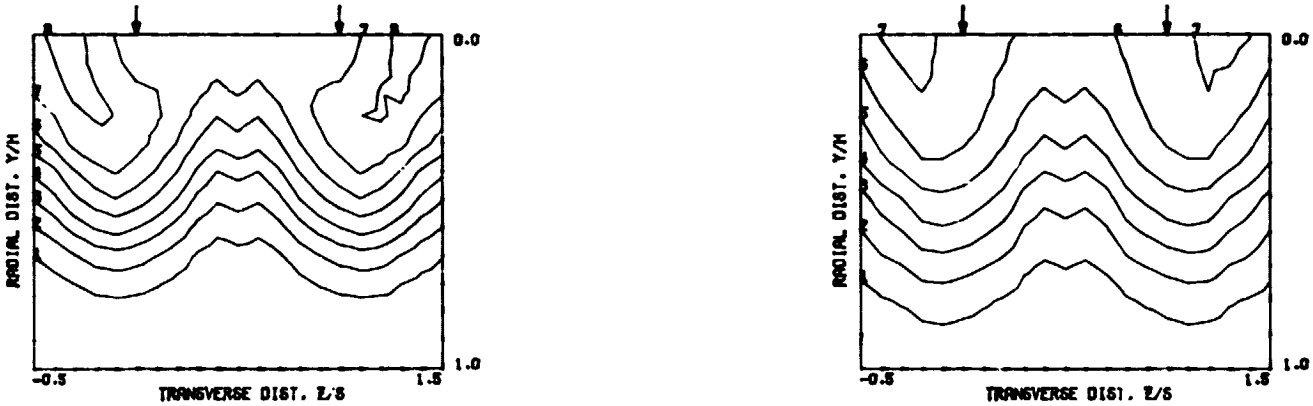

MEASURED THETA CONTOURS FOR TEST NO.33. TMAIN=CONST. J=7.05. S/D=2.0

ORIGINAL PAGE IS
OF POOR QUALITY

FOLDOUT FRAME

M/SEC TMAIN = 649.8 K TJET = 301.3 K THEB = 0.1969 BLORAT= 3.903 DENRATIO= 2.165 TRATIO=0.464

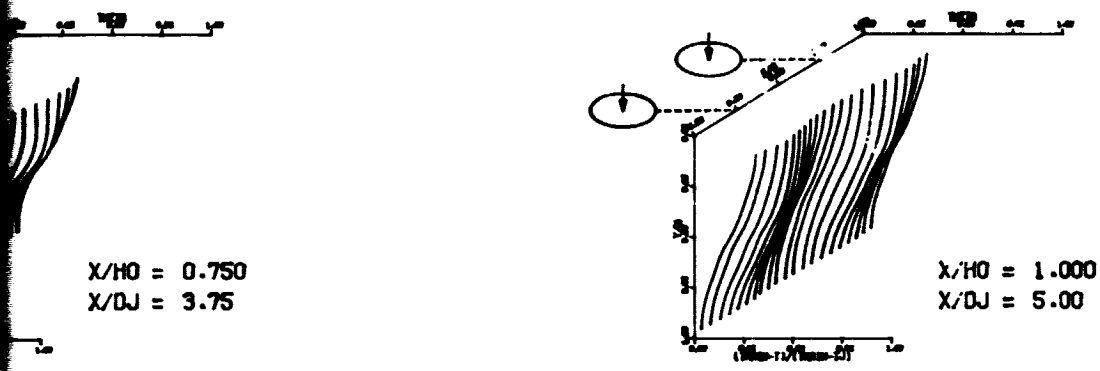

ION VI. TMAIN=CONST . J = 7.05 . S/D = 2.00 . H/D = 4.00

6 7 8 9 10

.3000 0.3500 0.4000 0.4500 0.5000

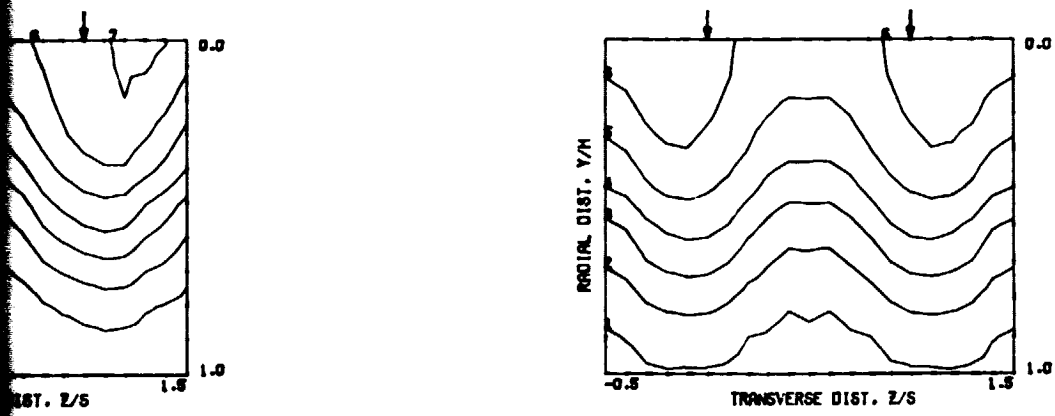

FOLDOUT FRAME

ORIGINAL PAGE IS OF POOR QUALITY

AIN=CONST. J=7.05. S/D=2.0. H/D=4.0

Figure 77

CONTOUR	1	2	3	4	5	6	7	8	9
VALUE	0.0500	0.1000	0.1500	0.1969	0.2500	0.3000	0.3500	0.4000	0.45

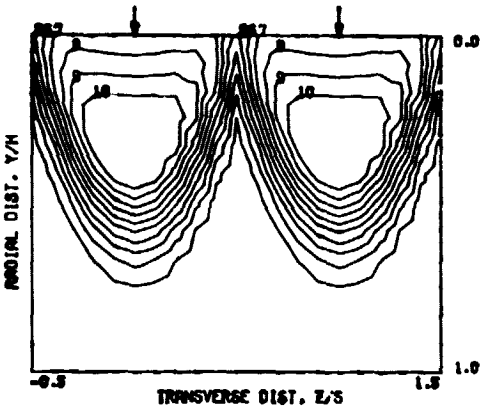

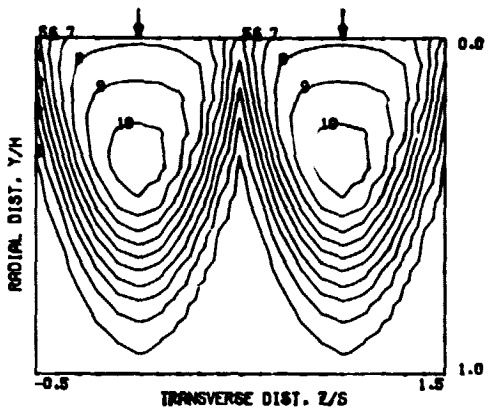

PREDICTED THETA CONTOURS FOR TEST NO.33. TMAIN=CONST. J=7.05. S/D=2.0.

S/DJ = 2.50 HO/DJ = 5.00 VRATIO = 1.80 TRATIO = 0.464 DENRATIO=2.165 TMAIN

X/H = 0.50 X/DJ =2.50

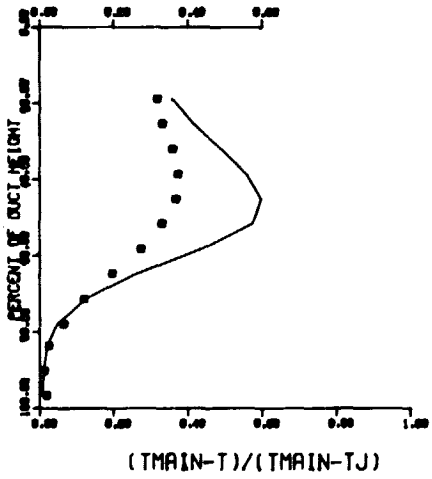

X/H = 0.75 X/DJ =3.75

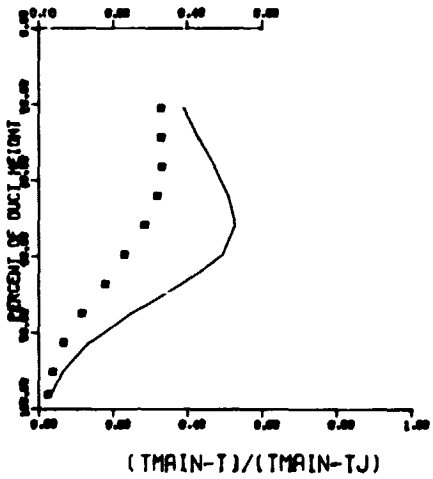

COMPARISON BETWEEN DATA AND CORRELATIONS FOR TEST NO. 33. TEST SECTION VI.UNIFOR

ORIGINAL PAGE IS
OF POOR QUALITY

FOLDOUT FRAME

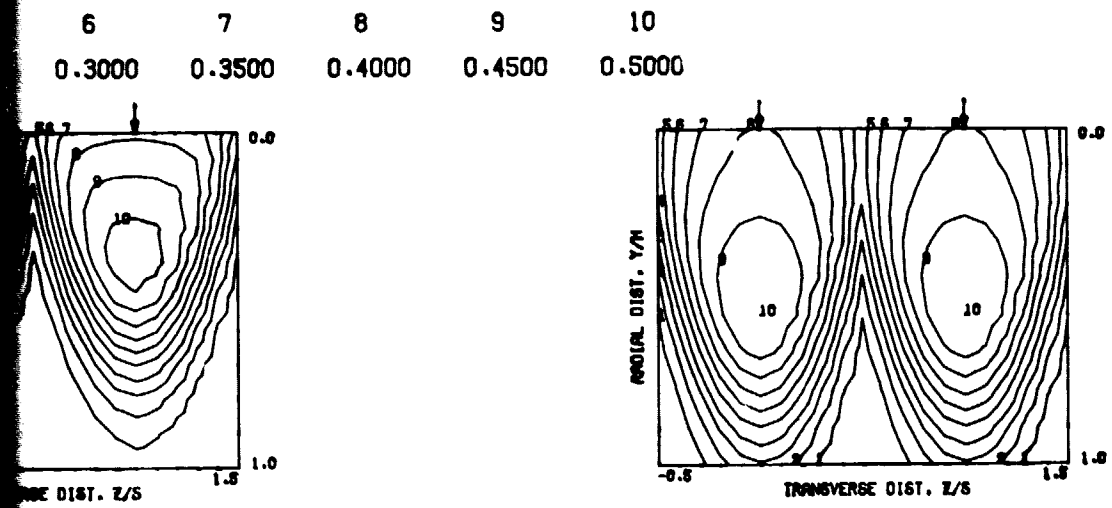

. TMAIN=CONST. J=7.05. S/D=2.0. H/D=4.0

TIO = 0.464 DENRATIO=2.165 TMAIN = 649.6 K TJET = 301.3 K THEB = 0.197

X/DJ =3.75 X/H = 1.00 X/DJ =5.00

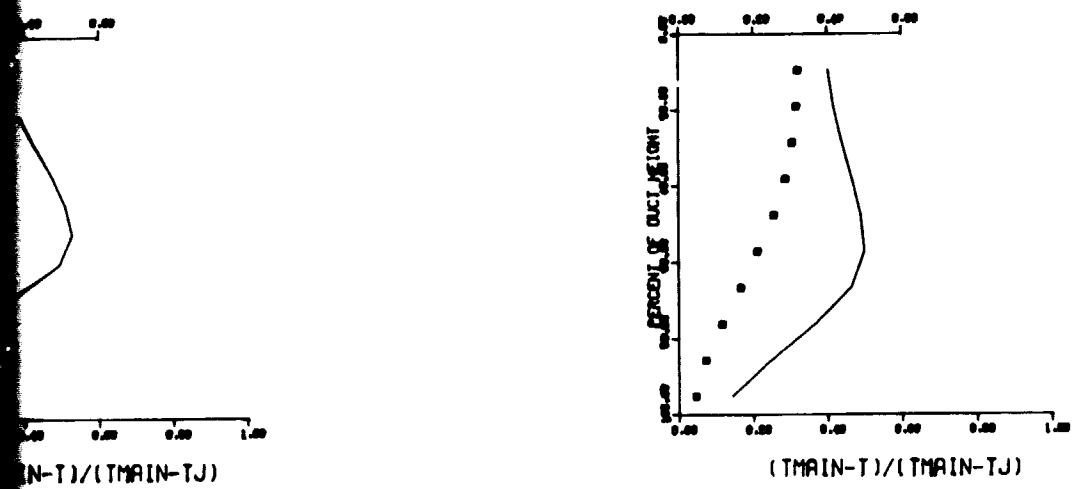

FOLDOUT FRAME

ORIGINAL PAGE IS
OF POOR QUALITY

NO. 33. TEST SECTION VI.UNIFORM TMAIN. J = 7.05 . S/D =2.00 . H/D =4.00

Figure 78

S = 0.0508 METERS S/DJ = 2.561 HO/DJ = 5.122 VMAIN = 16.2 M/SEC VJET = 55.9 M/SEC TMAIN = 650.8 K

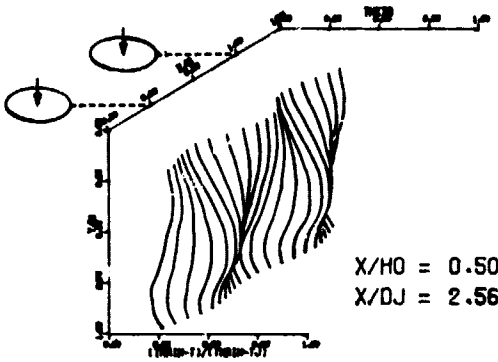

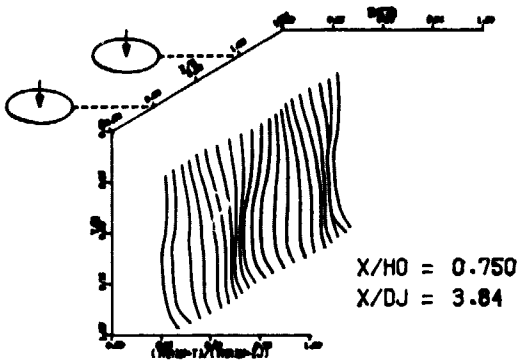

MEASURED THETA PROFILES FOR TEST NO. 34. TEST SECTION VI. TMAIN=CONST . J

CONTOUR	1	2	3	4	5	6	7	8
VALUE	0.0500	0.1000	0.1500	0.2000	0.2500	0.3144	0.3500	0.4000

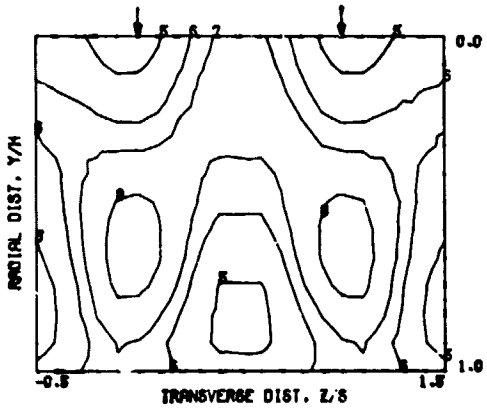

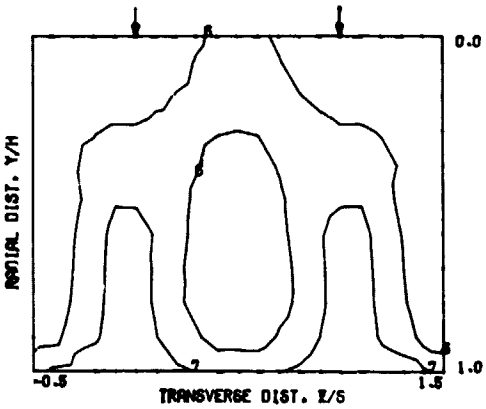

MEASURED THETA CONTOURS FOR TEST NO.34. TMAIN=CONST. J=26.4. S/D=

ORIGINAL PAGE IS
OF POOR QUALITY

FOLDOUT FRAME

SEC TMAIN = 650.8 K TJET = 296.9 K THEB = 0.3144 BLORAT= 7.657 DENRATIO= 2.225 TRATIO= 0.456

X/HO = 0.750
X/DJ = 3.84

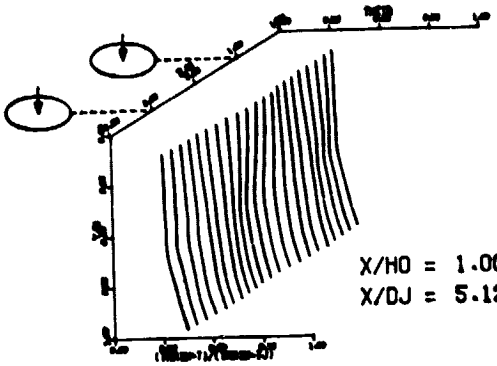

X/HO = 1.000
X/DJ = 5.12

VI. TMAIN=CONST . J = 26.40 . S/D = 2.00 . H/D = 4.00

	7	8	9	10
144	0.3500	0.4000	0.4500	0.5000

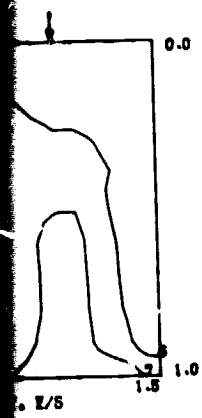

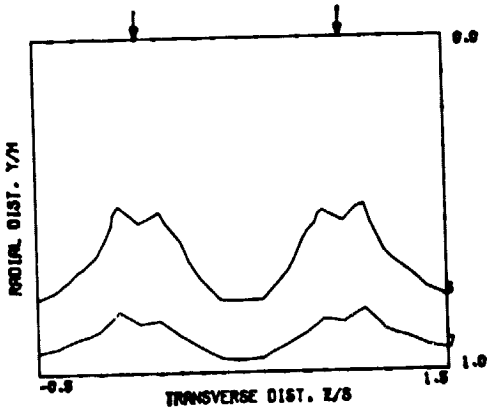

ORIGINAL PAGE IS
OF POOR QUALITY

IN=CONST. J=26.4. S/D=2.0. H/D=4.0

Figure 79

FOLDOUT FRAME

CONTOUR	1	2	3	4	5	6	7	8	9
VALUE	0.0500	0.1000	0.1500	0.2000	0.2500	0.3144	0.3500	0.4000	0.4

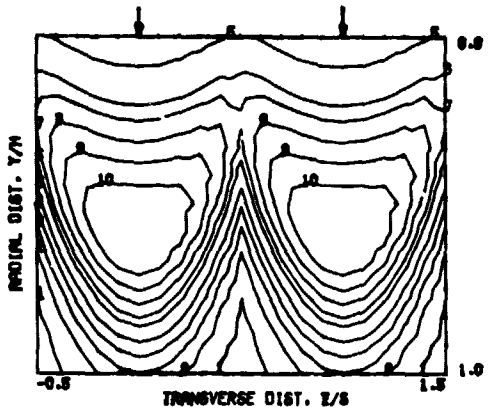

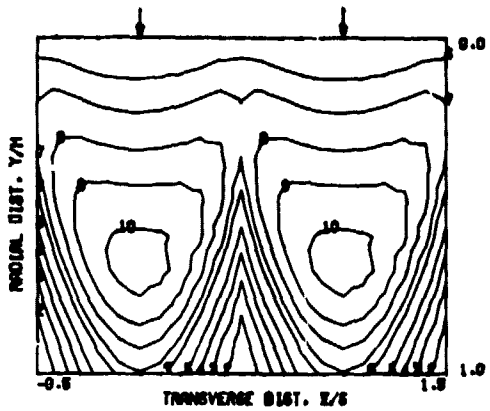

PREDICTED THETA CONTOURS FOR TEST NO.34, TMAIN=CONST, J=26.4, S/D=2.0

S/DJ = 2.56 HO/DJ = 5.12 VRATIO = 3.44 TRATIO = 0.456 DENRATIO=2.225 TMAIN

X/H = 0.50 X/DJ =2.56

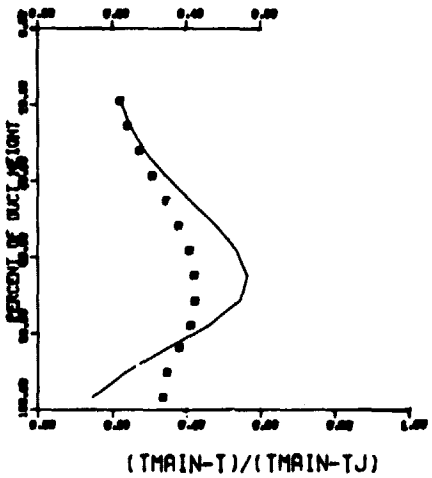

X/H = 0.75 X/DJ =3.84

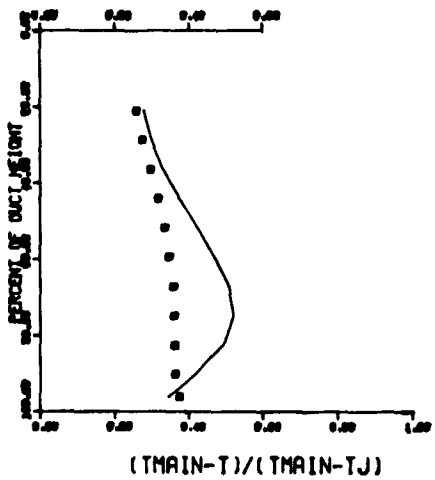

COMPARISON BETWEEN DATA AND CORRELATIONS FOR TEST NO. 34, TEST SECTION VI.UNIFO

FOLDOUT FRAME

ORIGINAL PAGE IS
OF POOR QUALITY

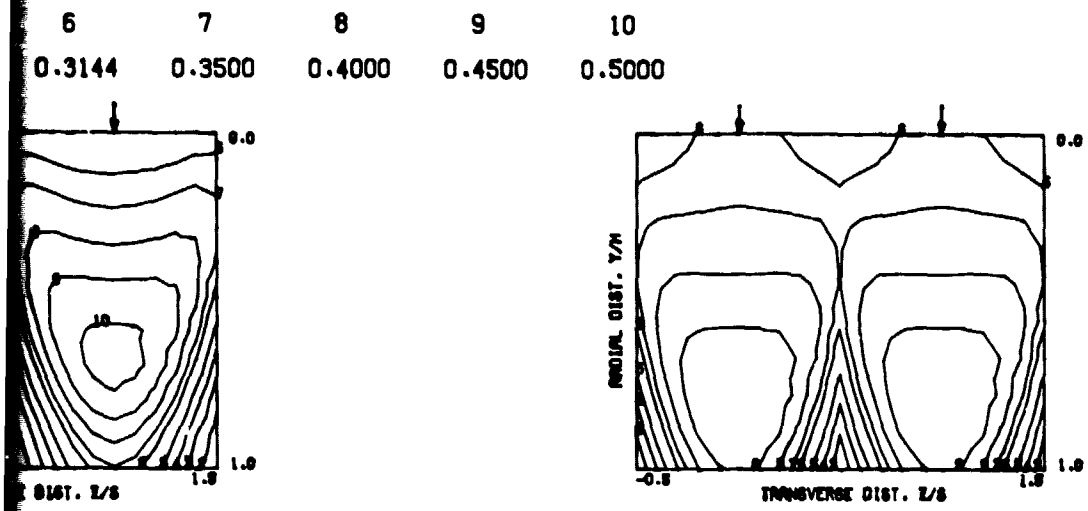

TMAIN=CONST. J=26.4. S/D=2.0. H/D=4.0

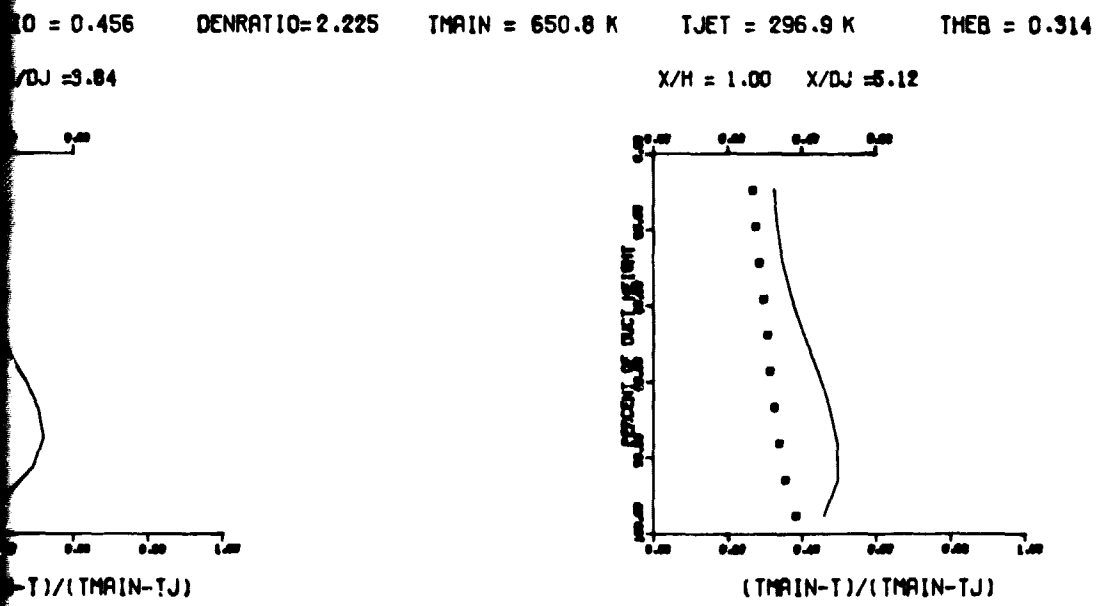

NO. 34. TEST SECTION VI.UNIFORM TMAIN. J = 26.40 . S/D =2.00 . H/D =4.00

Figure 80

ORIGINAL PAGE IS
OF POOR QUALITY

S = 0.0508 METERS S/DJ = 4.961 HO/DJ = 9.921 VMAIN = 18.7 M/SEC VJET = 70.9 M/SEC TMAIN = 561.4 K TJ

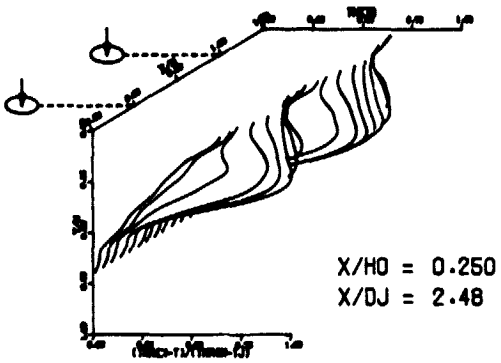

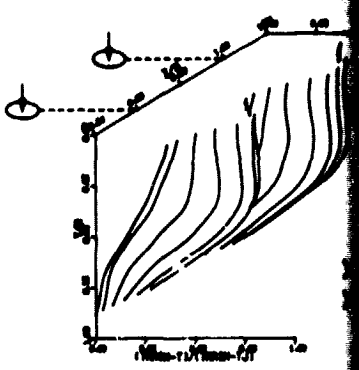

MEASURED THETA PROFILES FOR TEST NO. 35, TEST SECTION V, TOP COLD . J =

CONTOUR	1	2	3	4	5	6
VALUE	0.0500	0.1002	0.1500	0.2000	0.2500	0.3000

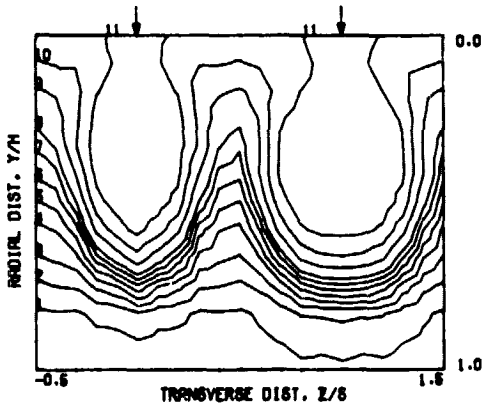

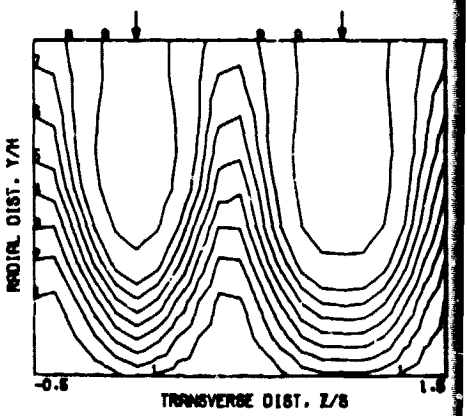

MEASURED THETA CONTOURS FOR TEST NO.35, TOP COLD.

FOLDOUT FRAME

ORIGINAL PAGE IS
OF POOR QUALITY

70.9 M/SEC TMAIN = 561.4 K TJET = 307.6 K THEB = 0.1002 BLORAT= 6.977 DENRATIO= 1.864 TRATIO=0.548

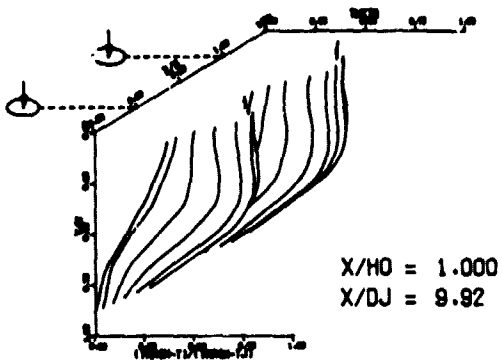

ECTION V, TOP COLD , J = 26.82 , S/D = 4.00 , H/D = 8.00

	4	5	6	7	8	9	10	11
00	0.2000	0.2500	0.3000	0.3500	0.4000	0.5000	0.6000	0.7000

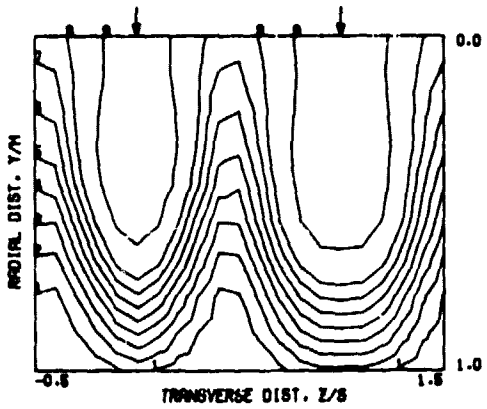

2 FOLDOUT FRAME

ORIGINAL PAGE IS
OF POOR QUALITY

OURS FOR TEST NO.35, TOP COLD, J=26.82, S/D=4.0, H/D=8.0

Figure 81

CONTOUR	1	2	3	4	5	6	7
VALUE	0.0500	0.1002	0.1500	0.2000	0.2500	0.3000	0.35

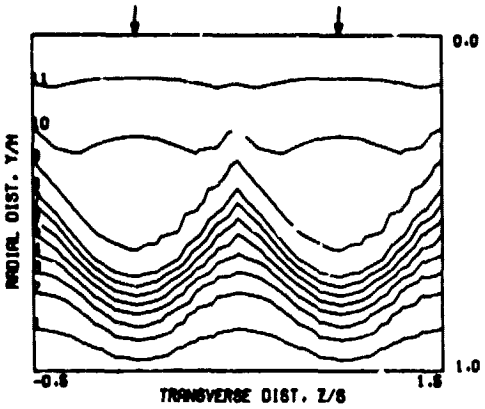

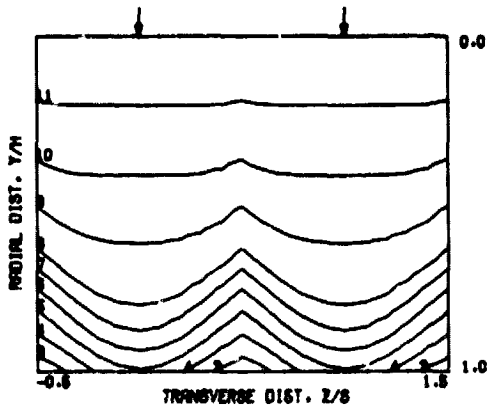

PREDICTED THETA CONTOURS FOR TEST NO. 35, TOP COLD, J

S/DJ = 4.96 HO/DJ = 9.92 VRATIO = 3.79 TRATIO = 0.548 DENRATIO= 1.864 TMAIN =

X/H = 0.25 X/DJ =2.48

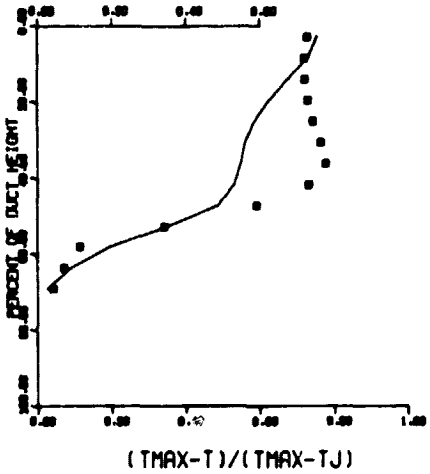

X/H = 1.00 X/DJ =9.92

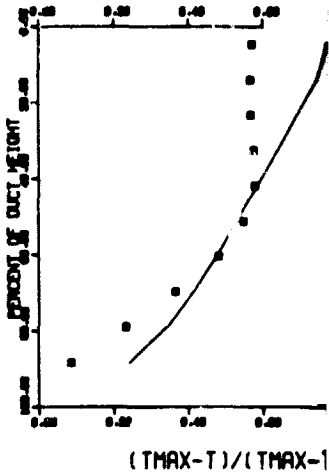

COMPARISON BETWEEN DATA AND CORRELATIONS FOR TEST NO. 35, TEST SECTION V, TOP CO

ORIGINAL PAGE IS
OF POOR QUALITY

FOLDOUT FRAME

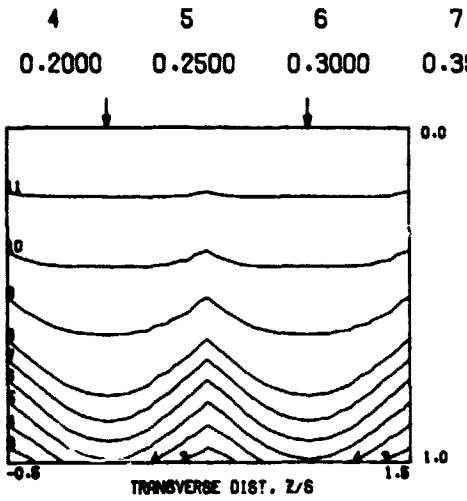

RS FOR TEST NO. 35, TOP COLD, J=26.82, S/D=4.0 H/D=8.0

D = 0.548 DENRATIO= 1.864 TMAIN = 561.4 K TJET = 307.6 K THEB = 0.055

X/H = 1.00 X/DJ =9.92

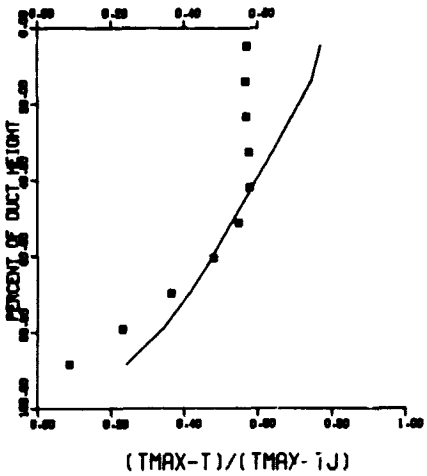

FOLDOUT FRAME

ORIGINAL PAGE IS
OF POOR QUALITY

O. 35, TEST SECTION V, TOP COLD , J = 26.82 , S/D =4.00 , H/D =8.00

Figure 82

S = 0.0508 METERS S/DJ = 5.163 HO/DJ = 10.327 VMAIN = 18.8 M/SEC VJET = 139.1 M/SEC TMAIN = 568.2 K T

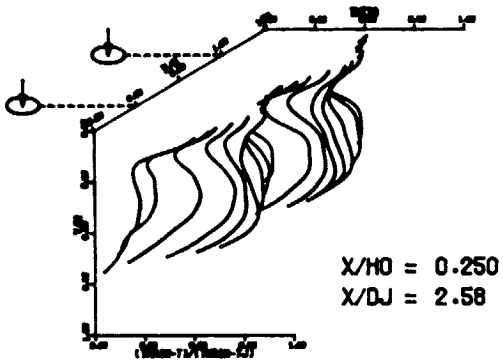

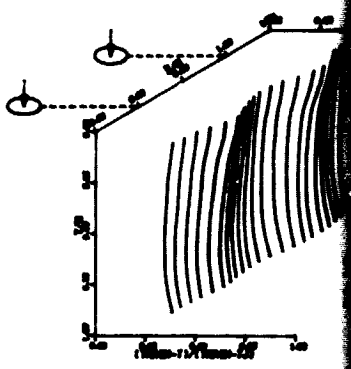

MEASURED THETA PROFILES FOR TEST NO. 36. TEST SECTION V. TOP COLD . J =

CONTOUR	1	2	3	4	5	6
VALUE	0.0500	0.1000	0.1500	0.1768	0.2500	0.3000

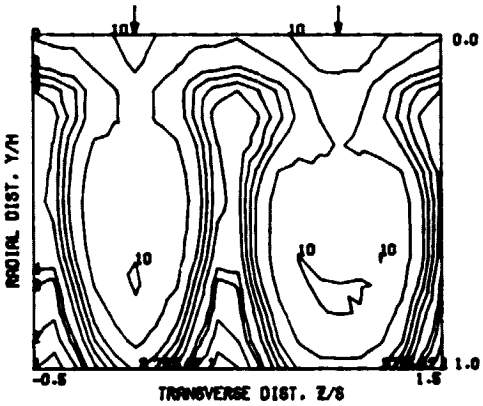

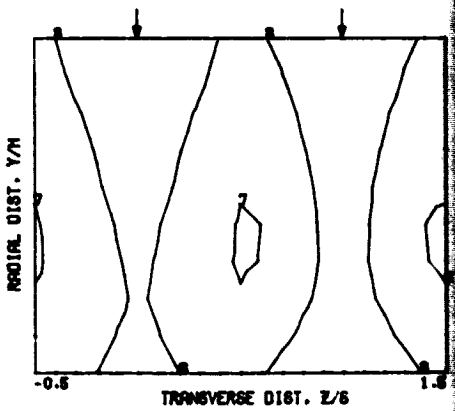

MEASURED THETA CONTOURS FOR TEST NO.36. TOP COLD.

FOLDOUT FRAME

ORIGINAL PAGE IS
OF POOR QUALITY

.1 M/SEC TMAIN = 568.2 K TJET = 305.2 K THEB = 0.1768 BLORAT= 14.583 DENRATIO= 2.012 TRATIO=0.537

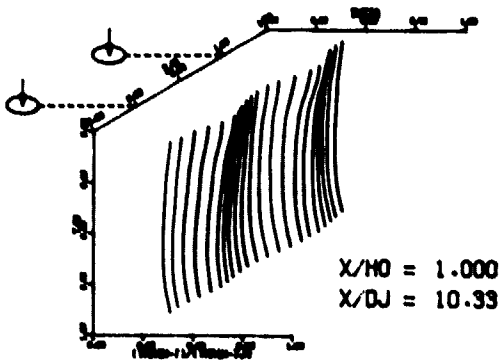

ION V. TOP COLD , J = 109.80 , S/D = 4.00 , H/D = 8.00

4	5	6	7	8	9	10	11
0.1768	0.2500	0.3000	0.3500	0.4000	0.5000	0.6000	0.7000

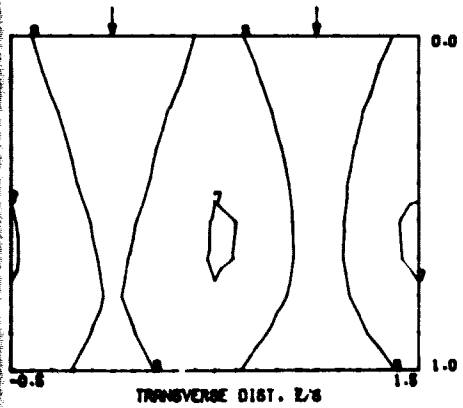

FOLDOUT FRAME

FOR TEST NO.36. TOP COLD. J=109.8. S/D=4.0. H/D=8.0

Figure 83

ORIGINAL PAGE IS
OF POOR QUALITY

CONTOUR	1	2	3	4	5	6
VALUE	0.0500	0.1000	0.1500	0.1768	0.2500	0.3000

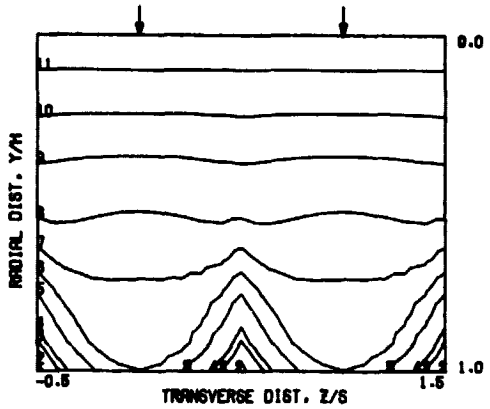

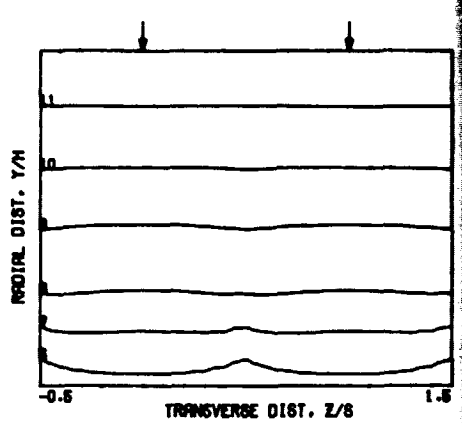

PREDICTED THETA CONTOURS FOR TEST NO. 36, TOP COL

S/DJ = 5.16 HO/DJ = 10.33 VRATIO = 7.39 TRATIO = 0.537 DENRATIO=2.012 TMA

X/H = 0.25 X/DJ =2.58

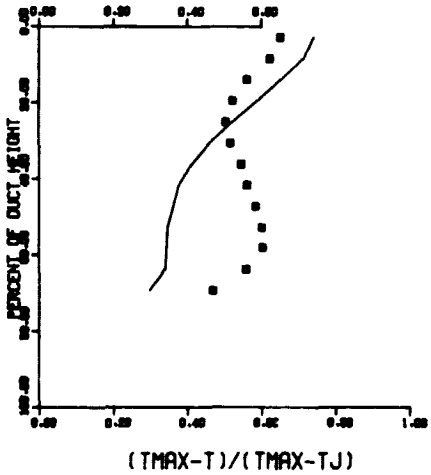

X/H = 1.00 X/DJ =1

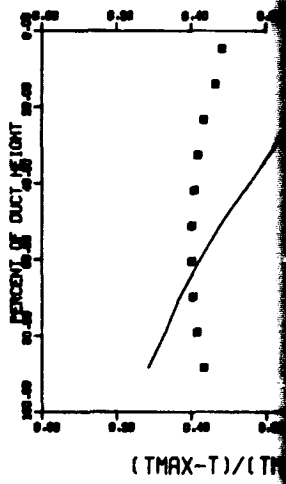

COMPARISON BETWEEN DATA AND CORRELATIONS FOR TEST NO. 36, TES. SECTION V, TOP

ORIGINAL PAGE IS
OF POOR QUALITY

FOLDOUT FRAME

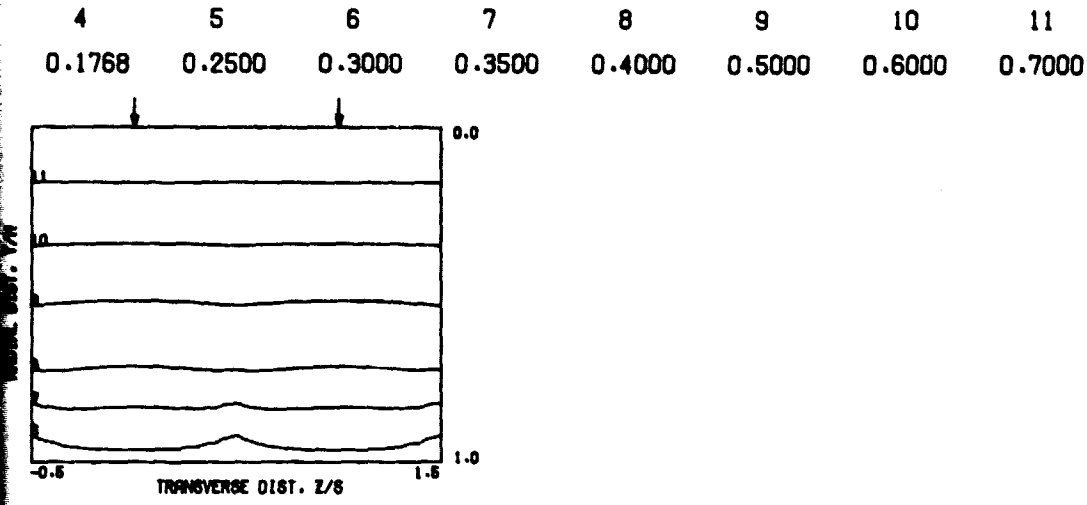

RS FOR TEST NO. 36, TOP COLD, J=109.8, S/D=4.0 H/D=8.0

D = 0.537 DENRATIO=2.012 TMAIN = 568.2 K TJET = 305.2 K THEB = 0.101

X/H = 1.00 X/DJ =10.33

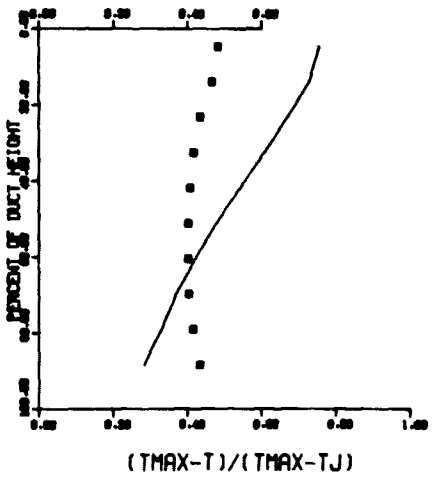

ORIGINAL PAGE IS
OF POOR QUALITY

. 36, TEST SECTION V, TOP COLD , J = 109.80 , S/D =4.00 , H/D =8.00

Figure 84

FOLDOUT FRAME

S = 0.0508 METERS S/DJ = 4.698 HO/DJ = 9.396 VMAIN = 16.0 M/SEC VJET = 40.7 M/SEC TMAIN = 417.3 K TJE

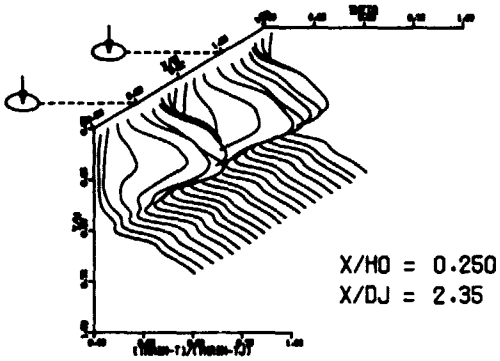

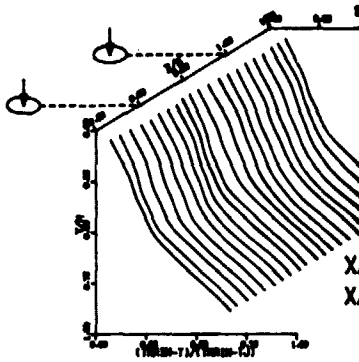

MEASURED THETA PROFILES FOR TEST NO. 37, TEST SECTION V, TOP HOT , J =

CONTOUR	1	2	3	4	5	6
VALUE	0.0500	0.0641	0.1500	0.2000	0.2500	0.3000

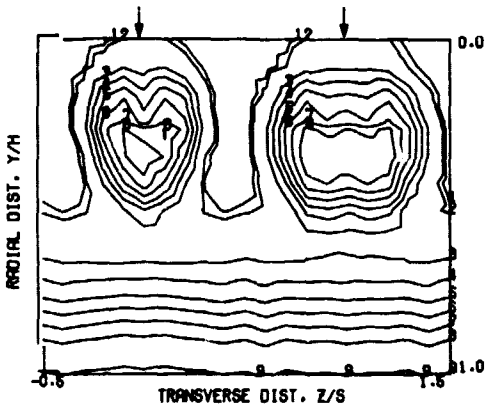

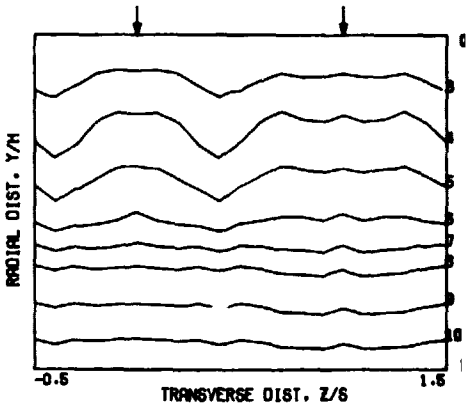

MEASURED THETA CONTOURS FOR TEST NO.37, TOP HOT,

ORIGINAL PAGE IS
OF POOR QUALITY

FOLDOUT FRAME

M/SEC TMAIN = 417.3 K TJET = 319.0 K THEB = 0.0641 BLORAT= 3.850 DENRATIO= 1.316 TRATIO=0.764

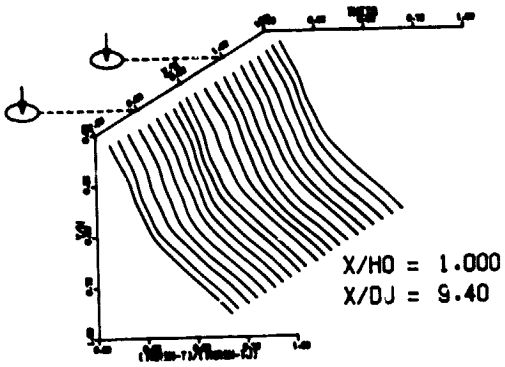

N V, TOP HOT , J = 8.51 , S/D = 4.00 , H/D = 8.00

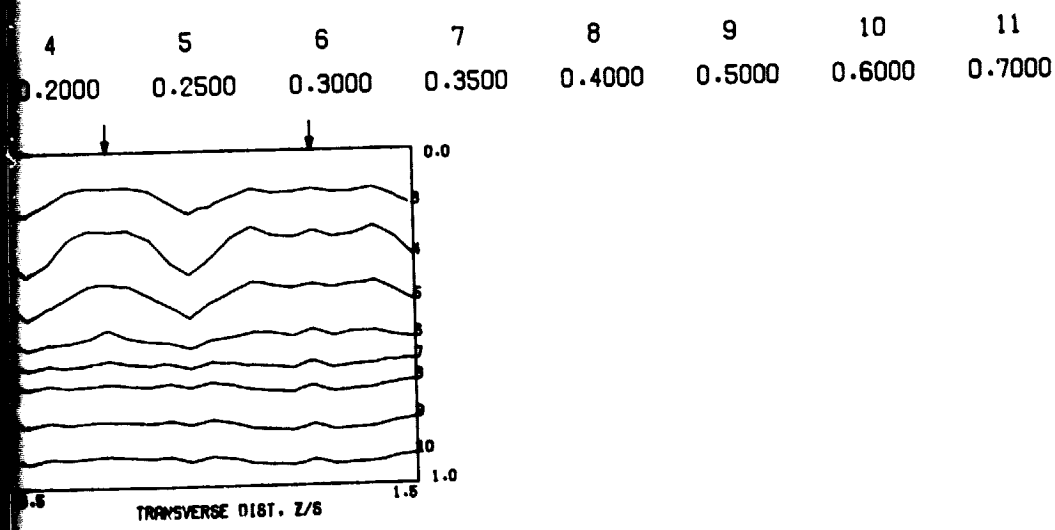

ORIGINAL PAGE IS
OF POOR QUALITY

FOLDOUT FRAME

FOR TEST NO.37, TOP HOT, J=8.51, S/D=4.0, H/D=8.0

Figure 85

CONTOUR	1	2	3	4	5	6
VALUE	0.0500	0.0641	0.1500	0.2000	0.2500	0.3000

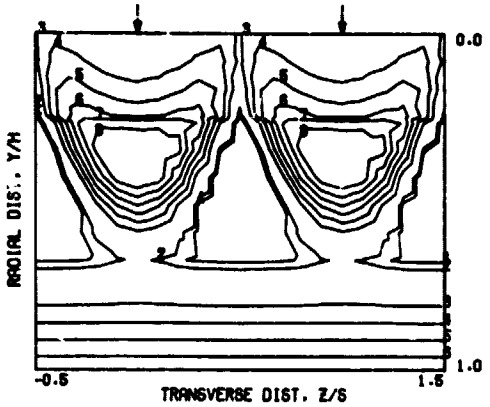

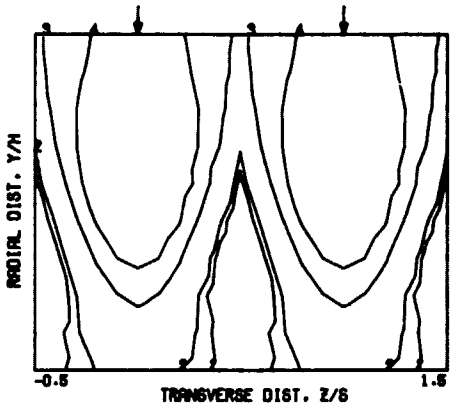

PREDICTED THETA CONTOURS FOR TEST NO. 37, TOP HOT

S/DJ = 4.70 HO/DJ = 9.40 VRATIO = 2.54 TRATIO = 0.764 DENRATIO= 1.316 TMAI

X/H = 0.25 X/DJ =2.35

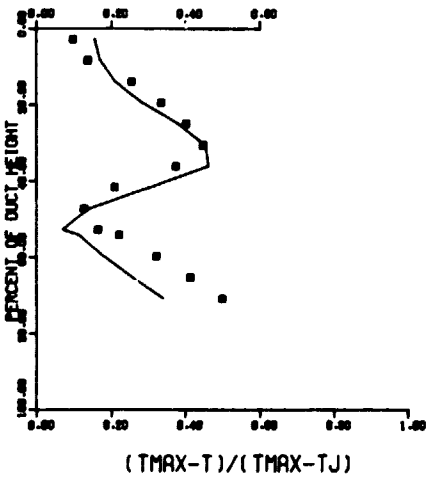

X/H = 1.00 X/DJ =9.

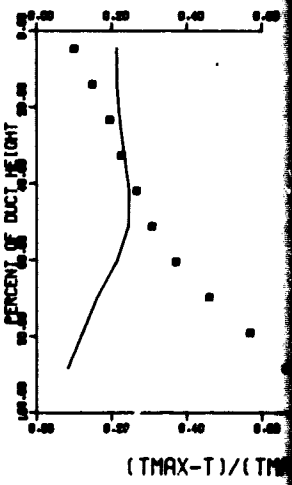

COMPARISON BETWEEN DATA AND CORRELATIONS FOR TEST NO. 37, TEST SECTION V, TOP

FOLDOUT FRAME

ORIGINAL PAGE IS
OF POOR QUALITY

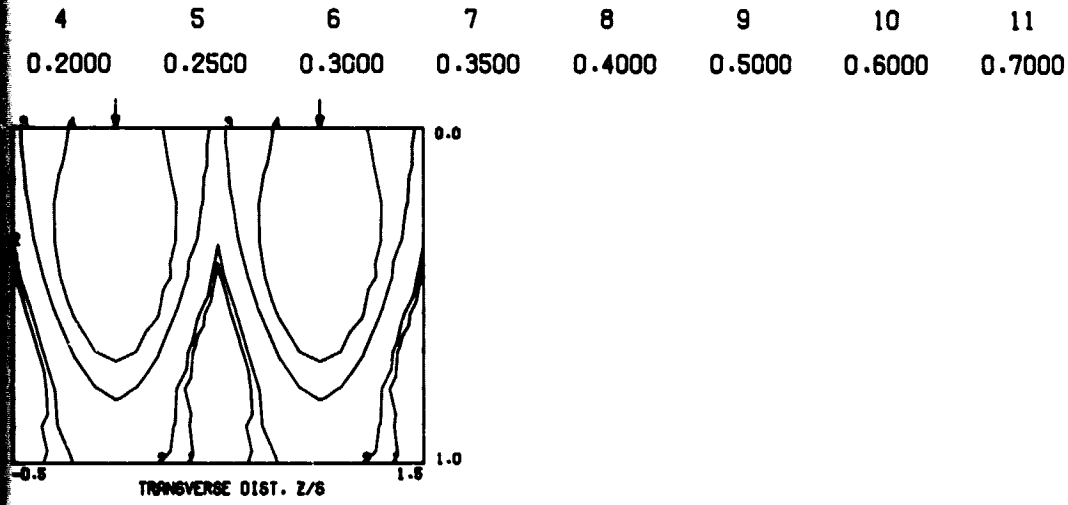

S FOR TEST NO. 37, TOP HOT, J=8.51, S/D=4.0 H/D=8.0

= 0.764 DENRATIO=1.316 TMAIN = 417.3 K TJET = 319.0 K THEB = 0.014

X/H = 1.00 X/DJ =9.40

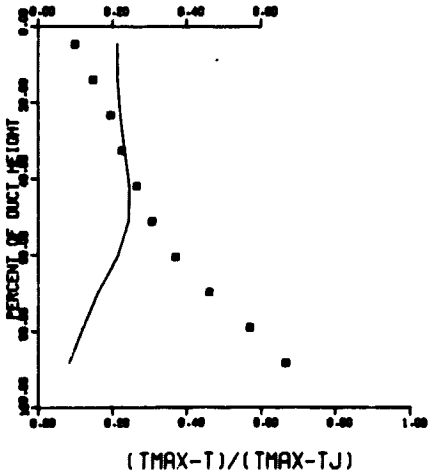

ORIGINAL PAGE IS
OF POOR QUALITY

. 37, TEST SECTION V, TOP HOT , J = 8.51 , S/D =4.00 , H/D =8.00

Figure 86

FOLDOUT FRAME

S = 0.0508 METERS S/DJ = 4.925 HO/DJ = 9.851 VMAIN = 16.0 M/SEC VJET = 75.4 M/SEC TMAIN = 416.1 K TJET

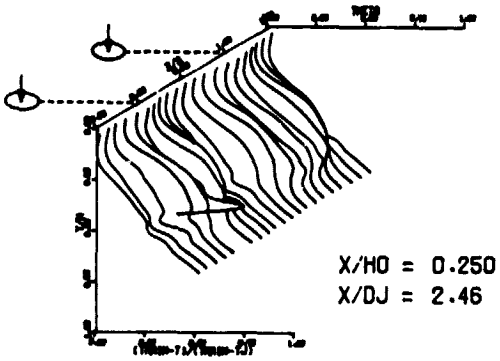

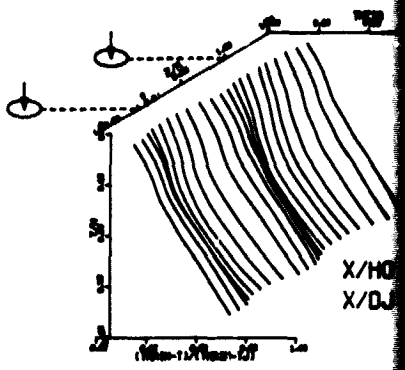

MEASURED THETA PROFILES FOR TEST NO. 38, TEST SECTION V, TOP HOT , J = 30

CONTOUR	1	2	3	4	5	6	7
VALUE	0.0500	0.1067	0.1500	0.2000	0.2500	0.3000	0.3

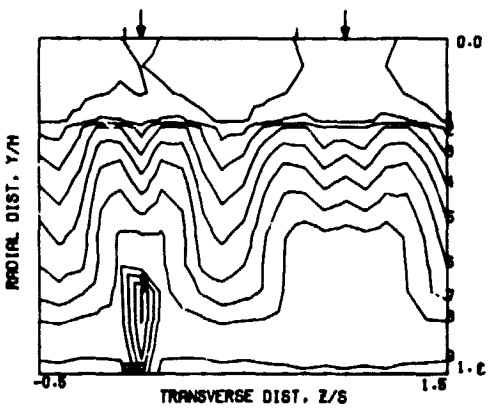

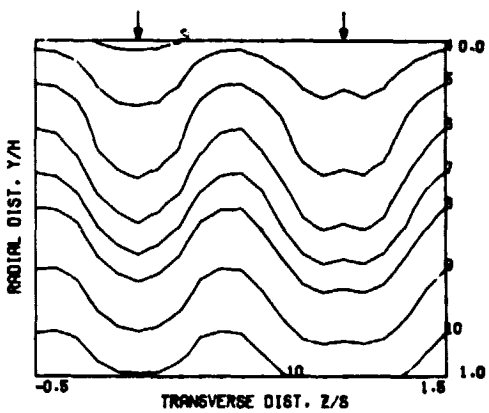

MEASURED THETA CONTOURS FOR TEST NO.38, TOP HOT, J

ORIGINAL PAGE IS
OF POOR QUALITY

FOLDOUT FRAME

M/SEC TMAIN = 416.1 K TJET = 314.5 K THEB = 0.1067 BLORAT= 7.163 DENRATIO= 1.356 TRATIO= 0.756

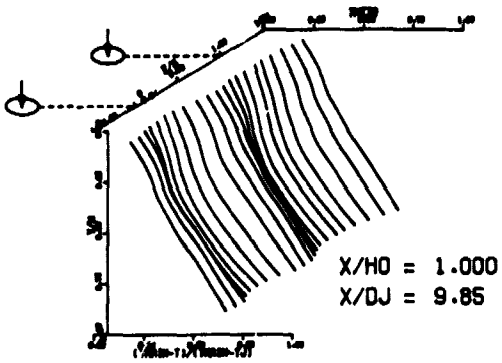

N V, TOP HOT , J = 30.24 , S/D = 4.00 , H/D = 8.00

4	5	6	7	8	9	10	11
0.2000	0.2500	0.3000	0.3500	0.4000	0.5000	0.6000	0.7000

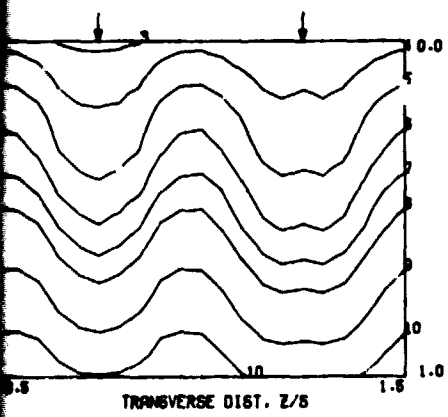

FOR TEST NO.38, TOP HOT, J=30.24, S/D=4.0, H/D=8.0

ORIGINAL PAGE IS
OF POOR QUALITY

FOLDOUT FRAME

Figure 87

CONTOUR	1	2	3	4	5	6
VALUE	0.0500	0.1067	0.1500	0.2000	0.2500	0.3000

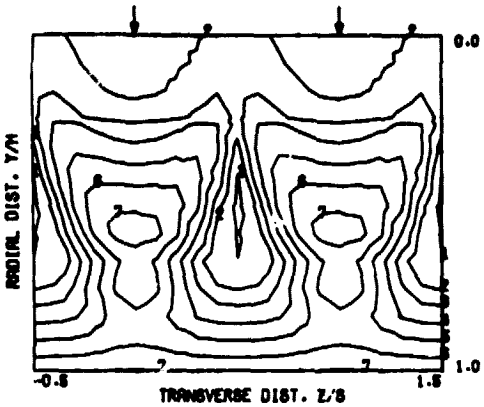

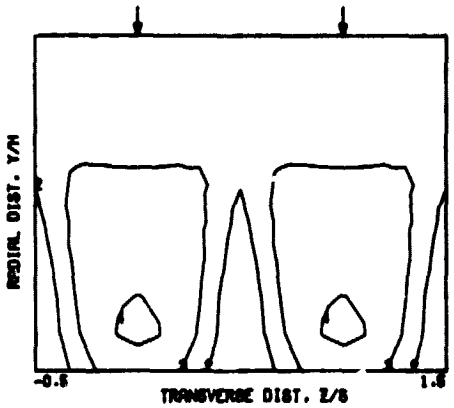

PREDICTED THETA CONTOURS FOR TEST NO. 38. TOP HOT

S/DJ = 4.93 HO/DJ = 9.85 VRATIO = 4.72 TRATIO = 0.756 DENRATIO= 1.356 TMA

X/H = 0.25 X/DJ =2.46

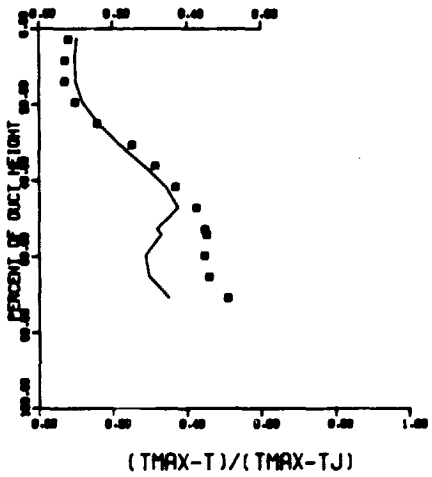

X/H = 1.00 X/DJ =

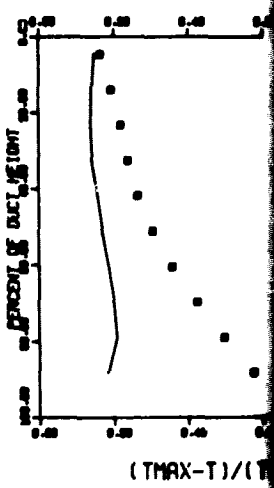

COMPARISON BETWEEN DATA AND CORRELATIONS FOR TEST NO. 38. TEST SECTION V. TOP

ORIGINAL PAGE IS
OF POOR QUALITY

FOLDOUT FRAME

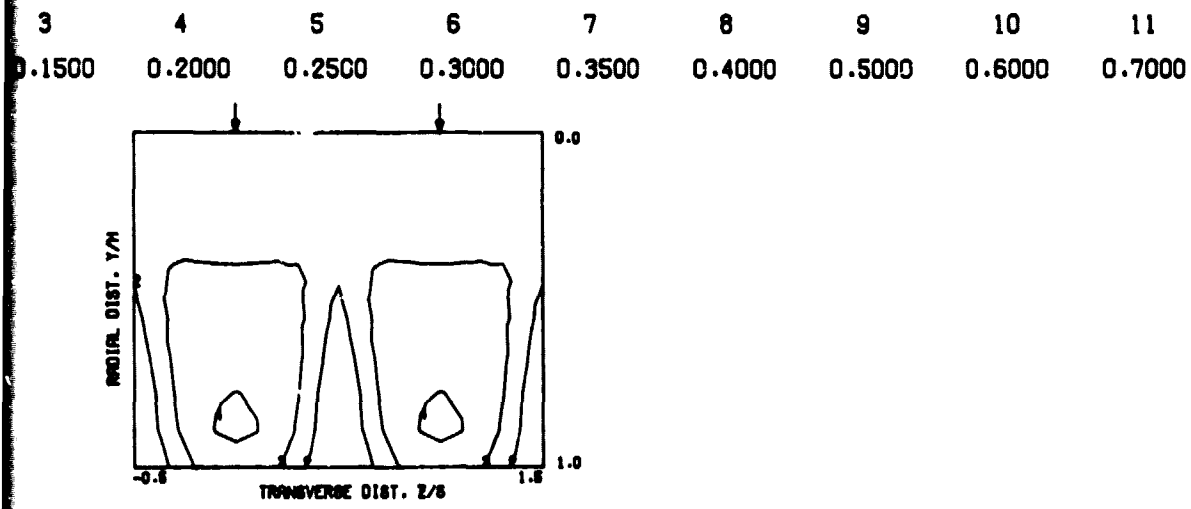

CONTOURS FOR TEST NO. 38, TOP HOT, J=30.24, S/D=4.0 H/D=8.0

TRATIO = 0.756 DENRATIO= 1.356 TMAIN = 416.1 K TJET = 314.5 K THEB = 0.023

X/H = 1.00 X/DJ =9.85

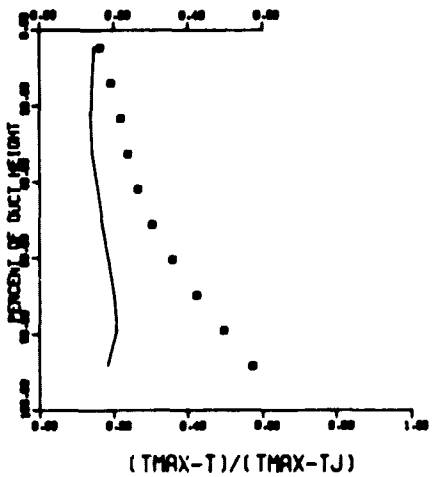

FOLDOUT FRAME

TEST NO. 38, TEST SECTION V, TOP HOT , J = 30.24 , S/D =4.00 , H/D =8.00

Figure 88

ORIGINAL PAGE IS
OF POOR QUALITY

APPENDIX A

LIST OF SYMBOLS

A	test section cross-sectional area at survey plane
D	geometric orifice diameter
D_j	effective orifice diameter
H_o	duct height at the jet injection plane
H	local duct height at the survey plane
J	momentum ratio $\left(\rho_j V_j^2\right) / \left(\rho_m V_m^2\right)$
P_t	stagnation pressure
P_s	static pressure
S	orifice spacing
T	temperature
V	velocity
X	X direction, parallel to duct axis
y	y direction, parallel to orifice centerline (radial direction)
Z	Z direction, normal to duct axis (transverse direction)

Greek

θ	temperature difference ratio
ρ	density
α	jet injection angle

Subscripts

av	average
EB	equilibrium value
j	jet property
max	maximum
m	cross-flow property, average value

APPENDIX B

REFERENCES

1. Holdeman, J. D., R. E. Walker, and D. L. Kors, "Mixing of Multiple Dilution Jets with a Hot Primary Airstream for Gas Turbine Combustors," AIAA Paper 73-1249, Las Vegas, Nevada 1973 (also NASA TM X-71426).

2. Holdeman, J. D., and R. E. Walker, "Mixing of a Row of Jets with a Confined Cross-flow," AIAA Journal, Vol. 15, No. 2, Feb. 1977, pp 243-249.

3. Walker, R. E., and D. L. Kors, "Multiple Jet Study, Final Report," NASA CR 121217.

4 Walker, R. E., and R. G. Eberhardt, "Multiple Jet Study Data Correlations," NASA CR-134795, 1975.

5. Kamotani, Y., and I. Greber, "Experiments on a Turbulent Jet in a Cross-Flow," AIAA Paper 72-149.

6. Ricou, R. P., and D. B. Spalding, "Measurements of Entrainment by Axisymmetrical Turbulent Jets," Journal of Fluid Mechanics II, 25-32 (1961).

7. Kamotani, Y., and I. Greber, "Experiments on Confined Turbulent Jets in Cross-flow," NASA CR-2392 (1974).

8. McAllister, J. D., "A Momentum Theory for the Effects of Cross-flow on Incompressible Turbulent Jets," Ph.D. Thesis (University of Tennessee, 1968).

9. Abramovich, G. N., The Theory of Turbulent Jets, Cambridge, Massachusetts, MIT Press, 1963.

10. Keffer, J. F., and W. D. Baines, "The Round Turbulent Jet in a Cross-Wind," J. Fluid Mech. 15, 481-496 (April 1963).

11. Stoy, R. L., and Y. Ben-Haim, "Turbulent Jets in a Confined Cross-Flow," J. Fluids Eng. 95, 551-556 (December, 1973).

12. Sucec, J., and W. W. Bowley, "Prediction of the Trajectory of a Turbulent Jet Injection into Cross-Flowing Stream," J. Fluids Eng. 98, 667-673 (December 1976).